THE BIOCHEMISTRY OF ANTIGEN PRESENTATION

Thesis submitted in partial fulfilment of the requirements

for the degree of Doctor of Philosophy

by

Sebastian Hartmut Springer

Queen's College

and

Molecular Immunology Group,

Institute of Molecular Medicine,

University of Oxford

Trinity Term (July), 1996

Abstract:

The biochemistry of antigen presentation

Sebastian H. Springer, D.Phil. thesis, Trinity Term 1996

Queen's College and Institute of Molecular Medicine, Oxford

This thesis describes studies on the binding of peptides to the murine major histocompatibility complex (MHC) class I molecule H-2D^b (D^b). The expression of the recombinant soluble D^b molecule in chinese hamster ovary cells and its subsequent purification by nickel affinity chromatography, gel filtration, and preparative native isoelectric focusing are reported. The product is the correct molecule, homogeneous, a dimer of dimers, and free of endogenous peptide.

A novel binding assay based on the enhancement of natural tryptophan fluorescence by the binding of peptide is introduced. This assay is used to determine melting curves of the empty and peptide-loaded protein, and to measure association rate constants by stopped-flow fluorescence spectroscopy.

Radioligand binding measurements of equilibrium as well as association and dissociation rate constants and their temperature dependence are reported. In agreement with earlier observations, the ratio of association and dissociation rate constants is much larger than the equilibrium association constant.

Fluorescence anisotropy decay spectroscopy gives evidence for conformational alterations in the D^b molecule upon peptide binding,

The data, possible errors and ways to avoid them, and mathematical models of binding are discussed to obtain an overall picture of the binding process.

To Angela

Table of contents

Authorship declaration

I declare that this thesis represents my own work,

except where stated below.

It has never been submitted for any other degree.

The fluorescence binding assay for class I molecule-peptide interactions is the fruit of my collaboration with Klaus Döring at the Max Planck Institute for Biology, Tübingen, Germany. Some of the steady-state fluorescence measurements described were done by him, with protein material isolated, purified, and provided by me; this fact is acknowledged in the individual figure legends.

All steady-state fluorescence anisotropy and fluorescence anisotropy decay measurements were performed by Klaus Döring with protein material isolated, purified, and provided by me.

During a short period of this thesis (four weeks), I received technical help from Michael Rogers who worked on the development of the preparative isoelectric focusing method.

Acknowledgements

During this thesis, I have received generous help and support from many people, only some of which I am able to thank here.

Alain Townsend created an environment in which this work was possible. He formulated the original problem, and was a constant source of help, support, and critical evaluation.

Enzo Cerundolo made the original observation of the 'mismatch kinetics', and generously shared data, ideas, teaching, and a positive mood.

All members of the Townsend laboratory cooperated to make this such an exciting place to work, and freely shared advice and technical help. I would like to thank Enzo Cerundolo, Tim Elliott, Jonathan Skipper, and Siddhartha Mukherjee for an atmosphere of creativity and discussion. Diana Cowley, Jon Edwards, and Michael Rogers worked for the success of this project.

Klaus Döring co-developed the fluorescence assay and taught me what I know about it. He made many measurements, in good and hard times, and helped me to understand them. His supervisor, the late Fritz Jähnig, helped with many aspects of the work.

Jörn Werner was my 'biophysics tutor'. He helped me to come to terms with most of the biophysical methods described in the last part of the thesis, and was a constant source of advice and friendship.

Klaus and Jörn have both spent a lot of time reading this thesis and preventing many embarassing errors.

Sheena Radford allowed me to use the Perkin-Elmer fluorimeter, the stopped-flow fluorimeter, and the CD spectrometer; she and Michael Groß, Andrew Miranker, Nico van Nuland, and Kevin Plaxco gave practical help and advice on the use of these machines.

Without my wife, Angela Köhler, this thesis would have been truly impossible. She tolerated our long time apart with heroic cheerfulness, and during our short times together spent many hours over mathematical models of class I peptide binding. This work is dedicated to her as a sign of my gratitude.

My friends in Oxford and elsewhere helped me to enjoy the time outside - and therefore inside - the laboratory. I wish to thank Sue Kyes, Rosalind Bark, Erika Miranda, Jörn Werner, Bodo Stern, Amir Attaran, Siddhartha Mukherjee and many others for constantly reminding me to remain a sane person.

Meine Mutter, Sabine Springer, hat mich in jeder denkbaren Weise unterstützt. Sie und mein Vater haben mich ermutigt, das anzustreben, woran ich glaube. Dadurch ist diese Arbeit möglich geworden. Ihnen beiden gebührt mein besonderer Dank.

I would like to thank my past academic teachers, in Frankfurt, Stuttgart-Hohenheim, and Tübingen. Special thanks must go to Stefan Jentsch for his advice and encouragement.

I would also like to thank Tim Elliott for advice, new ideas, and the use of his FPLC; Chris Higgins, my graduate advisor, for strategic advice and the use of equipment; Chris Newbold for expert advice on biochemical problems, and the use of his FPLC and other equipment; Rosalind Harding for help with mathematical problems; Michelle Rugless for the use of the analytical isoelectric focusing equipment; Tony Brett for help and advice with computation; Jean Edouard Gairin for the gift of five peptides; Yieh-ping Wan (Du Pont NEN, Boston) for the gift of tritiated SV-324-332 peptide; Marty Feinberg (Univ. Rochester) for the program CRNT (Chemical Reaction Network Toolbox) and advice on its use; and Alain Fersht (Cambridge), Ed Hulme (NIMR, London) and Mike Schimerlik (Oregon) for mechanistic suggestions.

Financially, this work was supported by the Wellcome Trust and the Townsend-Jeantet Prize Trust. I have also received financial support from Queen's College, Oxford, and the Studienstiftung des Deutschen Volkes.

1. Materials and methods

Methods have a tendency to evolve with time; the protocols given here reflect their state at the time of writing.

Centrifugations of eppendorf tubes are performed in an eppendorf centrifuge at 13000 rpm unless indicated otherwise.

All percentages are volume percent (v/v) unless indicated otherwise.

'15 ml centrifuge tube' and '50 ml centrifuge tube' mean the conical bottom plastic tubes, e.g. Beckton Dickinson-Falcon Nr. 2097 and 2090.

All companies mentioned are UK based unless indicated otherwise.

1.1. Chemicals and reagents

All chemicals and reagents were from Fluka, Sigma, or Merck BDH unless indicated otherwise. dNTPs were from Pharmacia (FPLC grade). Restriction enzymes and other molecular biology enzymes were from New England Biolabs. For molecular biology and protein work, reagents were of the highest available purity unless indicated otherwise.

1.2. Buffers and solutions used frequently

lysis buffer

50 mM	Tris·Cl pH 7.4
150 mM	NaCl
5 mM	EDTA
0.5%	NP-40
0.5%(w/v)	MEGA-9 (N-nonanoyl-N-methylglucamine)
2 mM	PMSF (Phenylmethylsulfonylfluoride)
5 mM	iodoacetamide

wash buffer

50 mM	Tris·Cl pH 7.4
150 mM	NaCl
5 mM	EDTA
0.5%	NP-40

TBS (Tris-buffered saline)

50 mM	Tris·Cl pH 7.5
150 mM	NaCl

PBS (phosphate-buffered saline) was prepared according to Sambrook et al. ([1]).

	1 l
NaCl	8 g
KCl	0.2 g
$Na_2HPO_4 \cdot 2H_2O$	1.44 g
KH_2PO_4	0.24 g
adjust pH to 7.45	

this gives 145 mM Na^+, 4.5 mM K^+, 140 mM Cl^-, and 10 mM phosphate.

It was found that the commercially available PBS tablets (Oxoid PBS nr. BR14a, Unipath) are coated with an agent that causes foaming of the PBS solution. These tablets were therefore not used.

TE (Tris-EDTA, DNA buffer)

10 mM	Tris·Cl
1 mM	EDTA
	pH 7.4 was generally used.

TBE (Tris-Borate-EDTA, DNA agarose gel buffer)

(final 1x)	5x, 1l

90 mM	Tris base	54 g
90 mM	boric acid	27.5 g
0.2 mM	EDTA	2 ml 0.5 M

1.3. Antibodies

1.3.1. Antibodies used in this study

Antibodies were used for immunoprecipitation of class I molecules during binding assays or for analytical purposes, for the staining of cells, and for western blotting.

The monoclonal antibody (mAb) W6/32 recognises a conformational epitope on human class I molecules [2].

The mAb 28.14.8S (IgG_{2a}) reacts with the α_3 domain of H-2D^b (and also with H-2L^d) independent of bound or unbound peptide [3, 4, 5].

The mAb B22.249 (IgG_{2a}) reacts with the a1 domain of H-2Db only in the presence of bound peptide [4, 6].

1.3.2. Production of monoclonal antibody from hybridomas

was performed according to Ey's protocol [7]).

1.4. Molecular biology

Molecular biology strategies and techniques were generally performed according to Sambrook et al. [1], or from the suppliers of the molecular biology enzymes. Some techniques were modified or taken from different sources; these are found below.

1.4.1. M13 cloning

1) preparation of competent bacteria

1. From an o/n culture, grow bacteria in 50 ml LB to a density of 600 nm. Remove 2 ml and save at 4 °C. Spin down remaining cells (5', 3000 g)
2. Resuspend well-drained cell pellet in 2-4 ml ice-cold 50 mM $CaCl_2$. Leave on ice for 20'.
3. (optional) Spin down the cells, resuspend cell pellet in 2.5 ml of ice-cold $CaCl_2$. Store at 4 °C. The cells are competent for up to 2 days.

2) transformation of competent bacteria

4. To 10 ml tubes containing 150 µl of competent cells, add 10 ng-1 µg M13 RF DNA. Incubate on ice for 40'.
5. Melt LB top agar and cool to 48 °C in a water bath. To 30 ml top agar, add 100 µl 10% X-gal (in DMF) and 100 µl 0.1M IPTG (in ads). Keep at 48 °C.
6. Heat-shock cell/DNA mixture for 2' at 42 °C.
7. To each tube, add 2 drops of bacteria (from step 1) and 3 ml of prewarmed LB-top agar. Immediately pour onto LB-agar plate and swirl to distribute.
8. Incubate plates at 37 °C overnight.

3) preparation of M13 RF DNA

9. Inoculate 100 ml of LB medium with a bacterial colony (from an M9 minimal plate if JM101 or similar to prevent loss of the F episome). Grow to an OD_{600} of 1.0. Store at 4 °C, evtl. overnight.
10. Phage stock: Inoculate 100 ml of LB medium with one blue plaque from an mp vector plate. Grow overnight.
11. Inoculate 900 ml of LB with the OD 1.0 culture from step 9. Grow to an OD of 1.5.
12. At this point, add the 100 ml of phage stock. Infect by shaking at 37 °C for 15 min. Add 0,5 ml of chloramphenicol solution (30 mg/ml in ethanol). Shake for 1-2 hrs at 37 °C to allow accumulation of RF DNA.
13. Prepare ccc DNA from these cells using the magic maxiprep method.

1.4.2. Plasmid isolation

Maxipreparations according to [1] with subsequent purification over two Cesium chloride gradients were used to prepare DNA for cell transfections.

1.4.3. DNA sequencing

For DNA sequencing, the Sequenase kit from USB (United States Biochemicals) was used, and the instructions supplied were followed in general.

1.4.4. Oligonucleotides

were obtained from the in-house synthesis, or from R&D/British Biotech. The in-house oligos were delivered on columns and had to be cleaved off and deprotected.

Cleavage and deprotection of oligonucleotides

1. Tap the beads into one end of the column (preferentially the end without the coloured ring). Carefully open the column with a spatula. Empty the beads into a screw-cap eppendorf tube.
2. Add 500 µl 25% ammonia solution. Incubate (6 hrs -) o/n.
3. Spin down the beads. Place the supernatant into a fresh eppendorf tube. Wash the beads with 400 µl TE.
4. Unite the ammonia and TE supernatants, and adjust with TE to 1 ml.
5. Uncap a NAP10 column (Pharmacia), pour off buffer, cut off the bottom seal, and equilibrate with 3 fillings of TE.
6. Apply the oligo solution to the column. When the flow stops, elute with exactly 1.5 ml TE.
7. Determine the concentration of the oligo by reading the OD_{260} (at 1/100 dilution). 1

OD_{260} unit represents 33 µg/ml of single-stranded DNA.

After the ammonia cleavage step, the oligos can also be precipitated with ethanol, or the ammonia evaporated in the speed-vac centrifuge. The protocol given was found to perform best.

1.4.5. Polymerase chain reaction (PCR)

For PCR, polymerases from Perkin-Elmer (AmpliTaq) and Stratagene (Pfu) were used.

Reactions were performed on Perkin-Elmer Cetus thermocyclers.

Ultrapure dNTPs from Pharmacia were used for PCR reactions.

The manufacturer's instructions, especially the AmpliTaq manual, were closely followed in the setting up and running of the reactions.

All oligonucleotides were designed to have an annealing temperature of 70 °C.

PCR experiments were carried out with 'hot start': all reagents with the exception of the polymerase were mixed, the reaction overlaid with 100 µl of light mineral oil, and heated to denaturing temperature for 5'. The reaction was then cooled to 80 °C, the polymerase added, and the first cycle started (with the denaturing step).

For Taq polymerase, the following buffer was used as a standard (given as 10x):

100 mM	Tris·Cl pH 8.8 (25 °C)
500 mM	KCl
15 mM	$MgCl_2$
1%(v/v)	Triton X-100

The optimum concentration of magnesium chloride was experimentally determined for each PCR experiment.

Extension temperature was 72 °C, and cycle time typically 1' for denaturation, 1' for annealing, and 1' for extension.

For Pfu polymerase, the following buffer was used as a standard (given as 10x):

200 mM	Tris·Cl pH 7.5 (RT)
100 mM	KCl

100 mM	(NH4)2SO4
20 mM	MgSO4
1%(v/v)	Triton X-100
1 mg/ml	bovine serum albumin

Extension temperature was 72 °C, and cycle times typically 1' for denaturation, 1' for annealing, and 10' for extension.

1.5. Mammalian cell culture

Cell and tissue culture practices generally followed Harlow and Lane [8], unless indicated otherwise. Some of the protocols below represent minor modifications.

When manipulating cells, all steps were performed under sterile conditions at room temperature unless indicated otherwise.

All medium and liquid reagents added to cells should be at 37 °C unless indicated otherwise.

Incubations of cells are at 37 °C, in an atmosphere containing 5% CO_2.

Cells are usually centrifuged at 500 g (corresponding to 1200 rpm in a benchtop swing-out centrifuge) for 5 minutes.

All cell culture plasticware was purchased from Falcon unless indicated otherwise.

All cell culture media and solutions were purchased from Gibco BRL unless indicated otherwise.

1.6. Expression of proteins using the glutamine synthetase amplification system

These protocols are based on advice and protocols from Christopher Bebbington (Celltech), Neil Barclay (Dunn School of Pathology), Simon Davis (IMM) and Mike Puklavec (Dunn School).

1.6.1. Transient transfection of COS-1 cells

To assess the plasmid construct, transient transfection into COS cells and analysis of the supernatant for product is useful. The following protocol is from Christopher Bebbington.

1. Trypsinise a subconfluent 75 cm^2 flask of COS-1 cells. Resuspend in D10. Pipet cells up and down carefully to dissolve cell clumps. Check for single cell suspension under the microscope.
2. Count cells. Aliquot into 75 cm^2 flasks at $2.5 \cdot 10^6$ cells per flask. Leave cells overnight to settle down.
3. Ethanol-precipitate aliquots of 19-38 µg DNA to sterilize. Resuspend in 4.7 ml DMEM/Tris. Add 1.18 ml DEAE-dextran per aliquot. Mix by pipetting.
4. Wash the cells twice with serum-free DMEM. Drain medium from cells. Add DEAE-dextran/DNA complex. Leave for 6-8 h in tissue culture incubator. Rock gently from time to time. Do not let the cells dry out.
5. Remove cell supernatant. Add 6 ml 10% DMSO in HBS. Leave on the cells for 2-5'.

   The time is not critical but must be above 2'.
6. Remove cell supernatant. Wash with serum-free DMEM. Replace with 12 ml D10.
7. Culture cells for 48-72 h and harvest the supernatant for analysis of product secretion.

1.6.2. Stable transfection of CHO K1 cells

The protocol is optimised for (adherent) CHO K1 cells. Lymphoid cells that grow in suspension will need a different transfection protocol to get enough DNA in.

1. On day -1, seed 10^6 cells into each of four medium-sized flasks and incubate overnight

in GMEM-S medium.

On day 1: Transfect the cells, using the calcium phosphate method (steps 2-6). Flasks 1-3 receive DNA, flask 4 is a mock transfection.

2. Prepare the recombinant plasmid: ethanol-precipitate 40 µg and redissolve in 50 µl of sterile 10 mM Tris·Cl pH 7.5.
3. In a 15 ml centrifuge tube, mix the 50 µl of DNA solution with 2 ml sterile HBS. Draw up 100 µl 2.5 M $CaCl_2$ in a sterile tip, and slowly run it down the side of the tube over ca. 1'. Leave at RT for 30' for the precipitate to form.

   The precipitate should be checked under the microscope.
4. Aspirate the supernatant from the cells. Wash once with 1 ml HBS. Add the DNA precipitate and distribute over the monolayer. Leave at RT for 30' with occasional redistribution.
5. Add 20 ml of 37 °C GMEM-S, and incubate at 37 °C for 4 h.
6. Draw off the medium and replace with 20 ml fresh GMEM-S. Let the cells recover overnight.

   The flasks will have 1-2·10^6 cells each at this point.
7. The next day (day 2), trypsinise the flasks and resuspend the cells in 10 ml GMEM-S. Distribute the contents of each flask into a 96-well plate in 100 µl aliquots. Leave the cells to settle down overnight.
8. The next day (day 3), select with 15, 20 and 25 µM L-methionine sulfoximine (L-MSX) (Sigma) respectively (The mock transfection receives 20 µM L-MSX): Add to each well 100 µl GMEM-S containing the double concentration of L-MSX.
9. Leave for individual clones to come out.

   This can take 2-3 (-4) weeks. The 25 µM plate has normally between 10 and 30 clones, the other plates slightly more.
10. Test all wells with clones for expression, using dot-blot methods, RIA or ELISA.
11. Pick the 3-5 strongest secretors. Grow up 10^7 cells of each and freeze them down.

1.6.3. High copy-number selection of lines

1.6.3.1. Selection by sandwich RIA

1. Precoat PVC Elisa plates (Falcon 3911, 3912) with capture antibody: Add 50 µl of a 20 µg/ml solution of antibody in PBS (0.01% azide) to each well. Shake on Elisa plate shaker for 30'.
2. Withdraw antibody solution (and reuse). Wash plates with 500 ml of PBS over the sink: pour on, shake off.
3. Immerse plates in bucket with blocking buffer (5% dried skimmed milk in PBS, 0.01% azide). Leave for >2 hrs.

   Coated plates can be stored in the refrigerator after this step.
4. Wash plates 5x under running tap water. Dry plates with tissue.
5. Put on 50 µl of culture supernatant per well. Shake for 30'.
6. Withdraw supernatants. Wash plates 5x under running tap water.
7. Put on 50 µl of iodinated antibody: ca. 1-5 µg/ml, ca. 600 000 cpm per well, in blocking buffer. Leave for ≥ 2 hrs.
8. Withdraw antibody solution (and reuse). Put plates into bucket under running tap for ≥ 1 hr.
9. Dry plate. Cut up and place single wells in screwcap eppendorf tubes. Count in gamma counter.

1.6.3.2. Further amplification

At this stage, selection was performed by incubating 5 ml of tissue culture supernatant from the clones with 20 µl Ni^{2+}-nitriloacetic acid agarose (Ni-NTA agarose, Qiagen) for 2 hours in the presence of 10 mM imidazole, washing with phosphate buffered saline (PBS), and eluting the protein with Laemmli sample buffer containing 10 mM EDTA.

The eluate was directly analysed by SDS-PAGE and the amount of D^b secreted was estimated from the intensity of the bands.

1.6.3.3. Bulk production of protein

For the production of large amounts of protein, secreting cells were grown in gassed roller bottles until stationary. The medium was then withdrawn, and sometimes the cells were re-fed with new medium for another week.

1.6.4. Reagents and media

GMEM-S (selective medium for CHO cells)

Glasgow's modified Eagle's medium, supplemented (from Advanced Protein Products) with 10% dialysed FCS and antibiotics, without glutamine.

serum-free DMEM

500 ml DMEM with L-glutamine (GIBCO 041-01965)

5 ml Nonessential amino acids 100x (GIBCO 043-01140)

5 ml Penicillin / streptomycin 100x

DMEM/Tris

20 ml serum-free DMEM

5 ml 250 mM Tris·Cl pH 7.5

DEAE-dextran solution is 1 mg/ml DEAE-dextran in TBS. Filter-sterilize. Store at 4 °C.

D10 is DMEM with 10% FCS, 2 mM glutamine, 100 IU/ml penicillin and 100 µg/ml streptomycin.

R10 is RPMI-1640 with 10% FCS, 2 mM glutamine, 100 IU/ml penicillin and 100 µg/ml streptomycin.

HBS ('transfection buffer")			**50 ml:**
200 ml:			
140 mM	NaCl	1.4 ml 5M	5.6 ml
5 mM	KCl	100 µl 2.5 M	400 µl
1 mM	Na_2HPO_4	100 µl 500 mM	400 µl
0.1%	glucose	250 µl 20% or 50 mg	200 mg
20 mM	HEPES (Na salt)	260.3 mg	1.040 g
	pH 7.05, filter-sterilize.		

The pH is critical and should be 7.00 - 7.10.

1.7. Proteins: analytical techniques

1.7.1. Bradford assay for protein concentration

This assay, based on the colour change of Coomassie Brilliant Blue G-250 upon binding to proteins, is rapid and simple. It is less sensitive towards detergent and Tris buffer than the Lowry assay. The protocol follows Dawson et al. (9].

1. To prepare the Bradford reagent, dissolve 100 mg Coomassie Brilliant Blue G-250 in 50 ml of 95% ethanol. Add 100 ml of 85% (w/v) phosphoric acid. Dilute to 1 l with water.
2. For measurements, use sample solutions of 10-100 µg/ml, and add a tenfold volume of dye reagent. Mix and read absorbance at 595 nm.

1.7.2. BCA assay for protein or peptide concentration

In this assay, cupric ion (Cu^{2+}) is reduced by the assayed protein to cuprous ion (Cu^{+}) by the biuret reaction. Bicinchoninic acid (BCA) forms a purple complex with Cu+ that absorbs strongly at 562 nm. This assay was mainly used for determining peptide concentrations. The BCA assay kit from Pierce (# 23320) was used, and the instructions of the manufacturer followed.

1.7.3. Determining protein concentration from the E_{280}

Tyrosine, tryptophan, and cysteine contribute to the absorption of a protein at 280 nm. The molar extinction coefficient of a protein can be calculated from its amino acid composition, following the method of Gill and von Hippel [10].

The formula used is

$$\varepsilon_{280,M} = 1280 \cdot n_{Tyr} + 5690 \cdot n_{Trp} + 120 \cdot n_{Cys},$$

where $\varepsilon_{280,M}$ is the molar extinction coefficient at 280 nm [$M^{-1}cm^{-1}$] and n_{Tyr}, n_{Trp}, and n_{Cys} the numbers of tyrosine, tryptophan, and cysteine residues in the protein, respectively. The extinction coefficients of the proteins were calculated with the GCG program 'peptidesort' [11] which uses this formula. It gives the extinction coefficient in the fully denatured state (6M guanidinium hydrochloride). A comparison showed that indeed the extinction coefficient in the folded state was three times higher (see results section).

1.7.4. Polyacrylamide gel electrophoresis of proteins

Hoefer Pharmacia equipment was used for all protein electrophoresis, either the SE 600 'full-size' or the SE 250 'mini' versions.

1.7.4.1. Denaturing SDS-PAGE

SDS-PAGE was carried out using the discontinuous buffer system of Laemmli [12], and

ready-made Protogel mixture (30% acrylamide, 0.12% N,N'-methylenebisacrylamide; National Diagnostics).

In general, acrylamide concentrations were 12% in the resolving gel, and 4% in the stacking gel.

Gel preparation

1. Assemble the gel plates and spacers according to the manufacturer's instructions.
2. Prepare resolving gel mixture. Add APS last. Pour resolving gel, leaving at least 2.5 x the length of the comb free space at the top for the stacking gel. Overlay with water or n-butanol and leave to set.
3. Carefully rinse top of resolving gel, and drain any remaining water. Prepare stacking gel mixture. Add APS last. Pour stacking gel. Insert the comb, being careful not to trap air bubbles. Leave to polymerise.
4. Pull the comb and assemble the gel running tank. Use LSB running buffer to rinse the sample wells.

Sample preparation

For samples in solutions that are weakly buffered, low in osmotic strength, and detergent-free, 3 x LSB sample buffer can be used. Otherwise, it is advisable to TCA-precipitate samples:

1. To the solution of sample protein, add the same volume of 30% (w/v) trichloroacetic acid (TCA). Leave to stand on ice for 30'.
2. Spin in eppendorf centrifuge for 20'. Very carefully withdraw supernatant with a drawn-out pasteur pipette.

   The pellet can be almost invisible, smeared over the tube wall, or non-adherent depending on the nature of the sample solution. Take extreme care not to lose it.
3. Wash at least three times with ice-cold acetone, spinning every time for 2'. Withdraw the last drop of liquid and leave to dry at RT for 2'.
4. Resuspend the pellet in LSB by pipetting. Heat to 100 °C for 3'. Spin down. The sample is ready for application.

TCA precipitation works with very small amounts of sample, down to the lower nanomolar range. I have not found it necessary to add carriers.

Occasionally the TCA is not fully removed by the acetone washes. If the color of the sample buffer changes to yellow when added to the pellet, add a few drops of 2M Tris base.

Protein A sepharose pellets from immunoprecipitations can be directly boiled with LSB. All samples were boiled at 100 °C for 3'.

Running the gel

1. Using a Hamilton syringe or drawn-out pipette tips, apply the samples to the gel.
2. Close the lid and apply voltage. Gels were usually run at constant current, with a starting current that gave 80-100 volts. The voltage increases during the run.
3. The run is finished when the bromophenol blue dye reaches the bottom of the gel. Take the gel sandwich apart and proceed to stain the gel.

Coomassie blue gel stain

All incubation times depend on the thickness of the gel. The times here are given for 1.5 mm gels. Volumes are given for 'full-size' gels and may be cut in half for 'mini' gels.

1. Incubate the gel in 500 ml acetic acid fixing solution for 30'.
2. Incubate the gel in 500 ml staining solution for 30'.
3. Rinse briefly in destaining solution a few times, then destain in 500 ml overnight.

Some mixed-be ion exchanger, or tissue, can be added to the solution to soak up the stain from the gel.

4. Store the gel in destaining solution.

silver stain

For occasional silver staining of gels, the silver staining kit from Bio-Rad was used, and the enclosed instructions followed. Prior to silver staining, the gels were Coomassie-

stained and destained thoroughly.

For all silver staining steps, only thoroughly washed glass vessels and water of the highest available purity were used.

reagents

12% resolving gel mix

final conc.		**(full-size)**	**(mini)**
0.4 x	Protogel mix	16 ml	4 ml
	water	13.4 ml	3.35 ml
0.375 M	Tris·Cl pH 8.8	10 ml 1.5 M	2.5 ml 1.5 M
0.1%	SDS	400 µl 10%	100 µl 10%
0.05%	APS (ammonium peroxodisulfate)	200 µl 10%	50 µl 10%
3.33 mM	TEMED (N,N,N',N'-tetramethylethylenediamine)	20 µl	5 µl

4% stacking gel mix

final conc.		**(full-size)**	**(mini)**
0.13 x	Protogel mix	1.3 ml	0.65 ml
125 mM	Tris·Cl pH 6.8	2.5 ml 0.5 M	1.25 ml 0.5 M
	water	6.1 ml	3.05 ml
0.1%	SDS	100 µl 10%	50 µl 10%
0.05%	APS	50 µl 10%	25 µl 10%
6.66 mM	TEMED	10 µl	5 µl

Laemmli sample buffer (LSB)

4%(w/v)	SDS
20%	glycerol

10%	β-mercaptoethanol
0.004%(w/v)	bromophenol blue
	in 0.125M Tris·Cl, pH 6.8

Laemmli running buffer (LRB) 4 l

25 mM	Tris base	12 g
188 mM	glycine	56.4 g
0.1%	SDS	4 g

acetic acid fixing / destaining solution

10%	acetic acid
20%	methanol

Coomassie staining solution (2 l)

2 g	Coomassie Brilliant Blue R-250
833 ml	methanol
333 ml	glacial acetic acid
833 ml	water
	stir overnight, and filter.

1.7.4.2. Native PAGE

For native discontinuous polyacrylamide gel electrophoresis, solutions and buffers identical to the SDS page system (above) were used, but SDS was omitted everywhere. Fixing and staining of the gels followed the same protocols as above.

1.7.5. Native isoelectric focusing (IEF) of proteins

For native IEF, the Resolve Systems Hemoglobin test kit (Isolab, Mechelen,

Netherlands) was used. The plastic-backed ultrathin gels supplied with the kit seem to resolve well in the range between 5.1 and 8 pH units. To run the gels, the instructions supplied with the kit were followed exactly. Sample resolution and visibility was best with between 1 and 20 µg material applied per lane. After electrophoresis, the gels were stained according to the following protocol:

1. Incubate the gel in 250 ml of fixing solution for 10'. Occasionally, swirl gently.

   Do not place the tray on a shaker as persistent shaking will detach the gel from its backing.

   After TCA fixation, protein bands can usually be seen as white precipitates.
2. Wash the gel in 500 ml distilled water for 10'. Repeat this process until all whitish ampholyte precipitates in the gel have disappeared.
3. Wash the gel twice in 200 ml ethanol.
4. Dry the gel in a stream of warm air.
5. Incubate the gel in staining solution for 20' or until the bands have the desired strength.
6. Destain, possibly with a change of destaining solution.

   If a dye precipitate appears on the surface of the gel, it can be - carefully - wiped of with a piece of paper towel.
7. Dry the gel in a stream of warm air, or standing upright on the bench.

TCA fixing solution

20%(w/v)	trichloroacetic acid
2%(w/v)	5-sulfosalicylic acid
	in aq.dest.

staining solution (can be reused)

5 g/l	Coomassie Brilliant Blue R-250
	stir for 1 hr; filter. Filter again if particles appear.

destaining solution

35% methanol

10% acetic acid

1.7.6. Immunoprecipitation from metabolically labelled cells

The cells should be in logarithmic growth phase.

If the cells are to be virus-infected before immunoprecipitation, follow steps a-d.

Otherwise begin with step 1.

a. Spin down the cells to be infected (5 x 10^6 - 2 x 10^7 cells per lane).

b. Add 2-10 pfu/cell of vaccinia virus in VDM.

c. Add R10 to a final cell density of 5 x 10^6 / ml. Leave for 90' to infect.

d. Spin down cells and resuspend in R10 at the same cell density. Leave at 37 °C for 1 h.

1. Spin down cells (and wash once in PBS).

Divide the cell lines into individual samples only after labelling (step 6).

2. Resuspend cells in methionine-free RPMI + 10% FCS at a density of 2 x 10^7 / ml.

3. Incubate for 1 hr at 37 °C.

4. Add 100 µCi [^{35}S]-Methionine (7 µl) per 10^7 cells. Shake gently.

5. Incubate for 2-3 hrs at 37 °C with occasional gentle shaking.

6. Spin down the cells. Resuspend in the same volume of PBS. Aliquot into Eppendorf tubes.

7. Spin the tubes for a short time in a microcentrifuge (5"-1'). Remove supernatant.

From now on, perform all operations in the cold room with ice-cold buffers.

8. Add 1 ml lysis buffer (containing protease inhibitors) per sample (1 ml per 2 x 10^7 cells). Resuspend gently.

9. Incubate on ice for 20'.

10. Spin in a microcentrifuge for 5' to pellet the nuclei. Transfer supernatant to a fresh tube.
11. To prepare the Staphylococcus A cells, spin down an aliquot and wash three times with lysis buffer. Resuspend in the same volume of lysis buffer.
12. To the supernatants from step 10, add 200 µl of Staphylococcus A suspension per 2 x 10^7 cells.
13. Rotate overnight at 4 °C to preclear.
14. The next day, spin the tubes to remove the bacteria and transfer the supernatant to a fresh tube.
15. Add antibody (10-15 µg/ml for purified monoclonals, or 1 x sample volume of 4-fold concentrated hybridoma s/n).
16. Rotate at 4 °C for 90'.
17. Add BSA to 1% (from 10% stock solution).
18. Check pH; adjust to 8.0 using Tris-base if necessary.
19. Add 100 µl Protein A - Sepharose (5% (w/v) suspension in lysis buffer) per sample.
20. Rotate for 45' at 4 °C.
21. Spin down the Sepharose beads and draw off the lysate.
22. Wash the beads four times with 1 ml wash buffer.

    After the washes, the beads can be stored frozen.

23. Add 30-50 µl Laemmli sample buffer. Boil for 5'. Run SDS-PAGel as usual.
24. Fix the gel and stain with Coomassie to check for the amount of antibody.
25. Soak the gel in Amplify for 30'. Dry the gel on filter paper and expose film.

Laemmli sample buffer, Coomassie stain see section on SDS-PAGE

Lysis buffer , wash buffer see Buffers and solutions used frequently

1.8. Proteins: preparative techniques

1.8.1. Chromatography equipment

All protein chromatography was performed using standard equipment: Gilson or ISCO peristaltic pumps, Pharmacia valves, Pharmacia column equipment, an ISCO UA-5 absorbance monitor, and Gilson or ISCO fraction collectors.

For the initial gel filtration experiments, a FPLC (Pharmacia) system (with 0.5 x 20 Sephacryl S-100 HR) and an HPLC gel filtration set-up (with a TosoHaas TSKgel G2000SWXL column) were also used.

Protein chromatography was initially performed at 4 °C, later at room temperature.

1.8.2. Isolation of Db·His from the cell culture supernatant using Nickel affinity chromatography

To isolate the recombinant protein from the CHO cell supernatant, batch and column procedures can be used. The protocol of a batch isolation follows.

1. Spin down the supernatant from the CHO cells (Beckman J-6B, 1000 ml containers, 3000 rpm, 30', 4 °C).
2. Carefully decant the supernatant and filter it through a Whatman GF/C filter to remove remaining cells.
3. Add 1/10 volume of 10x PBS; this will bring the pH to 7.0-7.4. Add sodium azide to 0.02%(w/v). Add imidazole to 5 mM. The supernatant can now be stored at 4 °C.
4. To the supernatant, add a 1:1 slurry of Nickel beads (Ni^{2+}-NTA agarose beads, Qiagen) washed in PBS. The amount of beads depends on the amount of protein present. From crude supernatant, 1 ml of packed beads binds 2-10 mg of protein.
5. Stir the bead suspension using an overhead stirrer, or a stirring bar 'jacketed' with rubber, overnight at 4 °C.
6. Filter the suspension under vacuum over a 5 µm cellulose acetate filter (Sartorius) on a sintered-glass disc filter holder. The beads are retained by the filter membrane.

7. Wash the beads on the filter with 200 ml PBS + 5 mM imidazole.
8. Resuspend the beads on the filter in PBS + 5 mM imidazole. Transfer the slurry into 50 ml centrifuge tubes. Repeat until all the beads have been transferred.
9. Spin down the beads (Sorvall RT6000B, 1500 rpm, 10', 4 °C). Wash three times with PBS + 5 mM imidazole. After the last wash, withdraw as much supernatant as possible.
10. To elute, resuspend the beads in PBS + 100 mM imidazole. Leave on ice for 20'. Spin and withdraw supernatant. Repeat and pool supernatants.
11. Check supernatants for protein by measuring OD_{280}. Proceed to purify by gel filtration.

1.8.3. Size exclusion chromatography (gel filtration)

For low pressure gel filtration, two columns were used: initially a 1.5 x 100 cm Sephadex S-200 HR column (flow rate 40 ml/hr, sample size 1.5 ml, maximum load 20 mg protein, fraction size 3-4 ml); later a 5 x 100 cm Sephadex S-300 HR column (flow rate 120-200 ml/hr, sample size 20 ml, maximum load 1 g protein, fraction size 50 ml). Gel filtration buffer was PBS + 0.02% sodium azide.

The column effluent was fractionated and the protein concentration determined by measuring OD_{280}. Peaks were pooled and either used for binding assays, or further purified by Nickel affinity chromatography, heat treatment, or preparative isoelectric focusing.

1.8.4. Preparative isoelectric focusing

For preparative IEF, a Rotofor machine (Bio-Rad) was used, and the manufacturer's instructions were followed with respect to set-up, assembly, buffers, running, and cleaning. The machine was connected to a cooling bath, and coolant was circulated through the central cooling finger at 2 °C.

Electrode buffers used were 0.1M orthophosphoric acid for the anode, and 0.1M sodium hydroxide for the cathode.

Samples were prepared by treatment with neuraminidase (Sigma N-2133, purified by affinity chromatography), 1 U / 40 mg protein, PBS, 37 °C, 2 hrs), and subsequent dialysis against 10 mM Tris·Cl, pH 7.5, overnight. They were then mixed with rotolytes (rotolyte mixture : sample solution, 1:1) and applied to the separation chamber.

For the separation of D^b·hβ_2m dimers, RotoLytes (Bio-Rad), pH range 6.0 - 7.2, were used in 1:1 proportion, giving a pH gradient from 6.4 to 7.0 according to the manufacturer's instructions. In practice it was found that the gradient was slightly wider, with the first and last two fractions reaching extreme pH values probably due to leakage of electrolyte through the ion exchange membranes.

Running conditions were 12 and 15 W constant for the small and large chamber, respectively. Running time was 6 hours, with a (water) prerun of 1 hr. After an initial lag, the voltage usually increased with 2-3 V/min, after 4-5 hours slowing down to about 0.5 V/min. In this late period the separation improved no further.

Under these conditions, only small amounts (-10 mg) of protein could be purified with high yields. Higher amounts of protein precipitated on the membranes that separate the fraction chambers. It remains to be shown whether this yield can be increased by the addition of glycerol or other agents.

Following the harvesting of the fractions, OD_{280} was measured to determine protein concentration, and the fractions were analysed by native isoelectric focusing and SDS-PAGE. Peaks were pooled and dialysed against PBS to be used in binding experiments, or for crystallisation.

1.8.5. Heat treatment of D^b·hβ_2m complexes

1. Equilibrate a PD-10 column (Pharmacia) with PBS + 0.02%(w/v) azide according to the manufacturer's instructions. Place into an hot air circulation oven set to 50 °C. Allow to warm up. Also prepare some PBS at 50 °C.

2. Concentrate 0.1-10 mg of protein to 2 ml in PBS. Place into 50 °C waterbath. Leave for 30'.
3. The following steps are carried out in the 50 °C oven: Apply the 2 ml of protein solution to the PD-10 column. Wash out the vial with 500 µl of PBS and also apply to column.
4. Elute with 3.5 ml 50 °C PBS. Collect eluate.
5. Analyse eluate by measuring OD_{280}, and by native isoelectric focusing.

1.9. Peptides

1.9.1. Peptide synthesis

Generally, peptides were obtained from SNPE Neosystems at immunograde (>80%) or higher purities. Peptides used in binding experiments were checked for purity on HPLC and HPLC-purified if necessary (see below).

1.9.2. Determining peptide concentration

As with proteins, the concentration of peptides that contain tyrosine residues can be determined very accurately by following the spectroscopic method of Edelhoch [13] or again Gill and von Hippel [10]. Determining the tyrosine absorption proved very useful as most peptides employed in this study contain tyrosines (originally for iodination). Edelhoch finds the $\varepsilon_{275.5,M}$ of the model substance Gly-L-Tyr-Gly to be 1280 $M^{-1}cm^{-1}$ in 6M guanidinium hydrochloride. I have found the following values with a defined solution of tyrosine:

solution	$\varepsilon_{275.5,M}$
6M GuaHCl	1475
0.1M HCl	1340
0.1M NaOH	2330
PBS	1335

As a result, peptide extinctions were usually measured in PBS and the concentrations calculated using a molar extinction coefficient of 1340 $M^{-1}cm^{-1}$.

For peptides containing no tyrosine residues, concentration was determined by comparing the HPLC peak area with a peptide of known concentration.

1.9.3. HPLC for peptide analysis and purification

Peptide analyses and purifications were on Rainin Dynamax C18 reverse phase HPLC analytical and semipreparative columns (Anachem) mounted on a Gilson modular HPLC system that was controlled by a Rainin-built Macintosh based HPLC controller with a Rainin interface. The supplier's instructions were followed with regards to flow rates, eluents, and cleaning procedures.

The solvent system was

buffer A: 0.1% trifluoroacetic acid (TFA) in HPLC water

buffer B: 0.1% TFA, 80% acetonitrile in HPLC water.

A typical gradient was 0 - 60% B in 30'.

If desired, the eluting material was collected as 1 ml fractions, lyophilised, dissolved in distilled water, sterile-filtered by spin filtration, and stored at -80 °C.

1.9.4. Radioactively labelled peptides

For the preparation and counting of radioactively labelled peptides, please see the corresponding sections under 'Class I - peptide binding assays'.

1.10. Class I - peptide binding assays

1.10.1. Iodination of peptides

All manipulations are done at room temperature. Radiation safety procedures must be followed.

1. Prepare two G10 spun columns (see below) per peptide to be iodinated.
2. Dissolve the peptide(s) at a concentration of 1 mM in PBS.
3. Wash iodobeads (Pierce; 2 beads / peptide) twice with 1 ml PBS.
4. Place each iodobead in one eppendorf tube. To each tube, add 40 µl PBS.
5. From a $Na^{125}I$ solution containing 100 mCi/ml (Amersham, # AMS 30), add 5 µl (500 µCi) to each tube. Mix and leave for 5'.
6. Add peptide solution according to ca. 50 µg of peptide (but not more than 50 µl). Leave for 5'.
7. Prespin the G10 spun columns 2' at 2000 rpm. Load the reaction mixture onto a G10 spun column. Centrifuge 2' at 2000 rpm.
8. Load the eluate onto another spun column. Centrifuge 2' at 2000 rpm.
9. Count 1 µl of the eluate in a gamma counter. Determine the exact peptide concentration of the starting solution (step 2) by the BCA method (Pierce). Assume a recovery of 80-90 %. Calculate the specific activity. Alternatively measure the concentration of iodinated peptide directly in the BCA assay.

   The specific activity is normally around 10^{15} cpm per mole of peptide. As the maximum specific activity for compounds containing one iodine atom is $4.86 \cdot 10^{18}$ dpm/mol, this gives a labelling efficiency of 0.01% at 50% counting efficiency.

10. Iodinated peptides were sometimes purified on HPLC to re-add a pure iodinated peak to unlabeled peptide.

Preparation of G-10 spun columns

1. Insert the body of a 1 ml syringe (without needle) downwards into a 15 ml centrifuge tube. Into the bottom, insert a small piece of siliconised glass wool (and stuff it slightly with the plunger), or a 2 mm siliconised glass bead (taking care that it sits in the center).
2. Fill the syringe with a slurry of Sepharose G-10 in water or PBS (+ 0.02% azide; the Sepharose needs to be autoclaved in the liquid). Spin at 1500 g for 1'. At this point, the gel settles and cracks become visible. Top up with more sepharose slurry and repeat centrifugation until the column volume is approx. 0.9 ml.
3. Wash the column twice by adding 100 µl of water or PBS (the peptide will end up in this buffer) and spinning at 1500g for 2'.
4. The column can be stored at 4 °C if capped tightly.

1.10.2. Iodine counting

All ^{125}I samples were counted in a Beckman gamma counter. Counting times were between 1 and 10 minutes, taking care that at least 1000 counts were registered from each sample to minimise the error. Counting results were expressed as counts per minute (cpm) without corrections.

1.10.3. Tritiated peptide, and tritium counting

Tritiated FAPGN-[3,5-^{3}H]Y-PAL peptide was a kind gift of Du Pont NEN (Boston, MA). Its specific activity was 46.5 Ci/mmol ($1.71 \cdot 10^{15}$ Bq/mol).

As the maximum specific activity for a compound containing one tritium is 28.7 Ci/mmol (half-life of tritium: 12.4 years = $3.91 \cdot 10^{8}$ seconds), this corresponds to 1.61 tritium atoms per peptide molecule, or 80% labelling efficiency.

Tritium-containing aqueous samples were diluted to 1 ml, and 10 ml of Ready-Safe scintillation cocktail (Beckman) was added in a standard scintillation vial. The samples

were mixed by shaking and left to stand for 1 hr before counting to let the chemiluminescence decay. Even so it was found that the counts were not constant over time, making it difficult to determine absolute numbers e.g. of binding sites.

It was also found that the Ready-Safe cocktail will not tolerate more than 50 mM EDTA in the initial sample, otherwise a white smear develops at the bottom of the vial.

Counting was done in a Beckman scintillation counter using a wide open counting window. Counting accuracy was set to 2%, making sure that no errors were introduced at this stage. This resulted in counting times of seconds up to 30 minutes per sample, depending on the activity present.

1.10.4. Binding assay with molecules from T2D^b cells

All binding experiments were done at 4 °C unless mentioned otherwise.

1.10.4.1. Equilibrium binding

The determination of binding constants for peptides and class I molecules using transfected T2 cells was introduced by Cerundolo and Townsend [14, 15].

1. Grow T2D^b cells to a density of $5 \cdot 10^5$ cells/ml.
2. Harvest aliquots of 10^7 cells by centrifugation, and wash once in PBS. Transfer the cells to an eppendorf tube.
3. To lyse the cells, add 500 µl of lysis buffer (see: buffers and solutions used frequently), and resuspend gently by pipetting. Leave on ice for 20'.
4. Spin out the nuclei in an eppendorf centrifuge for 5'. Transfer the supernatant to a fresh eppendorf tube.
5. Add radiolabeled peptide in a small volume.
6.. Add 100 µl of a 10% (w/v) suspension of washed Staphylococcus A bacteria and rotate overnight to preclear.
7. Spin out Staphylococcus bacteria and transfer the supernatant to a fresh tube.
8. Add B22.249 or 28.14.8S to 10-15 µg/ml. Rotate for 90'.

9. Check the pH of the solution by spotting on color indicator paper. If the pH is below 7 adjust it by dropwise adding 2M Tris base.
10. Add RIA grade BSA to 1%(w/v).
11. Add 150 µl of a 5%(w/v) suspension of washed protein A sepharose in wash buffer. Rotate for 45'.
12. Spin down the beads. Discard supernatant. Wash the beads four times with 1 ml wash buffer each. For the last wash, transfer the suspension to a new tube. After the last wash, carefully withdraw the last liquid with a drawn-out Pasteur pipette.

13a. For radioiodinated peptides, count the pellet directly in the gamma counter.

13b. For tritiated peptide, elute the protein from the beads by adding 100 µl of elution buffer and heating to 100 °C for 5'. Wash the beads with another 400 µl of elution buffer, and with 500 µl of water. Combine the supernatants in a scintillation vial. Add 10 ml scintillation liquid and count in scintillation counter.

1.10.4.2. Dissociation rate constant (off-rate) determination

Again, the protocol followed was essentially that of Cerundolo [15]. As in this paper, an initial rapid loss of a small proportion of binding sites was seen in some cases; in these cases, the value for t=0 was not included in the calculation.

1. Prepare cell lysate as in the equilibrium constant protocol above.
2. Add radiolabeled peptide (40-1000 µM) and leave to reach equilibrium overnight at 4 °C.
3. The next morning, perform immunoprecipitation as above. Time is counted from the initial wash of the bead pellet.
4. After washing the pellets (step 12 above), add 500 µl of lysis buffer containing 20 µM unlabeled peptide, and if desired additional $h\beta_2m$ at 1 µM.
5. At various times, spin down aliquots and wash four times. Change tubes for the last wash and withdraw supernatant liquid carefully.
6. Count in gamma counter or elute and count in scintillation counter as above.

1.10.4.3. Association rate constant (on-rate) determination

To determine on-rates, concentrations of peptides were used that gave approximately half-saturation in an accompanying binding assay.

1. Prepare a T2D^b cell lysate as in the equilibrium binding protocol, and imunoprecipitate the D^b molecules in a sufficient number of aliquots (usually ten for a single on-rate curve).
2. After the beads have been washed (step 12 above), resuspend them in 500 µl of lysis buffer.
3. Individually for each aliquot, add radiolabeled peptide in a small volume (t=0). Mix by inversion and place on a rotator.
4. At various times, spin out the beads in individual aliquots, and wash four times with wash buffer as above (step 12).
5. Count as above (steps 13a, 13b).

1.10.5. Binding assays with recombinant molecules

In general, binding experiments with recombinant molecules were performed in PBS without detergent or protease inhibitors. Binding experiments were done at 4 °C unless mentioned otherwise.

The following protocol was used to separate bound from free peptide:

1. Mount vacuum minicolumns (Promega, # A721C) on a vacuum manifold. Use 2 ml syringe bodies as funnels. Apply vacuum. Prewash the columns with 2 ml blocking buffer and 10 ml column wash buffer.

   This pretreatment is necessary as the batches of columns vary in their background binding of peptide.

2. Apply an aliquot of a binding assay, containing D^b molecules bound to Nickel beads, to a column. Wash with 5 ml column wash buffer.

For radioiodinated peptide, put columns directly into or onto scintillation vials, and count. For tritiated peptide, elute the protein as follows:

3. Detach the column from the vacuum manifold. Using a 1 ml syringe, draw in 500 µl of 50 mM EDTA in PBS through the column. This leads to the dissociation of the protein from the column. Leave at RT for 10'.
4. Expel the EDTA solution through the column into a scintillation vial. Repeat step 3. Add the second eluate to the first.
5. Add 10 ml of scintillation liquid, mix, and count.

Reagents

column blocking buffer

5%(w/v)	dried skimmed milk
0.5%	Tween 20
	in PBS

column wash buffer: 0.5% Tween 20 in PBS

1.10.5.1. Equilibrium binding constant

1. In 500 µl PBS, combine 1-5 µg of $D^b \cdot h\beta_2m$ complex, 40 µl of a 1:1 slurry of washed nickel beads, and radiolabeled peptide. Leave on a rotator to equilibrate overnight.
2. Separate bound from free as described above.

1.10.5.2. Dissociation rate constant

1. In a 15 ml centrifuge tube, combine per time point: 1-5 µg of $D^b \cdot h\beta_2m$ complex, 40 µl of a 1:1 slurry of washed nickel beads, and PBS to 500 µl. Add radiolabeled peptide to 1 µM and allow to equilibrate for at least two hours.
2. Spin down the nickel beads, discard the supernatant, and wash the beads four times with the maximum possible volume of PBS (t=0).

3. Resuspend the beads in PBS, containing unlabeled peptide to 20 µM, to a volume of (500 µl · number of points). Aliquot into eppendorf tubes, and place on rotator.
4. At appropriate times, take aliquots and separate bound from free as described above.

1.10.5.3. Association rate constant

1. In a 10 ml glass beaker, placed in a 4 °C waterbath to keep the temperature constant, combine per time point: 1-5 µg of D^b·hβ_2m complex, 40 µl of a 1:1 slurry of washed nickel beads, and PBS to 500 µl. Stir using a stirring bar.
2. At t=0, add radiolabeled peptide in a small volume. Help initial mixing by pipetting up and down.
3. At appropriate times, withdraw 500 µl aliquots and separate bound from free as described above.

1.11. Fluorescence spectroscopy

1.11.1. Steady-state fluorescence spectroscopy

Steady-state fluorescence spectroscopy was recorded using a Perkin-Elmer LS-50B fluorimeter with a pulsed light source.

Thermal control was with a programmable circulating water bath (Neslab RTE-111); the temperature readout from the fluorimeter was used for temperature standardisation. (An in-cuvette temperature sensor was used without much success.)

Samples were placed in a 1 ml quartz cuvette (Hellma) with a magnetic stirring bar, and stirred continuously during measurements.

Protein concentration was usually around 100 nM as determined by OD_{280}.

Usually, excitation and emission slit widths were adjusted so that the signal from the protein was approx. 5-700 fluorescence units before the addition of peptide.

For emission scans, background scans (buffer) were performed and subtracted from the data to eliminate the Raman peak.

The exact settings appear with the individual experiments.

For **emission scanning** experiments, excitation was at 295 or 300 nm (see individual experiments), and emission was scanned between 320 and 420 nm, with the emission peak around 340 nm.

For **time-drive** measurements, excitation was again at 295 or 300 nm, and emission was recorded at 350 nm.

1.11.2. Stopped-flow fluorescence spectroscopy

Stopped-flow fluorescence experiments were performed in an Applied Photophysics BioSequential DX-17MV sequential two-syringe stopped-flow fluorimeter equipped with SpectraKinetic 05-109 monochromators. Excitation wavelength was 300 nm; emission was measured above 320 nm with the built-in cutoff filter.

Thermal control was with a programmable circulating water bath (Neslab RTE-111); the temperature readout from the fluorimeter was used for temperature standardisation.

The large syringe (2.5 ml) usually contained 50 nM $D^b \cdot h\beta_2m$ complex (as measured by OD280) in PBS; the small syringe (250 µl) contained peptide at 10x the desired final concentration. One filling of both syringes was good for ten shots.

Two thousand data points were recorded in the duration of a single binding curve.

To evaluate the data, about ten to thirty shots for a given set of conditions were averaged using the built-in software. Curves of the following equation:

$$y = a + b \cdot t + c \cdot (1 - e^{-k \cdot t})$$

were then fitted to the data sets (see results).

1.11.3. Fluorescence steady-state anisotropy spectroscopy

was performed at the Max Planck Institute for Biology in Tübingen by Klaus Döring, in a Perkin-Elmer LS-50B spectrofluorimeter with polariser and analyser filter wheels.

Excitation and Emission wavelengths were as above. In the course of the experiment, the position of the filters was changed, and the initial data analysed, using the built-in software.

1.11.4. Fluorescence anisotropy decay (FAD) spectroscopy

FAD measurements, and data analysis, were performed by Klaus Döring in Tübingen with the set-up described previously [16, 17]. Tryptophan fluorescence was excited at 300 nm with polarised laser light pulsed to 4.1 MHz. Emitted light was detected at 350 nm. Data were corrected for background and the decay of total fluorescence intensity, and a multiexponential decay curve was fitted as described in the results section.

1.12. Circular dichroism measurements

CD spectra were recorded with a JASCO J-720 computer controlled CD/ORD spectrometer. Thermal control was with a programmable circulating water bath (Neslab RTE-111); a small thermocouple inserted into the cuvette was used for temperature standardisation. All measurements were performed with sample that was extensively dialysed against PBS. Contact with plastic was avoided to prevent contamination with UV-absorbing substances. The concentration of D^b protein was 1.9 µM; however, for the near UV measurements, a 10 mm cuvette, and for the far UV measurements, a 1 mm cuvette (Hellma, Germany) was used.

Data were analysed using the built-in software.

1.13. Molecular modelling

For the display of protein structures, the programs RasMol (Glaxo, Greenford, UK) and (for the surface model in figure 21) GRASP [18] were used. I would like to thank Mike Smith for help with the former, and Jörn Werner for help with the latter.

1.14. General data analysis

For the fitting of curves to data points, the Macintosh program pro Fit (Cherwell Scientific, Oxford) was used. It allows the user to formulate algorithms (expressed in the PASCAL programming language). Some of these algorithms are printed below. The program fits using a Levenberg-Marquardt routine [19] which needs reasonable starting parameters. It minimises the χ^2 value of the fit (the squares of the deviations of observed from expected, divided by the value of the expected, are added to give the χ^2), and gives standard deviations for the individual fitted parameters. Usually, different sets of starting parameters were fed into the program, and the results of the fits compared. If they were different (in about one in ten cases), a random variation of the parameters (Monte Carlo fit) over a wide range was carried out with typically 100,000 fits. The values originating from the Monte Carlo fit were then fed into the Levenberg-Marquardt algorithm. The χ^2 value of that fit was always equal to or smaller than the lowest of the values obtained before.

Standard errors of the mean (σ_{n-1}) were propagated in calculations, wherever possible, according to the law of error propagation [20]: for a function f ($x_1,\ldots,x_n$) of the measured values $x_1,\ldots,x_n$ with their associated standard errors $\Delta x_1,\ldots,\Delta x_n$, the standard error Δf is:

$$\Delta f(x_1,\ldots,x_n) = \left(\sum_{i=1}^{n} \left(\frac{\partial f}{\partial x_i} \Delta x_i \right)^2 \right)^{1/2}$$

This gives the following rules for the propagation of errors (strictly valid only if $\Delta x \ll x$):

error required	formula
$\Delta\,(x/y)$	$\sqrt{(\Delta x/y)^2 + (x\Delta y/y^2)^2}$
$\Delta\,(x \cdot y)$	$\sqrt{(y\Delta x)^2 + (x\Delta y)^2}$
$\Delta\,(1/x)$	$\Delta x/x^2$

For data derived from curve fits, the standard error from the fitting routine was used. Wherever it was impossible to obtain standard errors, errors were estimated realistically, usually as 5% of the data. The error bars in the figures have the width of the standard errors.

2. Introduction

2.1. Immunity

The immune system serves to protect vertebrates from microorganisms and parasites and may also play a role in eliminating malignantly transformed cells. Its key feature is the so-called complementarity - specific molecular recognition of foreign structures.

In nonspecific immunity complementarity exists in the polysaccharide binding sites of complement and lectins, and the receptors of phagocytes; but it has a fixed genetic encoding and does not undergo an evolution or improvement during the immune reaction.

Adaptive immunity has two major arms: the humoral response, where factors (antibodies) are secreted by activated B lymphocytes and bind to antigens located in the extracellular compartment; and the cellular response, the immune system's way of looking inside cells for parasites or viruses.

In adaptive immunity, the different alleles of major histocompatibility complex (MHC) class I and class II molecules, and the large repertoire of T cells provide a far greater variety and better fine-tuning of complementarity in the course of the response; once the challenge is over, a memory of it persists, accelerating the next response to the same antigen.

This introduction aims to review how viral antigens are presented through MHC class I molecules, with an emphasis on the molecular function of the class I molecules.
Several tutorial reviews on this topic have recently been published [25-31].

2.2. The presentation of viral antigens to the immune system

Virally infected cells can be recognised and lysed by cytotoxic T lymphocytes (CTL). This recognition depends on the infected cell and the CTL sharing at least one 'class I' locus of the major histocompatibility complex (MHC) region of the genome (MHC restriction of antigen presentation [32, 33]).

Viruses spend most part of their reproductive cycle inside cells; therefore a mechanism exists to display protein fragments from the interior of the cell on the surface, for CTL recognition. Work from Townsend and collaborators [34-36] showed that the main viral antigens derive from intracellular proteins, that the expression of whole proteins is not necessary but that fragments of influenza nucleoprotein are enough for its recognition [37], and that incubation of the cells in peptide is sufficient for T cell recognition [38-40]. It is now generally accepted that fragments from mainly cytosolic viral proteins are displayed or 'presented' to CTL bound to the gene products of the MHC class I locus (subsequently called class I molecules).

2.2.1. Generation of epitopes in the cytosol

Peptide epitopes can be generated from proteins that lack signal sequences for endoplasmic reticulum (ER) import [41, 42]. The peptides generated in the cytosol must therefore be transported to the cell surface to associate with class I molecules (see the section on peptide transport). RMA-S and T2 cells, which are deficient in this transport step, have very few peptides available to bind to class I molecules; this shows that the cytosol is the major source of antigenic peptides ([43, 44]). Even the presentation of most secretory proteins fails in these cells (reviewed in [45]), again indicating cytosolic degradation (of nascent proteins?) and transport into the ER of the resulting fragments. Accordingly, the inhibition of lysosomal proteolysis does not inhibit class I antigen presentation [46].

There are exceptions to this rule [47-50], and there is also evidence for a role for

degradation in the ER in some cases (see below, and [51, 52]).

2.2.1.1. *Cytosolic proteolysis: ubiquitin, the proteasome and others*

The major proteolytic system in the cytosol is the proteasome, a large structure of 26S [53] made up of a 20S (700 kDa) catalytic core [54] and many regulatory subunits. The evidence for its involvement in antigen presentation is reviewed in [30].

Peptide aldehydes which inhibit the proteasome in vitro can block the presentation of certain peptide epitopes from proteins without affecting presentation of the corresponding peptides directly expressed in the cytoplasm [55-57].

Two of the proteasome's catalytic subunits, LMP2 and LMP7, are encoded within the MHC [58-61]. Under the influence of interferon-γ (IFN-γ), they are expressed instead of their constitutive homologues [62-64]. They alter the cleavage specificity of the proteasome for artificial substrates *in vitro* [65, 66], but numerous experiments with LMP2/7-deficient cells and LMP2 or LMP7 knockout mice (reviewed in [30]) have shown an antigen presentation defect only in a few limited cases, and the question remains whether the *in vitro* experiments mirror the cellular conditions [67].

Many proteins in the cytosol undergo conjugation with the small protein ubiquitin on lysine ε-amino groups via isopeptide bonds prior to degradation, probably by the proteasome (review: [68]; a slightly different view: [69]). Accelerating the ubiquitin-dependent degradation of influenza nucleoprotein by addition of an N-terminal arginine [70] partially overcomes the block in the presentation of the influenza NP-366-374 epitope in vaccinia-infected target cells [71]. This implicates the ubiquitin system in the generation of epitopes, but without any certainty.

To current knowledge it seems that CTL epitopes are not evenly distributed in proteins (reviewed in [26]). The reasons for this, and its general significance, are unknown. Only in some cases there is experimental evidence that surrounding amino acid residues [72-75] or its position influence the generation of an epitope from a protein (evidence for:

Cerundolo et al., in preparation; [76]; evidence against: [77, 78]; reviewed in [26]).

2.2.2. Peptides cross the ER membrane

2.2.2.1. TAP transporters and their specificity

The mutagenised murine cell line RMA-S and the human cell lines LBL721.174 (.174)[79] and T2 (derived from .174) [80] were found to be defective in the surface expression of class I molecules and the presentation of cytosolic antigen [43, 44]. 721.174 was known to harbour a large deletion in the MHC class II region [81].

Other cell lines with this phenotype are LBL721.134 [79, 82] and BM36.1 [83] (reviewed in [84]).

Work with these cells has led to the identification of the *TAP1* and *TAP2* genes in the MHC class II region, members of the ABC transporter family (reviewed in [85]). RMA-S was later found to harbour a point mutation in the TAP2 gene that leads to a premature stop codon [86].

Transfection with the missing or mutated *TAP* genes restores antigen processing in these mutants. The gene products, TAP1 and TAP2 (transporter associated with antigen presentation), assemble as heterodimers in the ER and cis-Golgi membrane [87].

In lysates of RMA-S and T2 cells, class I molecules can be stabilised by adding specific peptide [43]. This and the observation that in these cells peptide antigen can be presented when introduced into the ER [51] is consistent with an essential role for the *TAP1/2* genes in peptide transport across the ER membrane.

Biochemical studies have shown that TAP 1/2 binds peptide independently of ATP [88, 89], and that peptide transport into microsomes [90, 91], microsomes of TAP-transfected insect cells [92], and the ER of permeabilised cells [93] is TAP- and ATP- dependent (although not that it is mediated by the TAP heterodimer). This peptide transport shows size limitations (7-12 residues, longer possible but with low efficiency [94]).

Preferences of the transport step for certain C-termini and, to a lesser degree, for residues within the peptide have been demonstrated [95-97], but it is unclear to which extent this influences the availability of epitopes in vivo; in the rat it has been shown that TAP2

alleles (*a* and *b*) control the HPLC profiles of peptides eluted from the class I molecule RT1.A^a [98].

2.2.2.2. *Retrograde transport of peptides*

Neefjes and collaborators [99] have observed the release of peptides from the ER where they had previously been transported by the TAP transporter, the degradation of the bulk of these peptides in the cytosol, and the re-entry of a small fraction into the ER. They suggest this as a mechanism by which peptides that fail to associate with class I molecules (because they are too long) may be recycled through the proteolytically active cytosol to get a 'second opportunity' to attain the right length. The efflux from the ER seems catalysed, is ATP-dependent, but not mediated by the TAP transporter. Its specificity is unknown.

Export of glycopeptides from the ER of cells has been shown in other systems [100]; a finding that is compatible with this idea, [101].

2.2.3. MHC class I molecules

MHC class I molecules as found on cell surfaces consist of the MHC-encoded heavy chain (HC), the noncovalently linked light chain called beta-2 microglobulin (β_2m), and a peptide molecule usually 8-11 amino acids long.

The amino acid sequences of class I heavy chain alleles were first determined in the early 1980s, either from proteins [102-104] or from cDNA [105-110]. The HC polypeptide consists of three extracellular domains termed α_1, α_2, and α_3, followed by a transmembrane segment and a cytoplasmic tail which varies in length between the alleles; the total molecular weight is 42-44 kDa. The five domains are encoded by separate exons. The first three domains have been classified as immunoglobulin domains based on homologies to antibody sequences which are not high (28-40%) but include matches in highly conserved and infrequent amino acids [104].

The α_1 and α_2 domains are polymorphic (about 30% variation between allelic

sequences), whereas the a3 domain is highly conserved within any one species.

All class I molecules characterised so far share a site for N-linked glycosylation at position 85 in the α_1 domain, and murine class I molecules have other potential N-linked glycosylation sites at positions 172 and 256 in the α_2 and α_3 domains. The α_2 and α_3 domains have one internal disulfide bridge each. Class I molecules have been reported to be phosphorylated at their cytosolic domain [111]; however, no functional connection exists yet [112]. Figure 1 shows the primary structure of a class I molecule, with disulfides and glycosylation sites.

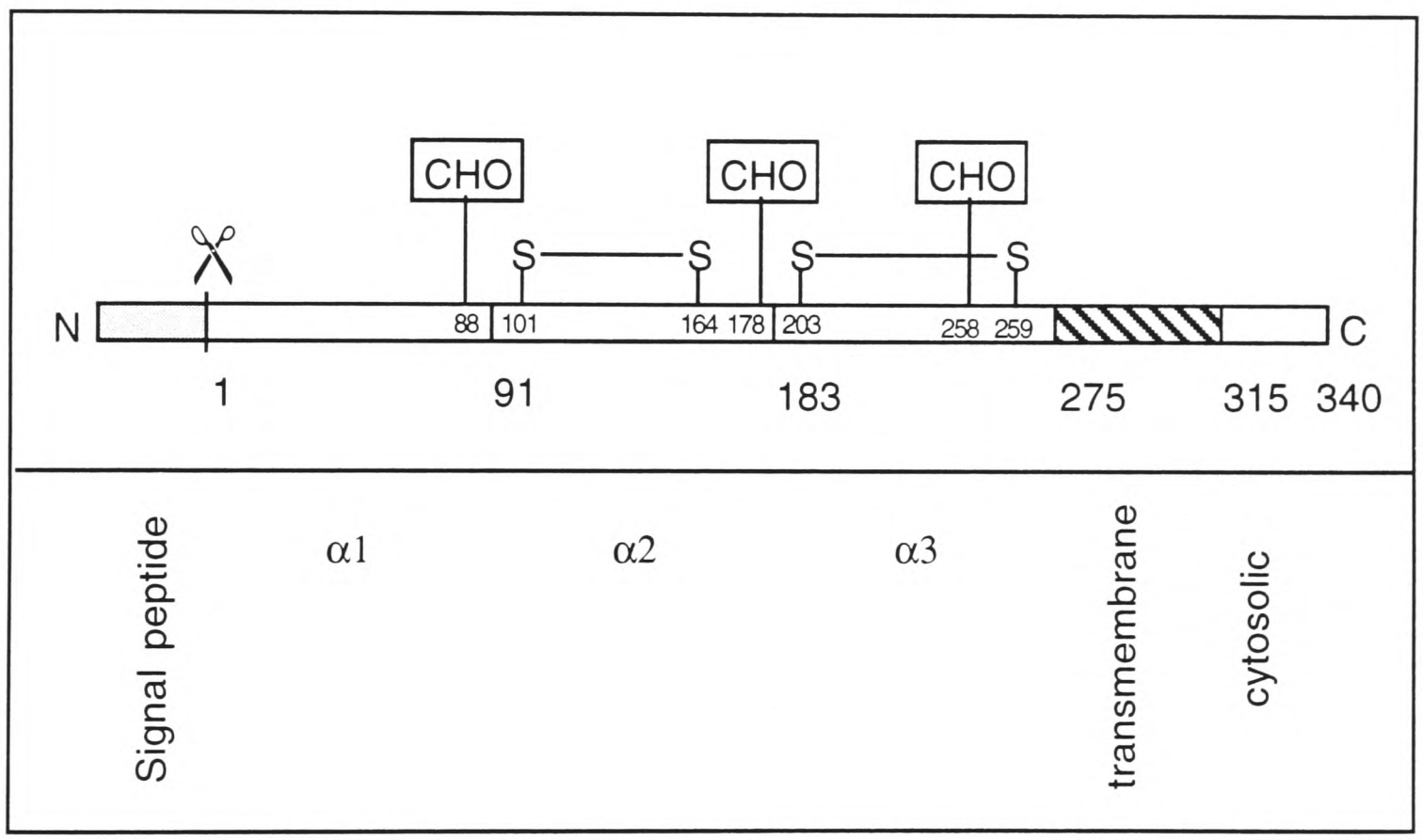

Figure 1: Top panel, primary structure of a murine class I molecule; with disulfide bonds (S–S) and glycosylation sites (CHO). Amino acid residues are counted from the start of the α_1 domain. Bottom panel, assignment of domains. In murine class I molecules, each domain is encoded by one exon (the cytosolic domain by several).

There are some 'special' or 'nonclassical' class I molecules that have very limited allelic variation and/or a different attachment to the plasma membrane, such as HLA-E [113,

114] or Qa [115]. These molecules have not been shown so far to participate in the antiviral immune response.

The light chain, β_2m, is not encoded in the MHC. It was first shown to associate with heavy chain in 1973 [116]. The first sequence reported was that of human β_2m [117]; the polypeptide is 99 residues long and has a molecular weight of 11,600 Da. β_2m from mice [118] is 69% identical; there is similar conservation between other species. β_2m is only slightly polymorphic: there is only one form in humans, and three allelic forms in the mouse varying by a single amino-acid substitution.
β_2m is not absolutely necessary for the surface expression of (low levels of) H-2D^b HC, as experiments in β_2m-negative cells (R1E, [5, 119]) have shown.

2.2.3.1. The structure

The determination of the crystal structure of HLA-A*0201 [120] and subsequently of other class I molecules (see table 1 in [121]) has elucidated the overall structure of the complex, and the way peptides are bound to it (figures 21 to 24; reviewed in [121-123]):
The membrane-proximal α_3 domain adopts the immunoglobulin fold and together with the symmetrically bound β_2m supports an eight-stranded antiparallel β-sheet that is formed by the α_1 and α_2 domains. On top of this sheet, away from the cell membrane, two long curved helices (one from the α_1 and one from the α_2 domain) delineate the sides of a groove that is 30 Å long, 11 Å deep, and 12 Å wide in the middle, the binding site for the ligand peptides [124].
The polymorphic residues in the α_1 and α_2 domains are found to point into the peptide binding groove and up from the helices. It is assumed that the T cell receptor binds from this side [125], so the polymorphisms would confer unique peptide- and TCR- binding properties on each MHC allele.
Figures 21 to 24 show several views of the complex of the murine class I molecule H-2D^b with the influenza nucleoprotein residues 366-374 peptide (NP_{68}-366-374; ASNENMDAM), solved by Nathenson and collaborators [126].

2.2.3.2. *Binding rules for peptides*

Biochemical evidence that peptides are natural ligands for class I molecules came from the laboratories of Nathenson [127] and Rammensee. Acid extracts from whole EL4 (H-2^b) or P815 (H-2^d) cells infected with influenza virus [128, 129] or from class I molecules isolated from these cells [130] were separated on HPLC, and distinct fractions were shown to be sensitise target cells for lysis by CTL. The population of peptides extractable from whole cells is governed by the MHC haplotype [129].

Pool sequencing of the peptide fractions [130] revealed the length requirements for peptide binding, and common amino acids at particular positions of all peptides present, termed anchor residues. There are at least two anchor residues for each class I allele (review: [131, 26]), one of which is always the C-terminal residue. The other anchor is usually at position 2, but can be at 3 or 5. For example, H-$2K^d$ binds nonameric peptides with tyrosine in position 2 (P_2) and a hydrophobic residue (leucine, isoleucine, valine) at the C-terminus (P_ω); H-$2D^b$ binds nonameric to undecameric peptides with asparagine at P_5 and hydrophobic residues at P_ω; and H-$2K^b$ binds octameric peptides with phenylalanine and tyrosine at $P_{\omega-3}$, and hydrophobic residues at P_ω. Besides the main anchor residues, there are also 'secondary anchors' that play a role in the stability of the peptide-class I complex (see below; reviewed in [121]).

The combination of peptide length and anchor residues bound by a given class I allele is termed the 'binding motif' for that allele. Binding motifs allow the prediction of CTL epitopes from protein sequences. They are, however, not motifs for the binding of peptide to class I molecules but rather presentation motifs that can also reflect the selectivity of earlier cellular steps in cellular epitope generation (see below; [131]). True binding motifs are now beginning to be established in several systems [132-134]; Matsumura and collaborators have incubated H-$2K^b$ molecules with a random mixture of peptides [132] and find no preference for hydrophobic amino acids at the last position of the K^b-binding peptide.

2.2.3.3. *Interactions between peptides and class I molecules*

The molecular interactions that lead to the tight binding of many different peptides to a given class I molecule are summarized in [123, 135, 136, 121].

In the bound state, the peptide is deeply embedded in the binding groove, with 72-84% of its surface buried [137]. The loss of 1400 $Å^2$ surface area on class I HC and peptide together, providing for ca. 100 van der Waals contacts [138], is enough in itself to overcome the loss of entropy upon binding and provide for a stable complex [139]. Hydrogen bonds (between 21 and 36 in the complexes crystallised so far [138]) and ionic interactions are more likely to play a role in the selectivity of the binding. The fact that there are always two anchor residues is interesting in terms of the binding entropy [132].

The peptide is held in the binding groove, in an extended conformation, through interaction with several subsites or 'pockets' (definition: Wiley and collaborators [140]) along its sequence, termed A to F. A and F pocket are preserved in their structure, while B to E pockets are polymorphic. Individual pockets have been shown by transplantation experiments to provide regional binding specificity [123].

There are many interactions between the class I molecule and the peptide backbone, but relatively few with individual peptide side chains (overview in [137]). The binding of charged and polar atoms of the peptide main chain is sequence-independent and provides a larger proportion of the overall binding affinity than the interactions involving the peptide side-chains.

Especially important is the tight binding of the amino (A pocket) and carboxyl (F pocket) termini of the peptide, where hydrogen bonds with highly conserved residues of the class I molecule are formed: three at the N-terminus, two at the C-terminus, one (by the penultimate peptide carbonyl group) with Trp-147 of the class I heavy chain.

These interactions are energetically more important than the anchor residues [141] (HLA-

A2) [142] (HLA-B27). Isosteric substitutions of one peptide terminus with methyl groups give lower-affinity complexes [141], while double substitutions abolish peptide binding.

The class I side chains that form these hydrogen bond networks with the peptide come from different subunits of the heavy chain:

N terminus	Tyr-159, Tyr-171	α_2 α-helix
	Tyr-7	β-sheet
	Tyr-59 (indirect)	α_1 α-helix
C terminus	Tyr-84	α_1 α-helix
	Thr-143, Lys-146	α_2 α-helix
	Tyr-123, Trp-133 (ind.)	β-sheet

The completion of these networks through the binding of peptide should play a role in stabilising the structure of the whole class I molecule; the very well-defined binding of the termini also ensures that all peptides are oriented in the same way.

Each class I molecule also forms hydrogen bonds with main-chain atoms of the peptide that are not universal. They provide additional sequence-independent binding energy.

The interactions of the heavy chain with peptide side-chains impose sequence specificity on the binding, mainly for sterical reasons: the peptide has to fit into the B to E pockets which vary greatly between alleles.

The most universal side chain pocket is the E pocket, for the peptide C-terminal side chain (P_ω).

The B pocket binds P_2 which for most alleles is an anchor residue. It comes in various sizes: deep and negatively charged in HLA-B27 (to bind arginine), smaller and without a negative charge in HLA-A2 (leucine), and even smaller in HLA-A68 (valine, threonine).

In some murine class I molecules, the anchors are more in the center of the peptide and bound by the C pocket, which is large and hydrophobic in H-2K^b (Phe, Tyr at $P_{\omega-3}$) and smaller and polar in H-2D^b (Asn at P_5 bound by three hydrogen bonds).

The structure of the pockets is known from the crystallisation studies, and they can be modelled for uncrystallized class I molecules; based on this, predictions for anchor residue preferences can be made [142].

The replacement of anchor residues with alanine or glycine severely compromises binding, showing that the binding energy contribution of the anchor residues is important [132, 143].

From crystal structures of different peptides bound to one class I allele [138, 144] it became evident that there are also pockets with a less stringent binding specificity for peptide side-chains: 'loose' or stereochemically flexible pockets that can accommodate different residues (for example the D pocket in HLA-B27 [145] and the D pocket in HLA-A2 [144]) or that repel only negatively charged residues (the B pocket in A2 [144, 146]), and 'part-time' pockets that only sometimes engage peptide side-chains depending on their conformation (the E pocket in HLA-A2 [144]). For both 'loose' and 'part-time' pockets, peptide side chains that bind productively will increase the stability of the complex; but those that do not interact will not necessarily inhibit complex formation. Another 'optional contribution' to the stability of the complex could come from peptide residues that do not bind to the class I molecule itself but make it easier for the peptide to pack in the groove, or from brigding water molecules that help to accommodate various residues (these occur mostly in the middle of the peptide).

These observations support the concept of 'secondary anchors' that can influence the binding affinity of peptides (see above; [146, 147]), and even allow to raise the accuracy of prediction of high-affinity binding peptides to 70% when taken into account.

The approach that some residues need to be avoided at secondary anchor positions [146] has been especially fruitful. Gairin and collaborators [134] showed that out of 45 peptides with a H-2D^b presentation motif (only taking the primary anchors into account), most did not bind due to dominant negative structural elements at some non-anchor residues (for example negative charge at P_2 or P_3), whereas other residues (P_6) were only minimally involved.

Deviating from the extended conformation, peptides can 'bulge out' from the groove or 'zig-zag' ([144, 148](HLA-A2.1), [149, 150] (HLA-A68) and Cerundolo and Collins, in preparation; review: [151]).

Other examples of non-canonical binding have been found in the alternative N-terminal binding for an HTLV-1 Tax octapeptide to A2 (the nonamer also binds [152]), and the extended C-terminus (by a single glycine) of a calreticulin decapeptide that leaves the groove at the C terminus [149].

It is unlikely, however, that a peptide truncated at the C terminus would bind class I, because P_ω is always an anchor residue.

Conformational differences in the class I heavy chain between complexes with different peptides have been reported (for HLA-A2 [144] and H-2K^b [138]) as slight changes in the N-terminal α_2 α-helix, including side chains that would be visible to the T cell receptor, with a potential influence on T cell recognition.

2.2.4. Class I synthesis and assembly

2.2.4.1. The assembly of the heavy chain-β_2m complex

Class I molecules are cotranslationally translocated into the lumen of the endoplasmic reticulum, where both β_2m and peptide are present. There are some indications as to the

way in which the trimeric complex forms (see for reviews [14, 153, 31]):

The binding of peptides to empty HC·β_2m complexes *in vitro* proceeds fast and stabilises the heavy chain into the native conformation recognised with MAb B22.249 (for murine class I) or W6/32 (for human class I). Both optimal-length and extended peptide function in this reaction [43, 15]. Only optimal-length peptides, however, can induce this conformational change in the absence of β_2m, and only at far higher concentrations [153].

Heavy chain and β_2m associate in the absence of peptide to a complex which is unstable in detergent and has the HC in the native conformation. If peptide is added to the lysate, the class I molecules are stabilised [43, 14].

The same HC instability occurs in cells that have no β_2m [154], or no peptide available in the ER; but addition of the missing partner in a lysate will stabilise the trimeric complex.

Investigations demonstrating HC association with TAP (see below), correct *in vivo* folding of H-2L^d heavy chain in the presence (against much less in the absence) of β_2m [155], and differential immunoprecipitation experiments [156] suggest that most newly synthesized class I molecules associate with β_2m first and bind peptide later. However, experiments carried out with β_2m-deficient mice [157] show that functional D^b HC can be detected at the surface of β_2m-negative cells [119]. These cells can be lysed by alloreactive and influenza nucleoprotein-specific [158] CTL.

2.2.4.2. *Interactions with calnexin, calreticulin, and TAPs*

It has been hypothesized that ER proteins assisting the folding process ('chaperones') could help assemble the heterotrimeric class I complex.

There is no absolute need for this, as complex formation has been demonstrated *in vitro* without additional proteins [159-161]; dependence on chaperones has not been demonstrated *in vivo* to this date.

Class I heavy chains associate with the 88 kDa protein calnexin early after synthesis

[162, 163] and remain bound in the absence of β_2m, as shown in β_2m-deficient human (Daudi, [164]) and murine (R1E, [165]) cells. In TAP-deficient murine RMA-S cells [165], class I HC·β_2m dimers remain bound to calnexin, suggesting that calnexin-bound HC associates with β_2m and then dissociates from calnexin, in a TAP-independent (in human cells, [167]) or TAP-dependent manner. In fact, it seems to be 'handed over' to TAP as HC/β_2m dimers have been shown to associate with the TAP dimer [168, 169] and dissociate under the influence of peptide.

A role of TAP and/or calnexin for the ER retention of peptide-free class I molecules has been supported by class I - calnexin cotransfection experiments into Drosophila cells [170]. However, in other experiments, neither retention of different class I alleles [171] nor antigen presentation [172] could be correlated with calnexin presence or binding.

In human cells, association of both BiP and calnexin with HC is seen [165]; however, here, the dissociation of calnexin from HC seems independent of the presence of TAP [167] but possibly triggered by β_2m binding instead. For the retention of empty human class I molecules in human cells, another retention mechanism must be postulated.

Murine class I molecules in TAP-deficient human cells (or more exactly, class I molecules having murine α_1 and α_2 domains [173]) are transported to the cell surface associated with hβ_2m [174], again suggesting species differences in the retention process.

2.2.4.3. Interaction of D^b with the human invariant chain

Human invariant chain has been coprecipitated with H-2D^b in detergent lysates of T2 cells by Cerundolo [175] .It dissociates from D^b upon peptide addition. This is unlikely to have functional significance but is consistent with a conformational change of the D^b heavy chain upon peptide binding.

2.2.5. The loading of peptide onto class I molecules

The human tumor rejection antigen gp96/grp94 has been shown to bind immunogenic peptides in the ER, and therefore implicated in the delivery of peptides to class I molecules [176, 320]; however, the evidence is still only circumstantial.

2.2.5.1. The timing

In normal cells, most heavy chains fold and associate into the trimeric complex within five minutes [156]. Detailed pulse-chase experiments have revealed differences between alleles in the rate of maturation [177, 321-323]; for review see [31]. During this time, the loading with peptide must take place.

2.2.5.2. The place

The adenovirus protein E3/19K stably associates with some class I molecules to retain them in a pre-Golgi compartment [178, 179] in a stable and β_2m-associated form. Class I heavy chains with a cytosolic domain from E3/19K are also retained, and loaded with intracellular peptide. This strongly implicates a pre-Golgi compartment in the peptide loading of class I.

Other experiments with transport-inhibiting agents (Brefeldin A: [180, 181, 182]; okadaic acid: [183]) have confirmed this conclusion.

2.2.5.3. ER trimming of peptides

The amount of additional proteolysis, or 'trimming', that peptides experience in the ER is under discussion (reviewed in [29]), although there is certainly proteolytic activity within the ER: the signal peptidase can generate peptides that bind to class I molecules (shown for HLA-A2 binding peptides by Engelhard and Cresswell and their respective collaborators, [184, 185]).

Snyder et al. [52] found that the C-terminal (but not the N-terminal) epitope could be

released and presented to CTL in TAP-negative cells infected with a vaccinia construct encoding two epitopes in tandem. Extending these results, Elliott et al. [51] found that the optimal NP-266-274 epitope was generated in the ER out of the 170 amino acid IMP fragment of influenza nucleoprotein (NP). The full-length NP, when introduced into the ER, gives rise to epitopes for HLA-B8, but not for H-2D^b and K^k, indicating a limitation of the ER's proteolytic capacity.

If peptides are imported into the ER as longer precursors and then trimmed, this could happen before or after initial binding to class I. It is remarkable in this context that the proteasome has a tendency in vitro to produce peptides with basic or hydrophobic C termini that match the specificity of class I molecules (see [29]). Rammensee has suggested a model by which longer peptides first bind with their C-terminus to a class I molecule which then acts as a template for N-terminal trimming [186]. However, peptides elongated at the N- terminus show a much reduced binding affinity to class I.

2.2.5.4. What happens afterwards?

Following the loading with peptide, class I molecules are transported to the cell surface, generally in a short time (see above). On the surface of cells, especially of those lacking peptide supply or β_2m, there are empty class I molecules [43, 187] and heavy chains [5], but they are unstable and rapidly lose their native conformation. Empty HC·β_2m dimers on the cell surface are stabilised at room temperature when the HC·β_2m interaction is stronger [187], or by the addition of antibodies conformationally specific to the HC·β_2m complex [188].

2.2.6. Epitope generation: general considerations

In summary, it seems that the generation of a peptide epitope from a protein can be governed at several levels: proteolysis (availability and copy number of the protein, position of the epitope in the protein, generation of the right precursors by the primary

protease (especially preventing the premature destruction of the epitope), binding and transport by chaperones and the TAP proteins, 'trimming' in the endoplasmic reticulum, and finally binding to the class I molecule.

Most important of all these is certainly the peptide's ability to assemble class I complexes. All natural epitope peptides have been found to do this *in vitro* [143]; but the reverse is not true. Therefore, additional restrictions must exist. Interesting in this context is the observation of Matsumura and collaborators [132] that the C-terminal residue in the 'binding motif' is not stringently required by the class I molecule HLA-A2 (see above); maybe the fact that certain C-terminal residues are observed points to the specificity of a different step in epitope generation.

Cerundolo et al. have pointed out [15] that complex assembly (also seen with many extended peptides) is not enough for antigen presentation: the resulting complex must also exhibit a slow off-rate to reach the cell surface and remain present there. (An epitope that has a fast off-rate and is still presented is the melanoma gp100 A2 epitope [189].)

2.3. The class I - peptide binding process under scrutiny

2.3.1. Previous studies

Since it has been clear that class I molecules bind peptides, the binding process has been under study to help understand which role it plays in the selection, and the display on the surface, of a peptide epitope. The methods used include:

· binding of iodinated peptides to immunoisolated class I molecules from transport-competent cells [190]

· binding of iodinated peptides to immunoisolated class I molecules from transport-incompetent cells [15, 161]

· binding of radiolabeled peptides to recombinant soluble class I molecules [191-193]

· stabilisation of class I molecules in lysates by peptide [194]

· binding of radiolabelled peptide in vitro to class I molecules on the cell surface [195,

196]

· cell surface stabilisation of class I molecules by peptide [187, 197];

· reconstitution of acid-denatured class I molecules by peptide on the cell surface [197]

· binding of purified class I molecules from assembly-competent cells to glutaraldehyde-immobilized peptide [198]

· competitive inhibition of T cell recognition [199, 200]

· surface plasmon resonance [201] with immobilised peptide and recombinant class I molecule

· fluorescence change in dansylated peptide binding to recombinant class I molecule [202]

What can be said from these studies about the specific affinities and the kinetic constants of peptides? The following summary cites only studies that aim to give numeric values for interaction constants. Table 1 gives an overview of some of the data. (Where units are not given, they are $M^{-1}s^{-1}$ for on-rates, M^{-1} for equilibrium constants, and s^{-1} for off-rates.)

Early studies by Frelinger [203], Bouillot and coworkers [198], and Parham [204, 205] failed to show high-affinity specific peptide binding, probably because the peptides used were too long, and their immobilisation was highly unspecific.

Barber and collaborators added iodinated D^b-binding peptides to EL4 cells and lysed them afterwards [195]. Bound and free ligand were separated with the B22 antibody. They find association constants of $1.18 \cdot 10^6$ M^{-1} (NP-Y365-380), $1.3 \cdot 10^8$ M^{-1} (NP-Y367-374), and $2.17 \cdot 10^9$ M^{-1} (NP-366-374, by competition); and for NP-Y356-380 at 37 °C, kon= 726 $M^{-1}s^{-1}$ and koff= $4.08 \cdot 10^{-4}$ s^{-1}; k_{on}/k_{off}= $1.78 \cdot 10^6$ M^{-1} is in rough agreement with the equilibrium constant.

They show in subsequent papers [161, 206] that the NP-Y367-374 peptide associates much faster with HC·β_2m binary complex than with heavy chain, and the complexes are more stable.

Townsend and collaborators introduced RMA-S or transfected T2 cells as a source of empty binary complexes. The so-called 'assembly assay' first devised by this group [14, 207, 194] allows one to estimate the contribution of different peptides to the formation of stable tertiary complexes. Upon the binding of peptide, HC·β_2m dimers acquire specific serological epitopes (see below, 'conformational change'). If fresh lysates from radiolabeled RMA-S or T2 cells expressing the class I molecule of interest are incubated with peptide overnight, immunoprecipitation with conformation-specific antibody reveals the degree of complex formation and hence gives a measure of the equilibrium affinity of the tested peptide. Thus, the affinity of the 14mer NP-50-63 for D^b was shown to be $>5 \cdot 10^5\ M^{-1}$ [14], and that of NP-366-374 $5 \cdot 10^7\ M^{-1}$ [194]; modifications of anchor residues and extension of the peptide decrease binding affinity. The affinities thus measured agree with directly determined affinity constants ([194, 15]).

In another series of experiments, Cerundolo *et al.* [15] use immunoprecipitation from $T2D^b$ and T2A68 cell lysates (with peptide added at the point of lysis) to determine the affinity constants of iodinated peptides, for example NP-Y365-379 ($3.8 \cdot 10^5\ M^{-1}$), NP-Y367-374(34) ($1.9 \cdot 10^7\ M^{-1}$), and NP-Y367-374 ($1.38 \cdot 10^7\ M^{-1}$). They measure the off-rates in the presence of a large excess of cold peptide and find them faster at elevated temperatures and with elongated peptides; especially, C-terminal elongations were more unstable than N-terminal.

Another paper [208] gives the association rate constants (on-rates, k_{on}) for two peptides: the k_{on} for NP-Y367-379, 572 $M^{-1}s^{-1}$, corresponds to the one predicted from a simple one-step binding model ($K_a = 5.46 \cdot 10^6\ M^{-1}$, $k_{off} = 7.59 \cdot 10^{-5}\ s^{-1}$; predicted $k_{on} = 414$). However, for the optimal-length NP-Y367-374 peptide, the measured on-rate, 5585 $M^{-1}s^{-1}$, is two orders of magnitude too high for the predicted ($K_a = 2.33 \cdot 10^7$, $k_{off} = 8.9 \cdot 10^{-7}\ s^{-1}$; predicted $k_{on} = 20.7\ M^{-1}s^{-1}$). The same phenomenon was seen with A68-binding peptides (Enzo Cerundolo, pers.comm.). The authors propose that a conformational change in the class I molecule causes the mismatch kinetics, and that only peptides of the optimum length, like NP-Y367-374, can bring it about, suggesting a

mechanism for peptide selection for class I molecules. This observation has been the starting point for my thesis work (see below).

Margulies and collaborators initially used L^d molecules secreted from transfected L cells and various methods of separating bound from free [191]; in these experiments, they always find two-slope Scatchard plots, with affinity constants approx. $3 \cdot 10^6$ and $3 \cdot 10^4$. They begin to use surface plasmon resonance (SPR), an evanescent wave detection method [201], to find biphasic dissociation rates of 10^{-4} and $5 \cdot 10^{-4}$ s^{-1}; they measure on-rates of 10^3 to 10^4 $M^{-1}s^{-1}$. In another paper [209], they test at which position the peptides binding soluble L^d, D^d, K^b, and A2 can best be immobilised onto the sensor through a cysteine thiol group. The use the technique to study differences between a dominant OVA-257-264 (SIINFEKL) and a subdominant OVA-55-62 (KVVRFDKL) peptide in binding to soluble K^b [210]. The dominant peptide has a 10-fold faster on-rate and two-fold slower off-rate. When affinity measurements by RMA-S surface stabilisation are performed, the K_a found is one order of magnitude too low for the ratio of on/off-rates (see table) - an observation similar to the one made by Cerundolo *et al.* [208]. They do not comment on this finding. The group then went on to compare off-rates between A2-, D^d-, and K^b- binding peptides immobilised at different residues [211] to find them in the $2\text{-}6 \cdot 10^{-6}$ s^{-1} range, and to show that tetrameric and pentameric peptides can bind to D^d and L^d [212]).

It is important to say that measurements of kinetic constants with surface plasmon resonance are often erroneous due to mass transport problems unless controlled extremely carefully [213]. The Margulies group has also never published affinity constants measured by SPR.

Kourilsky and collaborators have produced single-chain K^d molecules in COS-1 cells [214] and baculovirus [215], and demonstrated peptide binding to these constructs. The developed a novel assay for class I - peptide binding looking at the change of fluorescence upon binding of a dansyl group attached to the N terminus of the peptide

[202, 216, 217], and use this to demonstrate affinity constants of 0.5-1.6·10^6 M^{-1}, and off-rates of 10^{-3} s^{-1} (for iodinated, 6·10^{-5} s^{-1} in a control experiment). As the N-terminus is vital for the tight binding of peptide, it could be expected that this modification will only lead to weak complexes. Also, in their experiments the on-rates are independent of the peptide concentration [217] because the binding sites are already occupied with endogenous peptide. These two disadvantages of their system make the parameters obtained difficult to compare with any other data.

Neefjes and Ploegh and collaborators have demonstrated binding to empty class I molecules on the cell surface, cell surface stabilisation, and upregulation of class I molecules by peptide [196]. Adding peptide to cells and immunoprecipitating after lysis, they find that iodinated SV-324-332 (FAPGNYPAL) has the same association kinetics to K^b as the tritiated (chemically unchanged) version, but the dissociation of the iodinated peptide is much accelerated [218]. They conclude that iodinated anchor residues impede optimal binding.

Buus and collaborators have isolated K^k, D^k, D^b, and K^b molecules from B cell lines by immunoaffinity chromatography [190]. Only 2% of their material binds peptide. They conduct binding assays with iodinated peptides and separate bound from free ligand by gel filtration. A C-terminally extended 18mer binding to K^k (Ha-255-271Y) has an extremely slow on-rate ($t_{1/2}$= 20 hours (k_{obs}= 1.4·10^{-5} $M^{-1}s^{-1}$) at 4 °C), a K_a of 3.3·10^6 M^{-1} , and a slow off-rate (10^{-6} s^{-1} at 4°C). As with all material isolated from transport-competent cells, there is the danger that those class I molecules that have no peptide loaded onto them might be preferentially those that are partially denatured or otherwise incompetent to bind peptide; the extremely slow on-rate here could be due to such a preparation artefact.

Bjorkman and collaborators have produced peptide-free, well-characterised soluble K^d·hβ_2m complexes in CHO cells that are immunopurified, denatured in 6M guanidinium

hydrochloride, and subsequently renatured [219]. In a very careful series of equilibrium dialysis experiments with tritiated NP-147-155 and cold competitors [193], they measure binding constants for many different peptides. For optimal peptides, affinities lie between $4 \cdot 10^6$ and $3 \cdot 10^7$ M^{-1}; N-and C-terminal extensions and deletions, amino acid exchanges, and iodination of the anchor tyrosine all have detrimental effects. Unfortunately, these data are not accompanied by kinetic measurements.

Peterson and collaborators [220] have performed assembly assays with Drosophila cells expressing K^b, D^b, L^d, A2.2, A2.1, and B27 with β_2m from their respective species. They investigate the temperature destabilisation of different peptide complexes in comparison. In another paper [192], after showing by native isoelectric focusing that their K^b class I molecules are empty, they determine the following parameters for iodinated VSV-8 peptide (titrating the $K^b \cdot \beta_2$m complex onto a fixed concentration of HPLC-pure ligand!, and separating bound from free by gel filtration): Ka= $3.03 \cdot 10^7$ M^{-1}; k_{on} (23°C) = $5.9 \cdot 10^4$ $M^{-1}s^{-1}$; k_{off} (37 °C) = $3.2 \cdot 10^{-4}$ s^{-1}. They do not comment on the three-fold discrepancy between k_{on}/k_{off} and K_a, but find (by competition) that the unlabeled peptide binds with $K_a = 2.7 \cdot 10^8$ M^{-1}. N-terminally elongated peptides bind not as well, but C-terminally elongated bind with the same affinity.

In a subsequent paper [132], they perform complete alanine scans of VSV-8 and OVA-8 peptides (by competition binding with iodinated VSV-8) which establish that a hydrophobic residue at P_8 is not needed for tight binding. The peptide $Ser_8$3Y5Y (SSYSYSSS) binds with $K_a = 5 \cdot 10^7$, identical to OVA-8. After incubating K^b in a mixture of random peptides, washing, and heating to 47 ° for one hour in detergent, acid elution shows that tyrosine and phenylalanine are dominant at positions 3 and 5, constituting a real class I binding motif (and not a 'presentation motif', see above).

Gairin and collaborators have looked at peptide selection by D^b molecules in a cell surface stabilisation assay, or by competition for cell surface binding against an iodinated standard peptide. They determine optimal lengths for peptides and find that the binding

affinity is decreased by one order of magnitude with an extension of one amino acid [221]. They also compared 45 optimal-length peptides with the Db binding motif [134] and found $K_{a,i}$= 1-3·10^8 M^{-1} for the best binders. Most of these peptides did not bind at all, and the authors identify dominant negative structural elements at non-anchor residues, for example negative charges at P_2 or P_3. Another paper [133] tests many variations of one peptide in the same assay, including an alanine scan. For the binding onto cells, k_{obs}= 5.6·10^{-4} s^{-1} at [peptide]= 5·10^{-10} M, giving an on-rate off 1.12·10^6 $M^{-1}s^{-1}$ at 37 °C!

Study	class I allele	peptide	temp. °C	k_{on} ($M^{-1}s^{-1}$)	k_{off} (s^{-1})	k_{on}/k_{off} (M^{-1})	K_a (M^{-1})
a: IP	H-2D^b	NP-Y365-380	37	726	4.08·10^{-4}	1.77·10^6	1.18·10^6
		NP-Y367-374	37				1.3·10^8
b: IP	H-2D^b	NP-Y367-374	4		1.2·10^{-6}		1.37·10^7
c: IP	H-2D^b	NP-Y367-379	4	572	7.6·10^{-5}	7.5·10^6	5.46·10^6
		NP-Y367-374	4	5585	8.9·10^{-7}	**6.3·10^9**	2.33·10^7
d: ‡	H-2K^b	OVA-55-62C6	25	650	1.6·10^{-5}	**4.1·10^7**	1.0·10^6
		OVA-257-264C6	25	5900	9.1·10^{-6}	**6.5·10^8**	4.0·10^7
e: ED	H-2K^b	NP-147-155	25				1.45·10^7
f: IP	H-2K^b	VSV-8	23*	59000	3.2·10^{-4}	**1.8·10^8**	3.03·10^7

Table 1: rate and equilibrium constants from the literature. Studies: a, [195]; b, [15]; c, [208]; d, [210]; e, [193]; f, [192]. Techniques: IP, immunoprecipitation; SPR, surface plasmon resonance; ED, equilibrium dialysis; ‡, kinetic constants by SPR, equilibrium constant by RMA-S stabilisation; *, off-rate measured at 37 °C.

Looking at the table, it is remarkable that the affinity constants for optimal-length peptides seem in general agreement between 10^7 and 10^8 M^{-1}, changing little with temperature.

Also, once the complexes have formed, they appear stable with half-times of many hours. The on-rates in the table lie between $5 \cdot 10^2$ and $6 \cdot 10^4$ $M^{-1}s^{-1}$, but they differ more widely in the experiments discounted here. Non-matching kinetics (discrepancies between the k_{on}/k_{off} ratio and the K_a constant) have been found in three independent studies, the clearest being [208].

2.3.2. The idea of 'conformational change' and its history

Can the idea of a conformational change of class I molecules upon peptide binding be substantiated from the literature? So far, three observations have been made that relate to conformational alterations (see review: [27]): conformational changes of the HC·β_2m complex upon peptide binding as recognised by antibodies, conformational changes in free HC upon peptide or β_2m binding, and conformational differences between complexes of a class I molecule with different peptides or buried mutations in the binding site.

2.3.2.1. Acquisition of conformational epitopes upon peptide or β_2m binding

Serological changes in the α_1 and α_2 domains of class I molecules upon assembly with β_2m have been known for a while [5, 222, 223]. In RMA-S detergent lysates the majority of class I HC·β_2m complexes are unstable, rapidly dissociating and losing their 'conformational epitopes'. Townsend *et al.* have demonstrated that this can be prevented by the addition of specific peptide [14]. This relates to the following class I molecules and antibodies:

· the conformation of HLA-A2 recognised by MA2.1 (α_1 domain)

· the conformation of D^b recognised by B22.249 (α_1); the MAb 28.14.8S (anti-α_3) is nonsensitive

· the conformation of K^b recognised by Y3 ($\alpha_1+\alpha_2$); nonsensitive: 76:3.

Similarly, empty dimers can be stabilised with conformation-specific antibody on cell

surfaces [188]. These conformational epitopes in the α_1 and α_2 domains of class I molecules are not peptide-dependent in the strong sense as they can also be induced by the binding of β_2m.

2.3.2.2. *Conformational change of heavy chain only*

Elliott *et al.* have shown that these epitopes can also be acquired by free D^b [153] and K^b [143] heavy chain, in the absence of β_2m, upon the binding of peptide. It does not need the α_3 domain of the class I molecule [143]. The requirements of the peptide are the same than for the binding to HC·β_2m complexes. The underlying phenomenon is, of course, synergistic binding of peptide and β_2m to the heavy chain.

2.3.2.3. *Structural differences between complexes*

When structures of the same class I molecules with different peptides were compared, it became evident that small conformational differences in the protein exist between the ternary complexes (for K^b: [138]; for A2: [144]). They are small changes, mainly in the side chains, but also at the N-terminal end of the α_2 helix, and they could be visible to antibodies or the T cell receptor.

Attempting to extend these observations, several groups have found 'peptide-induced structural microheterogeneities' in class I molecules, none of which is very substantial. Rohren *et al.* [224] studied the binding of conformation-dependent MAbs to 19 K^b·peptide complexes on cells using flow cytometry; they show that it is dependent on residue 2 of the peptide, and conclude that the buried P_2 has induced a change in conformation! However, the authors do not show that in all of the complexes P_2 is indeed buried; instead, it could be a 'part-time' anchor that could point up in some complexes, disrupting antibody recognition. There is a number of similar studies with the same *caveat* (see [225-229]).

In a variation [230], mutations at the bottom of the binding groove were shown to lead to a strong allogeneic response to the mutant, even when the same peptide was bound. This was interpreted as a change in class I structure but could also reflect a different way in which the mutated molecule accommodated peptide.

Finally, Ojcius *et al.* [231] report a break in the Arrhenius plot (see below) of the dissociation kinetics of endogenous low-affinity and of dansylated peptides from K^d and invoke a conformational change upon peptide dissociation.

2.3.2.4. L^dalt - conformational change dependent on peptide binding?

The group of Hansen and collaborators have described a conformation of the H-2L^d molecule detected by the specific antibody 64-3-7 which they call L^dalt (for alternative) [324-326]. It is not associated with peptide, and only a subpopulation has β_2m bound to it. In pulse-chase experiments in L·L^d cells, it is detectable immediately after synthesis, and it disappears from cell lysates when peptide is added; but it is also present at the cell surface and can be increased there by the dissociation of bound peptide. L^dalt molecules lack other conformational epitopes around the peptide binding site. It seems that the epitope recognised by 64-3-7 is truly peptide (absence)-dependent and β_2m-independent, making this the only system in which a conformational change of the heavy chain upon peptide binding can be clearly implied.

None of the other 'conformational changes' can be accounted with security for the irregularities in the kinetics and equilibrium data. The conformational antibody epitopes of B22.249 and similar exist without peptide in empty HC·β_2m complexes, and the conformational differences in the crystal structures do not necessarily mean a conformational change upon binding - the peptides could bind to one of many conformational substates of the free heavy chain. The case for a conformational change will be discussed further in the section about kinetic modelling.

2.4. Comparison with MHC class II molecules

MHC class II molecules, present on 'professional antigen presenting cells', present peptides mainly from glycoproteins or secreted proteins (with a few exceptions)[232, 27, 28]. Their overall structure is very similar to class I molecules, but the open-ended groove enables them to bind longer peptides than class I molecules can [233]. In binding studies with purified HLA-DR molecules, Sadegh-Nasseri and McConnell [234] demonstrated two association rates: a fast ($t_{1/2}$= 2 minutes) and a slow on-reaction. The fast complexes thus formed could later be distinguished on SDS-PAGE as 'floppy' (slow-migrating) dimers from the slowly formed 'compact' complexes [235, 236]; subsequent pulse-chase studies have not unequivocally confirmed that these two complexes lie on one reaction pathway [237, 238], but they seem to reside in distinct subcellular compartments [239].

For class II molecules, a conformational change upon peptide binding has therefore been suggested. The change to an acidic pH on transition into the class II loading compartment could induce the protein to undergo conformational changes; in contrast, class I molecules have to operate in an environment of constant pH.

2.5. The aim of this thesis

The mismatch kinetics observed by Cerundolo *et al.* [208] point towards a more complex mechanism than a simple on-step association. However, they were performed in detergent lysate, in the presence of cellular proteins and other solutes, and with iodinated peptide.

The first objective of this work was therefore to create a system in which class I - peptide interaction could be studied in a pure, detergent-free state; this would enable me to extend these observations to full sets of measurements under controlled conditions. These data would then be extended into a mathematical analysis of the binding process. Another line of investigation was to look directly for changes in the class I molecule associated with peptide binding that could provide evidence for conformational steps.

2.5.1. The H-2D^b molecule

For this work, H-2D^b was chosen as a model class I molecule for several reasons. Firstly, its cell biology is well described; secondly, its structure [126] and many of its natural epitopes [131] are known; thirdly, it is a stable and fast-maturing class I molecule that forms a very tight complex with human β_2m without altering its binding specificity [240]; fourthly, the mismatch effect was observed there first; and fifthly, a large amount of binding data with many different peptides, in detergent, was already available.

3. Functional expression of soluble D^b-His_6 in CHO cells

3.1. Planning and initial cloning steps

The first objective of this work was to generate peptide-free, soluble H-$2D^b$ molecules for a study of peptide binding in a defined *in vitro* system. For the initial construction, four considerations were therefore important: firstly, truncation of the gene at the right point so that the transmembrane domain would be abolished but the function of the protein retained; secondly, the addition of a tag or 'handle' that would aid in the purification of the protein in large amounts; thirdly, generation of a 5' environment of the gene that would allow for its efficient expression; and fourthly, the introduction of additional restriction sites before and after the coding sequence to ensure compatibility with different expression systems.

Many studies have shown that class I molecules bind peptide independently of their transmembrane and cytoplasmic domains [191, 192, 215, 219, 220, 241, 242]. However, there were reports that the abolition of residues 271 to 276 by proteolysis led to non-crystallisation of HLA-B27; these residues form part of the seventh β strand of the α_3 domain [142]. I chose a truncation for the H-$2D^b$ gene that corresponds to the one used by Bjorkman and collaborators [219]. It terminates the soluble protein just before the first amino acid of the transmembrane region, Val-285, retaining as much of the α_3 domain as possible. For the HLA-A*6801 gene, truncation before an earlier residue, Ile-282, was chosen as the α_3 domain is shorter in this molecule. The figure 20 (below) gives the full sequences of the resulting proteins.

To help the purification of the recombinant protein from cell lysates or supernatants, a sequence encoding six consecutive histidines was appended to the 3' end of both heavy chain genes, immediately following the truncation. 'Hexahistidine tails' have a high

complexing affinity for a resin containing nickel^{2+} chelated by nitrilotriacetic acid (NTA agarose or, in the following, Nickel beads) [243, 244]. Elution from the resin can take place with high or low pH, or, more physiologically, with increasing concentrations of imidazole that competitively displaces hexahistidine tails from the nickel (see below, and Materials and Methods section). However, binding is compromised by EDTA and β-mercaptoethanol, so that these reagents cannot be used in buffers.

The hβ_2m gene was not engineered with a histidine tail so that free β_2m would be unable to bind to the Nickel beads, and purified away from the complexes.

The efficient expression of homologous and heterologous constructs in eukaryotic systems has been shown to depend on the 5' surroundings of the gene. Of all the factors, presence of the so-called 'Kozak sequence' CCACCATG (with ATG being the start codon of the gene) was most important for an efficient translation of the mRNA [245]. I therefore decided to include this sequence in the construct.

The gene encoding H-2Db was amplified from a plasmid kindly provided by Dan Denney (pSSD14) by the polymerase chain reaction (PCR), using the primers in figure 2 to introduce a hexahistidine tail after amino acid 284 (instead of the transmembrane and cytoplasmic domains), and to add convenient restriction sites.

cDNA encoding A*6801 was produced from T2 cells transfected with A*6801, a kind gift from Peter Cresswell. The A*6801 gene was amplified as above but truncated after amino acid 281.

The cDNA encoding human β_2m (hβ_2m) was amplified from a plasmid kindly provided by Ken Parker by PCR using the primers in figure 2. Slight alteration of coding sequence was necessary to accommodate the NcoI site, changing the DNA sequence at the start of the coding region from ATGTCTCGC to ATGGCCCGC and therefore the second amino acid in the signal sequence from serine to alanine (note that amino acid 2 in D^b is also an alanine).

Of both class I heavy chains, full-length constructs without a histidine tail were also made for reasons of comparison.

```
Db 5'     CC'GAATTC'AAGCTT'CCACCATGGGGGCGATGGCTCCGCG
             Eco    Hind   Kozak+NcoI
                                MetGlyAlaMetAlaPro...

Db 3'     CC'GGATCC'TATCAGTGGTGATGATGGTGGTGCATGTAAGAGTCAGTGGACGGAG
             Bam
                   Amb OpaHisHisHisHisHisHisMetTyrSerAspThrSerPro...
          (reverse primer)

A*6801  5'
          CG'GAATTC'AAGCTT'CCACCATGGCCGTCATGGCGCCCC
             Eco    Hind   Kozak+NcoI
                                MetAlaValMetAlaPro..

A*6801  3'
          CC'GGATCC'TATCAGTGGTGATGATGGTGGTGGGTGGGCTGGGAAGACGGCTC
             Bam
                   Amb OpaHisHisHisHisHisHisThrProGlnSerSerProGlu
          (reverse primer)

β2m 5'    CC'AAGCTT'CCACCATGGCCCGCTCCGTGGCCTTAGCTGTG
             Hind   Kozak+NcoI
                          MetAlaArgSerValAlaLeuAlaVal

β2m 3'    CC'GGATCC'TTACATGTCTCGATCCCACTTAACTA
             Bam
                      OcrMetAspArgAspTrpLysVal...
          (reverse primer)
```

Figure 2: PCR primers used in cloning D^b, A*6801, and $h\beta_2m$. First line: primer sequence, second line (italics): restriction sites and Kozak sequence, third line: translation (retrotranslation for reverse primers).
(all sequences shown 5' to 3'; Ocr, Amb, Opa = stop codons)

The PCR products were initially cloned into M13, and 3 clones of each gene were fully sequenced. The sequences were found to coincide with the published sequences (Genbank accession numbers: D^b M18523, $h\beta_2m$ M17987; for A*6801, [246]). Clones were then transferred to pUC19 as EcoRI/BamHI fragments (pUC18 as BamHI/HindIII fragments for $h\beta_2m$).

3.2. Expression in CHO cells

3.2.1. Description of the system

The glutamine synthetase expression system, originally developed for the high-yield recombinant expression of antibodies, is described in [247] and [248]. The expression plasmid pEE14, with the gene or genes of interest inserted behind the strong human cytomegalovirus promoter/enhancer, integrates into a chromosomal location when transfected into chinese hamster ovary (CHO) cells. Selection for pEE14 is provided by the enzyme glutamate synthetase (GS; also encoded by the plasmid under the control of the weaker SV40 late promoter); this is essential for the cell in the expression medium GMEM-S which contains no glutamine but an elevated level of glutamate from which GS can produce this key metabolite.

The plasmid will replicate to a high copy number in COS cells and can therefore be used in a transient expression experiment to assess expression from a construct.

Especially high levels of expression can be selected for by using increasing concentrations the glutamine analogue and competitive glutamine synthetase inhibitor L-methionine sulfoximine (MSX); if this is used, only variant clones with large amounts of GS can survive, most commonly by amplification of a chromosome region which contains the plasmid. This system, used by Bjorkman and colleagues [219], has yielded up to 100 µg/ml of H-2K^{d}·hβ_2m soluble protein from cell supernatants in hollow-fibre fermenters.

3.2.2. Cloning procedure

The gene for D^{b}-His$_6$ was cut with HindIII and BamHI and cloned into the vector pEE6hCMV-B (containing the hCMV promoter), to give pEE6-D^{b}-His$_6$.

The gene for hβ_2m was cut with HindIII and BamHI and cloned into pEE14 to give

pEE14-β_2m. (For a map of these plasmids and their multiple cloning sites, see figure 3). The MluI/BamHI fragment of pEE6-D^b-His_6, containing the hCMV promoter and the D^b-His_6 gene, was then isolated and cloned blunt-ended into the BamHI site of pEE14-β_2m giving pEE14-D^b-His_6/β_2m (figure 4), a plasmid that contains in tandem (in the same orientation) the cDNAs for human β_2m (upstream) and H-$2D^b$, each under the control of a separate copy of the human cytomegalovirus promoter-enhancer, and the glutamine synthetase minigene under the control of the SV40 early promoter. I decided to place the β_2m gene upstream so that there would be excess β_2m and not excess heavy chain in case occlusion of the downstream promoter occurred, analogous to the mode of operation in the production of recombinant antibodies [248].

An analogous construct, pEE14-A68-His6/β_2m, was prepared from the A*6801 gene.

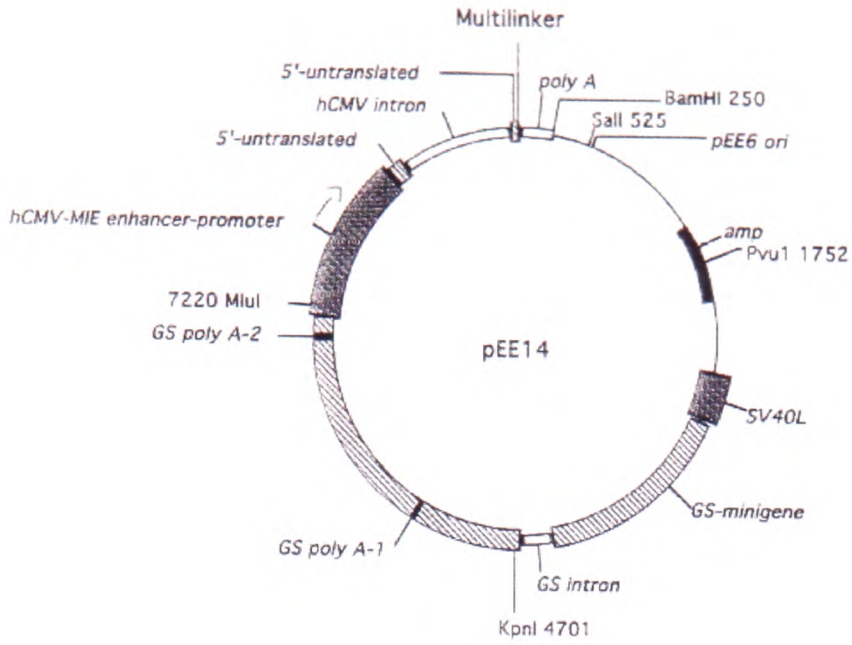

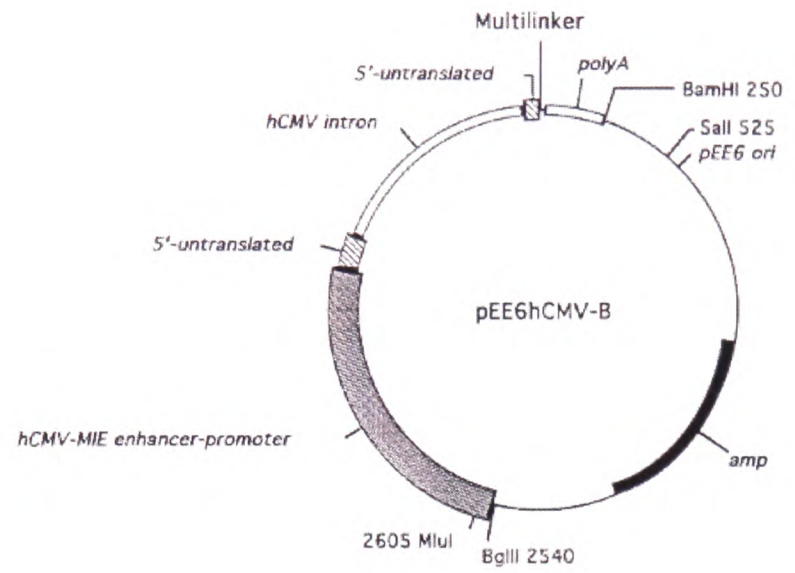


```
                                              HindIII
promoter  5' CTGCAGTCAC CGTCCTTGAC ACGAAGCTTG GGCTGCAGGT
-------->     GACGTCAGTG GCAGGAACTG TGCTTCGAAC CCGACGTCCA

        XbaI                SmaI/XmaI      EcoRI     BclI
CGATCGACTC TAGAGGATCG ATCCCCGGGC GAGCTCGAAT TCATTGATCA  3'
GCTAGCTGAG ATCTCCTAGC TAGGGGCCCG CTCGAGCTTA AGTAACTAGT
```

Figure 3: the plasmids pEE14, pEE6, and their multiple cloning cassette

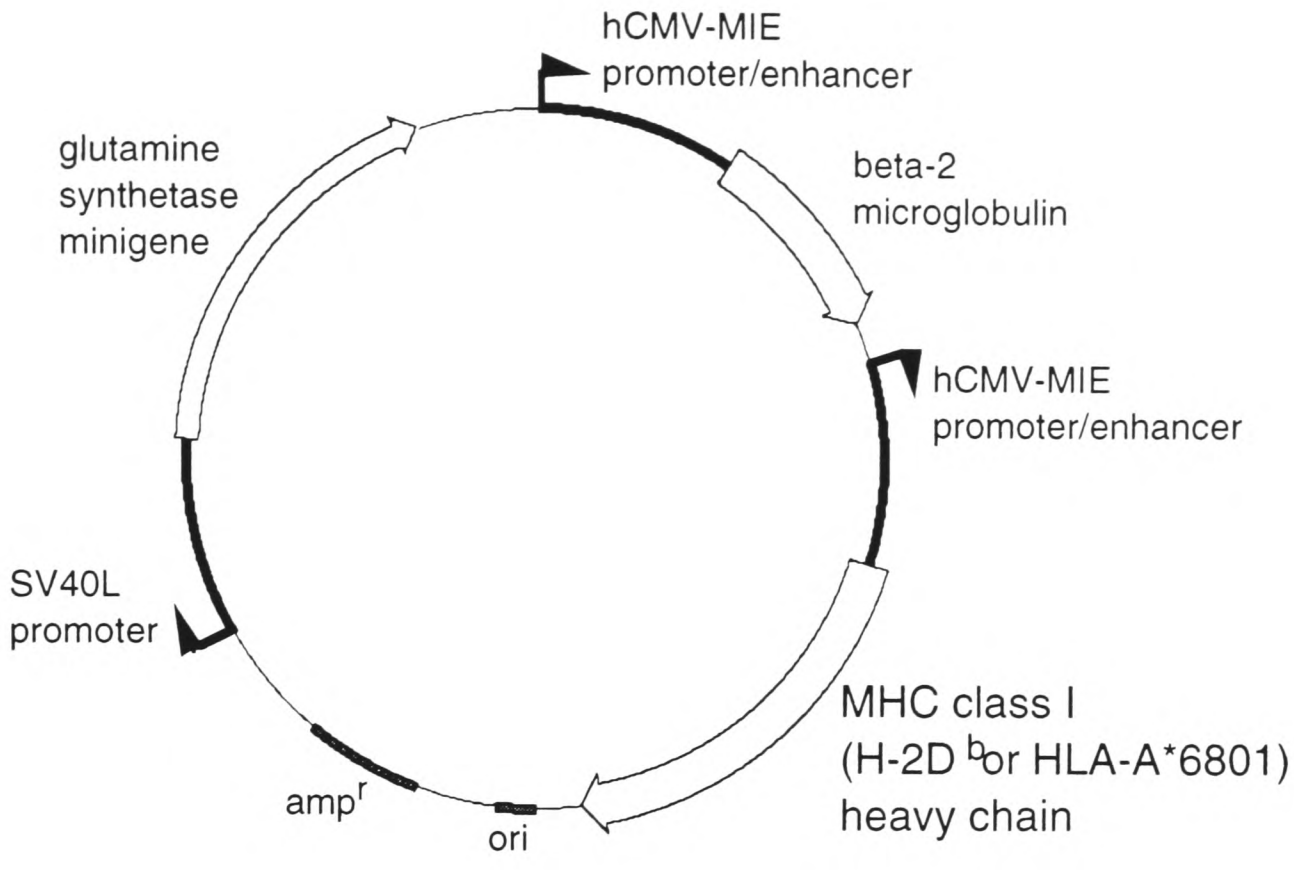

Figure 4: map of the plasmid pEE14-D^b-His_6/β_2m (with D^b) or pEE14-A68-$His6/\beta_2m$ (with A*6801). The sequence around the genes in the expression cassettes is given in figure 2.

3.2.3. Transient transfection of COS cells

I transfected pEE14-D^b-His_6/β_2m and pEE14-A68-$His6/\beta_2m$ into COS-1 cells. After 48 hours, expression of the heavy chains and associated β_2m could be demonstrated by immunoprecipitation from cell lysates (figure 5). The supernatant was dialysed against PBS and incubated with Nickel beads. Stepwise elution from the beads showed that binary HC·β_2m complexes had been secreted into the supernatant (figures 5 and 6). The molecules are of different size. In the cell lysate, D^b shows two strong heavy bands and one weaker band below; A68 shows one strong band and, approximately in line with the weak D^b band, and a weaker band below. This is consistent with glycosylation of D^b at 1 (weak), 2 or three sites; and of A68 at no (weak) or one site. D^b and A68 have three and

one potential glycosylation sites, respectively. In the supernatant fraction, the initial purification using Nickel beads is very effective (compare lanes b and e). Both proteins are eluted from the Nickel beads at 50 mM imidazole.

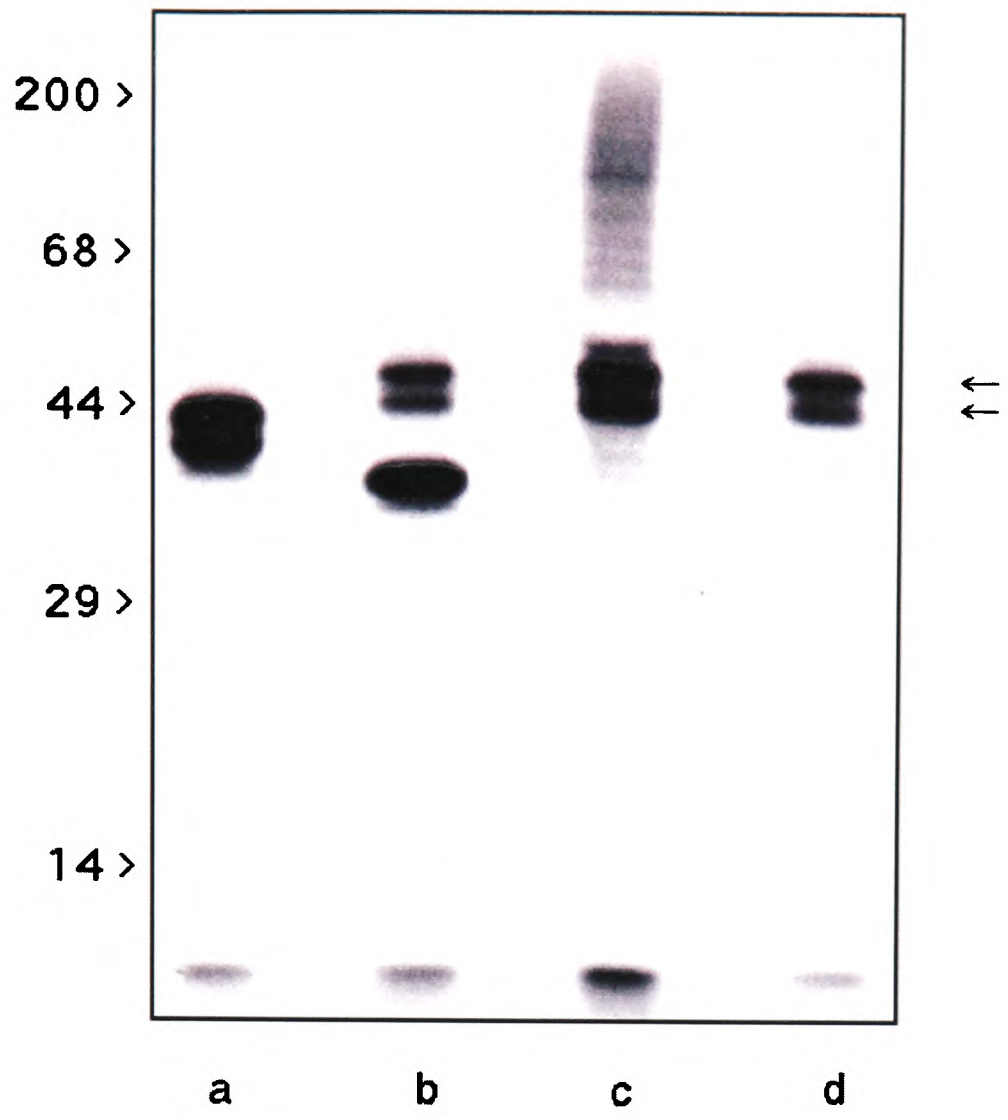

Figure 5: immunoprecipitation of radiolabelled D^b and A68 molecules from the lysate of transiently transfected COS-1 cells (autoradiograph).

lane a: cells transfected with pEE14-D^b-His_6/β_2m; immunoprecipitation with MAb 28.14.8S

lane b: cells transfected with pEE14-A68-His6/β_2m; immunoprecipitation with MAb W6.32

lane c: cells transfected with plasmid only; lane d: untransfected cells, immunoprecipitation in both with with MAb W6.32

The double arrow denotes class I molecules from the COS cells that cross-react with W6/32.

Marker sizes (in the left margin) are given in kDa.

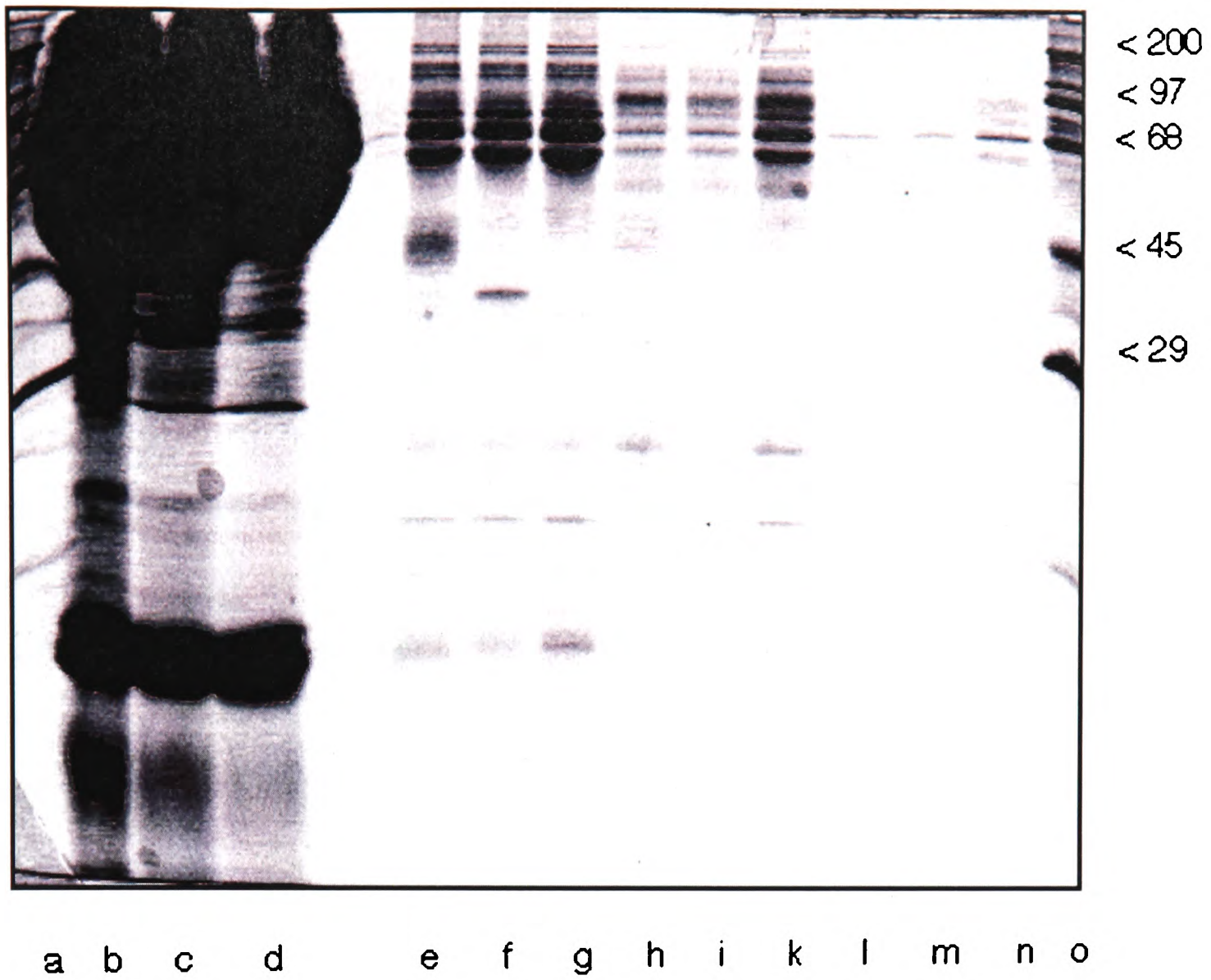

Figure 6: Nickel affinity chromatography of D^b-His_6 (b, e, h, l) and A68-His_6 (c, f, i, m) from the supernatant of transiently transfected COS-1 cells (Coomassie-stained SDS-PAGE gel). Untransfected cells in d, g, k, n. Beads were incubated with cell supernatant, washed, and eluted with 5 mM imidazole, b-d; 20 mM imidazole elution, e-g; 50 mM imidazole elution: h-k ; beads treated with EDTA/sample buffer to elute all remaining protein, l-n. D^b and A68 are both eluted with 20 mM imidazol. Specific association with β_2m can not be seen in this gel.

3.2.4. Transfection of CHO cells, selection, and amplification

I introduced pEE14-D^b-His_6/β_2m into CHO K1 cells as described in Materials and Methods. Initial transfectants, grown in GMEM-S medium at 20 μM MSX, came up after three to four weeks. They were selected for high expression using a radioimmunoassay with radioiodinated 28.14.8S antibody for detection of the Db protein. The highest secreting clones were reselected in higher concentrations (50-200 μM) of MSX using the same assay, or the quantification of SDS-PAGE analysis of protein bound to Nickel beads from the clone supernatant.

The best clones were transferred to roller bottles and, when grown to stationary phase, yielded approximately 10-25 mg of heterodimer per litre of culture supernatant (see below).

When transfected clones were labelled with [^{35}S]-methionine, complexes of D^b heavy chain and β_2m could be recovered in equal amounts from the supernatant by immunoprecipitation with the monoclonal antibodies 28.14.8S (anti-α_3) and B22.249 (anti-α_1/α_2), indicating that the great majority of the protein was folded and associated with β_2m (see figure 7).

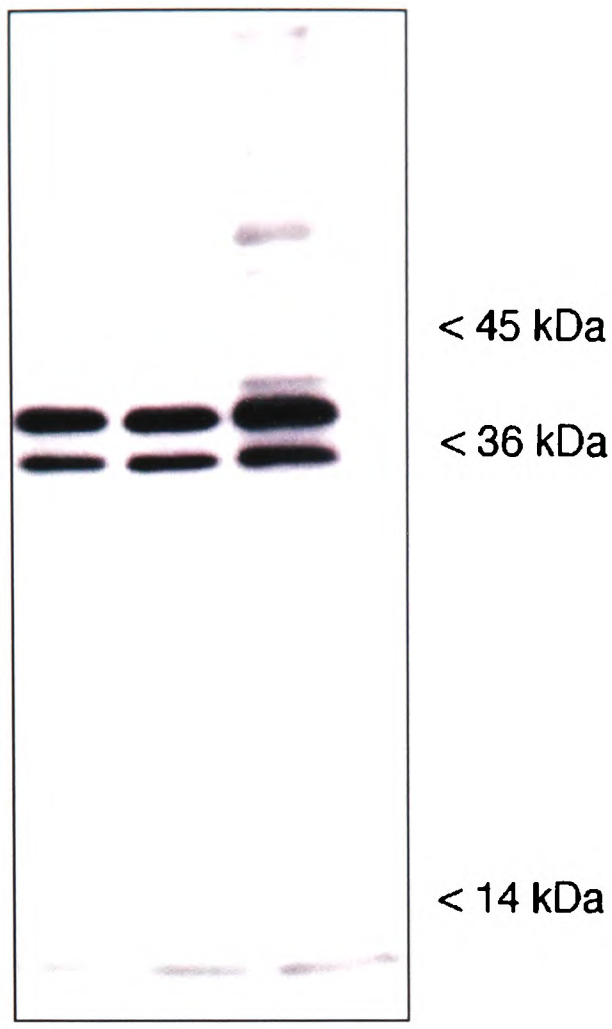

Figure 7: Precipitation of methionine - labeled D^b·hβ_2m from CHO cell supernatant, with (from left to right) 28.14.8S MAb, B22.249 MAb, Ni^{2+}-NTA agarose (autoradiograph). Equivalent amounts of D^b heavy chain and β_2m are precipitated with 28.14.8S and B22.249, indicating that the large majority of D^b heavy chains is associated with β_2m and folded correctly.

3.3. Purification of D^b-His_6·$\beta 2m$

The purification of the D^b-His_6·β_2m complexes was planned with four things in mind: firstly, the protein should at no stage see detergent that could interfere with subsequent steps, or bind to the protein and cause nonphysiological behaviour. Secondly, the protein should at no stage be denatured or β_2m dissociated, so that the material went into the binding assay in the same state as it had been produced by the cells. It was not clear whether class I molecules before they first see peptide exist in a 'special state' which might not be reattainable after de- and renaturation. If that was so, I certainly wanted to preserve that state. Thirdly, there should be as little contaminant protein as possible to make the more sensitive biophysical methods like CD, calorimetry, and crystallisation possible. Fourthly, the binding groove of the produced material should be uniformly empty to avoid interference from dissociating peptide in the binding studies, and later random tryptophan fluorescence enhancement due to a mixture of peptide already bound. The detailed protocols for each step are given in the materials and methods section.

3.3.1. Initial binding to Nickel beads from tissue culture supernatants

The initial purification step made use of the hexahistidine tail of the D^b-His_6 heavy chain. In a batch procedure, 5 ml of packed beads were stirred in 1 l of filtered cellular supernatant overnight, and protein eluted the next day with 100 mM imidazole, a competitor for histidine binding to the Nickel beads. The eluted protein was of a brown appearance and contained several strong contaminant bands, especially one around 68 kDa (see figure 8), but both heavy chain and β_2m were present (indicating that the complexes were still intact), and peptide was bound specifically in the radioligand and fluorescence binding assays, although with a pronounced slow on-rate component in the latter (see below).

When this eluate was analysed by native polyacrylamide gel electrophoresis, it appeared that with regard to size, two main populations were present: high molecular weight material which would only just enter a 12% native gel (> 500 kDa), and smaller species (see figure 10 below). From this and the slow fluorescence binding mentioned above, I concluded that some of the HC·β_2m complex was present as aggregates, probably due to the exposure of the secreted complexes to other proteins in the supernatant at 37 °C over several days that could lead to denaturation and nonspecific aggregation. (Aggregation of the purified molecules, as I observed later, is a slow process at 4 °C but accelerates with increasing temperature; see below.) It would be important to remove these aggregates as they could influence the specificity and kinetics of the binding reaction, make the determination of the number of binding sites difficult, and interfere with biophysical methods such as crystallisation, CD, and calorimetry. I therefore decided to perform separation by size (gel filtration) as the next step.

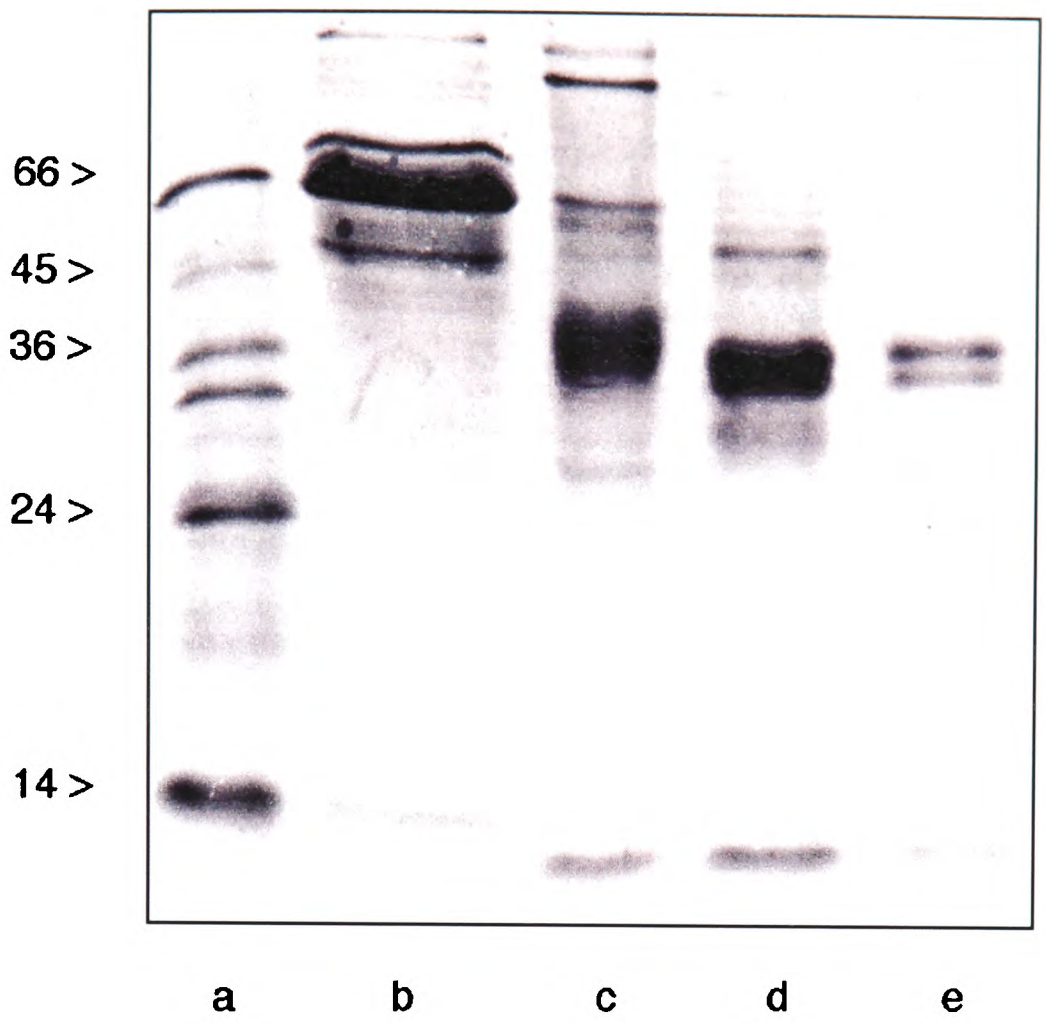

Figure 8: Overall view of the standard D^b·hβ_2m purification (Coomassie-stained SDS-PAGE gel). Lanes: a, markers; b, cell culture supernatant (CHO cells); c, material eluted from Nickel column with 100 mM imidazol; d, after gel filtration and neuraminidase treatment (hence the shift in size); e, the pure fraction from a native isoelectric focusing run.
Equal amounts of total protein (by OD_{280}) were applied to lanes b-d.

3.3.2. Gel filtration

Size exclusion chromatography was initially done in a 1.5 x 100 Sephacryl S-200 HR column, later in a large 5 x 100 Sephacryl S-300 HR column that worked better and allowed for the separation of 300 mg of protein in one run. As the elution diagrams in figure 9 show, two species of different sizes are clearly separated on gel filtration. As the native PAGE gel in figure 10 shows, the first peak consists of the high molecular weight aggregates, the second of the lower MW material. Figure 11 shows an SDS-PAGE analysis of the two peaks. The early peak contains the high molecular weight aggregates and also, interestingly, the major part of the 68 kDa contaminant protein (see figure 9); the late peak contains much purified HC·β_2m.

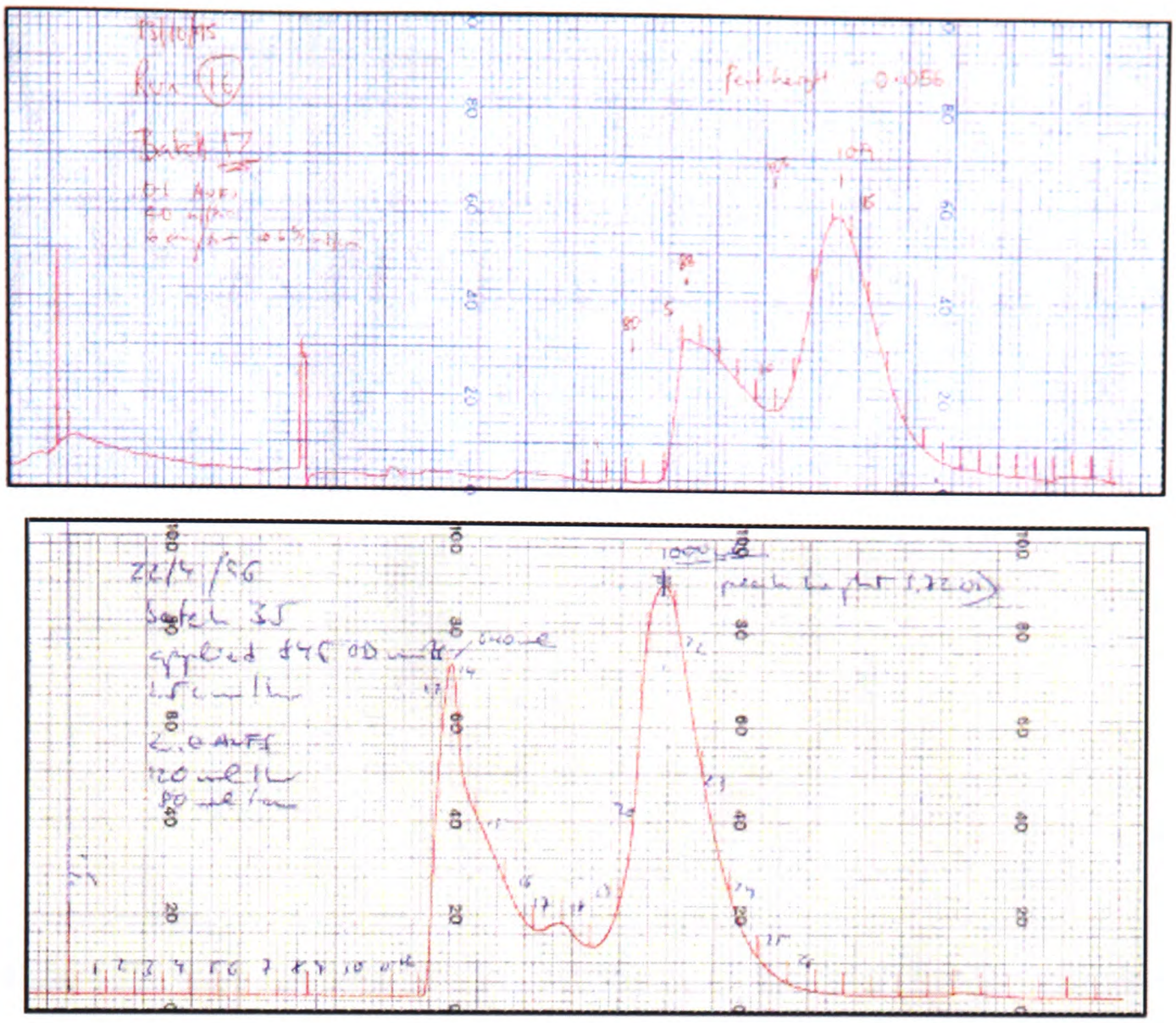

Figure 9: Elution diagrams of the gel filtration columns.

Top, 1.5 x 100 Sephacryl S-200 HR; bottom, 5 x 100 Sephacryl S-300 HR.

Injection is at the leftmost detector peak.

It can be seen that the separation of aggregates and monomeric protein is far better on the larger S-300 column.

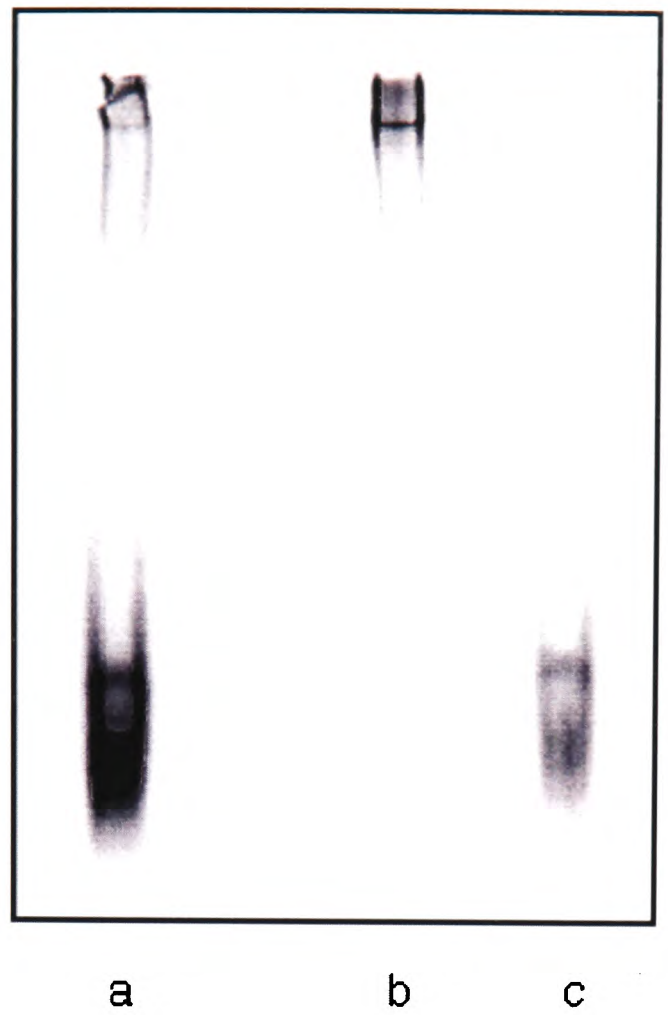

Figure 10: Native 12% polyacrylamide gel (Coomassie-stained) of the D^b·hβ_2m material before (lane a) and after gel filtration (early peak: lane b, late peak: lane c).

The high molecular weight fraction of the protein is clearly separated away from the material that is able to enter the gel on native PAGE.

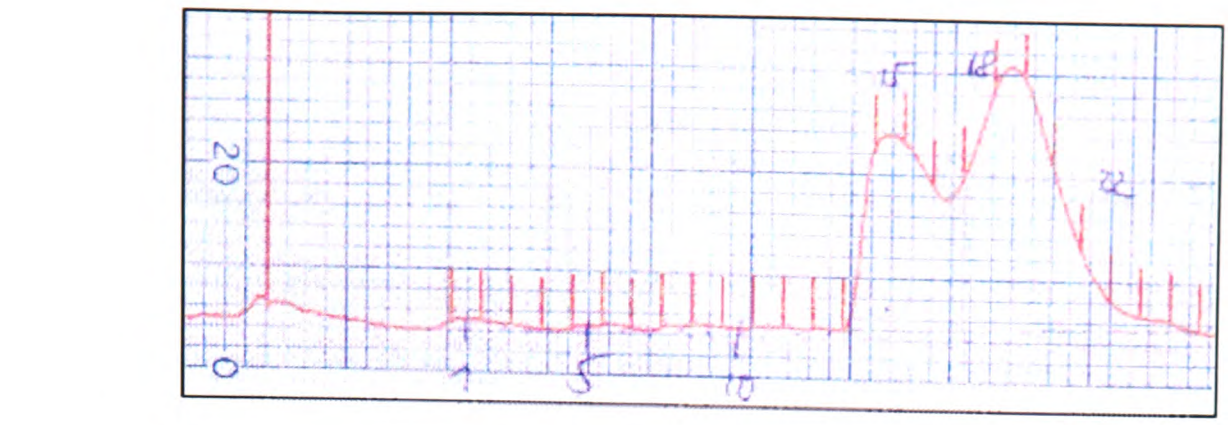

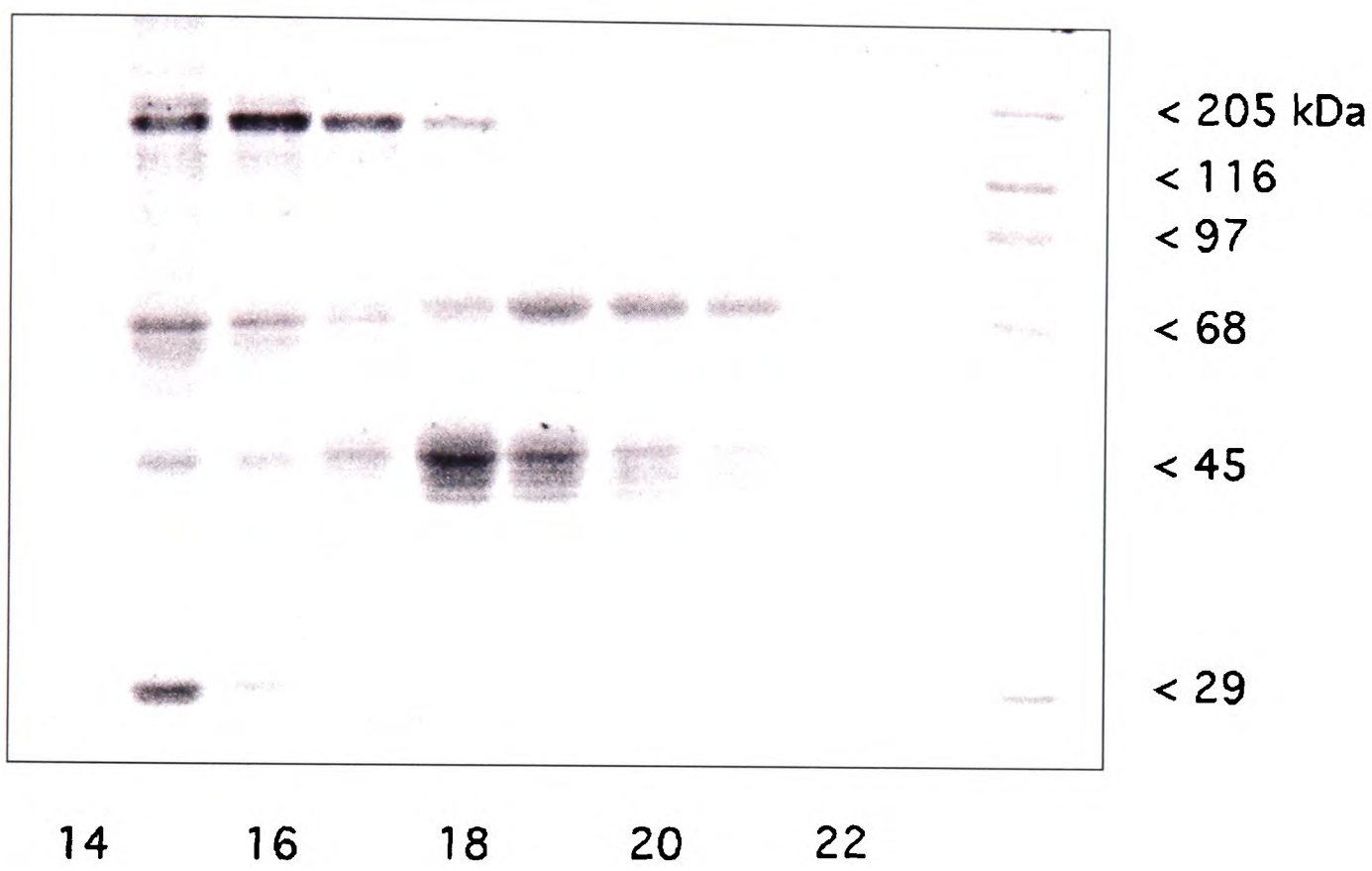

Figure 11: Analysis of a gel filtration separation on SDS-PAGE. Top panel, elution diagram with numbered fractions; bottom panel, SDS-PAGE analysis of the peak fractions. The early peak consists of some class I, the 68 kDa contaminant, and a 200 kDa protein.
The second peak is mainly D^b and the 68 kDa protein.

From an analytical run on an FPLC system calibrated with molecular weight standards (figure 12), it appears that D^b-His_6·β_2m was travelling as a complex of ca. 130 kDa under these conditions, and not in any higher aggregate. This would most likely represent a dimer of dimers, $(D^b\text{-}His_6\cdot\beta_2m)_2$, with glycosylation. This observation was later confirmed in the fluorescence anisotropy decay experiments looking at the radius of the whole protein in solution (see below). There is no biochemical or crystal structure evidence for 'class I dimers' to this date (although tetramers have been reported on one occasion [249]), and the crystal structures of class I molecules do not allow for an easy modelling of a dimer (as opposed to class II molecules that crystallise in dimers [233]) if the α_3 domain is to retain its place [121]. However, this domain is predicted to be quite flexible in relation to the peptide binding site, and therefore the formation of dimers of dimers is not impossible. It is interesting to note in this context that the positions of β_2m and the α_3 domain relative to the binding groove in the D^b crystal were found to be different from those in K^b [126], so that the possibility of variation between alleles in this matter exists. It is now feasible, using the recombinant molecules, to address this question in light scatter and ultracentrifugation experiments that would give a definite answer under equilibrium conditions; also, if a crystal is obtained, the structure might give further evidence on this point. An alternative explanation would be dimerisation involving the hexahistidine tail; this has not been reported from other proteins so far.

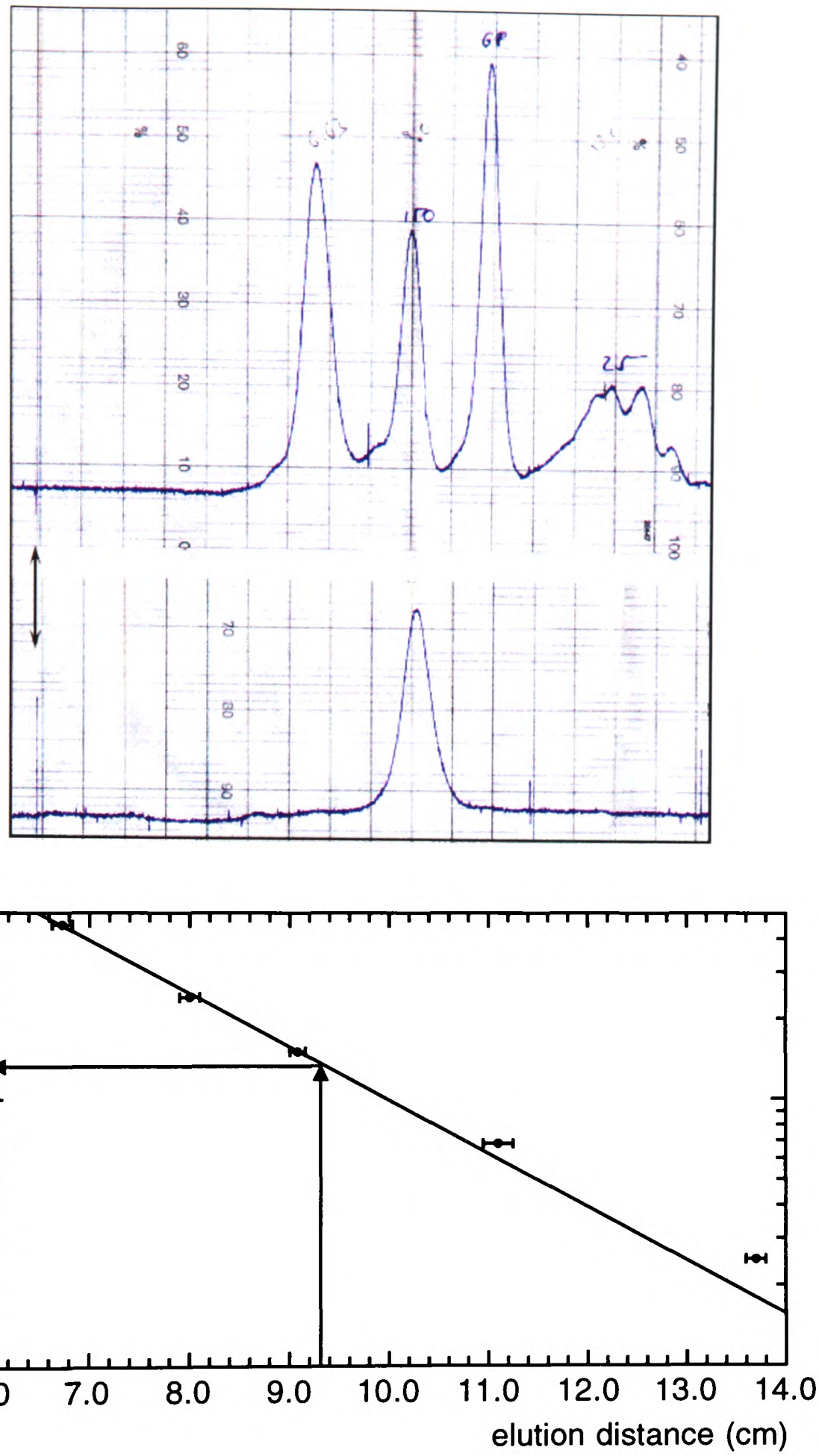

Figure 12: Determination of the molecular weight of the neuraminidase-treated final Db preparation on the S-200HR FPLC column.

Top panel, example of molecular weight standards (molecular weights 450, 150, 68, and 25 kDa; upper part) compared to the purified D^b complex (lower part) with the injection points lined up (double arrow).

Bottom panel, elution plot (molecular weight standards averaged from two experiments).

The elution volume of D^b indicates that the HC·β_2m complex is dimerised (MW: 130 ± 6 kDa)

3.3.3. Preparative isoelectric focusing

Following gel filtration, the D^b-$His_6 \cdot \beta_2 m$ protein was suitable for binding studies with radiolabeled peptides and by fluorescence, but not sufficiently pure for crystallisation attempts or calorimetric measurements as contaminating proteins were still visible on gels. It was also a concern that some of the D^b molecules would have bound to them endogenous peptides from the CHO cells, or peptides from in the medium: although the fetal calf serum used to grow the cells had been dialysed with a 10 kDa cut-off membrane to remove peptides, still some peptides might have originated from the hydrolysis of protein during the cell culture, or been secreted by the cells. Also, the purification protocol included no denaturing step that could have served to remove these peptides.

I decided to use native isoelectric focusing (IEF) [159, 192] to look at the state of occupancy of the Db molecules. To do this, the protein has to be treated with neuraminidase to remove the sialic acid residues which would make the protein heterogeneous in charge. Figure 13 shows an IEF experiment where the late peak from the gel filtration column was neuraminidase-treated, and different peptides were added subsequently . One prominent band, representing about 50% of the protein, shifts depending on the charge of the added peptide, probably representing empty $HC \cdot \beta_2 m$ complex that is capable of binding peptides. This gives an estimate of the proportion of complex that is still empty; and this gel also shows that it is possible to biochemically separate class I molecules on the basis of the charge of their peptide ligand. Peptide that had no D^b binding motif (NP-91-99) showed no influence on the pI of the band (data not shown).

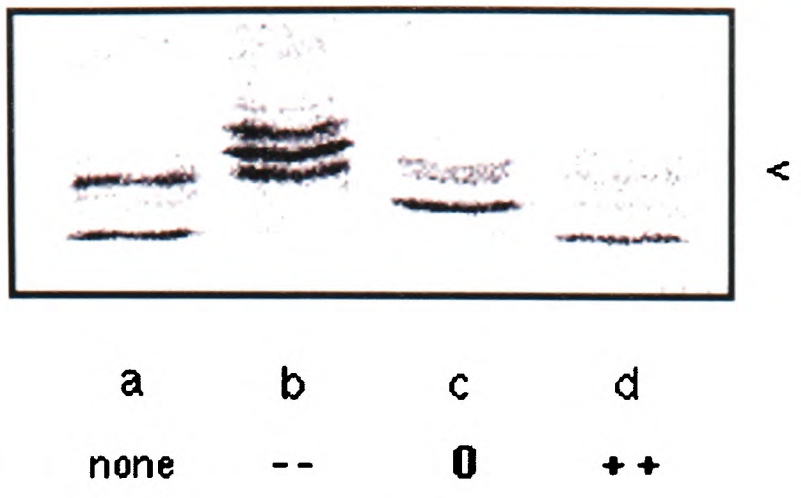

Figure 13: The effect of different peptides on the isoelectric point of the $D^b \cdot h\beta_2 m$ complex (Coomassie-stained native IEF gel; basic end down).

lane a: no peptide added; lane b: NP-Y367-379 (YSNENMDAM, 2 negative charges); lane c: SV 324-332 (FAPGNYPAL , neutral), lane d: GP-92-101 (CSANNSHHYI, 2 positive charges).

The lower D^b band shifts upon the addition of peptide; the upper band (arrowhead) remains constant throughout, probably representing molecules with peptide bound, or with denatured binding sites.

Upon the addition of neutral peptide, a slight acidic shift is visible.

The $D^b \cdot h\beta_2 m$ complex in this experiment had not been IEF purified prior to the experiment.

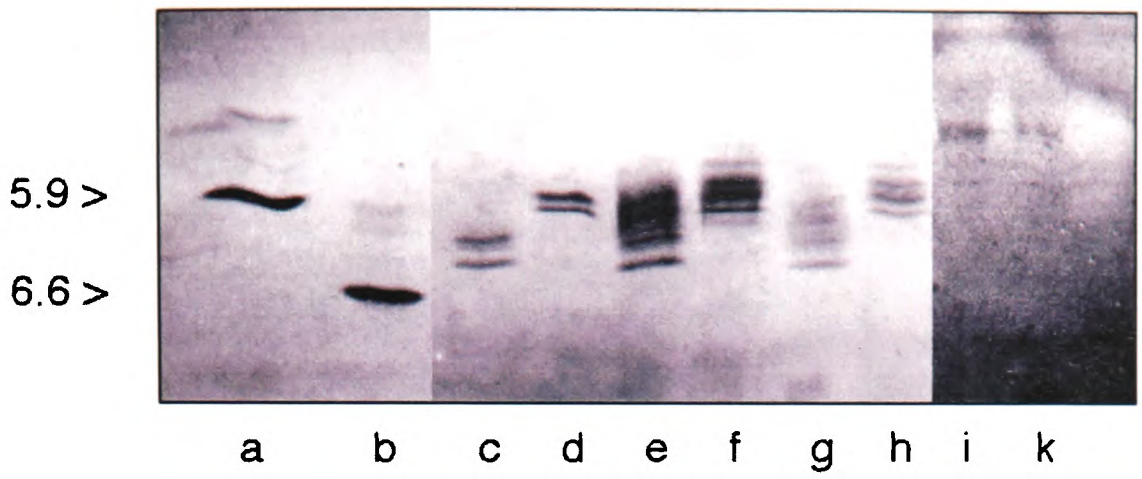

Figure 14: Purification by preparative IEF compared to thermal denaturation of the binding site, and the effect of peptide on the $D^b \cdot h\beta_2m$ complex and on heavy chain

(Coomassie-stained native IEF gel).

Lanes a, b: markers (annotated in the margin)

Lanes c, d: IEF-purified $D^b \cdot h\beta_2m$; g, h: starting material before IEF purification; e, f: the same material, heat-treated for 30' and subjected to gel filtration at this temperature; i, k: free D^b heavy chain.

Lanes c, e, g, i: no peptide added; lanes d, f, h, k: peptide NP-Y367-374 present.

D^b heavy chain shows a more acidic pI and does not bind peptide in this assay. The D^b complex before IEF purification shows some more acidic bands which do not shift on the addition of peptide. After purification, these bands have disappeared, and the two remaining bands both shift upon peptide addition. Heat-treatment of the same material does not have this effect.

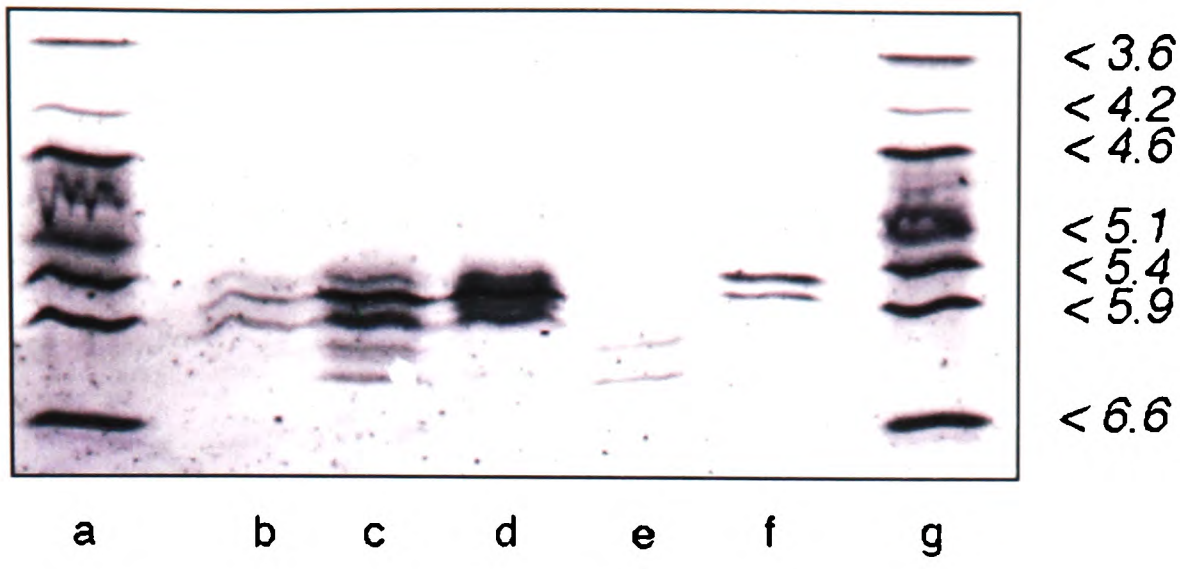

Figure 15: The two bands observed with empty D^b are not isoforms of bound β_2m (Coomassie stain of native IEF gel).

Lanes: a and g, markers (isoelectric points indicated in the margin); b: bacterially produced $h\beta_2m$ (courtesy of Karl Macintyre); c, mixture of recombinant $D^b{\cdot}h\beta_2m$ (lane e) and recombinant β_2m, incubated for 3 hrs at 37 °C; d, lane c plus NP-Y367-374 peptide; e, recombinant; f, lane e plus NP-Y367-374 peptide.

The ratio of the two bands in the empty D^b preparation is not altered when opportunity for exchange with β_2m is given, indicating that they do not differ in the β_2m species.

In figure 14, the effect of peptide on HC·β_2m complexes and free heavy chain is compared. Free heavy chain runs differently from the complex, and is not influenced by the addition of peptide in this experiment.

In figure 14, there are two bands of HC·β_2m complex that shift upon peptide addition (lanes c, d) This was sometimes seen in preparations, instead of a single band. To test the possibility that this heterogeneity in the isoelectric point was due to the binding of some hamster or bovine β_2m in exchange for the human molecule, this preparation of D^b-His_6·β_2m was incubated with an excess of recombinant hβ_2m (unfortunately not proven to be folded) for several hours at 37 °C. No change in the pattern of the bands was observed (see figure 15). The heterogeneity in the isoelectric point reported here is most likely to come from something else, for example incomplete removal of sialic acid residues in some batches. After treatment with PNGase which removes the sugars completely, collapse into a single band on native IEF was seen (Jon Skipper, pers. commun.).

As judged from the IEF markers, the empty HC·β_2m complex migrates at an isoelectric point (pI) of 6.3 (the second band at approx. 6.15), corresponding to the pI of 6.33 calculated from the sequence data (see below). However, in native IEF, the free HC focuses at a more acidic pH, about 5.2 (see figure 14, lane i), instead of the calculated 6.28; and also (bacterial) recombinant β_2m exhibits a pI of around 5.9 (figure 15, lane b) instead of the calculated 6.58. It is easily possible that upon folding the pI of a protein changes (see below). This demonstrates that pI values from native IEF gels cannot be used strictly to identify proteins.

It is remarkable that, in addition to the pI shifts imposed by the charge of the peptide, there seems to be an additional acidic shift with all three peptides tested (figure 13, lanes b to d). So, the pI of the complex shifts slightly to the acidic on the addition of the neutral peptide FAPGNYPAL, and the acidic shift upon ASN<u>E</u>NM<u>D</u>AM addition is far more

pronounced than the basic shift upon CSANNSHHYI binding.

The isoelectric point of a protein is the integral of the individual isoelectric points of its side chains. The isoelectric points of amino acid side chains strongly depend on their environment [250]. When a protein changes conformation, charged side chains can become buried in the interior (less accessible to water) or exposed at the protein surface. In both cases, their isoelectric points will change, and with them the pI of the whole protein. A shift in the isoelectric point of a protein can therefore indicate a conformational change [250, 251]. However, the effect on the pI from burial or exposure of side chains due to conformational change is difficult to separate from the consequences of burial of the peptide binding site, which contains charged residues, by the peptide. An isoelectric shift caused by the latter would not necessarily indicate a conformational change. The observation reported here is not in itself an indication of conformational change in the Db heavy chain upon peptide binding, but certainly compatible with this idea.

Another interesting observation is the upper (more acidic) band in figure 13, lane a, which seems not to shift upon the addition of any peptide. I had expected to see a wide range of different bands for the occupied complex, depending on the charge of the (random) peptides in the binding groove. In contrast, there was only one major band (although it is slightly more diffuse than the band corresponding to the empty molecule). Is it possible that the majority of D^b complexes isolated has one dominant peptide or peptide species bound? This could be either a dominant peptide from the cells, or something that bound from the supernatant. An alternative explanation is that this band represents denatured D^b heavy chain that is therefore unable to bind peptide, and that has again undergone an acidic shift in the pI (see above). Purification of this peak, and elution of peptide, would clarify this issue.

The separation effect between empty and loaded D^b complexes described above demonstrated that at least half of the protein was loaded with peptides or denatured and needed to be purified further. Fortunately, I was able to use it in a preparative method to

obtain empty molecules of the highest purity.

The Rotofor chamber (Bio-Rad) is a preparative IEF device consisting of a cylindrical chamber with electrode assemblies at either end, cooled by a central cooling finger, that is divided into twenty transverse sections by membrane disks. The sample solution, consisting of the protein in a low-salt buffer and an ampholyte mixture, is applied evenly to the cylinder, and in the course of the separation the proteins focus in one or several adjoining chambers. These are afterwards drained individually (experimental details in the materials and methods section).

Separation of neuraminidase-treated gel filtration eluate on the Rotofor gave two, sometimes three, major protein peaks. Figure 16 shows an analysis of the fractions by SDS-PAGE and native IEF. The major contaminant protein is purified away from the D^b complex which focuses in two peaks at the very acidic end and in the middle of the gradient. The acidic material runs on a native IEF gel in the more acidic position of the denatured/occupied protein, whereas the central peak runs in the place of the empty material and shifts almost entirely upon the addition of peptide (figure 16). This peak sometimes gave two bands in the native IEF analysis which might come from incomplete deglycosylation (see above) (Figures 14 and 15).

$HC \cdot \beta_2m$ complex thus purified gave an increased fluorescence enhancement in the fluorescence binding assay (20%) as compared to non-IEF purified (15%), indicating that a higher number of binding sites per mg protein was now available (data not shown).

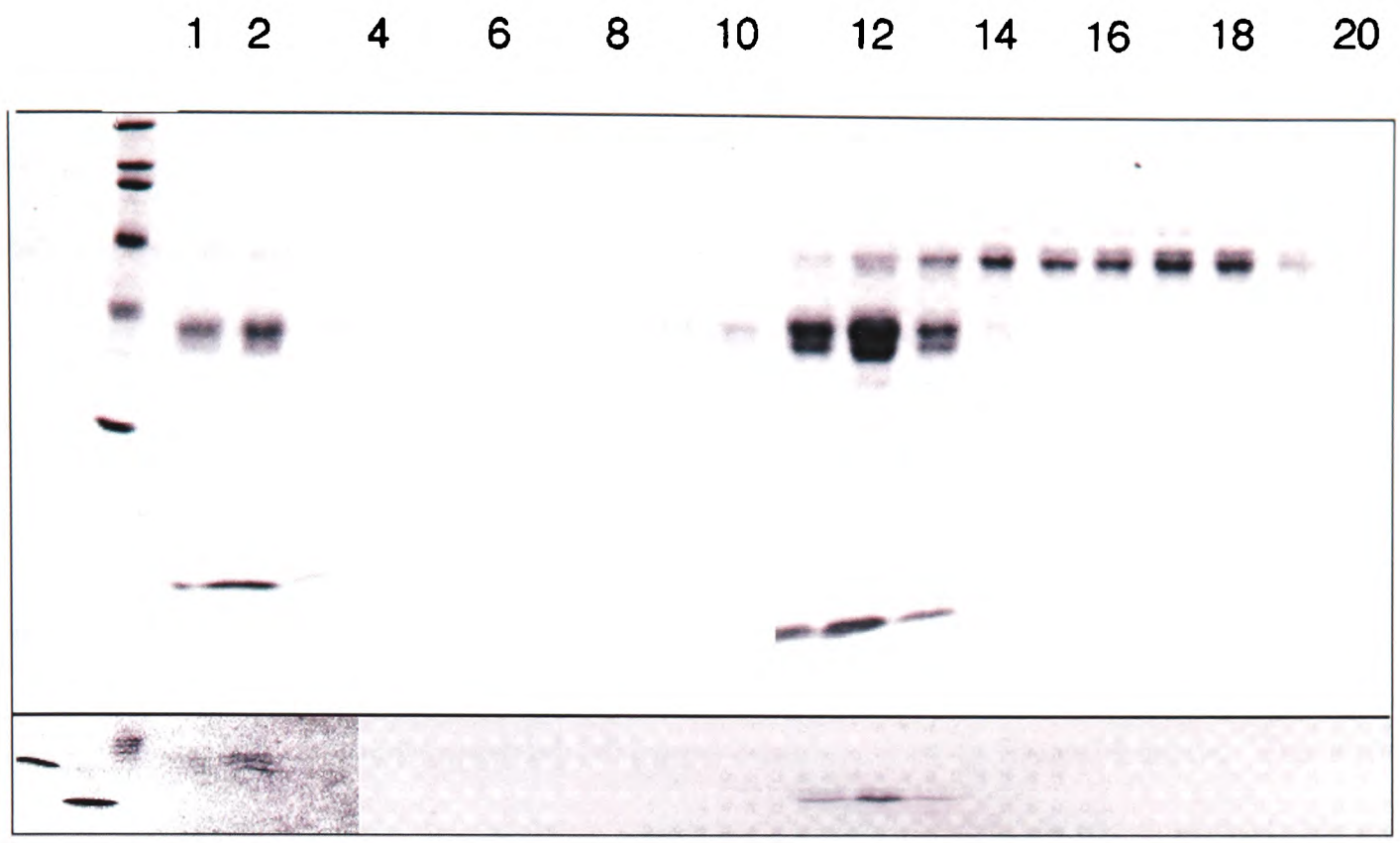

Figure 16: SDS-PAGE (top) and native IEF (bottom) analyses (both Coomassie stained) of the fractions of a preparative native IEF separation in a pH 6 - 7 gradient (Bio-Rad Rotolytes). Fractions are numbered at the top. Fraction 1 is the most acidic fraction. Molecular weight markers (leftmost lane) for the SDS-PAGE are 200, 116, 97, 68, 45, and 29 kDa; pI markers for the IEF (leftmost two lanes) are 5.9 and 6.6. A protein of 66 kDa is being purified away from $D^b \cdot h\beta_2m$ because of its more basic pI. D^b itself occurs in two places in the gradient: in the very acidic, and in the medium fractions. The very acidic material shows the acidic shift on native IEF, characteristic of peptide-occupied material. The D^b focusing in the middle of the gradient is pure unoccupied $HC \cdot \beta_2m$ complex. Both subpopulations of D^b are associated with β_2m.

It can be concluded that the separation by preparative native IEF allows to completely separate the occupied and denatured from the empty and binding-competent D^b-His_6·β_2m complexes. The material recovered from the central peak is almost homogeneous on SDS-PAGE and native IEF. It represented the highest degree of purity of D^b-His_6·β_2m available to us, and has been or is being used in fluorescence binding, fluorescence anisotropy decay, CD, calorimetry, stopped-flow fluorescence, and crystallisation studies.

3.3.4. Overview of the purification

An overall view of the purification of D^b complexes is given in figure 8 above. The above 'standard purification' can be further extended by including another nickel agarose column, eluted with an imidazole gradient, before the final Rotofor step. This helps to exclude the last remaining contaminant proteins.

3.4. Characterisation of the product

For the products encoded by the plasmid pEE14-D^b-His_6/β_2m, the GCG program 'peptidesort' [11] makes the following predictions (the leader sequences are not taken into account):

	D^b-His_6	β_2m	D^b-His_6·β_2m
molecular weight (kDa)	33749	11762	45511
isoelectric point	6.28	6.51	6.33
extinction coefficient ε_{280} (cm^{-1}·M^{-1})	84,590	19,180	103,770

The protein material that was recovered from the CHO supernatant following transfection

with pEE14-D^b-His_6/β_2m, and subsequently purified, consisted of two subunits of 32 and 11-12 kDa in size when completely deglycosylated (see below), corresponding to the theoretical molecular weights of HC-His_6 and β_2m. The reason for the slightly smaller apparent size of Db·His_6 is not clear, but it could be the consequence of abnormal migration on SDS-PAGE. The isoelectric point of the complex was 6.3 (with an additional band at 6.15 sometimes seen), as predicted from the protein sequences. The size of the protein on gel filtration is not consistent with a HC·β_2m heterodimer, but could indicate the formation of a dimer of heterodimers.

The complex exhibits a strong affinity for the Ni^{2+} NTA agarose, indicating that it is not C-terminally truncated. It also precipitates with the MAbs 28.14.8S (α_3 domain) and B22.249 (α_1/α_2 domains); the latter is conformation-specific and demonstrates that HC and β_2m are associated in a physiological manner (figure 7 above).

H-$2D^b$ has three potential glycosylation sites. On SDS gels, the isolated heavy chain appeared as a block (indicating heterogeneous glycosylation) that collapsed into two main bands upon exhaustive treatment with neuraminidase (see figure 8), indicating that two main size isoforms of sugars were present, and that varying amounts of sialic acid were attached to each. Upon treatment with endoglycosidase F or N-glycosidase F (PNGase F) these two main bands gave rise to a single band with the molecular weight of 32 kDa (figure 17).

Following purification by preparative isoelectric focusing, the protein appears homogeneous on SDS-PAGE and native IEF (here sometimes as two bands, see above). The IEF band shifts upon the addition of a charged peptide, indicating that all of the final product is able to bind peptide. This reaction is specific to D^b-binding peptides.

The protein preparation specifically bound peptides with the H-$2D^b$ anchor motif in radioligand and fluorescence binding studies (see below). To determine the nature of the binding and the number of binding sites per unit protein, a radioligand binding experiment with iodinated NP-Y367-374 peptide was performed with a protein concentration of 10 nM as determined by the extinction at 280 nm in the native state (see

figure 18). Scatchard analysis and direct fit of the Langmuir isotherm both gave an affinity constant of $5.4 \cdot 10^{7}$ and $3.1 \cdot 10^{-9}$ M binding sites. This would have indicated that only 32% of the protein molecules present will bind peptide, a figure in contrast to the complete shift of the IEF band upon peptide addition. It can also be excluded from a fluorescence binding experiment that further binding takes place at higher peptide concentrations (up to 100 µM; see below figure 40). However, a similar percentage of binding sites was obtained from this material in Robert Tampé's laboratory with the peptide NP-C367-374, fluorescein-labelled on the cysteine (Ingmar Dorn, pers. comm.).

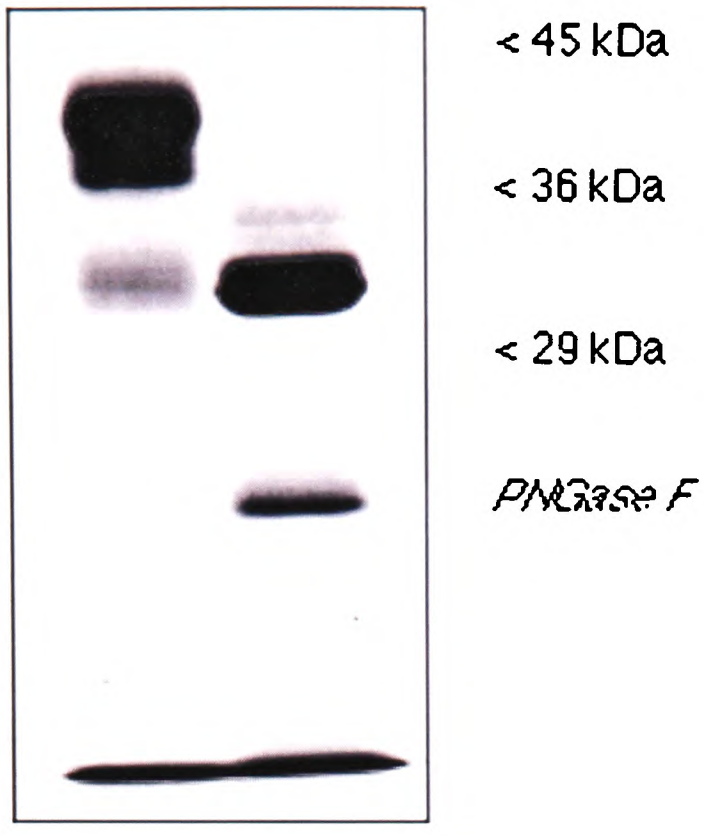

Figure 17: PNGase F treatment of D^b·hβ_2m (Coomassie-stained SDS-PAGE gel).
On PNGase F treatment, the heavy chain forms a tight band at approx. 32 kDa, showing that the glycosylation can be fully removed.

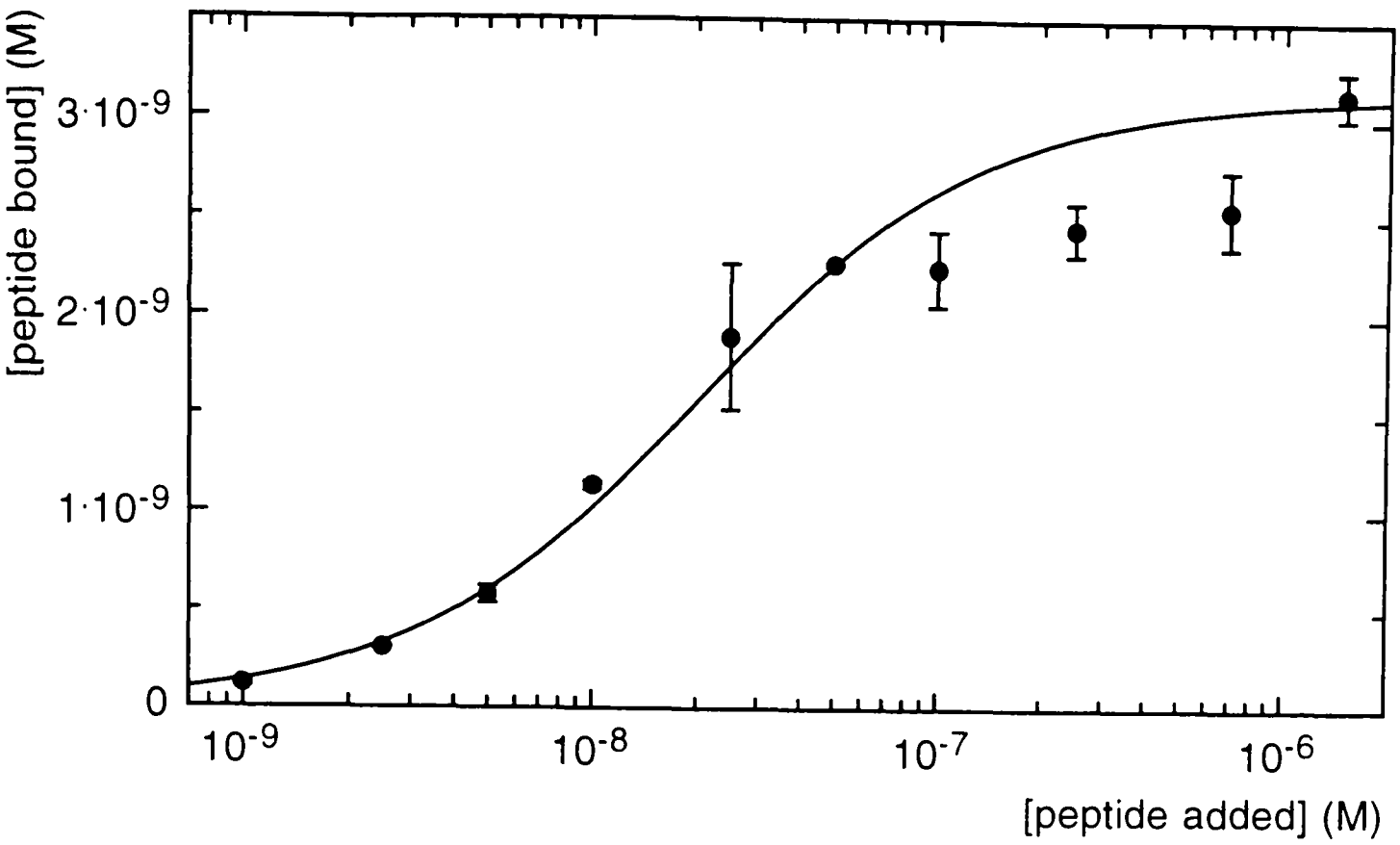

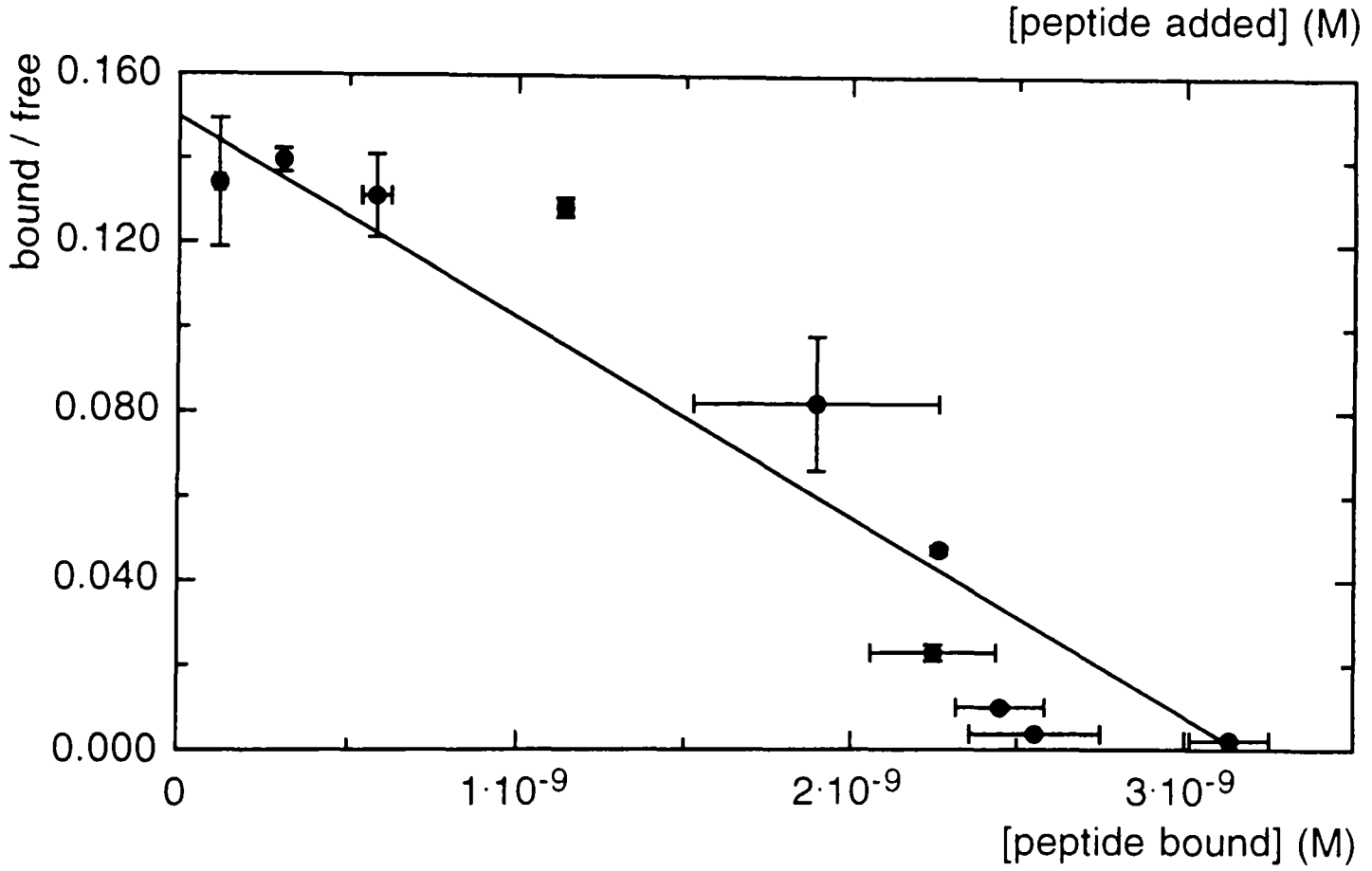

Figure 18: Determining the number of peptide binding sites in a D^b preparation, from a binding assay with iodinated peptide.

Comparison of two methods of data fit (see materials and methods).

D^b: 10^{-8} M by absorption.

Upper panel: semilogarithmic binding diagram with complete Langmuir isotherm fitted by least-squares analysis. Parameters are, sites: 3.14 (± 0.02) $\cdot 10^{-9}$ (31.4% of expected); Ka= 5.41 (± 0.15) $\cdot 10^{7}$ M^{-1}.

Lower panel: Scatchard plot.

Straight line fitted by least-squares analysis; Ka= 5.34 (± 0.61) $\cdot 10^{7} M^{-1}$; sites: 3.00 $\cdot 10^{9}$ (± 10%).

Therefore, the extinction at 280 nm of the purest available protein preparation was compared in water and 6M guanidinium hydrochloride, and found to be 3.2 times lower in the latter. As the extinction coefficients are calculated for denatured protein [10], it must now be taken into account that the extinction coefficient in the native state differs by a factor of 3.2 and is closer to 300,000. This number fits with the results of the Bradford protein assay (Ingmar Dorn, pers. comm.). If this correction is made, nearly 100% of the complex can be assumed to be binding-competent, a result in full agreement with the complete acidic shift on the IEF gel upon peptide addition.

It can be concluded that the final isolated protein is most probably a complex of D^b-His_6 and β_2m that is folded in its physiological conformation. It has no peptide in its peptide binding groove, and is able to bind peptide specifically upon addition. No other protein is associated with it.

The final protein preparations were stored at 4 °C and for at least two weeks showed no decrease in their peptide binding abilities. After this time aggregates began to form and the on-rate of binding slowed down (see below figure 31). The aggregates could normally be removed by repeating the gel filtration step. This stability is in contrast to the situation in detergent lysates where the empty complex dissociates overnight. In a parallel observation, Matsumura *et al.* [192] observed that their Drosophila-produced Kb complex was stable at 47 °C for up to one hour, but when 1% Triton X-100 was added, immunoreactivity with the conformation-specific antibody Y3 was rapidly lost; the molecules could be protected from detergent decay by the VSV-8 peptide. It seems that detergent generally destabilizes HC·β_2m complexes. (For the detergent influence on rate and equilibrium constants, see below.)

4. A novel assay for peptide binding to class I molecules using natural tryptophan fluorescence

In the study of the interactions of biomolecules, several considerations are important for the choice of an experimental method [23, 22, 21]: firstly, the wish to study the interaction in a system where all parameters are under control. Ideally, this is an *in vitro* system where only such components are present that have been deliberately added. This is often not possible when proteins are not at hand in sufficient quantity and purity, or have to be generated from cell lysates where detergent is a necessary ingredient.
Secondly, the desire to interfere with the natural mechanism of ligand-receptor binding as little as possible; ideally, neither the ligand nor the receptor should be altered in any way, and the detection should take place in an equilibrium situation where no unwanted or unforeseen dissociation effects can influence the data. In practice, this is often impossible by the necessity to introduce a label on receptor or ligand, and/or to separate bound from free ligand.
Thirdly, the ideal system would allow the monitoring of the kinetic properties as well as the equilibrium conditions, so that a full picture of the interaction can be obtained.

As concerns the interaction of class I molecules with peptides, all systems described so far have been troubled by one or the other technical shortcoming (see introduction). Therefore, to put forward the hypothesis of non-matching kinetics, a new experimental system was required. Natural tryptophan fluorescence measurements fulfil all the conditions mentioned above and have enabled us to control and extend the biochemical experiments done already.

4.1. Principles of tryptophan fluorescence

Fluorescence measurements are a convenient way to look at protein-ligand interaction: they are nondestructive, take place in real-time, and no separation of bound from free

ligand is required (Review in [252]). Fluorescence is the emission of light from an electronically excited state of a molecule, the excitation being caused by the absorption of light of a shorter wavelength (for details and foundations see [253-255]). In a fluorimeter, the sample is excited by a monochrome source, and light that is emitted from the sample is observed at a right angle to the incident beam.

The biochemical uses of fluorescence are based on the observation that the absorption and emission characteristics of a fluorophore depend on the dielectric constant - the hydrophobicity or hydrophilicity - of the surrounding medium [256]. Picture 19 shows this with a model compound, NATA (N-acetyl-tryptophanamide), in three different solvents. Generally, in more hydrophobic environment, an increase in fluorescence intensity and a blue shift of the emission maximum are observed [257]. Often, the absorption also increases.

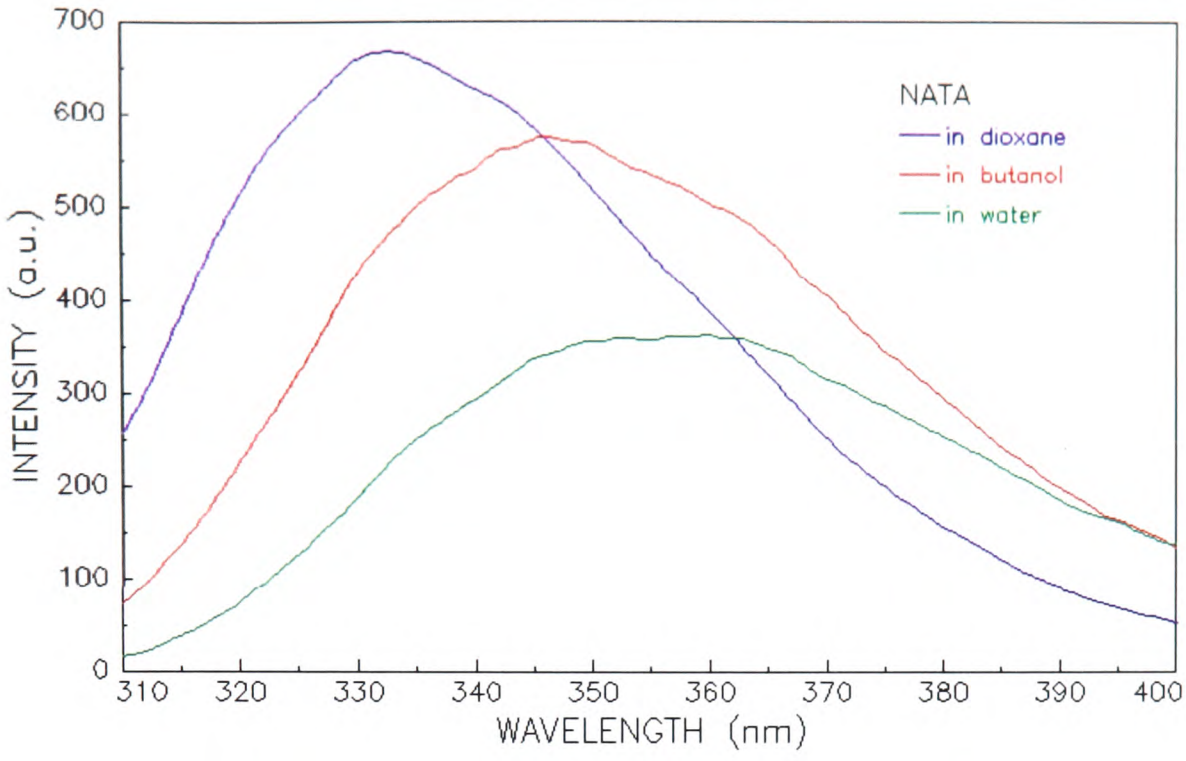

Figure 19: fluorescence emission spectra of N-acetyl tryptophanamide in water (green), butanol (red), and dioxane (blue). Excitation is at 295 nm. Fluorescence emission increases and the maximum shifts to shorter wavelengths as the environment of the fluorophore turns more hydrophobic. Measurement and graph by Klaus Döring.

Fluorophores, either natural (aromatic amino acids, see below) or artificially introduced, can therefore serve as a sensor for their chemical environment. If this environment is altered due to the burial or exposure of fluorescent groups, or the juxtaposition of charges, the fluorescent properties of the sample are bound to change. Any biological process in which the environment of a molecule is changed by binding, chemical transformation, or conformational changes, is in principle amenable to fluorescence analysis.

Fluorescence is a very fast process (typically in the order of nanoseconds [258]). Therefore, it is suited to the detection of fast events and the evaluation of kinetic constants ([259, 260]; review: [261]).

Most fluorescence receptor-binding studies use ligands that have been fluorescently labelled with fluorescein or the dansyl group [261]. In the MHC class I field, Kourilsky and co-workers have measured the binding of N-terminally dansylated peptide to H-2K^d (see introduction and [202]). Fluorescein has the advantage of an extremely strong fluorescence effect (high quantum yield), but it needs to be demonstrated by independent experiments that the covalent modification of the ligand does not influence the binding parameters - a proposition certainly not justified in the case of MHC class I molecules, where both N and C termini are tightly bound in a network of hydrogen bonds (review: [28]). In fact, fluorescent labelling of the peptide almost anywhere is bound to interfere with the kinetic or equilibrium parameters of the binding reaction.

It is, however, possible to use a completely non-interfering method: the natural fluorescence of proteins. Aromatic side-chains have strongly fluorescent properties ([256, 262], p. 200), and their fluorescence intensity has been shown to depend on their environment in the protein [256], on protein conformation [257], and on the binding of a ligand [260].

Tryptophan fluorescence is most easily followed in proteins because its excitation spectrum does not overlap with the spectra of tyrosine and phenylalanine: therefore tryptophans can be excited and detected selectively [263]; also, tryptophan has the highest fluorescence quantum yield of the aromatic amino acids, therefore its emission is the strongest. The method has been used to look at a variety of receptor-ligand systems (see below), for example antibody on-rate kinetics [264], and changes in tryptophan fluorescence between empty and occupied states of MHC class II proteins have been observed [265].

To follow natural tryptophan fluorescence, no modification whatsoever of the protein is necessary. The signal is recorded in real-time from a fluorescence cuvette containing a buffered solution of the protein at any convenient temperature, minimising interference with natural conditions. Furthermore, the method is nondestructive and allows the complete recovery of the sample after the measurement. As tryptophan fluorescence is weaker than fluorescein or dansyl fluorescence, care must be taken that no contaminant proteins, organic molecules (as buffers or detergents), or fluorescent impurities from vials and equipment are present.

I therefore sought to establish whether the binding of peptides to class I molecules could be measured with the help of fluorescence spectroscopy.

4.2. The structure of class I molecules, and their interactions with peptide, in the context of tryptophan fluorescence

Tryptophans occur infrequently in proteins of the immunoglobulin superfamily, but they tend to be highly conserved within and across families. They have been used to first assign class I molecules to this superfamily [266]. Figure 20 shows that there are 11 tryptophan residues in the D^b heavy chain, and 9 in A68 at conserved positions.

Some of these tryptophans are known from the D^b crystal structure (in the complex with ASNENMDAM peptide) to play a role in the binding of peptide [121] [126]:

Trp-73 hydrogen-bonds the P_6 and P_7 carbonyl oxygens;

Trp-133 (β-sheet) is involved in the second shell of a hydrogen bond network with the peptide;

Trp-147, conserved in virtually all class I molecules, binds the P_8 carbonyl oxygen via a hydrogen bond;

Trp-167 forms van der Waals interactions with the peptide N terminus.

Moreover, Trp-73 (α_1 helix) and Trp-147 (α_2 helix), together with Tyr-156, build a hydrophobic ridge (found also in D^f, D^q, D/L^{v1}, L^d, and L^q; [126]) in the peptide C-terminal half of the binding groove, between the C and E pockets, over which residues P_6 to P_8 are forced to rise out apparently with little or a 'relaxed' contact (see introduction) to the D^b molecule. This is probably one reason why variation in residues P_6 to $P_{\omega-1}$ has not been found to profoundly influence peptide binding [134], and why D^b will bind nonameric to undecameric peptides that probably form loops of different size over this ridge. These spatial relationships are demonstrated in figures 21 to 24.

```
-23  MGAMAPRTLL LLLAAALAPT QTRAGPHSMR YFETAVSRPG LEEPRYISVG
 27  YVDNKEFVRF DSDAENPRYE PRAPWMEQEG PEYWERETQK AKGQEQWFRV
 77  SLRNLLGYYN QSAGGSHTLQ QMSGCDLGSD WRLLRGYLQF AYEGRDYIAL
127  NEDLKTWTAA DMAAQITRRK WEQSGAAEHY KAYLEGECVE WLHRYLKNGN
177  ATLLRTDSPK AHVTHHPRSK GEVTLRCWAL GFYPADITLT WQLNGEELTQ
227  DMELVETRPA GDGTFQKWAS VVVPLGKEQN YTCRVYHEGL PEPLTLRWEP
277  PPSTDSYMHH HHHH*
```

```
-23  MAVMAPRTLV LLLSGALALT QTWAGSHSMR YFYTSVSRPG RGQPRFIAVG
 27  YVDDTQFVRF DSDAASQRME PRAPWIEQEG PEYWDRNTRN VKAQSQTDRV
 77  DLGTLRGYYN QSEAGSHTIQ MMYGCDVGSD GRFLRGYRQD AYDGKDYIAL
127  KEDLRSWTAA DMAAQTTKHK WEAAHVAEQW RAYLEGTCVE WLRRYLENGK
177  ETLQRTDAPK THMTHHAVSD HEATLRCWAL SFYPAEITLT WQRDGEDQTQ
227  DTELVETRPA GDGTFQKWVA VVVPSGQEQR YTCHVQHEGL PKPLTLRWEP
277  SSQPTHHHHH H*
```

Figure 20: Tryptophans in the D^b-His_6 (top panel) and HLA-A*6801·His_6 (bottom panel) heavy chain hexahistidine constructs. The full amino acid sequence of the expressed proteins is given, with the tryptophan residues in bold. The signal sequences are underlined; residues are counted excluding the signal sequence). There are 11 tryptophans in the D^b-His_6 and 9 in the A68 heavy chain (their positions are: 51, 60, 73 (D^b only), 107 (D^b only), 133, 147, 167, 204, 217, 244, 274) , and another two in $h\beta_2m$.

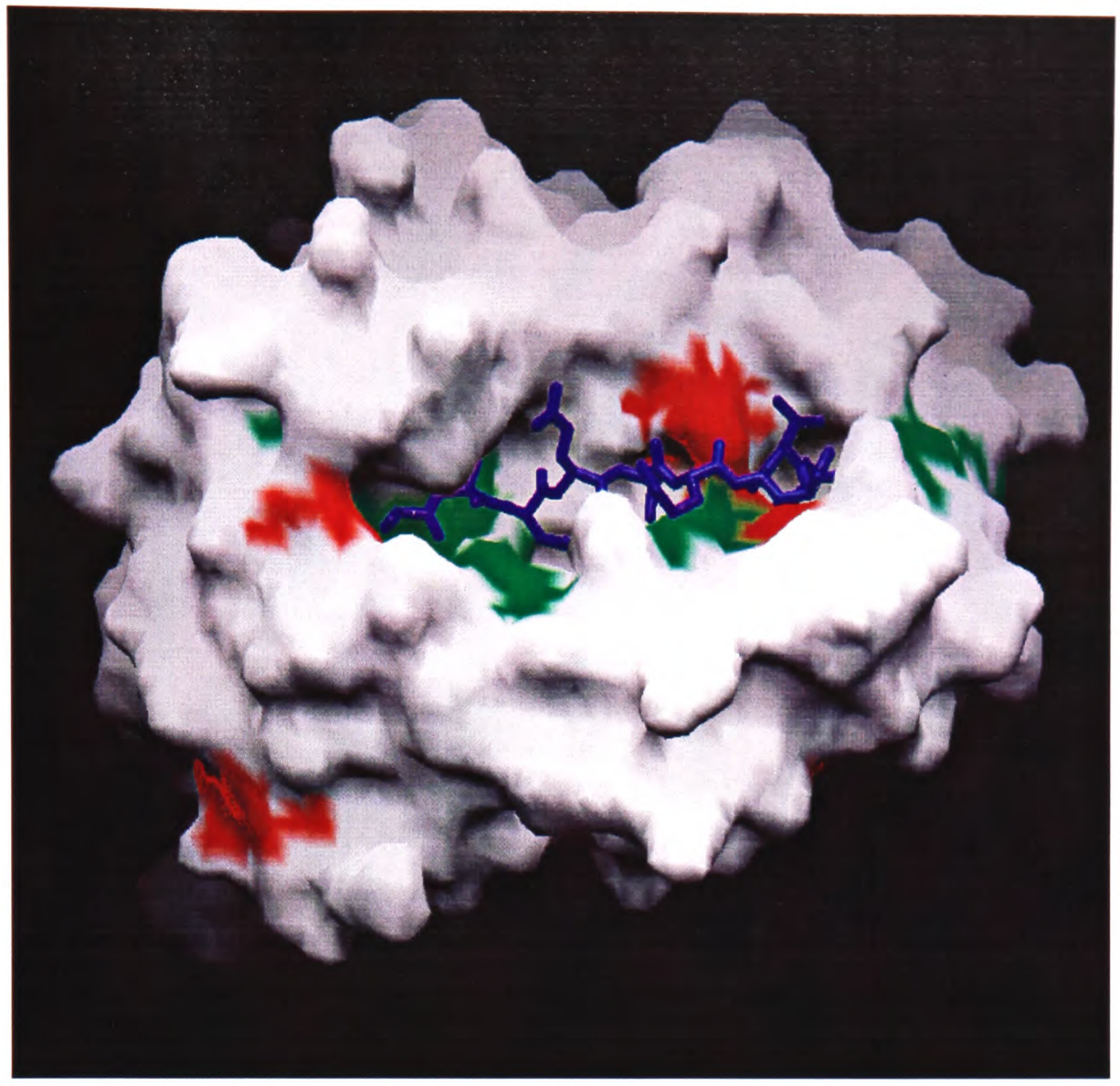

Figure 21: A surface plot (created using the program GRASP) showing the peptide binding site of H-2D^b. The NP(1934)-366-374 peptide ASNENMETM is shown in the groove as a stick model. The peptide N-terminus is on the left, the α_1 helix is the lower. Surfaces of tryptophans and tyrosines are shown in red and green, respectively.

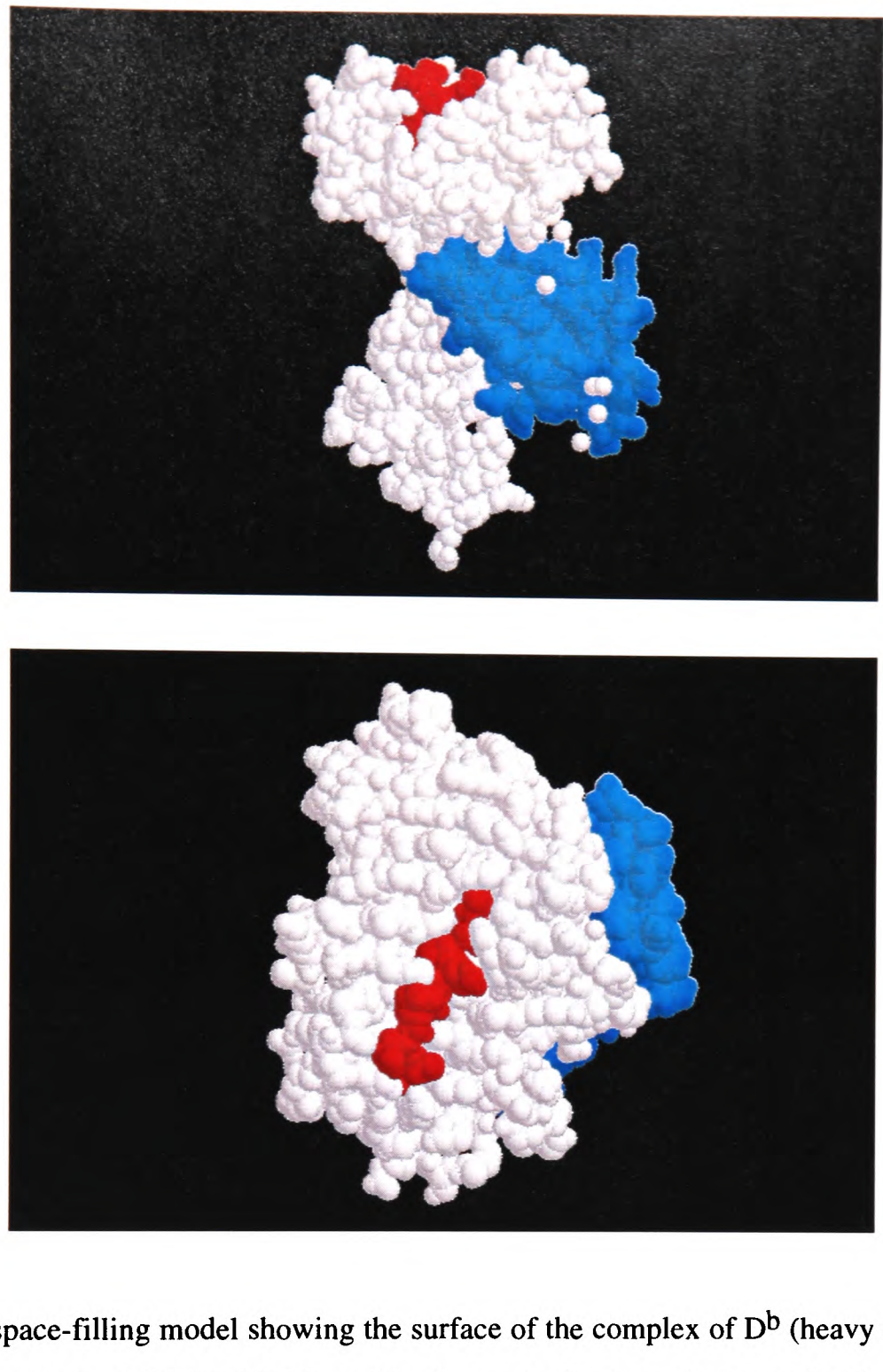

Figure 22: A space-filling model showing the surface of the complex of D^b (heavy chain white, light chain light blue) with the ASNENMETM peptide, demonstrating how deeply buried the peptide is in the binding groove. For this complex, 72% of the surface of the peptide are buried.

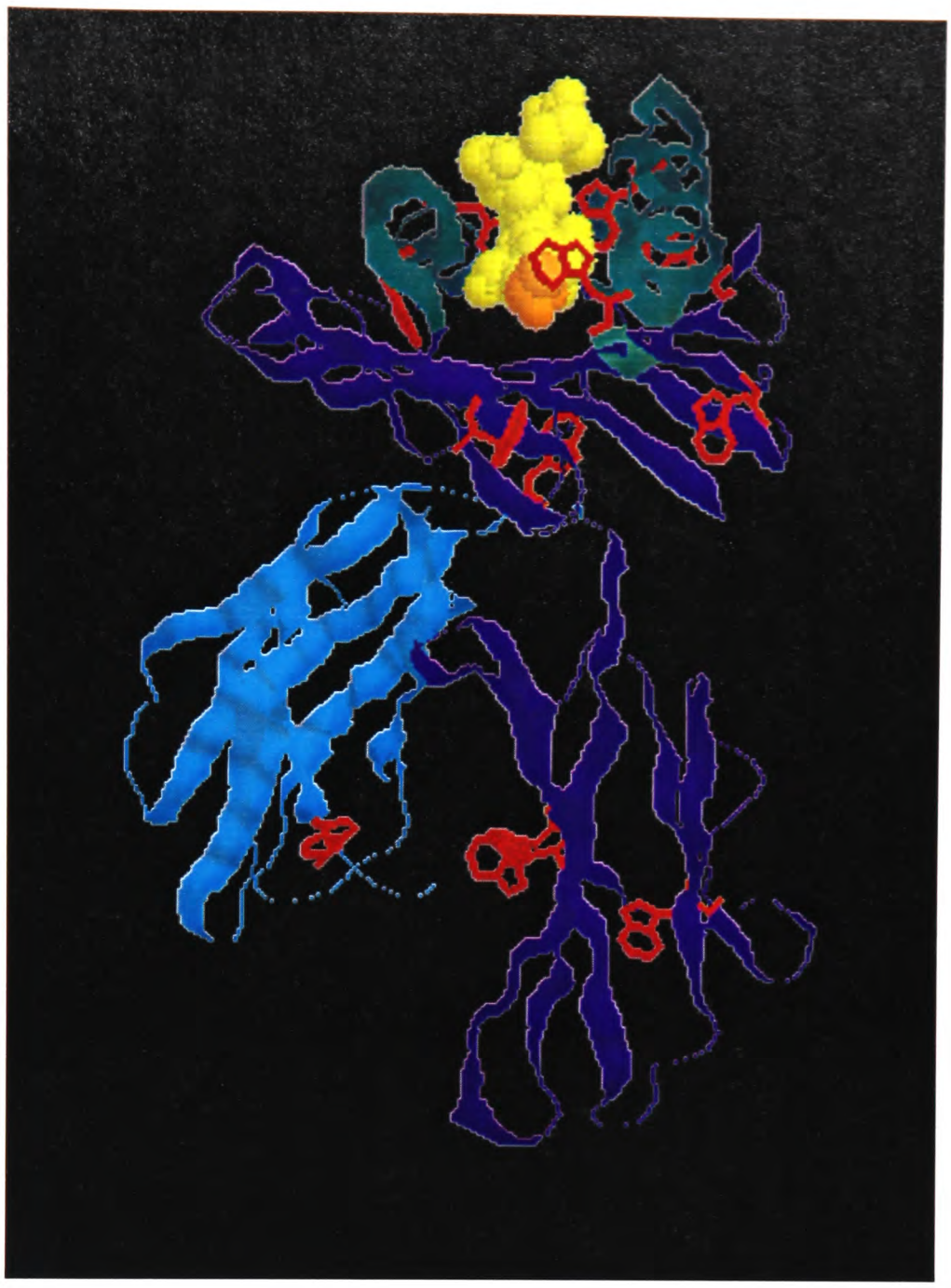

Figure 23: D^b (heavy chain blue, β_2m cyan) in complex with the ASNENMETM peptide, showing all tryptophan side-chains in red. There are eleven tryptophan residues in D^b, and two in β_2m.

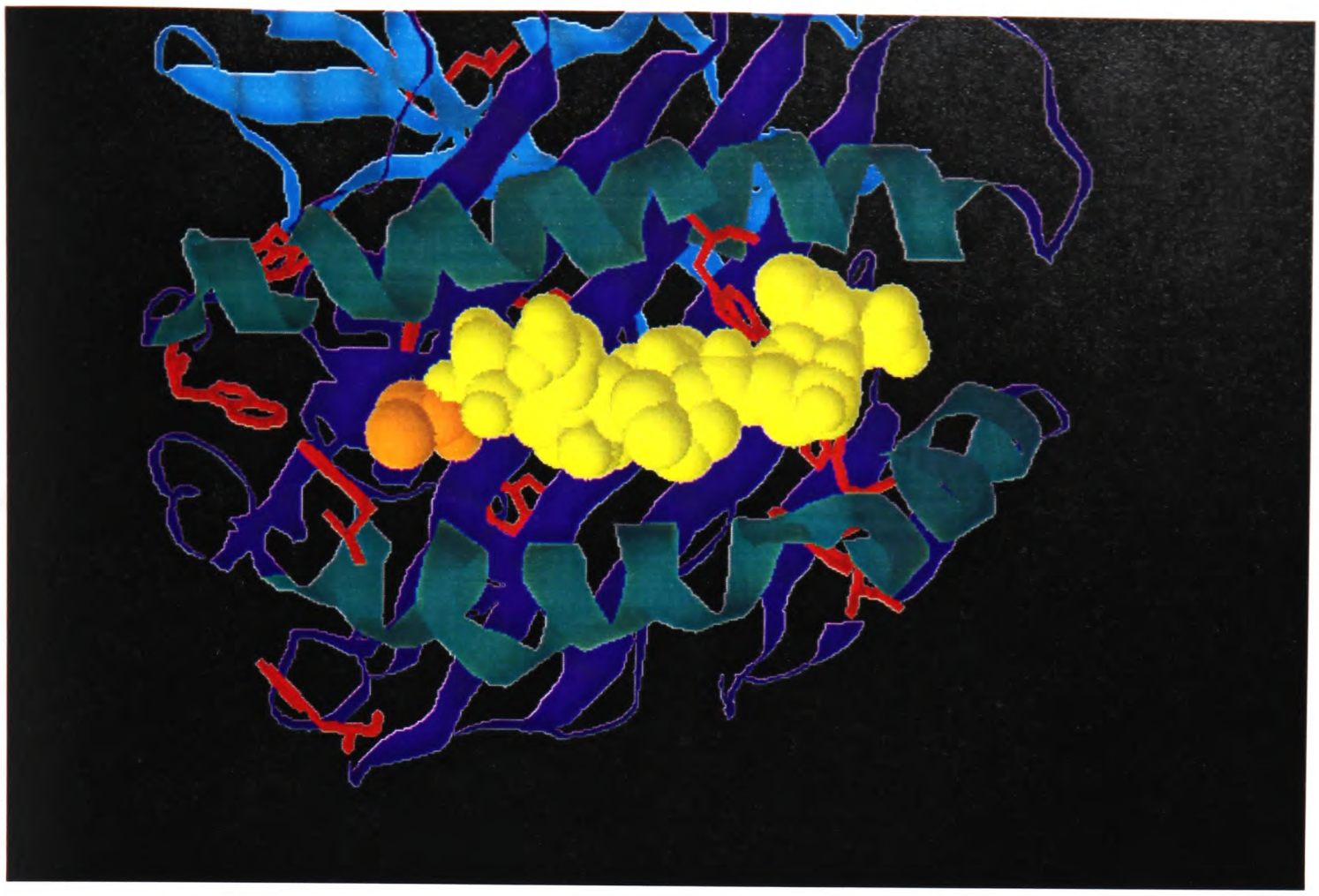

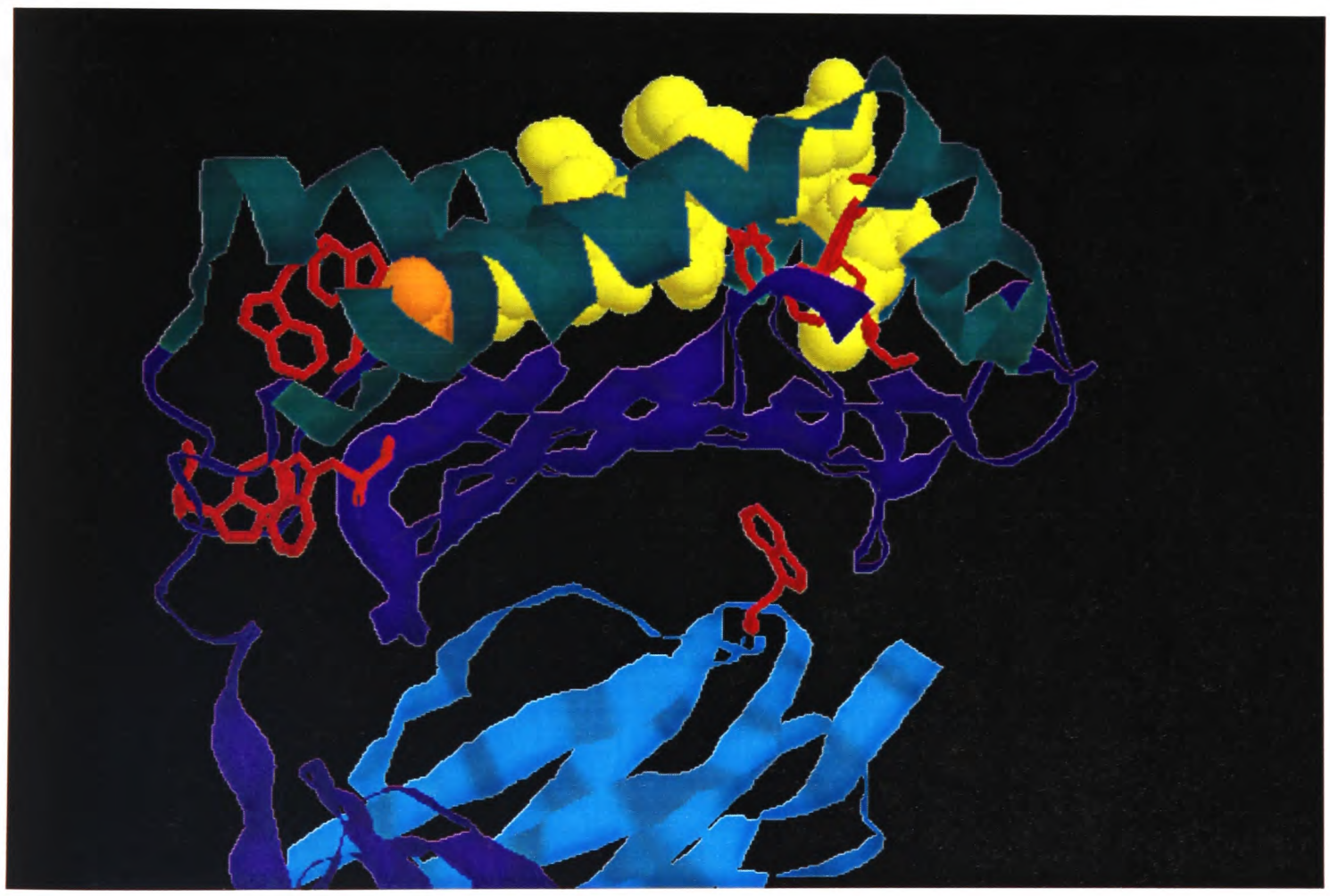

Figure 24: Close-up views of the D^b binding site with the ASNENMETM peptide to show how the tryptophans interact with the peptide. The peptide N-terminus is in orange. The α_2 helix (more strongly kinked) is the lower helix in the upper panel, and the helix in front in the lower panel. The tryptophan involved in van der Waals interactions with the N terminus is Trp-167; and Trp-147 (α_2 helix side) and Trp-73 (α_1 helix side) form the ridge over which the peptide bends out.

The hydrogen bonding interactions of tryptophan side chains usually involve the indole nitrogen ($N_{\varepsilon}1$) that is a member of the fluorophore ring. It is therefore plausible that upon alteration of hydrogen bonding networks that involve tryptophans, their fluorescent properties will change.

4.3. Steady-state tryptophan fluorescence experiments

An experiment was set up in which the fluorescence (excitation, 395 nm) of 100 nM D^b-$His_6{\cdot}\beta_2m$ heterodimer was recorded. Figure 25 shows the strong increase in tryptophan fluorescence (corresponding to ca. 6%) and a blue shift of 1.5 nm of the emission peak which were observed upon the addition of 100 nM NP-Y367-374 peptide, while no change was seen when 20 µM of the non-binder NP-91-99 were added. This demonstrated that there was an enhancement of the natural tryptophan fluorescence of Db upon peptide binding, and that this enhancement was sequence-specific and not the result of nonspecific interactions between peptide and protein.

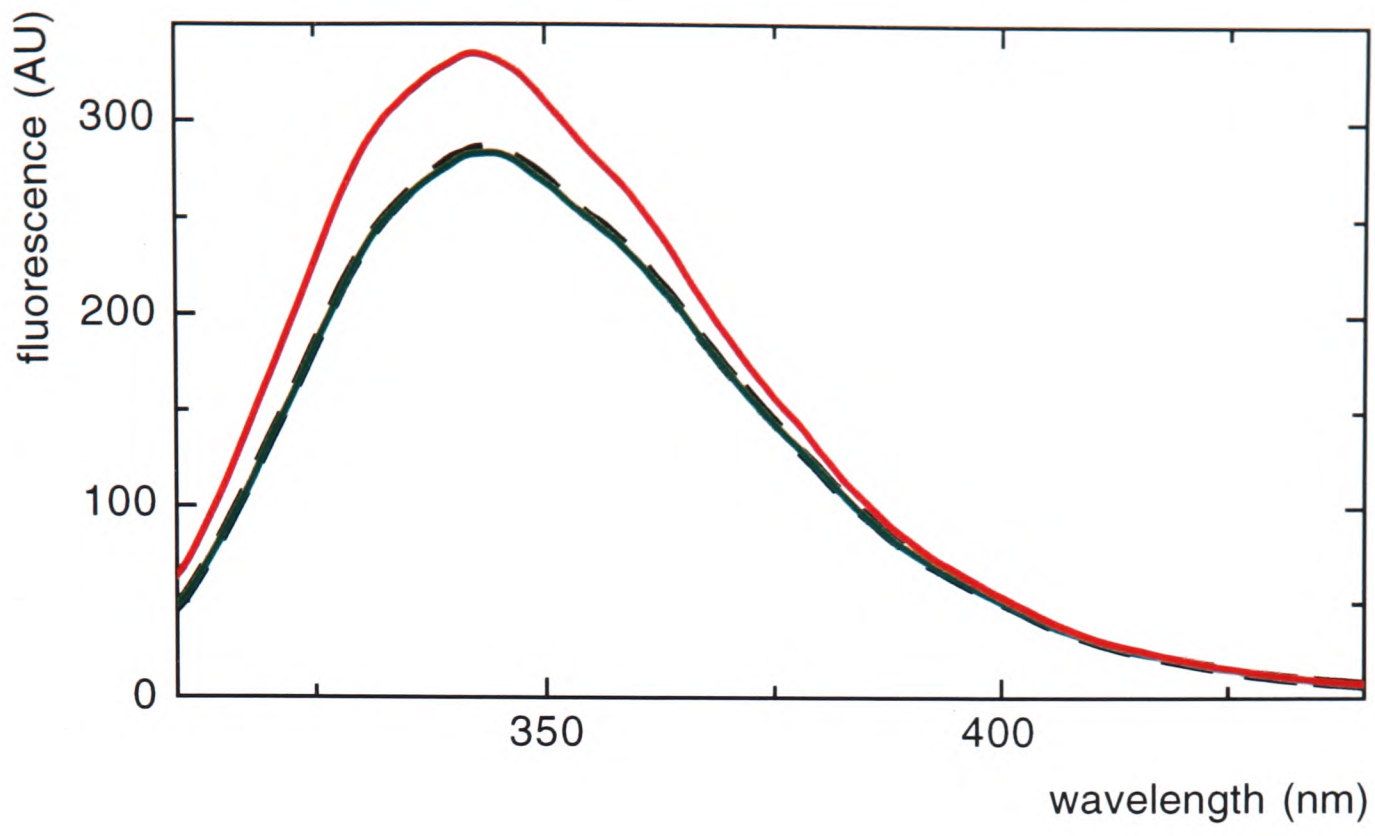

Figure 25: Fluorescence enhancement of D^b-His_6·β_2m upon addition of NP-Y367-374 peptide (emission scan; excitation at 295 nm). Curves [wavelength/value of maximum]: green: 100 nM protein [344/285.9]; red: 100 nM protein + 100 nM NP-Y367-374 peptide [342/334.8]; black/dashed: 100 nM protein + 20 µM NP-91-99 peptide (negative control) [344/283.8].

The fluorescence enhancement is specific for the NP peptide.

The value of the enhancement is 17.6%, and the blue shift is about 2 nm.

An increase in tryptophan fluorescence can be interpreted as a higher hydrophobicity value in the environment of the fluorophore [257]. The increase seen here could originate from: firstly, the shielding of the tryptophan residues in the binding groove (residues 73, 133, 147, 167) from water by the peptide, leading to a less polar environment for the fluorophore; secondly, the direct (residues 73, 147, 167) or indirect (residue 133) interaction of peptide side-chains with tryptophans via hydrogen bonds and alterations in the electron density of the fluorophore; or thirdly, it could be the consequence of a conformational change following peptide binding which brings other tryptophan side chains, even those distant from the binding site, more into the hydrophobic interior of the protein. As all of the thirteen tryptophan residues in the complex could act as fluorophores, the effect is likely to be a mixture of different contributions from different residues. (Direct hydrogen bonding interactions involving tryptophans would, theoretically, increase the polarity of the environmant of the tryptophans, and lead to a decrease in fluorescence; see below.)

To establish which effect made the greatest contribution, the peptide CSANNSHHYI (LCMV GP-92-101; kindly provided by Dr. Jean Gairin), was tested in an analogous experiment. Compared to NP-Y367-374 (YSNENMDAM), the loop P_6-$P_{\omega-1}$ is one amino acid longer and basic : Ser-His-His-Tyr opposed to Met-Asp-Ala. Although the structure of the GP-92-101 in the complex with D^b has not been determined, this loop is very likely to contact the Tyr/Trp_2 ridge in D^b in a different way.

The GP-92-101 peptide had been shown before to bind in the isoelectric focusing assay (see above figure 13). Change in the fluorescence signal was observed upon addition to the HC·β_2m complex, but in this case the fluorescence decreased (see figure 26).

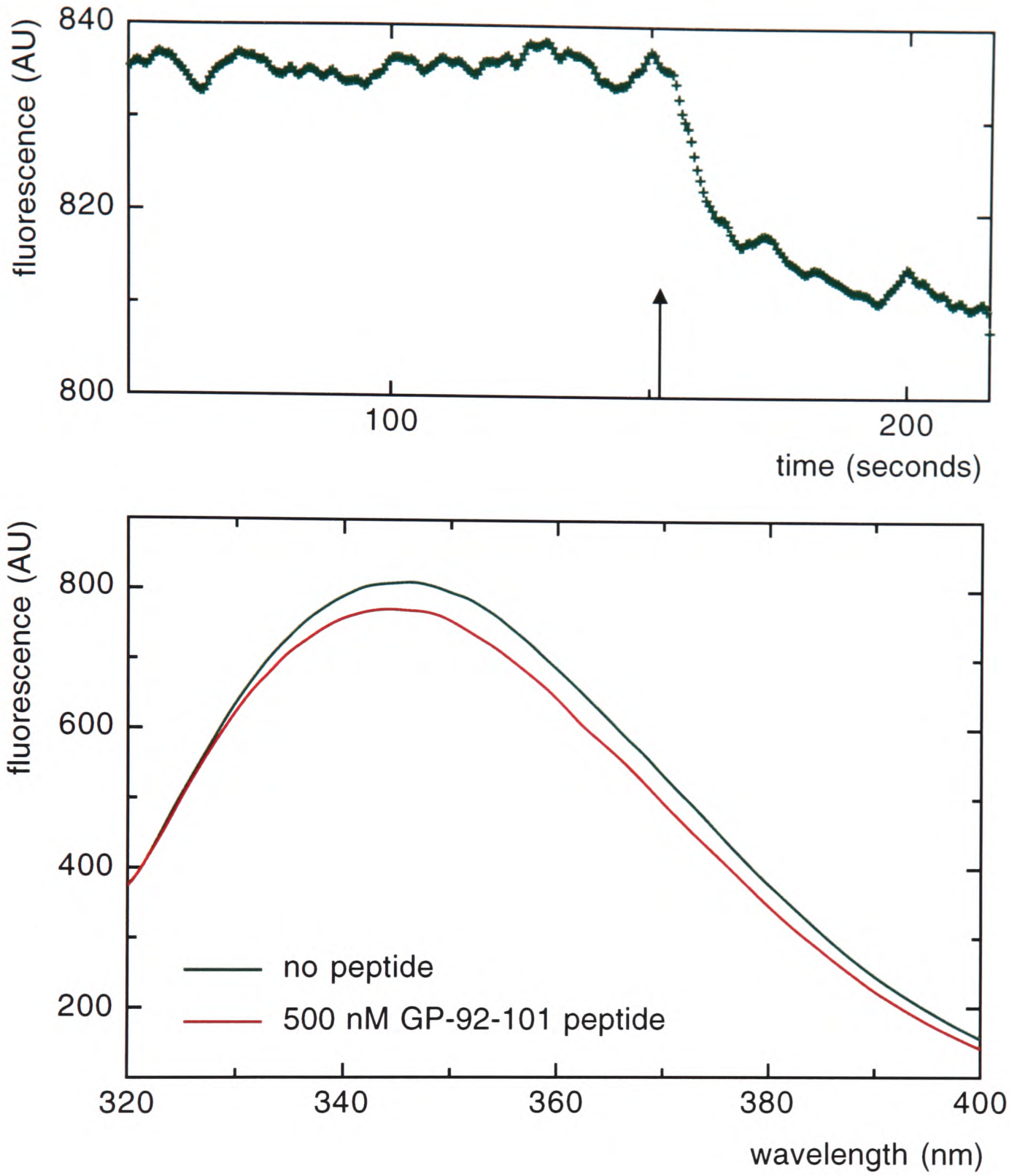

Figure 26: Reduction of fluorescence upon binding of the GP-92-101 peptide (CSANNSHHYI) to D^b. Top panel, timedrive (excitation 294 nm, emission 355 nm) with addition of 500 nM peptide at the arrow. The slowness of the decrease is probably due to insufficient mixing in the cuvette. Bottom panel, spectra before (green; maximum: 344.9 nm / 782.5 AU) and after (red; maximum: 344.5 nm / 774.7 AU corrected for dilution) peptide addition.

There is a blue-shift of 0.4 nm, and a fluorescence decrease of 4.5%.

This indicates that a major part of the fluorescence change depends upon the sequence of the peptide, and is therefore not caused by overall conformational change in the protein. It is more likely that those tryptophans that bind peptide-specific residues, Trp-73, Trp-147, and Trp-167, make the greatest contribution to the overall change, that their emission is strongly influenced by direct interactions with peptide side-chains, and that they can be influenced in different ways by different peptide sequences. Study of the fluorescence change properties of the hybrid peptides ASNENSHHYI and CSANNMDAM would resolve this matter; solution of the crystal structure of the GP-92-101 complex would provide an interesting second angle on this question.

Subsequently, other peptides were tested for their ability to alter the fluorescence of the D^b HC·β_2m complex. Some of the graphs are shown in figure 27 while the data are summarised in table 2.

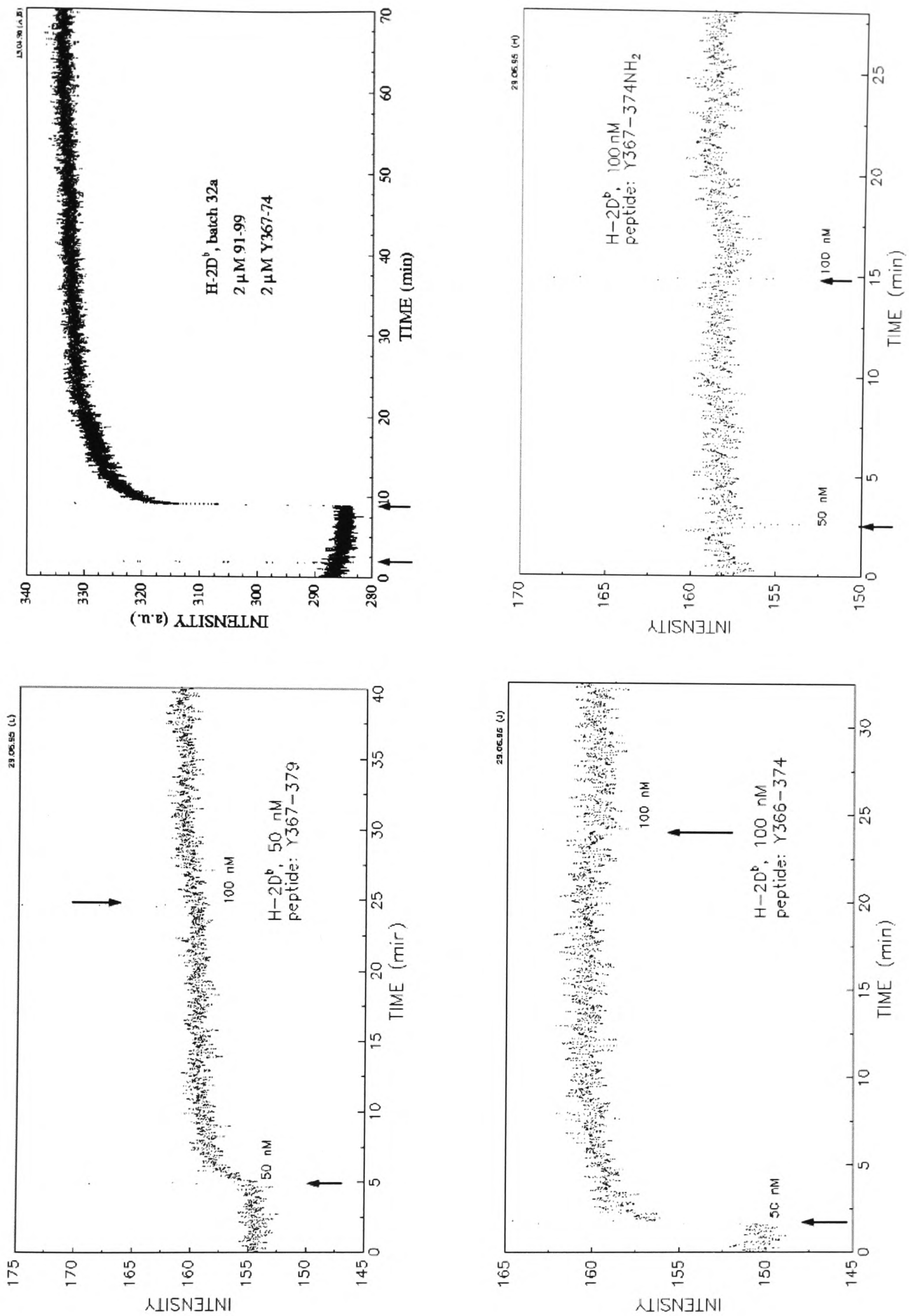

Figure 27: Fluorescence enhancements with different peptides. Time drives, observing fluorescence at 350 nm, with excitation at 300 nm. Protein and peptide concentration as given in the panels. Additions of peptide at the arrows. Enhancement values are in table 2.

Top left, NP-91-99 (first) and NP-Y367-374; top right, NP-Y374-374NH_2; bottom left, NP-Y367-379; bottom right, NP-Y366-379. Experiments done by Klaus Döring.

peptide	concentration (nM)	fluorescence enhancement	binding affinity M^{-1} (4 °C)
NP-366-374 ASNENMDAM	100	11 %	≈ Y367-374
NP-Y367-374 YSNENMDAM	100	12 %	$5.4 \cdot 10^7$ (1)
SV-324-332 FAPGNYPAL	100	13%	$9.24 \cdot 10^7$ (2)
NP-91-99 KTGGPIYKR	2,000	0 %	no binding
NP-Y367-374NH_2 YSNENMDAM-NH_2	50; 100	1 %	no binding
NP-Y366-374 YASNENMDAM	50	7 %	ND
NP-Y367-379 YSNENMDAMESSTL	50	5 %	$4.35 \cdot 10^6$ (1)
NP-Y365-379 YIASNENMDAMESSTL	50	2 %	$3.8 \cdot 10^5$

Table 2: Fluorescence enhancements for peptides at the given concentrations, at room temperature. In the last column, known affinities are given for comparison; they come from table 6 below and from work by Cerundolo ([15] and pers. comm.) (1): iodinated peptide, (2): tritiated peptide. ND, not determined.

The SV-324-332 peptide FAPGNYPAL shows a fluorescence increase comparable to NP-Y367-374. For the other peptides - all modifications or extensions of the NP-Y367-379 sequence - the fluorescence enhancements at a given concentration correspond to the binding affinity of the peptides as far as it has been measured by other methods such as assembly assay or radioligand binding assay (table 2 and below, table 6). However, the intensity of the fluorescence will not only depend on the amount of class I molecule

occupied at that particular peptide concentration, but also on the way in which the peptide side chains interact with the tryptophans of the class I molecule. A simple binding experiment is therefore not enough to determine the binding affinity of a completely unknown peptide; instead, if an effect is seen, a binding curve with different peptide concentrations (step titration) should be recorded (see below, figure 40).

4.4. Thermal stabilisation of D^b-His_6·β2m by peptide

While the protective effect of peptide against detergent denaturation of class I HC·β_2m complexes was first observed in the Townsend laboratory [43, 14], the thermal stabilisation of class I molecules by their peptide ligand has been measured by Bjorkman and collaborators for H-2K^d [219] and by Bouvier and Wiley for HLA-A2 [141], both by circular dichroism. I therefore undertook to use the fluorescence enhancement effect to assess the stabilisation of the D^b HC·β_2m complex in a thermal denaturation experiment.

100 nM HC·β_2m (not purified by IEF and therefore a mixture of peptide-occupied and unoccupied molecules) was heated in the fluorimeter at a rate of 1K per three minutes while fluorescence was recorded. On a background of a linear fluorescence decrease with temperature [256, 253], a sharp transition at 56 °C was observed in the presence of peptide (figure 28). When no peptide was added, a weaker transition around 28 °C took place, followed by a long 'tail'.

The most likely interpretation of these data is that the weak transition represents the denaturation of empty HC·β_2m complexes, and that the 'tail' represents the gradual denaturation of complexes with endogenous peptides of different binding affinities. The term 'denaturation' used here does not necessarily imply dissociation of β_2m from the HC at 30 °C; in fact, binding experiments conducted at this temperature indicate that the complex is still able to bind low concentrations of peptide, albeit much more slowly. It is more likely that the 'melting' or 'denaturation' signal comes from a partial unfolding of the empty binding site (discussed below: see figure 33), representing a second specific change in the fluorescence of the Db·β_2m complex (see additional evidence below).

With 1 μM NP-Y367-374 peptide present, the transition at 56 °C is very definite and no signs of denaturation are seen at lower temperatures (see the first-derivative curve in figure 28), although only partially empty D^b had been used. The most likely explanation for this is the rebinding of NP-Y367-374 peptide to D^b molecules that were thermally emptied of low-affinity peptides (as seen in the -peptide curve between 30 and 50 °C), and their subsequent stabilisation. This also indicates that the YSNENMDAM peptide is at the highest stability end of the range of peptides that are bound to our D^b complex when it is isolated (see below).

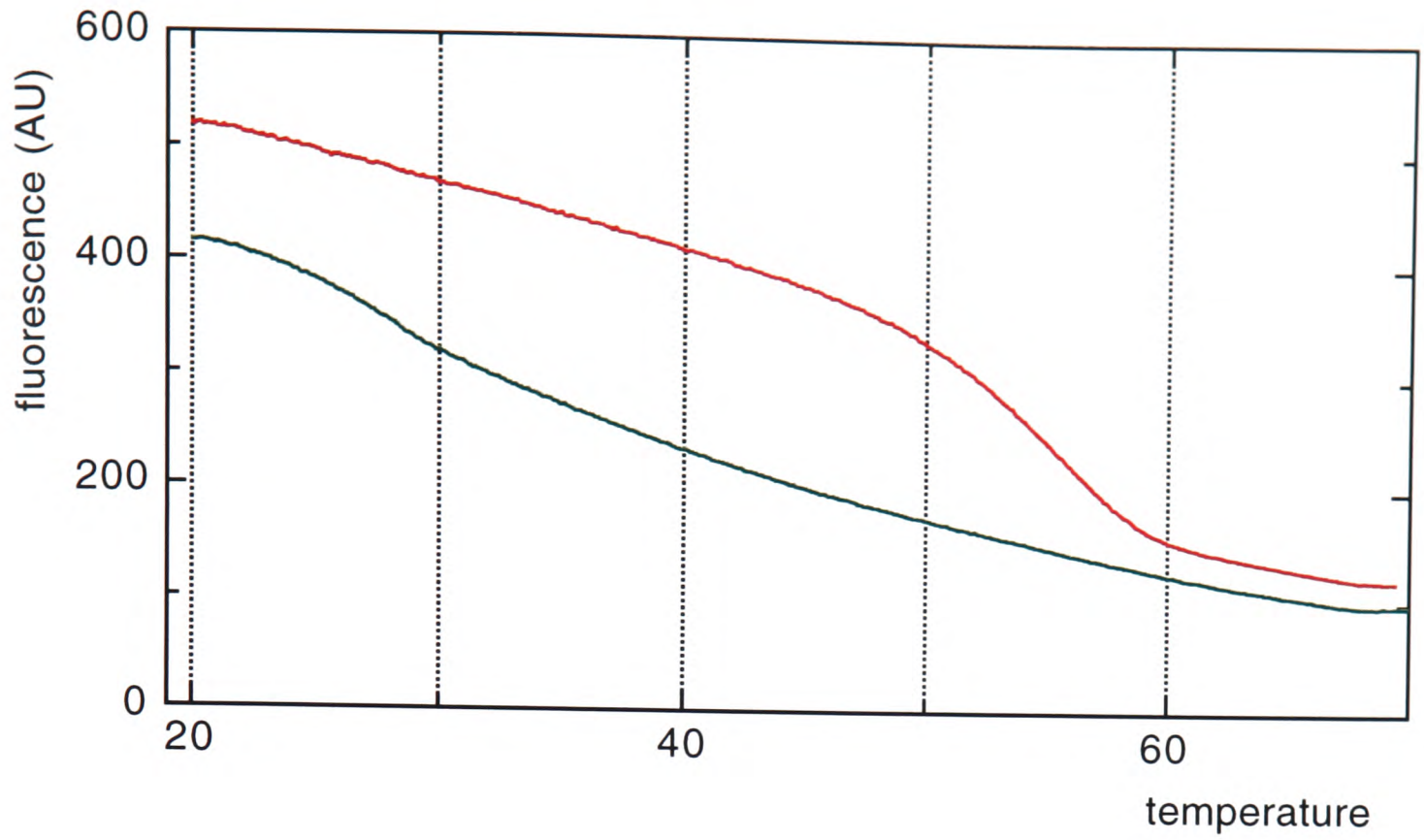

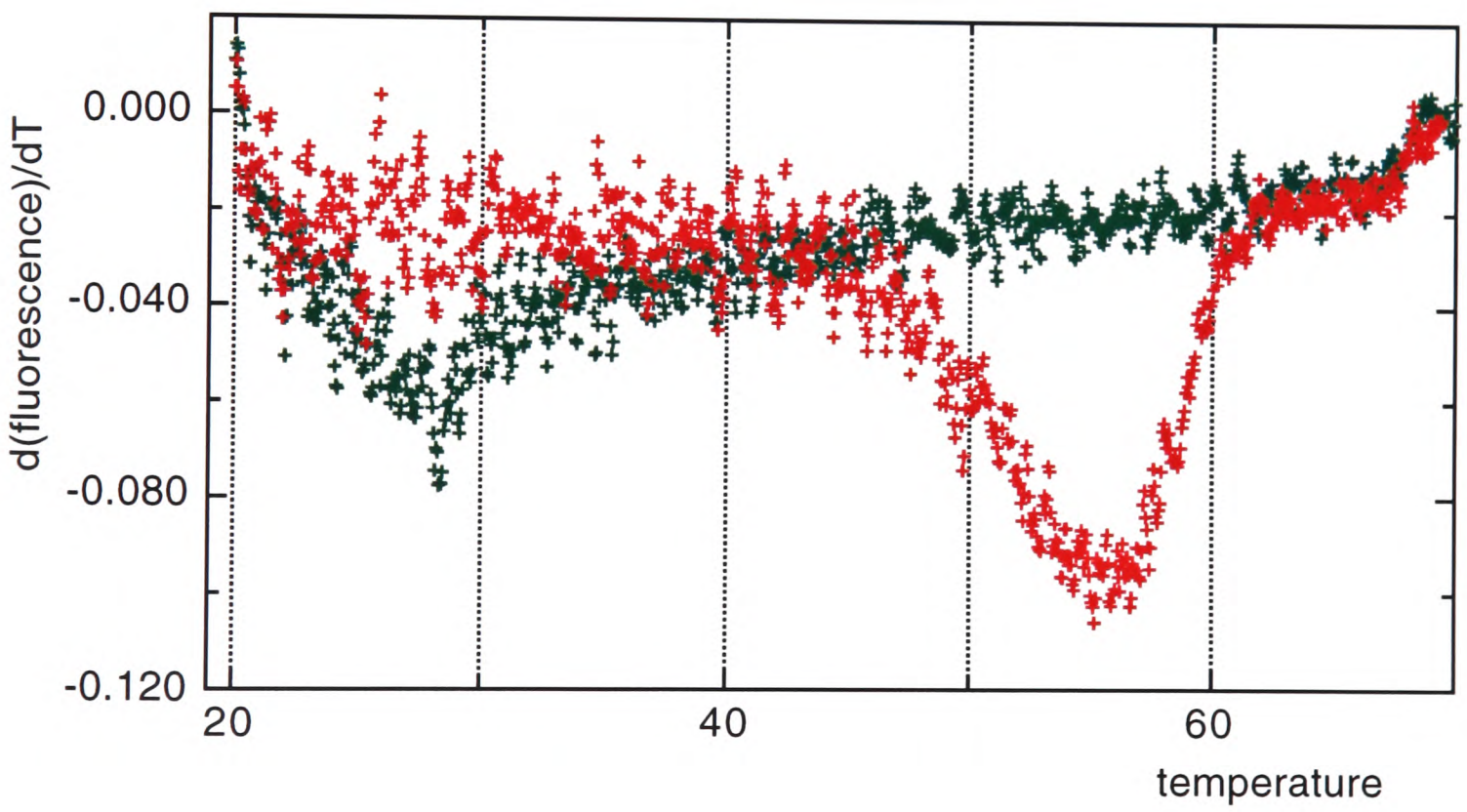

Figure 28: Thermal stabilisation of D^b-His_6·β_2m by NP-Y367-374 peptide.

Top panel, fluorescence (excitation, 295 nm; emission: 345 nm) of 100 nM D^b-His_6·β_2m in the presence (red) or absence (green) of 1 µM peptide, against temperature (heating rate 3 min/K); bottom panel, first derivative curves.

The peptide-incubated material shows a sharp transition at 56 °C; the untreated material shows a weaker transition at 28 °C and a long 'tail'. Deatails see text.

If this interpretation is correct, the data would indicate a slightly lower thermal stability of D^b compared to the data of Bjorkman et al. [219] who find an unfolding transition midpoint of 45 °C for the empty and 57 °C for the occupied K^d molecule, and also give the melting point for β_2m as 64 °C (see detailed description below).
Bouvier and Wiley [141] find 75.5 °C for HLA-A2 binding GLLGFVFTV (even beyond the melting temperature of β_2m!), and down to 42.8 °C with variants of this peptide.

A closer look at the denaturation curve of empty D^b in its first-derivative form (figure 28) suggests that the optimal nonamer, NP-Y367-374, is of very high affinity compared to the peptides endogenously bound to D^b in CHO cells: at least 90% seem to have already dissociated at a temperature of 50 °C.

I attempted to use this effect to remove peptide from the binding site of the (non-IEF-purified) HC·β_2m complexes by heating to 50 °C for 30 minutes and separating the complex from eluted peptides by Sephadex G-25 gel filtration (see materials and methods) at this temperature. The protein from the eluate was able to bind peptide when cooled back to room temperature, even with an increased fluorescence intensity enhancement (see figure 29: 19.2% against 15.4%, indicating that more sites per unit protein were now available to binding); however, on native IEF gels no purification effect was seen that was comparable to IEF-separated material (see figure 14, lanes e/f against lanes c/d). A possible reason for this is that some of the protein denatured during heating or cooling without peptide.

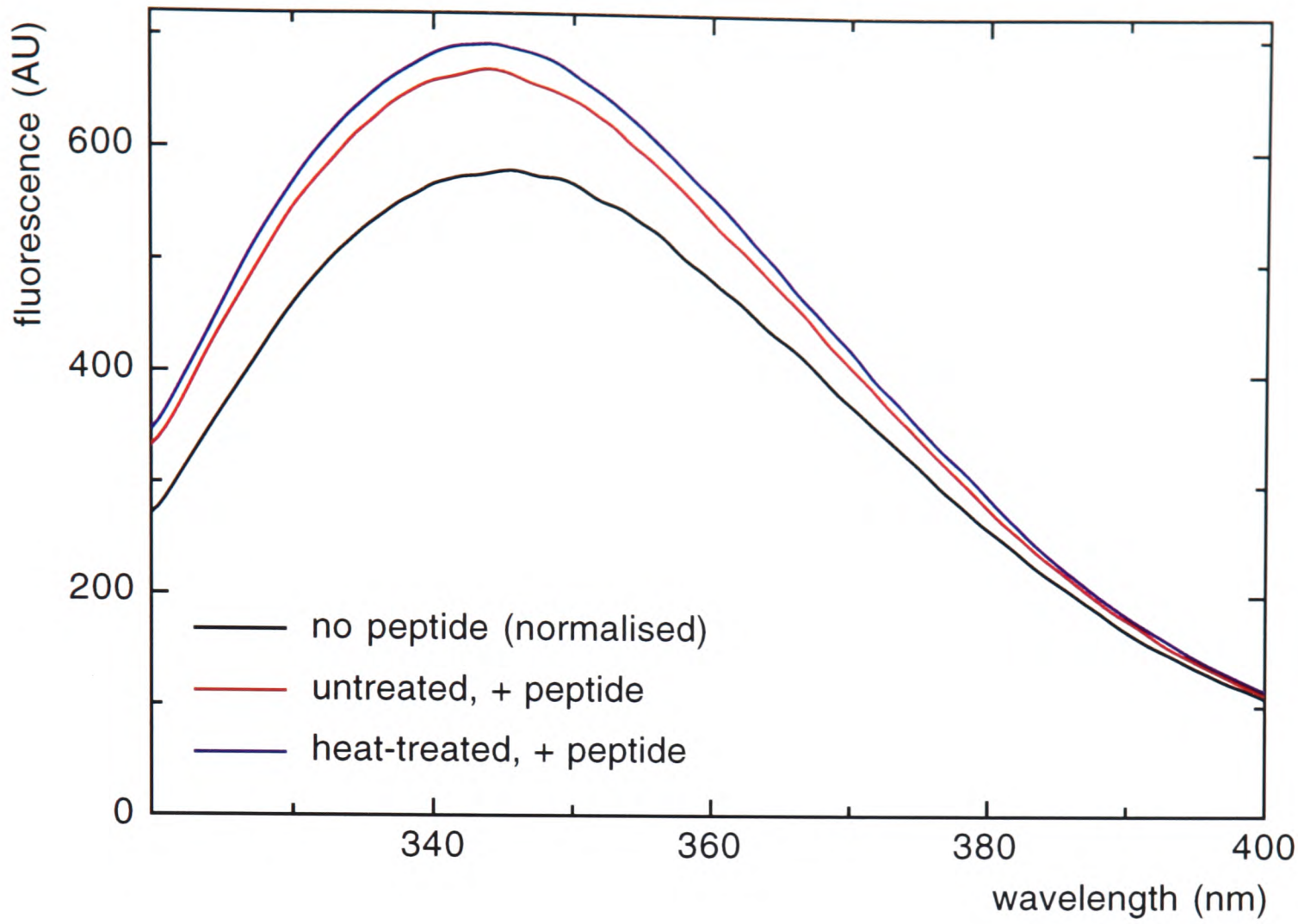

Figure 29: Heat-treatment of the D^b complex increases peptide binding (fluorescence emission scan). Identical fluorescence binding experiments were performed with untreated and heat-treated material. Peak values (maximum/fluorescence): no peptide, 345.5/581.13; untreated, 344.0/670.55 (15.4% enhancement); heat-treated, 344.0/693.05 (19.2% enhancement).

I have also conducted experiments to determine the temperature stabilisation of D^b using CD measurements analogous to Bjorkman's (see below).

4.5. Fluorescence time drives

I attempted next to determine the time-scale on which the fluorescence changes occurred. Fluorescence emission was recorded at a fixed wavelength (usually 345 or 350 nm) with time, and NP-Y367-374 peptide added at a given time.

In initial experiments using Nickel beads - eluted material, the on-reaction could be resolved into three different components (see figure 30): one component that was too fast to be recorded, and made up 50% or more of the intensity enhancement; a second component with a half-time in the range of minutes; and a third component that was extremely slow.

When the gel filtration purification was introduced, I could show that material from the early peak, containing the high molecular weight aggregates and many contaminating proteins, showed slow association with only the medium and the slow component (see figure 31, lower panel), whereas the low molecular weight peak showed the fast and the medium component, and also a greater fluorescence enhancement per unit protein than the early peak (12.1% against 4.2%, see upper panel in figure 31). This indicates that in the crude protein preparation, multimeric aggregates of HC·β_2m were dissociating in a pre-equilibrium, slowing down the peptide binding process.

Still, two association constants remained, one of them too fast to determine in a conventional fluorimeter (also termed steady-state fluorescence measurement): the increase was complete within seconds, and stirring in the fluorescence cuvette is not good enough to allow for full mixing in less than one minute.

The second, minute-range, component of the binding reaction could be reduced but never fully removed by heat-treatment of the molecules (see above) and by adding very small amounts of detergent (0.06% n-octyl tetraoxyethylene, C_8E_9; Klaus Döring, pers. comm.). It was still partially present in the material that had been purified by IEF. This slow time-constant could represent a real effect, such as the slow isomerisation of the complex after initial peptide binding (see discussion), or it could represent an artefact of protein denaturation or binding to the cuvette walls.

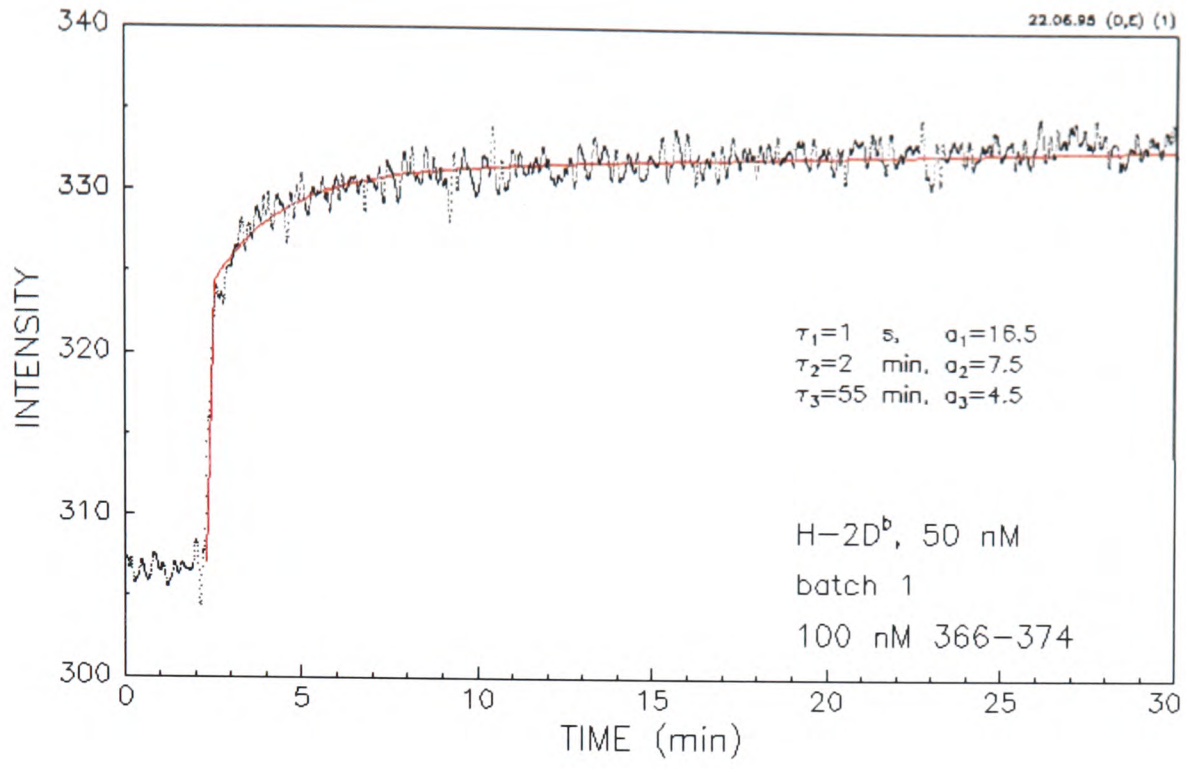

Figure 30: On-rate of fluorescence enhancement (time-drive of fluorescence intensity).

In this and all other time-drive experiments, excitation was at 300 nm and emission 350 at nm unless mentioned otherwise.

50 nM D^b complex (by absorption), not purified by gel filtration.

On the addition of 100 nM NP-366-374 peptide (the little downward peak in the curve due to the opening of the sample compartment), fluorescence increases rapidly. Three time constants derived by computer fit, and their respective amplitudes, are given in the caption.

The overall fluorescence enhancement in this experiment is 9%.

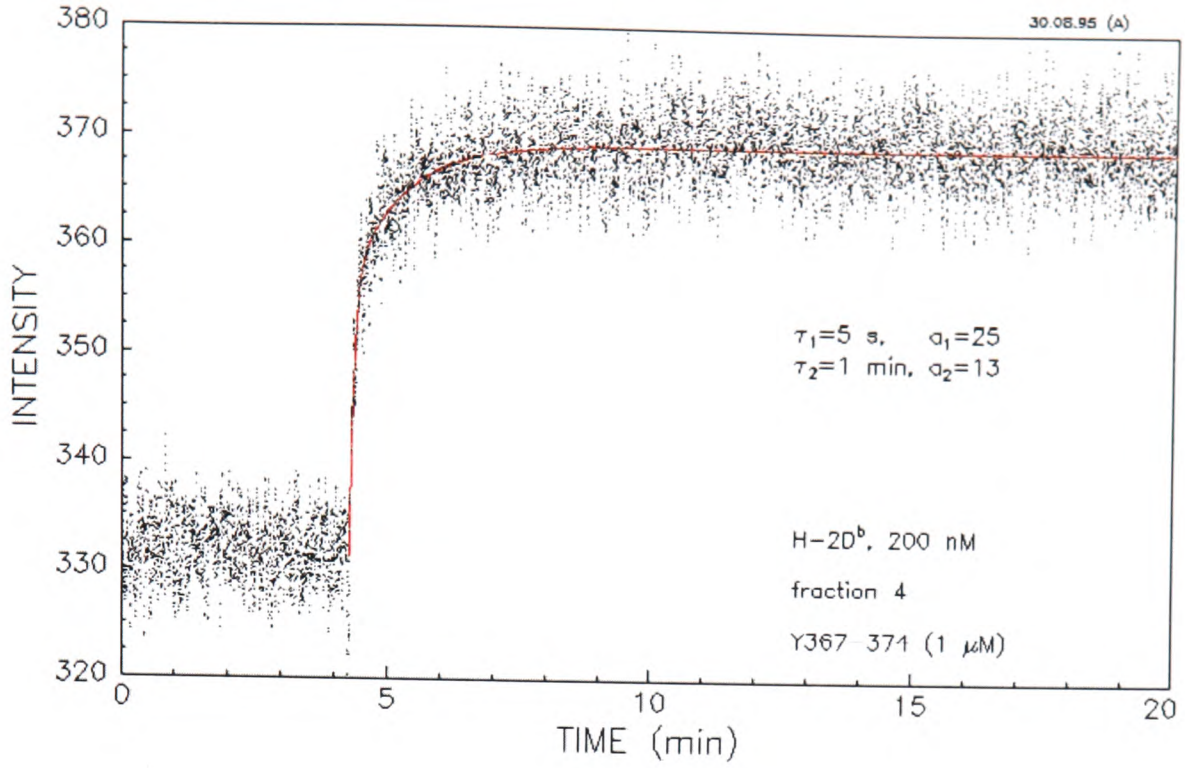

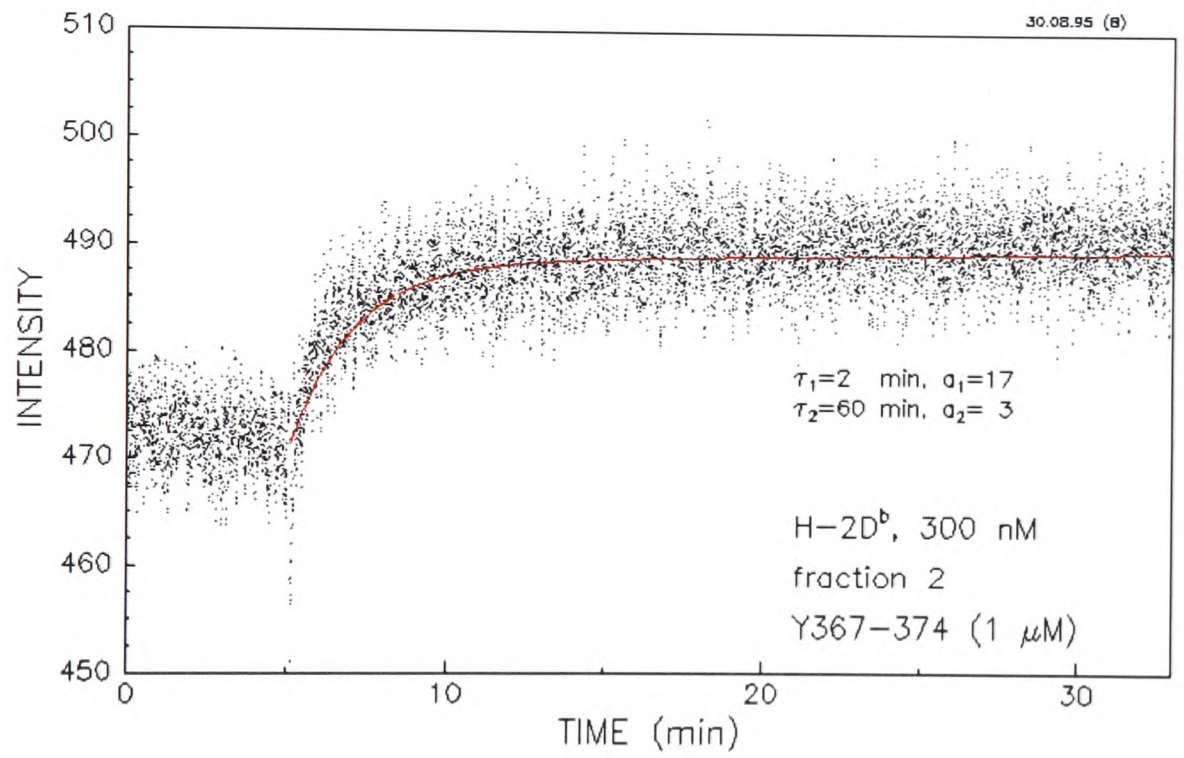

Figure 31: fluorescence enhancement time-course of fractions from the late peak (top; 200 nM protein) and the early peak (bottom; 300 nM protein) of the gel filtration eluate, using 1 μM NP-Y367-374 peptide.

The early peak binds less peptide per unit protein (4.2% enhancement as opposed to 12.1%), but also binds far more slowly, indicating perhaps the dissociation of aggregates.

The influence of temperature on the on-rate

I was interested to look at the temperature dependence of this binding reaction. Processes that involve conformational changes in proteins are very often strongly temperature-dependent, whereas diffusion and the rate of diffusion-controlled reactions vary little with temperature [267], so that temperature dependence of rates can be an important indicator of mechanistic details of a reaction. The on- and off- rates for peptides and D^b molecules measured by Cerundolo et al. [15, 208] were strongly temperature-dependent.

The time-drive experiments were therefore repeated at different temperatures. At temperatures between 4 °C and 25 °C, the binding curves looked indistinguishable (see figure 32). However, when the assay was done at 37 °C, the binding of peptide was much slower.

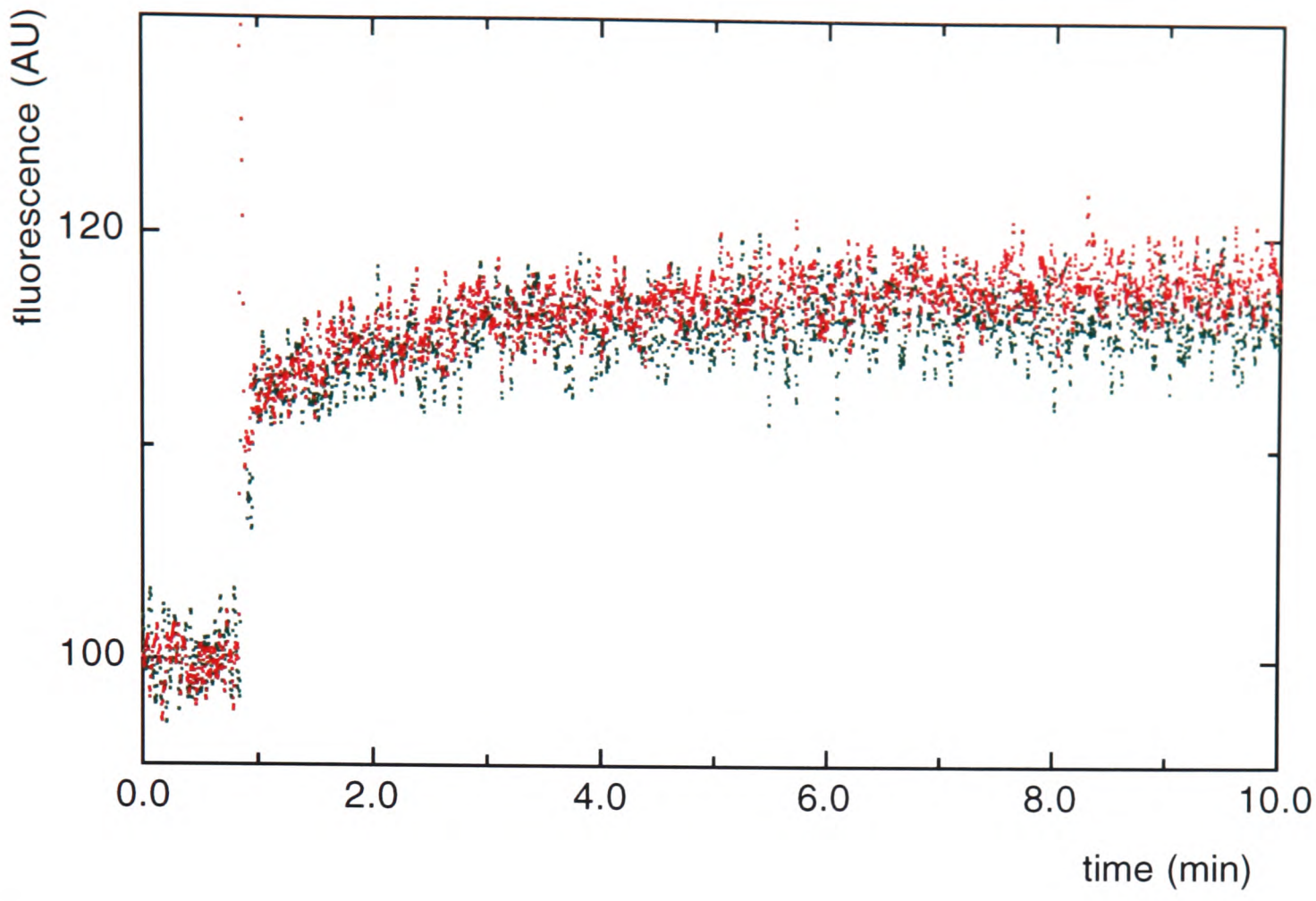

Figure 32: Comparison of on-rates at 4 °C and 15 °C (fluorescence time-drives). To 55 nM D^b in the cuvette (initial fluorescence values normalised to 100), 2 µM NP-Y367-374 were added at t= 50". Red curve, 4 °C; green curve, 15 °C. Experiment done by Klaus Döring.

There is no apparent difference in the on-rates in this apparative setup; this is due to the slow mixing in the cuvette that becomes time-limiting. See below, 37 °C, and stopped-flow experiments.

To determine why this was the case, the following experiment was carried out (see figure 33): one aliquot of a D^b solution had 1 µM NP-Y367-374 peptide added to it and was then heated from 20 to 37 °C. There was a decrease in the fluorescence signal (12%), most likely from the natural decrease of the fluorescence with temperature, but no profound effects.

Then, another aliquot was heated to 37 °C without the previous addition of peptide. Here the decrease of the fluorescence was much more pronounced (27%), indicating a structural alteration, and in agreement with the results from the melting curve (see above figure 28). This empty material now bound peptide very slowly, with a half-time of about 60 minutes, but, when followed for a long time, approached and almost reached the fluorescence of the peptide-pre-treated protein at 37 °C (compare the magenta and cyan curves in figure 33, lower panel).

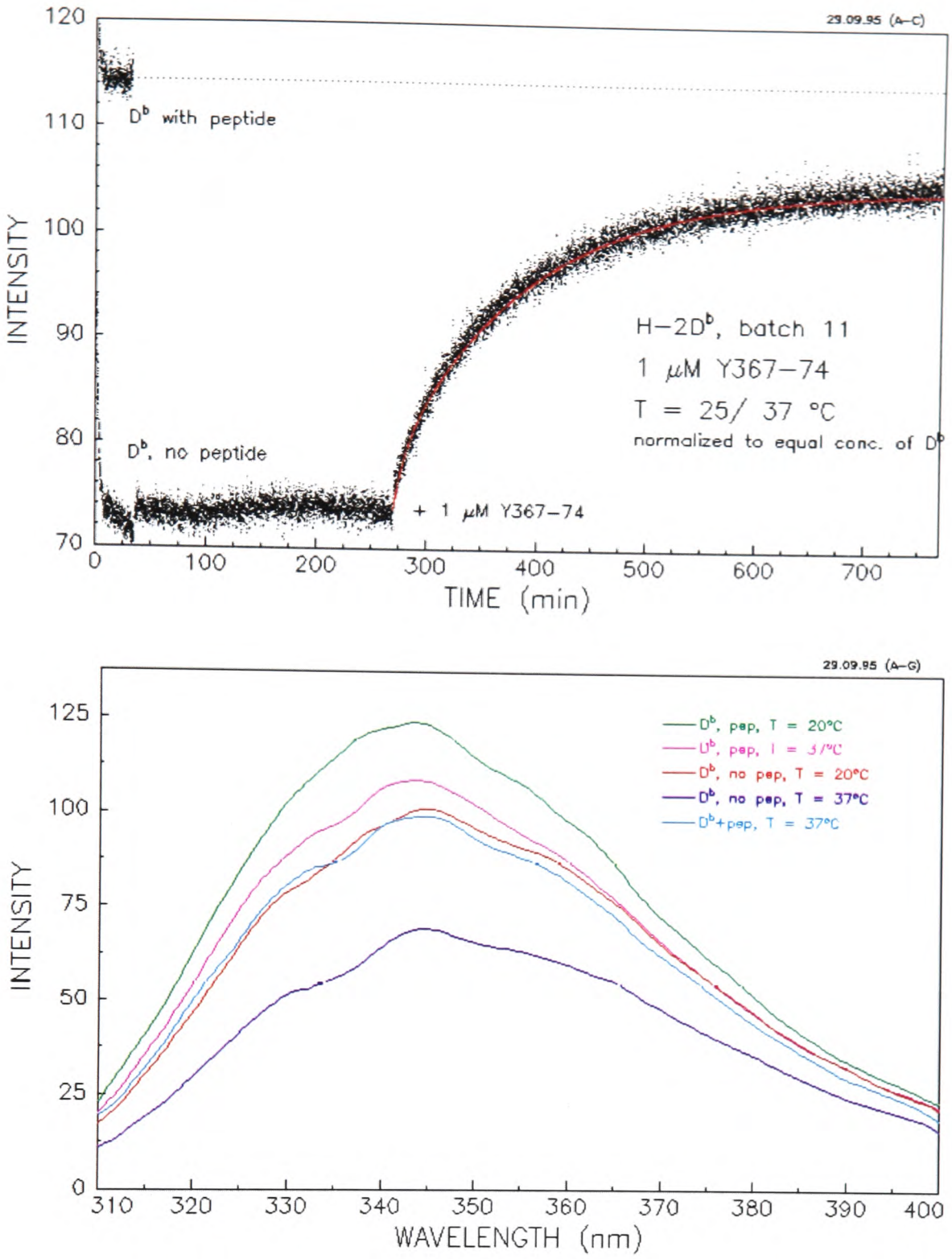

Figure 33: Melting of the peptide-binding domain of D^b at 37 °C.

Time-drive at 345 nm emission (upper panel) and spectra (lower panel).

Upper panel: the upper left-hand curve describes the fluorescence change of D^b-His_6·β_2m with added peptide from 20 °C (t=0, green spectrum below) to 37 °C (t=50', purple spectrum below). The lower curve describes the fluorescence change of empty D^b-His_6·β_2m from 20 °C (no peptide, t=0, int.= 100; red spectrum below) to 37 °C (t=50', int.= 74, blue spectrum below) and further upon the addition of peptide at 37 °C (278' to 760'; final point: cyan spectrum below).

At 37 °C, the binding of peptide is far slower than at room temperature (see time-drives above); the great decrease in fluorescence of the empty molecule upon heating points towards a denaturation process. This denaturation is fully reversible upon peptide binding (cyan curve) or recooling (not shown).

This last result demonstrated that the protein is not irreversibly denatured at 37 °C, but that it is able to bind peptide, albeit more slowly. A likely explanation for these results is that at 37 °C the peptide binding site is 'partially denatured', in a form that does not easily bind peptide anymore. The conformation of β_2m and the α_3 domain seems unchanged, as the protein returns to its normal fluorescence after peptide binding, and the conformation of these domains is not known to be influenced by peptide. Dissociation of β_2m at 37 °C as a cause for the slow binding is unlikely, because peptide binding to the heavy chain alone would require much higher concentrations of peptide [153].

These data agree with and extend the results of the thermal denaturation experiment (see above figure 28) that 'melting' of the empty complex takes place at or even below 30 °C. It can be concluded that at 30 °C and above, the binding site of the empty D^b molecule exists in a state that is reversibly and partially unfolded, and therefore unable to bind peptide with the same kinetic on-rate as when fully native. This suggests that at temperatures below the melting point, the binding site is not completely 'floppy' as it receives peptide, but that the peptide binds to a defined but unstable conformation of the binding site.

The 'molten' state of the binding site at 37 °C was fully reversible, as empty complex heated to 37 °C and cooled to room temperature again binds peptide with the usual rapid kinetics (data not shown); also, 37 °C is the temperature at which the protein is kept in the supernatant during the cellular growth and secretion period; if an irreversible change had occurred during that time, the experiments would not have been possible. (Biological implications of this finding are discussed in the last section.)

5. Binding to recombinant soluble molecules: a new, rapid on-rate confirms the kinetic mismatch

The most remarkable observation about the fluorescence time-drive data above was that they allowed us to observe an on-rate that was significantly faster than any on-rate onto class I molecules measured before (figure 30; see introduction). If the half-time of the fast component is taken to be 5 seconds, at a concentration of 100 nM of peptide the kinetic on-rate would be

$$\frac{\ln(2)}{5 \cdot 1 \cdot 10^{-8}} = 1.3 \cdot 10^{6}\ M^{-1}s^{-1} \text{ at room temperature.}$$

On-rates of this kind are too fast to be recorded in conventional fluorimeters. I therefore decided to determine exactly the novel fast on-rate component in a stopped-flow fluorescence spectroscopy experiment.

5.1. Stopped-flow fluorescence measurements

In stopped-flow fluorescence measurements, two solutions containing the reaction partners are mixed and immediately (within 10 milliseconds) injected into a fluorescence cuvette. Time is counted from the moment of injection. The fluorimeter then records emission, in a given wavelength window, with time. In 0.1 seconds, 2000 points can be recorded. This allows the real-time determination of association constants ([267-269]; for examples see [270-272, 260]).

I performed stopped-flow experiments mixing class I (50 nM) and peptide (variable concentration) solutions in a volume ratio of 10:1, as described in the materials and methods section. Figure 34 (top panel) shows a typical data set obtained from a single injection. To make ligand depletion negligible (see below), the receptor concentration has to be kept as low as possible, resulting in a weak fluorescence signal; therefore several curves have to be averaged for data analysis. The bottom panel in the same figure shows an average over 12 data sets.

To obtain the apparent on-rate constant k_{obs}, a curve fit to the data must now be performed. As the ratio between the fluorescence signal S and the concentration of bound ligand is unknown, it is best to fit the data by least-squares analysis to a single exponential curve like

$$S = \mathbf{S_{eq}} \cdot (1 - e^{-\mathbf{k_{obs}} \cdot t}),$$

as derived in the appendix, adding a background drift where necessary (fitted parameters in bold). The computer fit of this function to the data in figure 34 is given in the figure legend.

Another way of evaluating the k_{obs} constant is to linearise the data set via the relation

$$\ln\left(1 - \frac{S}{S_{eq}}\right) = -k_{obs} \cdot t,$$

also derived in the appendix. Following this, a plot of $\ln\left(1 - \frac{S}{S_{eq}}\right)$ against t has a slope of $-k_{obs}$. This plot necessitates the knowledge of the signal at equilibrium, S_{eq}, which can be difficult to estimate in a stopped-flow experiment because of the background drift of the signal; but it can be obtained from the least-squares fit to the exponential function mentioned above. Linearisation, as always, has the advantage that systematic errors can easily be detected, but the fits obtained using linearised data are less accurate. A linearised fit is shown in figure 35.

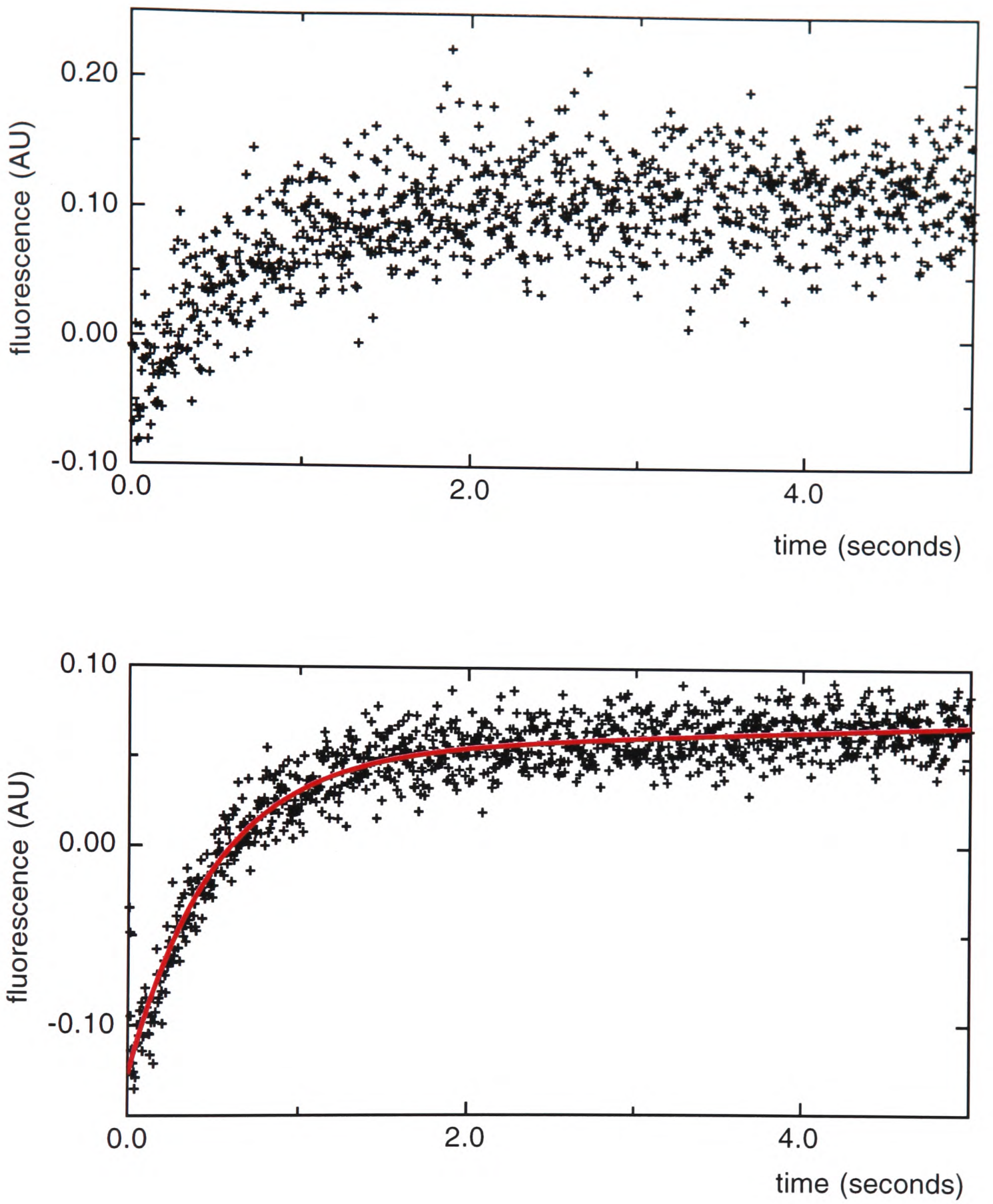

Figure 34: Stopped-flow experiment and averaging. 25 nM D^b, 879 µM NP-Y367-374 peptide final concentration, 15 °C. Top panel, single injection; bottom panel, average over 12 injections; red curve: computer fit of $y= -0.126 + 3.15 \cdot 10^{-3} \cdot t + 0.178 \cdot (1-e^{-2.01 \cdot t})$.

kobs= 2.01; kon= $2.3 \cdot 10^6$ from this experiment.

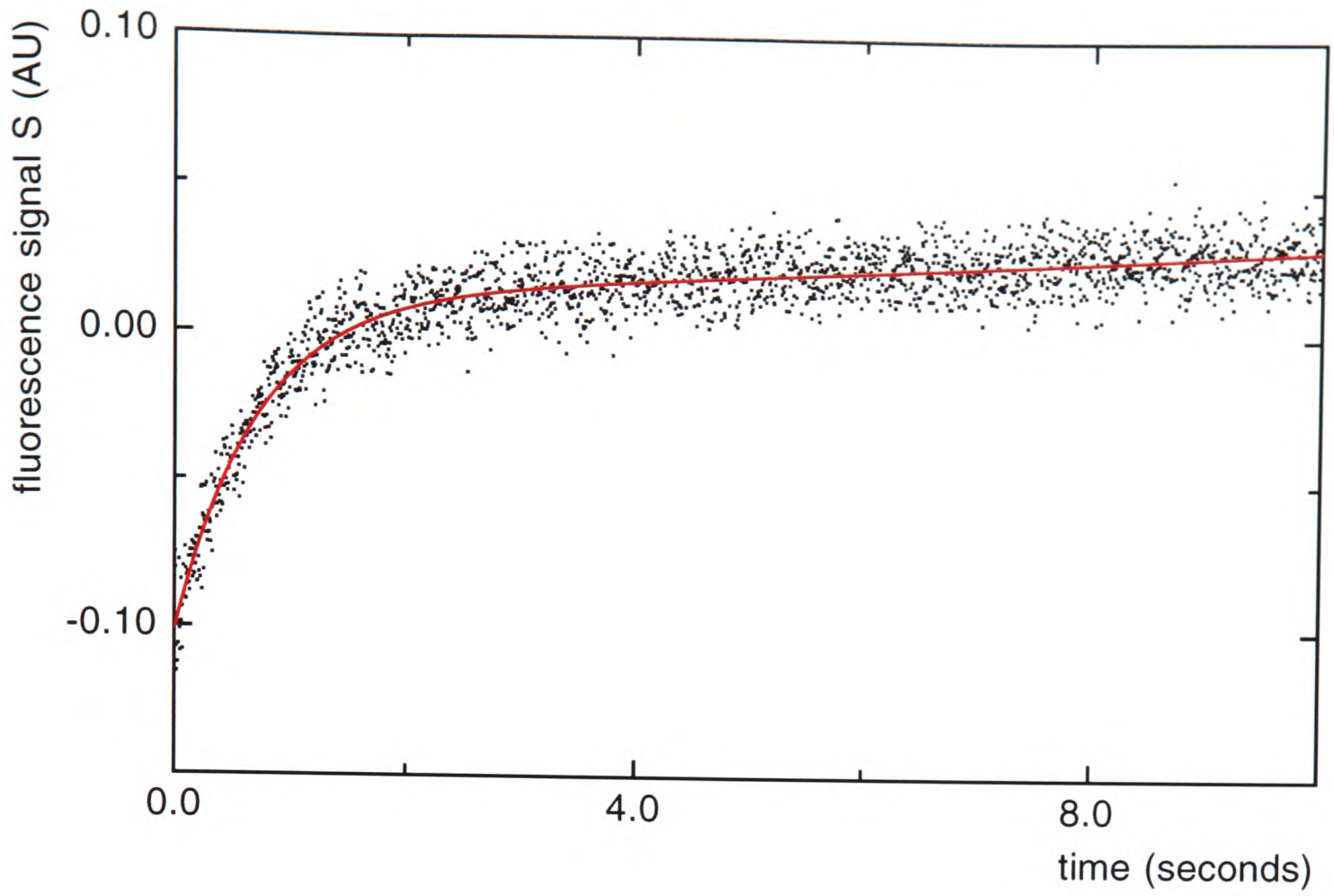

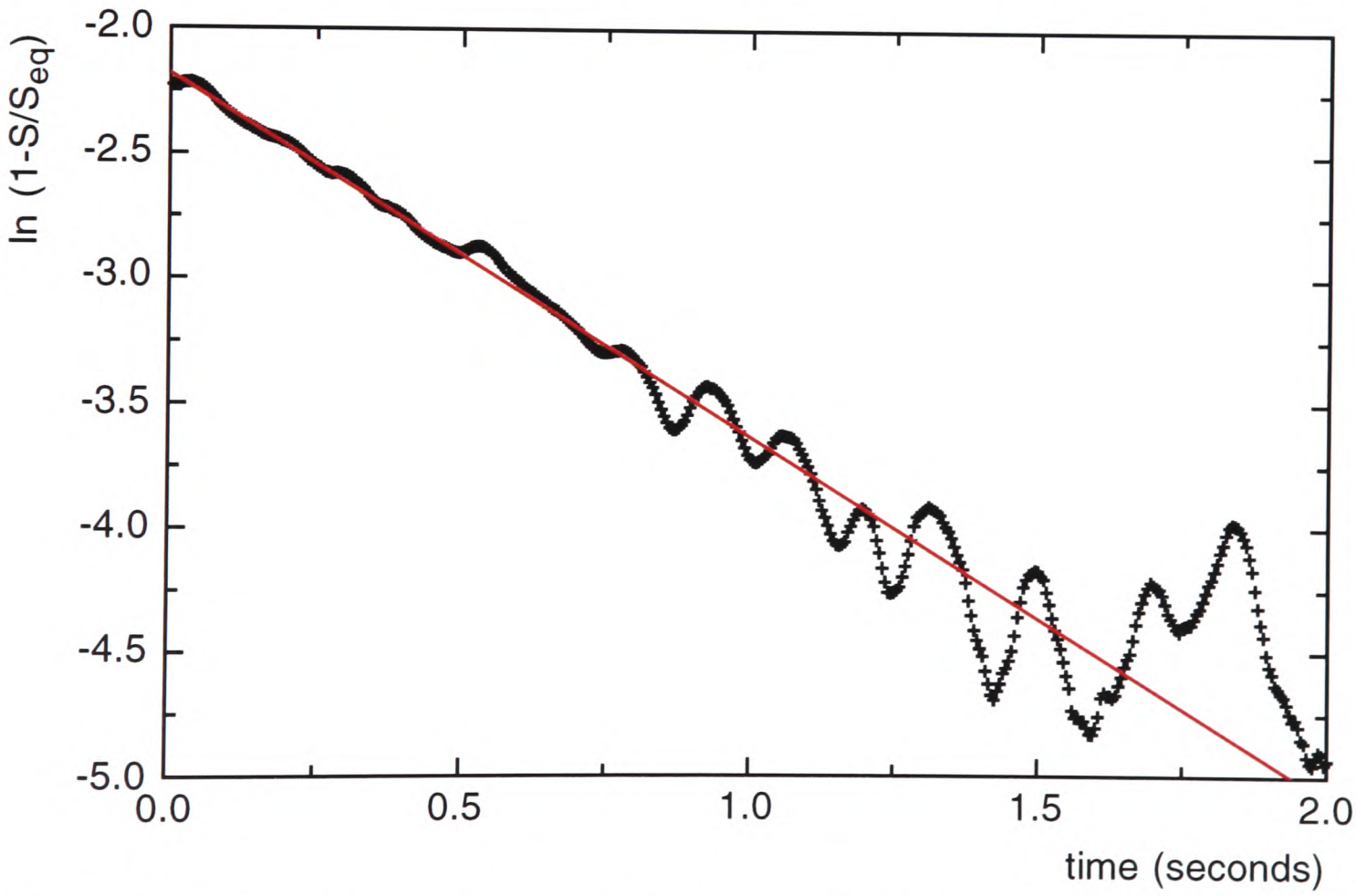

Figure 35: Derivation of on-rates from single binding curves. Upper panel: direct fit of integrated mass action equation to the binding curve of $4.82 \cdot 10^{-7}$ M NP-Y-367-374 peptide to Db at 25 °C gives kobs= 1.426 (±0.034), kon-= $2.96 \cdot 10^{6}$ (±5%). Lower panel: Initial rate fit of the same reaction smoothed over 10 data points. Straight line fitted to points between t=0.07 and t=0.5" gives k_{obs}= 1.454 (± 0.012), k_{on}= $3.02 \cdot 10^{6}$ (± 2%).

Note that due to logarithmising, only the data points up to 0.5 seconds can be used for the fitting.

From the k_{obs}, the on- and off- rate constants in the binding reaction (k_1 and k_{-1})can be calculated. As derived in the appendix,

$$k_{obs} = k_1 \cdot L_0 + k_{-1}$$

(with L_0 = concentration of ligand under non-depletion conditions) if a simple model of one-step binding

$$R + L <=> RL$$

is postulated, or if a subsequent step (e.g. a conformational rearrangement) is too slow to be recorded in the stopped-flow experiment. If $k_1 \cdot L_0 >> k_{-1}$ (in other words: the initial off-rate is negligible), k_1 can be derived directly from k_{obs} via

$$k_1 = k_{obs} / L_0 .$$

Otherwise, or if the magnitude of k_{-1} is not known, it is most convenient and acurate to measure k_{obs} at several $[L_0]$, and to plot the resulting values for k_{obs} against L_0. The slope of the curve is k_1, and k_{-1} is on the y-axis intersection. (About the accuracy of this estimation for k_{-1}, see below.)

I measured k_{obs}/L_0 plots for several peptides; the results are shown in figures 36 and 37, and table 3. All data could be satisfactorily fitted to straight lines. To obtain an idea of the standard error of the measurements, usually thirty injections were performed for each data point. They were then not averaged all together but split into three groups of ten injections which were averaged and evaluated separately, and the resulting k_{obs} values subjected to statistical analysis. Also, if possible, different recording time-scales on the stopped-flow fluorimeter were used to record the different groups. At some data points, the number of injections was less, but never less than 20. The standard deviations so obtained were taken into account when straight lines were fitted by least-squares analysis. A control experiment with the non-binding peptide NP-91-99 at 20 µM final concentration was performed; this gave no fluorescence change in the stopped-flow apparatus.

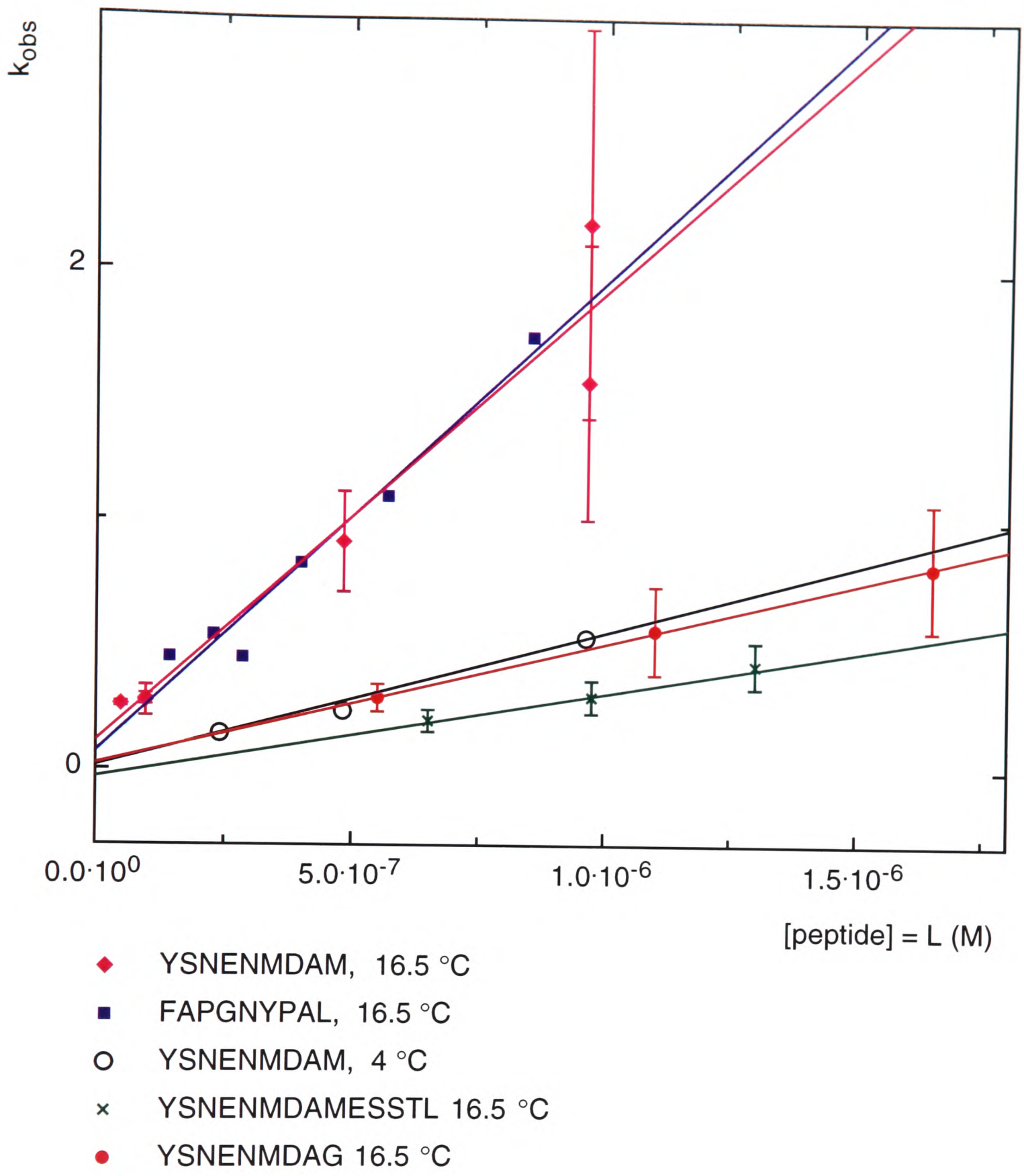

Figure 36: Determination of on-rate constants from stopped-flow data. k_{obs} is plotted against ligand concentration, and straight lines fitted. Table 3 indicates the results of the curve fits.

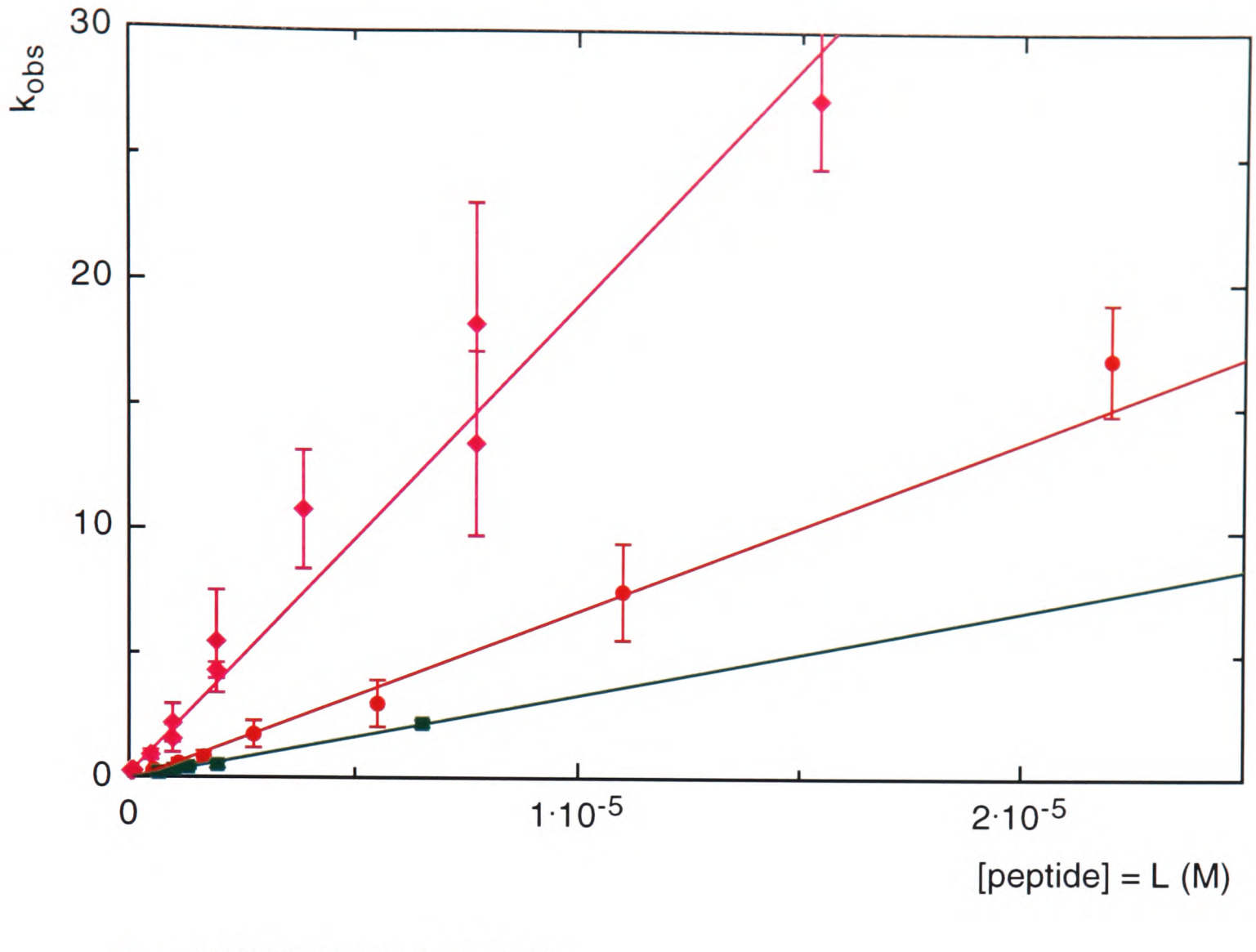

Figure 37: Determination of on-rate constants from stopped-flow data over a wide range of peptide concentration, for three peptides. k_{obs} is plotted against ligand concentration, and straight lines fitted. Table 3 indicates the results of the curve fits.

peptide	temperature	points (range)	k_1 ($M^{-1}s^{-1}$)	k_{-1} (s^{-1})
NP-Y367-374	16.5 °C	12 (all)	$1.81 \cdot 10^6$	0.113 (±0.14)
		1-6	$1.201\ (\pm 0.28) \cdot 10^6$	0.193 (±0.019)
	4 °C	4 (all)	$5.41\ (\pm 0.03) \cdot 10^5$	0.0137
	25 °C	1(direct fit)	$2.96 \cdot 10^6$ (±5%)	ND
		1 (IRF)	$3.02 \cdot 10^6$ (±2%)	ND
SV-324-332	16.5 °C	6 (all)	$1.89\ (\pm 0.18) \cdot 10^6$	0.0714 (±0.086)
NP-Y367-379	16.5 °C	5 (all)	$3.40\ (\pm 0.25) \cdot 10^5$	-0.030 (±0.044)
		1-3	$3.38\ (\pm 1.46) \cdot 10^5$	-0.022 (±0.126)
NP-Y367-374G9	16.5 ·C	7 (all)	$6.87\ (\pm 0.074) \cdot 10^5$	-0.107 (±0.07)
		1-3	$4.89\ (\pm 2.0) \cdot 10^5$	0.0215 (±0.13)

Table 3: stopped-flow measured on-rates. k_1 and k_{-1} are derived from computer least-square fits of the data, taking the standard deviations into account.

It is evident that k_{-1} cannot be meaningfully determined by this method. The three peptides for which kobs have been recorded over a wide range show a slight upward curvature in their kobs vs. [peptide] plots for unknown reasons, indicated here by the fact that curve fits over the first points (those visible in figure 36) give lower k_1 values.

Values for NP-Y367-374 derived from a single concentration point by direct fit (direct) or by initial rate fit (IRF) are included. k_{-1} cannot be determined in this way (ND).

Peptide sequences not given in the table are (see also abbreviations section):

NP-Y367-374	YSNENMDAM
NP-Y367-379	YSNENMDAMESSTL
NP-Y367-374G9	YSNENMDAG
SV-324-332	FAPGNYPAL

The experiments show extremely fast on-rates for the NP-Y367-374 (YSNENMDAM) and SV-324-332 (FAPGNYPAL) peptides (1.81 and 1.89 $\cdot 10^6$ $M^{-1}s^{-1}$, respectively). These two on-rates are almost identical, indicating that there might be a common or even general way in kinetic terms for peptides of optimal-length and -sequence to bind to D^b.

For the long peptide NP-Y374-379 (YSNENMDAMESSTL), and for NP-Y367-379G9 (YSNENMDAG) with a glycine substituted for methionine in position 9, the on-rates are substantially (three-to fivefold) slower. Both of these peptides are unable to properly bind at the C-terminus: while the longer peptide is probably extending beyond the groove [149] and therefore only participates in a modified C-terminal hydrogen bonding network in the F pocket, the glycine substitution cannot form the right van der Waals contacts in the E pocket (and indeed, its affinity for Db is lower; see below table 6). However, both peptides bind to D^b, and given the severity of the changes in their sequences, it is perhaps surprising that the reduction in the on-rates is not greater (see discussion).

The on-rate for NP-Y367-374 is strongly temperature-dependent: it is 3 $\cdot 10^6$, 1.8 $\cdot 10^6$, and 5.4 $\cdot 10^5$ $M^{-1}s^{-1}$ at 25, 16.5, and 4 °C, respectively. This difference was not seen by conventional fluorimetry because the reactions are generally too fast to resolve with that method (compare figures 36 and 32). The temperature dependence can be used to infer that even in this early step some conformational rearrangement of the protein, the peptide, or both is required. This is not surprising as the fluorescence effect is strongly sequence-dependent (see above) and therefore involves specific interactions of the peptide with D^b; to allow these specific interactions, at least some degree of rearrangement from the unordered solution structure of the peptides will be required. The temperature dependence of the on-rate I subjected to detailed thermodynamical analysis (see below).

The on-rates reported here are the highest that have ever been found for class I - peptide interactions (see introduction). I have therefore tried to obtain an estimate of the

theoretical limit for the on-rate of peptides onto class I molecules using kinetics theory. (A theoretical review is given in [273].)

The maximum rate of a reaction depends on the encounter probabilities of the components. According to the modified Smoluchowski equation [274, 273],

$$k_{encounter}\ (M^{-1}s^{-1}) = 4\pi\ \kappa\, a\, f \cdot (D_R + D_L) \cdot N_A/1000.$$

κ, the interaction parameter, is the product of the fractions of the molecule surfaces that will undergo the reaction. As about 80% of the peptide surface are buried in the complex, and about one sixth of the surface of the class I molecule, this factor is set to $0.8 \cdot 1/6 = 0.133$.

a is the interaction distance in cm, the sum of the radii of receptor and ligand. The dimensions of the extracellular portion of a class I molecules are about 70 x 40 x 40 Å [122], but from the fluorescence anisotropy decay measurements (see below) I assume r_R= 35.5 Å, and $V_R = 1.9 \cdot 10^{-19}$ cm^3. The size of the binding groove is approx. 30 x 11 x 12 Å [121], which might as well be used for the dimensions of the peptide. I therefore set

$$a = 36.7 + \sqrt[3]{30 \cdot 11 \cdot 12 \cdot \frac{3}{4\pi}} = 35.5 + 9.8 \approx 45 \text{ Å } (10^{-8} \text{ cm}).$$

f is the increase or decrease in the collision rate due to electrostatic interactions; it is generally difficult to estimate and, as class I molecule and peptide are both hydrated, here set to unity.

$\mathbf{D_R}$ and $\mathbf{D_L}$ are the diffusion constants of receptor and ligand, respectively. They can be calculated according to the Stokes-Einstein relation,

$$D_X = \frac{k \cdot T}{6\pi \cdot \eta \cdot r_X};$$

(with k= Boltzmann's constant, r_X= the radius of species X, and T= absolute temperature). The viscosity η is 1 centipoise in aqueous medium (= $1 \cdot 10^{-3}$ kg·s·m^{-1}), so that $kT/6\pi\eta$ resolves as $2.19 \cdot 10^{-13}$ cm^3/s. Thus, values of $D_R = 6.2 \cdot 10^{-7}$ and $D_L = 2.2$

$\cdot 10^{-6}$ $cm^2 s^{-1}$ are obtained.

The theoretical limit for the on-rate of peptide onto class I is therefore

$$4\pi \cdot 0.133 \cdot 45 \cdot 10^{-8} \cdot 1 \cdot 2.8 \cdot 10^{-6} \cdot 6.023 \cdot 10^{23}/1000 = \mathbf{1.3 \cdot 10^{9}\ M^{-1}\ s^{-1}}.$$

This number is to be taken as a minimum estimate for the limit; in other systems, the calculated maximal rates are often exceeded due to electrostatic rate enhancements [267, 273], but reaction rates below this limit are plausible from a theoretical point of view. The maximal on-rates that I have observed are, with approx. $2 \cdot 10^6$ $M^{-1}s^{-1}$, well within these limits. Voss [261] and Fersht [267] review reasons why on-rates can be slower than diffusion-limited. In the case of D^b and peptide, it is possible that the desolvation of the large peptide ligand, and of the binding groove which must contain highly ordered water due to its hydrophobic nature, takes a long time; that the need to preorientate the partners before binding decreases the interaction parameter; that electrostatic interactions play a larger role in the 'getting together' of ligand and receptor than acknowledged above; and that the ellipsoid shape of the molecules causes uneven rotation. The classical Smoluchowski equation can be modified to accommodate some of these effects [275]; however, it is most likely that conformational reorientations of both the protein and the peptide, which are difficult to treat mathematically, are necessary for the binding.

k_1 values for enzymes and substrates generally fall into the range of 10^6-10^8 $M^{-1}s^{-1}$ (see list in [267]). For the interaction of antibodies with small ligands and peptides, on-rates between 10^6 and 10^7 $M^{-1}s^{-1}$ [276, 277, 261, 278, 264], generally closer to 10^7 $M^{-1}s^{-1}$ [279], have been found in solution. More widely, the binding of small ligands to receptors often falls into this range (for example [260] for sugars binding to bacterial transport proteins). The fast reaction rates reported here are therefore in accordance with other systems; the question why they have not been measured before merits careful analysis of the previous data (see below and discussion).

In contrast to the determination of the initial on-rate k_1, the off-rate k_{-1} has been difficult to determine reliably from the L_0/k_{obs} plots of the stopped-flow data. The y-axis intersection varied widely and non-systematically between peptides and fitting approaches, and even reached negative values in some experiments.

The accuracy of the estimate for k_{-1} in this method depends on the magnitude of k_{-1}, and the ability to measure binding at ligand concentrations as low as possible to get close to the y-axis intersection in the k_{obs}/L_0 plot. Unfortunately, the latter is difficult in these experiments due to the (even further) reduction of the signal at low ligand concentrations, and the necessity to keep the initial receptor concentration one order of magnitude below the initial ligand concentration to avoid ligand depletion; furthermore, when at low L_0 the reaction takes a long time to reach equilibrium, the baseline drift of the stopped-flow fluorimeter begins to pose a problem. The only statement about k_{-1} that can be made from the stopped-flow experiment is that it must be smaller than the smallest k_{obs} measured, which puts it in the region between 0 and 0.1 s^{-1} for all the peptides investigated (for a discussion see below).

5.2. Measurement of on-rates using radioligand assays

Having performed the stopped-flow measurements, there were three reasons to measure the on-rate again using the traditional [208] binding assay: firstly, to corroborate the measurements using data from a different experimental system; secondly, to explore the causes of the difference to the on-rates published by Cerundolo and Townsend [208], and thirdly, to attempt to measure the association at low ligand concentrations and a known concentration of binding sites, allowing for the more accurate determination of the initial off-rate k_{-1} (see above for a description of the problems with the stopped-flow method; and below for the evaluation of the radioligand binding data).

For association constants in the order of magnitude of 10^7 $M^{-1}s^{-1}$, the observed rate

constant k_{obs} will be in the range of 10^{-1} to 10^{-2} s^{-1}, with half-times in the range of tens of seconds, even if the reaction is cooled to 4 °C and L_0 is kept as low as possible. The method used previously [208] used class I molecules prebound to protein A sepharose beads, and centrifugation in a microfuge followed by four consecutive washes was employed to separate bound from free ligand. This separation, typically taking 2-3 minutes, was too slow to allow for an appropriate resolution in the early stages of the binding process.

I therefore developed a filtration assay more in line with the assays commonly used in radioligand binding experiments ([269]; for detailed review and comparison with other techniques see [280]). The D^b-His_6·$h\beta_2m$ complexes were prebound to Nickel beads in a stirred, thermostatised (waterbath) vial in PBS buffer. At t=0, peptide was added in a small volume, and mixing was aided by pipetting the suspension with a micropipettor. At given time points, aliquots of the suspension were withdrawn and filtered through suction microcolumns in which the beads were retained. This procedure achieved separation times, including several washes, of <20 seconds; therefore it was possible to take time points at approximately this time interval. When doing experiments with iodinated peptides, the microcolumns could be counted directly; for tritium peptide counting, the protein was eluted from the Nickel beads with 50 mM EDTA or SDS-PAGE sample buffer (without dye) containing 50 mM EDTA. A detailed description of the method is found in the materials and methods section.

Using this assay, on-rates of tritiated and iodinated SV-324-332 (FAPGNYPAL) peptide at different concentrations, and under different conditions, were measured. Data were fitted, using a least-squares fit, to the following equation:

$$RL = \frac{L_0 \cdot R_0}{L_0 + 1/K_a} \cdot (1 - e^{-(k_1 \cdot L_0 + k_{-1}) \cdot t})$$

This formula is derived, and the fitting procedure described in detail, in the appendix. Figure 38 shows some on-rate curves and the respective fits, and table 4 gives an

overview of the data.

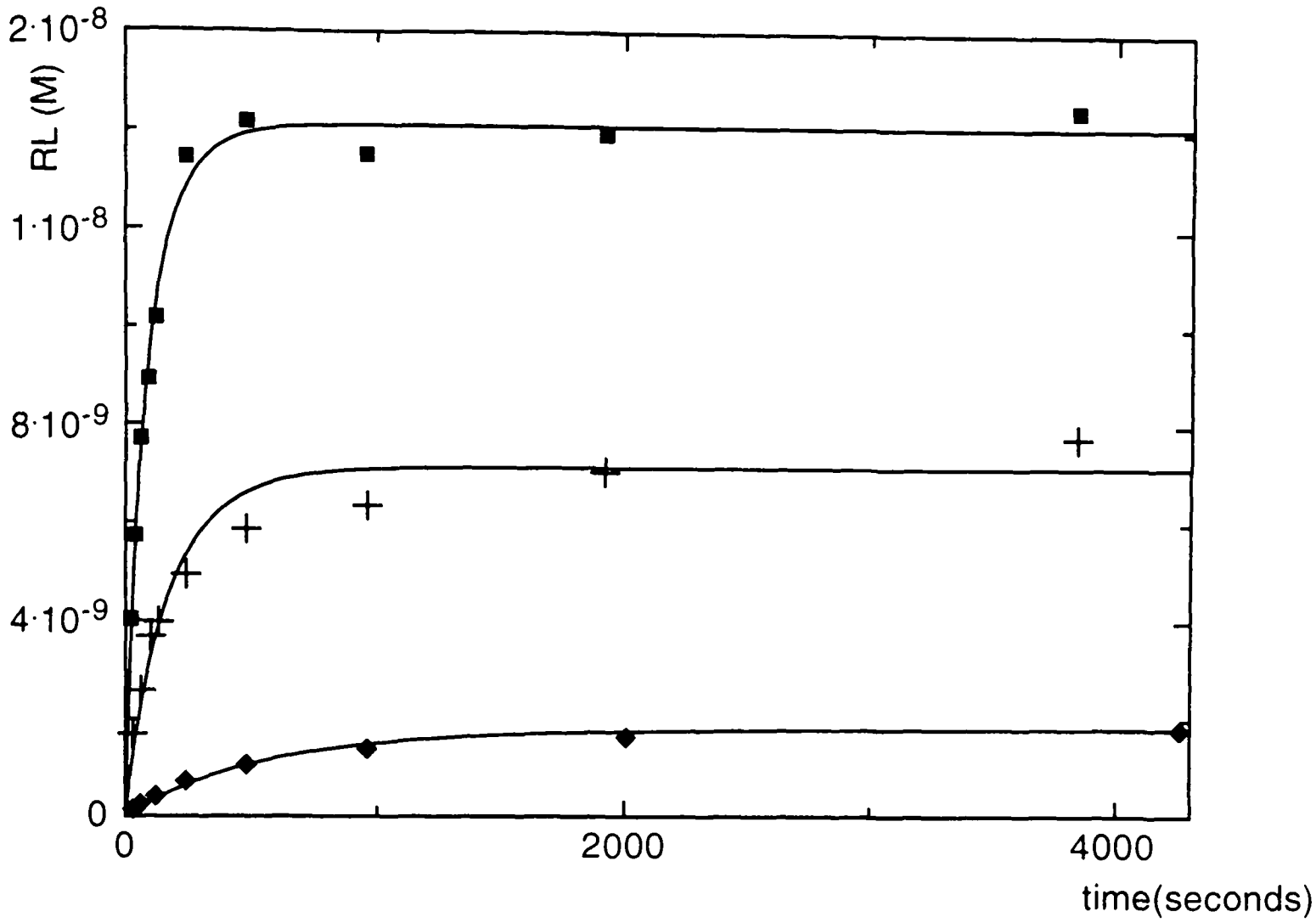

Figure 38: on-rate measurements of tritiated SV-324-332 (FAPGNYPAL) peptide onto D^b. Squares, 25 nM peptide and 24.5 nM protein; crosses, 15 nM peptide and 4.5 nM protein; diamonds, 2 nM peptide and 4.5 nM protein. Results of the curve fits see table 4.

exp.	conc. nM	det.?	k_{on} ($M^{-1}s^{-1}$)	k_{off} (s^{-1})	factor
a	2	–	**4.12 (±0.38) ·10^5**	0	0.90
b	15	–	**4.34 (±0.6) ·10^5**	0	1.55
c	25	–	**4.25 (±1.46) ·10^5**	1.38 (±1.39) ·10^{-3}	0.81
d	25	+	**2.34 (±0.24) ·10^5**	0	0.75
e	100	1)	**6.63 (±1.24) ·10^4**		1.00
f	25	2)	**9.59 (±3.18) ·10^4**	2.8 (±11) ·10^{-5}	0.76
g	25	3)	**3.56 (±0.6) ·10^4**	0	
h	100	4)	**8560**		

Table 4: table of on-rates determined by binding of radiolabeled SV-324-332 peptide as described in 'materials and methods'. (exp. = experiment; det.= detergent)

All on-rates measured at 4 °C.

1): iodinated peptide, no detergent;

2): in detergent, separation by immunoprecipitation;

3): T2D^b detergent lysate, immunoprecipitation

4): T2D^b detergent lysate, immunoprecipitation, iodinated peptide

These results suggest that the previous binding data obtained by Cerundolo et al. [15] can be reconciled with those from the stopped-flow experiment. The on-rate of 8560 (all on-rates are $M^{-1}s^{-1}$) for iodinated peptide in cell lysate (experiment h) is close to the one measured for NP-Y367-374 in the cited paper (5585). If tritiated peptide is used in the same assay (g), the on-rate increases to 36,000. Therefore, at least for the SV-324-332 peptide FAPGNYPAL, radioiodination alters the binding kinetics of the peptide. This was unexpected following the observation by Gairin and collaborators [134] that there are no clear correlations between particular amino acids in position P_6, and the affinities of peptides towards D^b. However, P_6 could play a different role in each peptide, for example to ease the packing of the peptide across the ridge (see introduction), which would not have been picked up in this experimental approach.

When - instead of cell lysate - recombinant molecules in detergent are used (experiment f), the on-rate increases to 96,000 $M^{-1}s^{-1}$. This could be due to differences between the recombinant and the natural molecule such as the absence of transmembrane and cytosolic regions from the former or differences in the state of conformation; or to the presence of cell lysate in one assay. Cerundolo et al. [175] have shown that in $T2D^b$ cells (which were used for this assay), human invariant chain is associated with the empty $D^b \cdot \beta_2 m$ complexes in the cell lysate, and that it is displaced by the addition of peptide. It is possible that processes like this create a pre-equilibrium that slows down peptide binding in cell lysates.

If the measurement is carried out in detergent using the filtration system, the on-rate is measured around 420,000 $M^{-1}s^{-1}$ in three experiments at different peptide concentrations (experiments a-c). This is in general agreement with the stopped-flow experiment, where 540,000 $M^{-1}s^{-1}$ at 4 °C was found.

A control experiment measured the on-rate in detergent with the filtration technique and found 230,000 (d) as opposed to 96,000 $M^{-1}s^{-1}$ (e) when bound and free ligand were separated via immunoprecipitation. The difference between these numbers, repeated in several experiments, could be due to the loss of an unstably bound proportion of peptide during the long washing period in the immunoprecipitation. However, upon prolonged washing of the microcolumns, even with detergent buffer, no reduction of the count was seen (data not shown).

These experiments demonstrate that iodination, detergent, and the presence of cell lysate all influence the measured on-rates, and emphasize how important a 'minimal interference' approach to binding measurements is. Influence of detergent upon kinetic parameters of MHC class II molecules (most likely the off-rate) has been demonstrated previously [281]. However, despite these effects the on-rates measured by Cerundolo *et al.* [208] for NP-Y367-374 were still faster than compatible with the equilibrium affinity and off-rate constants [15].

In these experiments, the total number of binding sites was known from the absorption measurement of the protein solution, and from the fact that material was used that shifted completely on an IEF gel upon peptide addition. This information should have made it possible to determine the off-rate constant of the initial complex, k_{-1}, by fit of the integrated mass action equation (see above and appendix). This is possible in two ways: the equation

$$RL = RL_{eq} \cdot (1 - e^{-(k_1 \cdot L_0 + k_{-1}) \cdot t}),$$

$$\text{with } RL_{eq} = \frac{L_0 \cdot R_0}{L_0 + 1/K_a},$$

can be used directly to fit the curve. Traditionally, K_a is inserted in this formula as the equilibrium affinity constant of the reaction ($K_{a,eq.}$), and expressed as k_1/k_{-1}. This generates a relationship between the equilibrium and the kinetic constants so that k_{-1} always has the value of $k_1/K_{a,eq}$. It lies in the nature of this fit that small systematic errors in the determination of R_0 (the total receptor concentration) or RL (for example shifts in the counting efficiency or sample recovery) will profoundly influence the fit, especially the value of k-1.

There is another problem to this fitting approach. If it is taken into consideration that a more complicated binding process underlies the observed reaction, the ratio k_1/k_{-1} does not necessarily have to be equal to $K_{a,eq}$. For example, in a binding model

$$R + L \underset{k_{-1}}{\overset{k_1}{\rightleftharpoons}} RL \underset{k_{-2}}{\overset{k_2}{\rightleftharpoons}} R'L,$$

where the isomerisation RL –> R'L is assumed to be a slow step, the overall equilibrium constant $K_{a,eq}$ is $k_1/k_{-1} \cdot k_2/k_{-2}$ (see appendix) while the affinity constant seen in the association step, K_1, is k_1/k_{-1}.

I found it therefore more appropriate to introduce an additional factor f to determine the

deviation of RL_{eq} from $\frac{L_0 \cdot R_0}{L_0 + 1/K_a}$ calculated with the known equilibrium $K_{a,eq}$. The fitting routine is described in the appendix. If this routine is used, k_{-1} obtained should derive entirely from the shape of the on-rate curve, and not from any equilibrium conditions; it can therefore differ substantially from $k_1/K_{a,eq}$. Indeed, when these fits were performed, it was not possible to obtain a meaningful number for k_{-1}: either, the best fit was obtained using a k_{-1} value of zero (experiments a, b, d, g), or the standard error was greater than the value obtained (experiments c, f).

To control for this rather complicated fitting routine, a simple fit to a single exponential was also performed. This fit does not take the depletion of ligand into account, which at these low concentrations of ligand is not strictly legitimate. Failure to implement ligand depletion leads to an overestimation of the rate constant (see below, and [21]), so that the numbers obtained can only serve as maximum values. However, this fit allows an assessment of the k_{-1} via a k_{obs}/L_0 plot. The data and fits are shown in figure 39, the results in table 5.

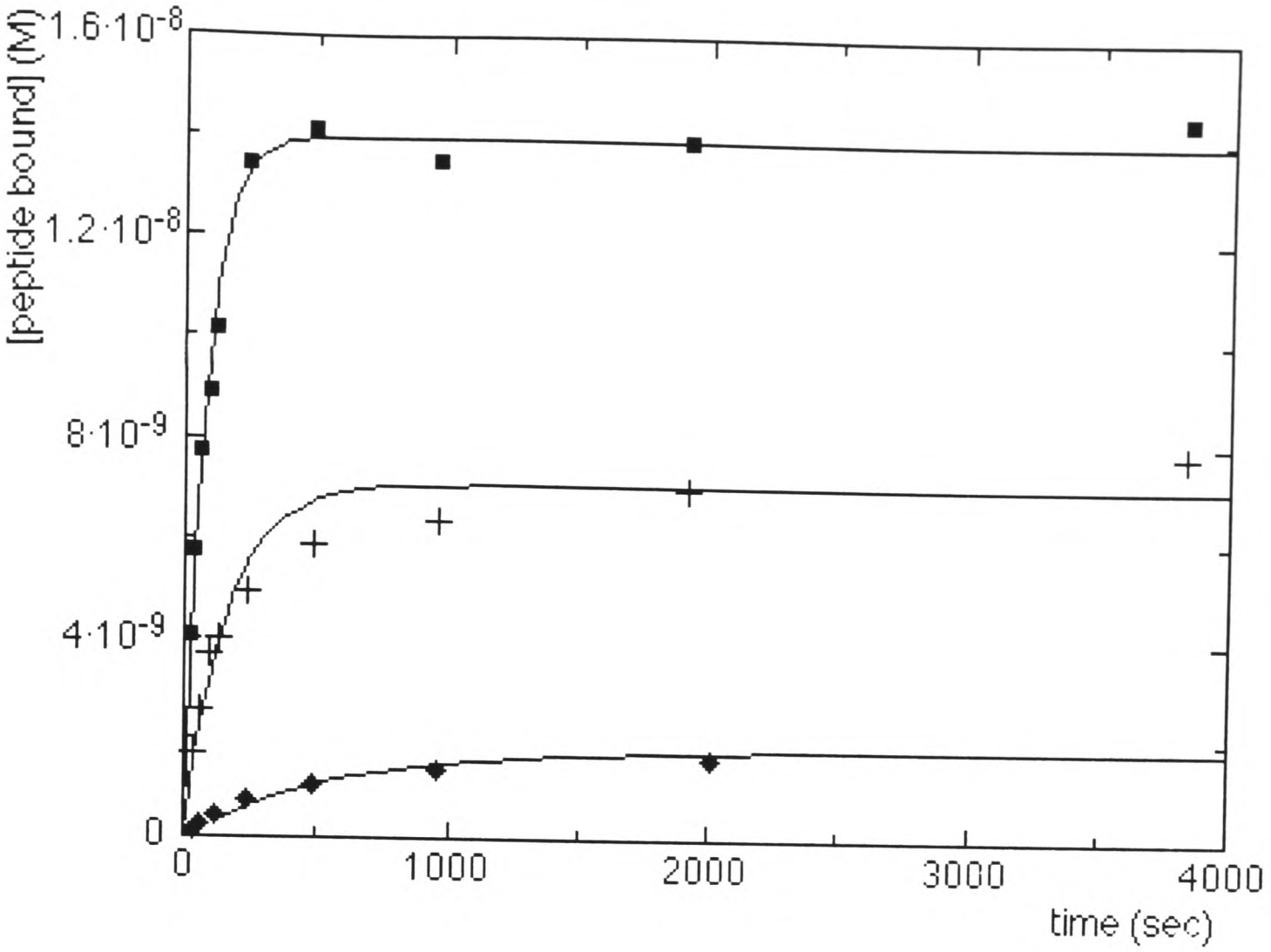

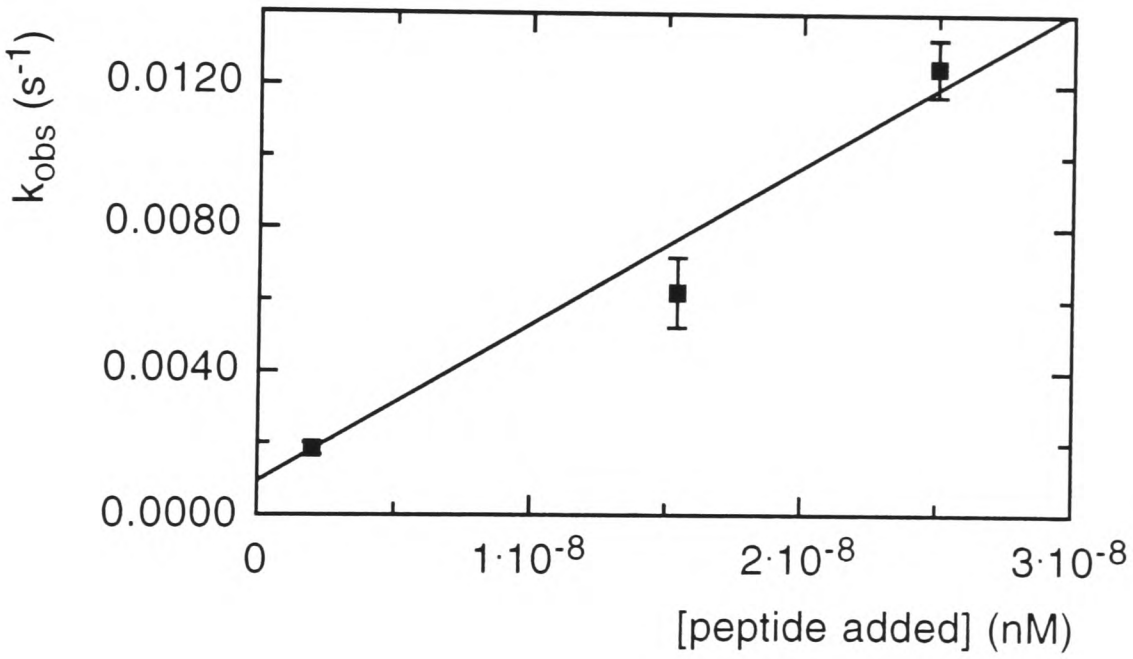

Figure 39: Simple fits to obtain k_{obs}, not taking ligand depletion into account (top panel), and secondary plot (with least-squares fit) of k_{obs} against L_0 (bottom panel), for tritiated SV-324-332 (FAPGNYPAL) peptide onto D^b. Squares, 25 nM peptide and 24.5 nM protein; crosses, 15 nM peptide and 4.5 nM protein; diamonds, 2 nM peptide and 4.5 nM protein. The results of the individual fits are in table 5.

The fit to the secondary plot gives $k_{-1} = 4.13\ (\pm 13) \cdot 10^{-4}\ s^{-1}$, and $k_1 = 4.55\ (\pm 0.91) \cdot 10^5\ M^{-1}s^{-1}$.

exp. (table 4)	[peptide] (nM)	[D^b] (nM)	amplitude (M bound)	k_{obs} (s^{-1})	k_{obs}/[peptide] ($M^{-1}s^{-1}$)
c	25	24.5	$1.40 \cdot 10^{-8}$ (± 0.015)	$1.25 \cdot 10^{-2}$ (± 0.08)	$9.16 \cdot 10^{5}$ (± 0.32)
b	15	4.9	$7.08 \cdot 10^{-9}$ (± 0.31)	$6.21 \cdot 10^{-3}$ (± 0.97)	$4.03 \cdot 10^{5}$ (± 0.65)
a	2	4.9	$1.81 \cdot 10^{-9}$ (± 0.045)	$1.83 \cdot 10^{-3}$ (± 0.17)	$4.96 \cdot 10^{5}$ (± 0.85)

Table 5: Results of the k_{obs}-fits. The exponents are also valid for the standard deviations. See figure 39.

A straight line, fitted through the data in the k_{obs}/L_0 plot (taking the standard errors into account), gives the following data: $k_1 = 4.55\ (\pm 0.91) \cdot 10^5\ M^{-1}s^{-1}$; $k_{-1} = 4.13\ (\pm 13) \cdot 10^{-4}\ s^{-1}$. The number for k_1 is in the same range as the values above, confirming the validity of the above fit. The number for k_{-1}, with its standard error three times the value, is the closest measurement of the initial off-rate constant that I have been able to perform. It seems that the only valid statement with respect to this off-rate is that it must be at or below (slower than) $1.5 \cdot 10^{-3}\ s^{-1}$.

Taken together, the radioligand on-rate experiments have confirmed the fast on-rates that were first measured with stopped-flow fluorescence, and have explained the discrepancy between these and the results published by Cerundolo et al. [15]. Having obtained these results, I felt it was important to measure also the equilibrium and dissociation rate constants to ensure that the kinetics mismatch was not due to an artefact in these observations.

5.3. Equilibrium binding experiments

5.3.1. Radioligand binding assays

I decided to measure affinity constants with the recombinant protein in different ways: with iodinated (see figure 18 above) and tritiated peptide, and by fluorescence step-titration (see figure 40). The data are summarized in table 6.

For the radioligand binding experiments, Langmuir isotherms (taking ligand depletion into account) were fitted to the data using least-squares analysis. Scatchard plots were also generated to detect systematic deviations from the binding curve, but not used for the fitting. Some curves are displayed in figures 41 and 42.

The determination of association constants by fluorescence step-titration poses a special problem: The relationship between the fluorescence signal S and the concentration of bound ligand is not known *ab initio*. It could be determined from the fluorescence enhancement at saturation and the known number of binding sites, but would be difficult to transfer from one experiment to another because it depends strongly on instrumental parameters such as the accuracy of the emission slit width setting (fluorescence is proportional to the square of the emission slit width). It is therefore more accurate to measure the increase in fluorescence at each titration step, and to plot the sum of these values against the total ligand concentration added (both numbers, of course, have to be corrected for the volume increase).

It is especially important in a fluorescence step-titration experiment to operate at a ligand concentration that is well below the dissociation constant K_d ($1/K_a$). If this is not the case, and the signal is plotted against the logarithm of the concentration to obtain the binding curve, an artificial 'binding curve' of $RL \approx R_0$ with $K_d = R_0/2$ (and never less than that) is obtained. It is therefore important, when binding results are plotted in a semilogarithmic plot, to carefully control R_0, and to check the conformity of the curve with a real binding reaction using a linearised plot (Alain Townsend, pers. comm.).

In the fluorescence experiment, the protein concentration was therefore set to 3.3 nM (as measured by absorption) which was the lowest value where fluorescence enhancement could be reliably measured in spite of the baseline drift (figure 40). The resulting curve shows that there is only one binding affinity over five orders of magnitude.

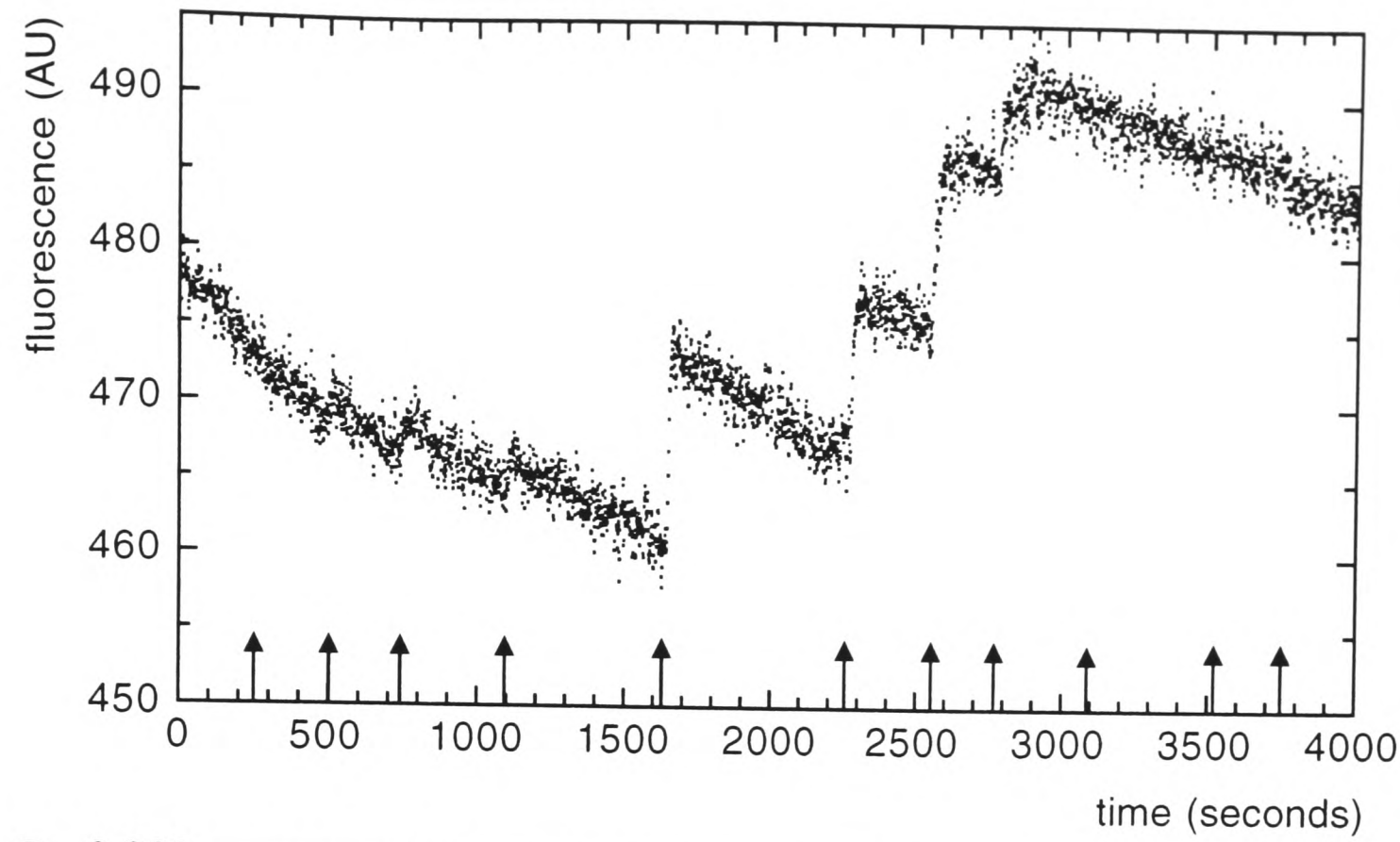

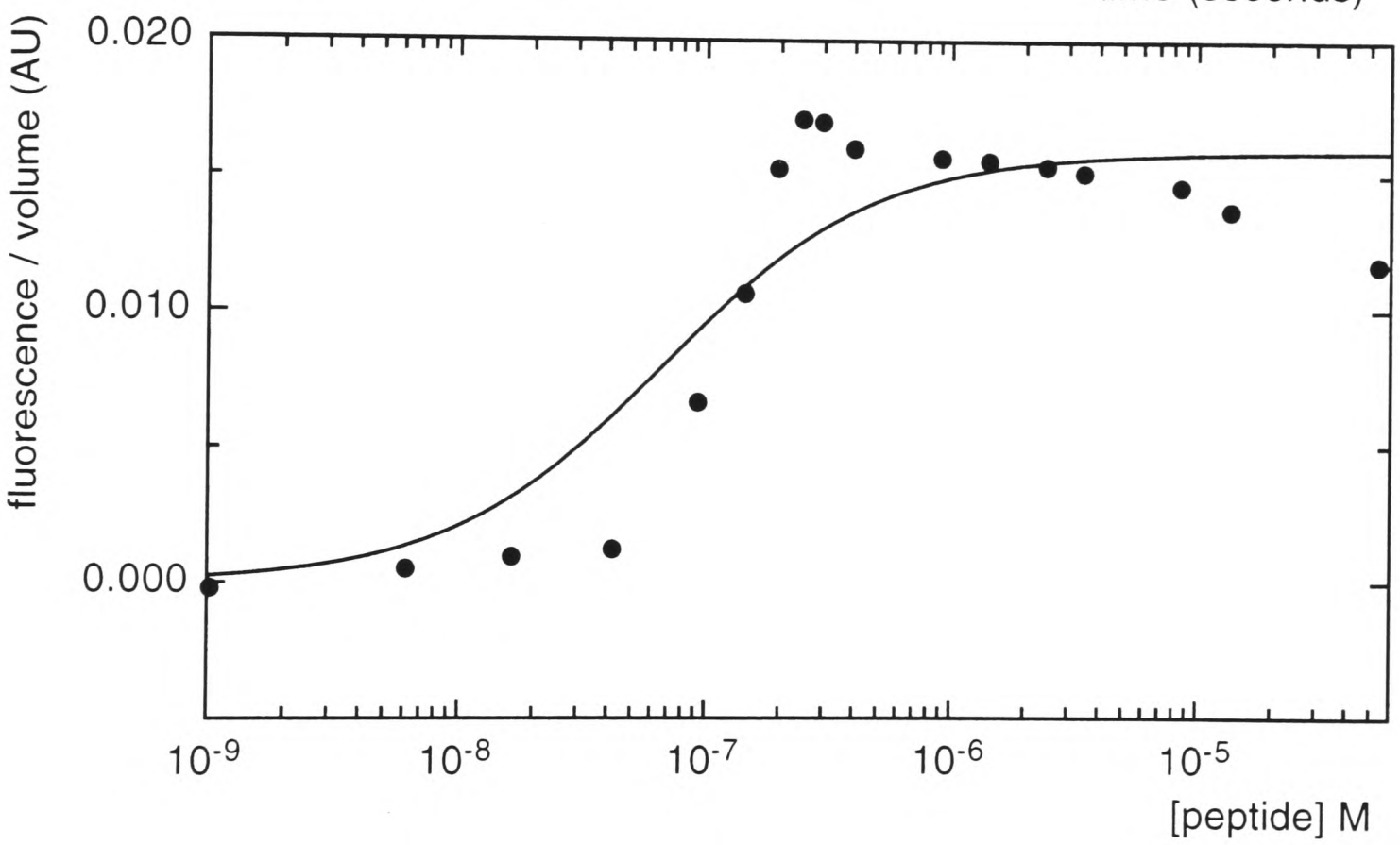

Figure 40: Fluorescence step-titration of peptide binding to the D^b-His_6•hβ_2m complex, done at 25 °C. 3.3 nM protein (by absorption).

Upper panel, titration curve. Excitation 280 nm, emission 342 nm. The arrows designate addition of peptide aliquots. Lower panel, fluorescence plotted against concentration of added peptide (both values normalised for the increase in volume during the titration).

Curve fitted: simple isotherm, no ligand depletion; Ka= 1.50 (±0.02) •10^7 M^{-1}.

Because of the very weak fluorescence signal and baseline drift at low protein concentrations (see upper panel), the fit to a binding curve is not very good. However, this shows that there is only one binding event between 10^{-9} and 10^{-4} M peptide.

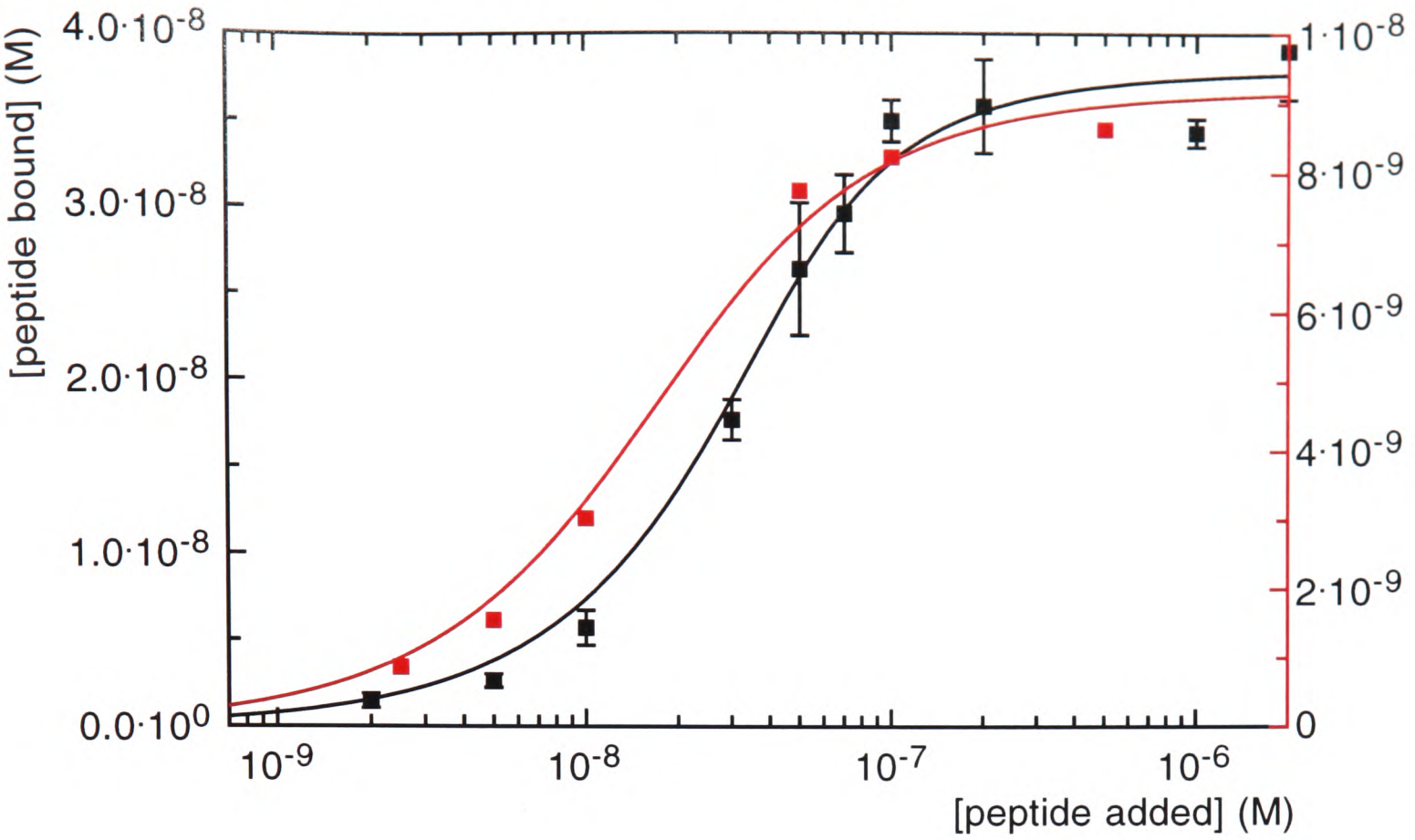

Figure 41: The affinities of D^b for the SV-324-332 peptide FAPGNYPAL are nearly identical in detergent lysates and in the recombinant system. Red curve (right hand-side y scale), binding of tritiated FAPGNYPAL peptide to D^b from T2Db lysate.
Black curve (left hand-side y scale), binding of the peptide to recombinant protein.
Results of the direct fits of the Langmuir isotherm:
cell lysate assay: K_a= 8.43 (± 1.76) $\cdot 10^7$; 1.055 (± 0.038) $\cdot 10^{-8}$ M sites;
recombinant protein: Ka= 9.25 (±1.86) $\cdot 10^7$; 3.78 (±0.11) $\cdot 10^{-8}$ M sites (added 3.67 $\cdot 10^{-8}$ M)

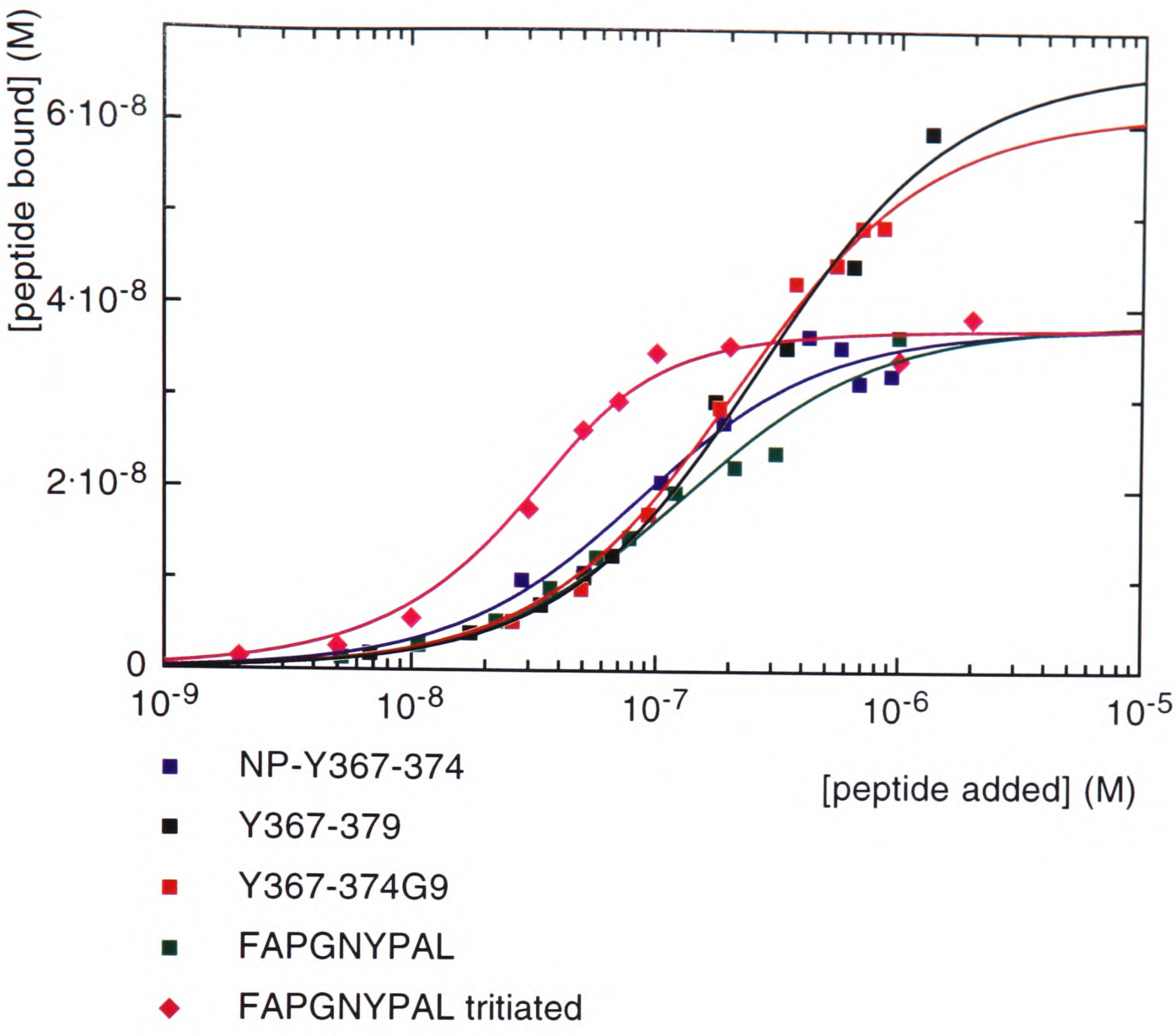

Figure 42: Most peptides tested have similar affinities to D^b complexes. Equilibrium binding experiments were performed with iodinated peptides (squares; peptides see legend).

Table 6 gives the results of the direct fits.

The control peptide NP-91-99 showed no binding under these conditions (data not shown).

The tritiated FAPGNYPAL peptide (magenta diamonds) bound more strongly than the same peptide in iodinated form.

exp.	peptide	type of assay	temperature	K_a ± st.dev. (M^{-1})
a	NP-Y367-374 (YSNENMDAM)	C (fig. 18)	4 °C	5,41 (±0.15) ·10^7
b		C	25 °C	1.48 (±0.37) ·10^7
c		C	37 °C	5.50 (±0.75) ·10^6
d		A [1)]	4 °C	2.3e+7
e		E	RT	1.50 (±0.60) ·10^7
f	SV-324-332 (FAPGNYPAL)	A [2)]	4 °C	2.04 (±0.42) ·10^7
g		C	4 °C	1.60 (±0.13) ·10^7
h		D	4 °C	9.24 (±1.86) ·10^7
i		B	4 °C	8.43 (±1.76) ·10^7
k	NP-Y367-379 (YSNENMDAMESSTL)	C	4 °C	4.35 (±0.69) ·10^6
l		A [1)]	4 °C	5.2 e+6
m	NP-Y367-374G9	C	4 °C	5.6 (±0.71) ·10^6

Table 6: binding constants for peptides to D^b molecules.

1), taken from Cerundolo et al.[15].

2), Enzo Cerundolo, pers. comm.

The types of assay are described in the following table:

types of assay:	source of D^b protein:	label	separation bound / free
A	$T2D^b$ cells	iodine	immunoprecip.
B	$T2D^b$ cells	tritium	immunoprecip.
C	recombinant	iodine	filtration
D	recombinant	tritium	filtration
E	recombinant	fluorescence binding assay	

These data show that the binding constants vary little between the detergent system with

molecules from T2D^b cells and recombinant molecules in PBS (for NP-Y367-374, compare d and a; for SV-324-332, compare i and h, and see figure 41; for NP-Y367-379, compare l and k), certainly not as much as the on-rates (compare with table 4). At 25 °C, the results of the fluorescence step-titration (e) fit very well with the binding assay using iodinated peptide. For the NP-Y367-374 peptide, there is a continuous decrease in K_a with temperature which I have used to look at thermodynamics of binding (see below).

For the SV-324-332 peptide, the binding affinities are higher when tritiated peptide is used (compare i to f and h to g). This difference is probably based on the presence of the iodine atom at P_6, and it could be due to the fourfold difference in the on-rate observed above.

Both the elongated peptide NP-Y367-379 and the G9 substitution NP-367-374G9 show affinities that are tenfold lower; this can only partially be explained by the four- to fivefold reduction in the on-rate for those peptides compared to NP-Y367-374 (see table 3). However, it could be shown that the C-terminal anchor residue is not absolutely necessary for the binding of a peptide, in agreement with the results of Matsumura and collaborators [132].

5.4. Off-rate measurements

I next decided to measure the kinetic dissociation constants, or off-rates, using the recombinant protein.

Radioligand binding experiments to determine off-rates are relatively straightforward and easy to interpret (see the appendix for a detailed description): The peptide is prebound to the protein, free peptide is washed away, and the complex is incubated with a large (usually 100-fold) excess of unlabelled ligand, eliminating rebinding of the labelled species. The concentration of RL is then determined at given time-points by withdrawing

aliquots of the reaction. This works in both the immunoprecipitation and the rapid filtration approach. Evaluation of the data makes use of following equation for a first-order decay (RL –> R+L):

$$RL = RL_0 \cdot e^{-k_{off} \cdot t}.$$

To obtain k_{off}, $\ln(\frac{RL}{RL_0})$ or $\ln(\frac{S}{S_0})$ (which is the same number) is plotted against the time according to the rearranged equation

$$\ln(\frac{RL}{RL_0}) = -k_{off} \cdot t$$

to assess any deviations from a first-order decay reaction, especially at long times when RL/RL_0 is small, and errors are exaggerated by logarithmising. k_{obs} can then be derived using an exponential least-squares fit.

Figure 43 shows some dissociation curves, and table 7 summarises the data.

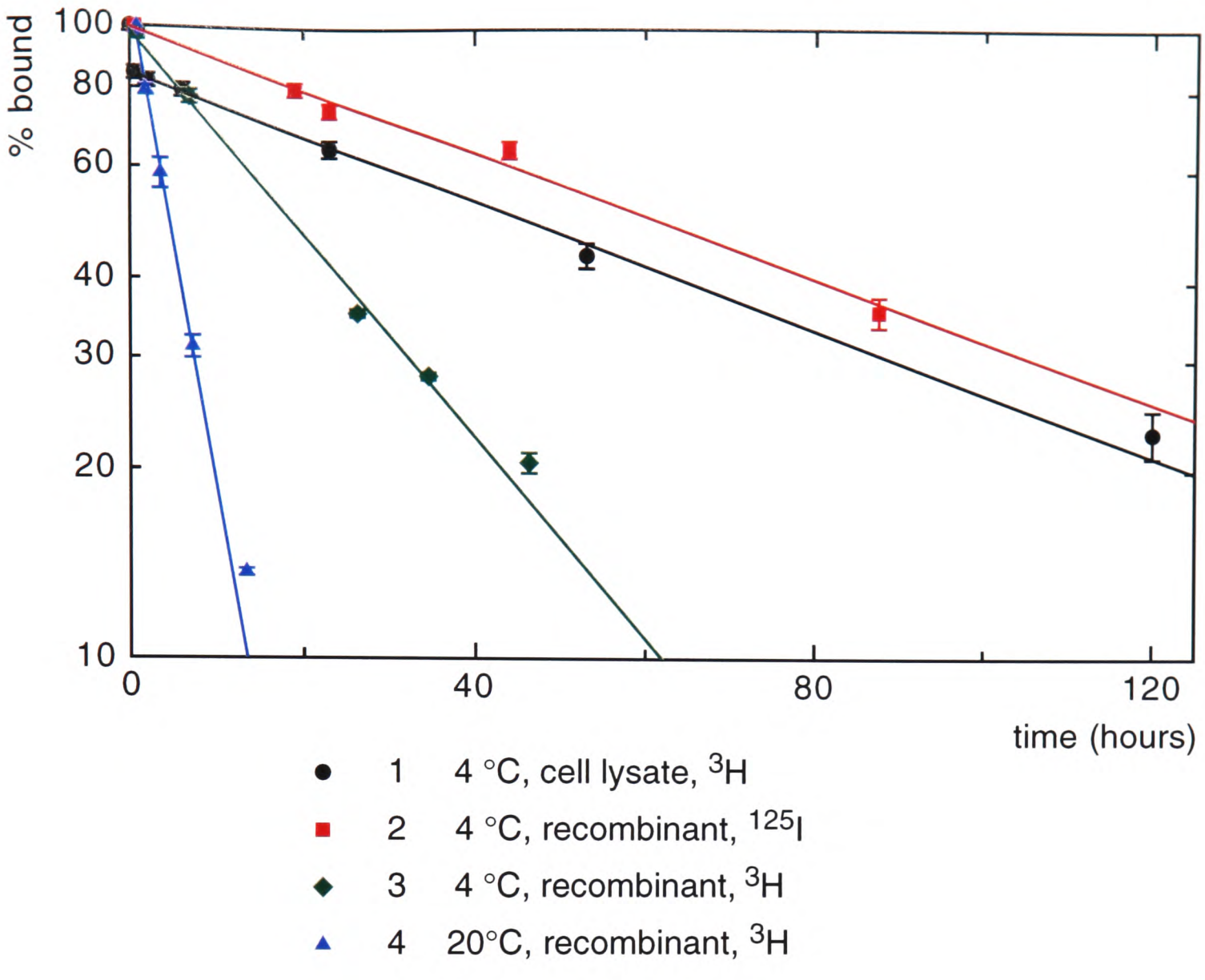

Figure 43: Dissociation rates (off-rates) measured with SV-324-332 (FAPGNYPAL) peptide. Y-semilogarithmic plot of the binding data, and straight lines representing a least-squares fit of exponential functions. The numbers in the legend refer to table 7. In the experiment from cell lysate, an initial drop of the counts is seen as often. The time-point for t=0 was therefore not included in the fit.

*	peptide	type of assay	temperature	k_{off} ± error (s^{-1})
a	SV-324-332 (FAPGNYPAL)	A [1]	4 °C	**3.85 ·10⁻⁶**
b/1		B	4 °C	**2.22 ·10⁻⁶ ±5%**
c/2		C	4 °C	**2.17 ·10⁻⁶ ±10%**
d/3		D	4 °C	**7.09 ·10⁻⁶ ± 2 %**
e/4		D	20 °C	**3.45 ·10⁻⁵ ±5%**
f	NP-Y367-374 (YSNENMDAM)	A [2]	4 °C	**1.24 ·10⁻⁶**
g		C	4 °C	**3.51 ·10⁻⁷ ±15%**
k	NP-Y367-379 (YSNENMDAMESSTL)	C	4 °C	**7.00 ·10⁻⁵ ±3%**
l		A [2]	4 °C	**7.69 ·10⁻⁵**
m		E	RT	**4.28 ·10⁻⁴ ±5%**

*: experiment / number in figure 43; 1): Enzo Cerundolo, pers. comm.; 2): [15]; the following index shows the types of assay:

types of assay:	source of D^b protein:	label	separation bound / free
A	$T2D^b$ cells	iodine	immunoprecip.
B	$T2D^b$ cells	tritium	immunoprecip.
C	recombinant	iodine	filtration
D	recombinant	tritium	filtration
E	recombinant	fluorescence binding assay (figure 44)	

For the SV-324-332 peptide, it is remarkable that the tritiated peptide dissociates more slowly than the iodinated from the cellular in the presence of detergent (2.2/3.9), but faster (7.0/2.2) from the recombinant in PBS. It is possible that detergent interactions with the protein influence the reaction parameters for different peptides in different directions; this could best be elucidated in a series that involve the temperature

dependence of the reactions to derive thermodynamical parameters.

For both iodinated SV-324-332 and the NP-Y367-374 peptides, the complex with D^b is more stable in the absence than in the presence of detergent (2.17/3.85 and 0.73/1.24, respectively). Tritiated SV-324-332 peptide behaves in an opposite way (7.09/2.22).

For the NP-Y367-379 peptide, the off-rates obtained with (l) and without (k) detergent coincide.

The temperature dependence of the dissociation rates can be used to estimate the energy barrier for the dissociation (see below).

In the fluorescence assay, off-rates could be measured by dilution experiments. However, dissociation times of this order of magnitude are difficult to measure because it is not easy to maintain the stability of the instrument baseline over a very long time, and experiments to this end did not give reliable results (Klaus Döring, personal comm.; data not shown). It was tried, however, to measure the off-rate of the long peptide NP-Y367-379 through its displacement by NP-Y367-374, which gives a stronger fluorescence enhancement (see above). The experiment is shown in figure 44: Db molecules were presaturated with 1 μM NP-Y367-379. When equilibrium was reached, 10 μM NP-Y367-374 peptide were added. Due to the displacement of the long by the short peptide, a slow increase in fluorescence was observed over the next 100 minutes, and a computer fit to the curve gave $\tau = 27$ minutes and therefore koff = $4.3 \cdot 10^{-4}$ s^{-1}. This number should not be influenced by the on-rate of the short peptide as this is at least four orders of magnitude higher under these conditions. The off-rate obtained is six-fold faster than the one measured biochemically at 4 °C.

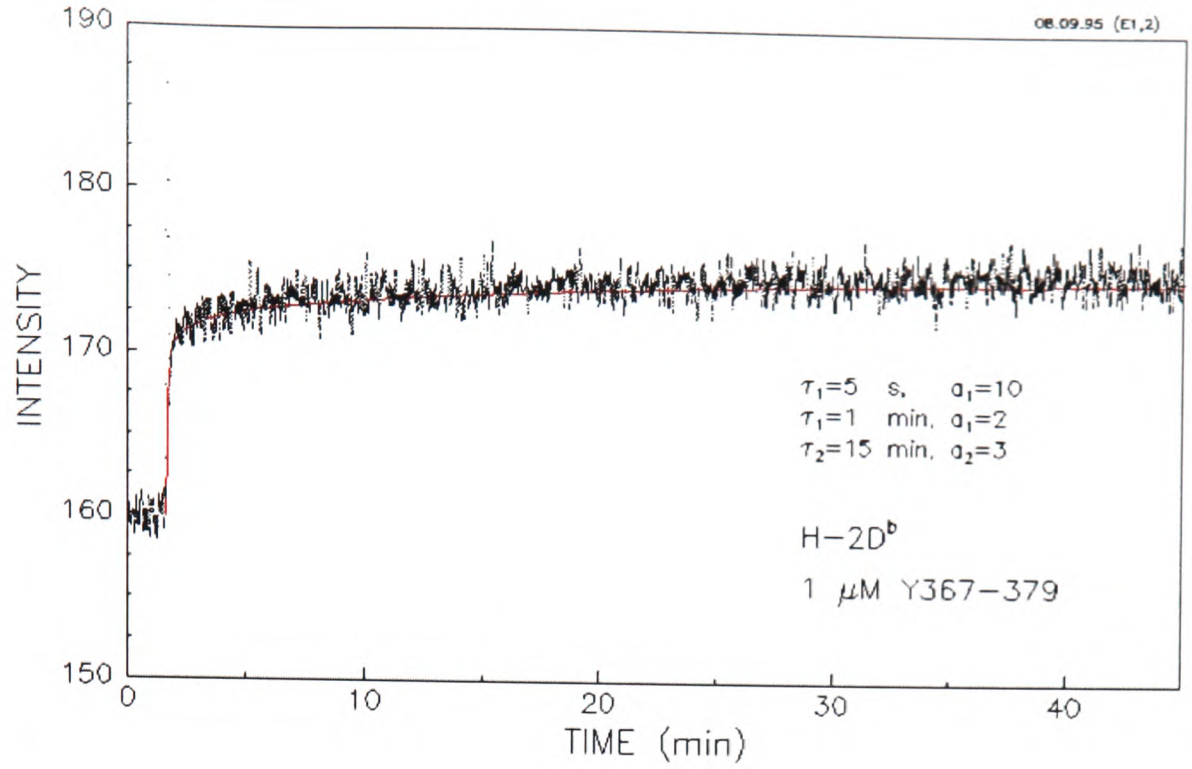

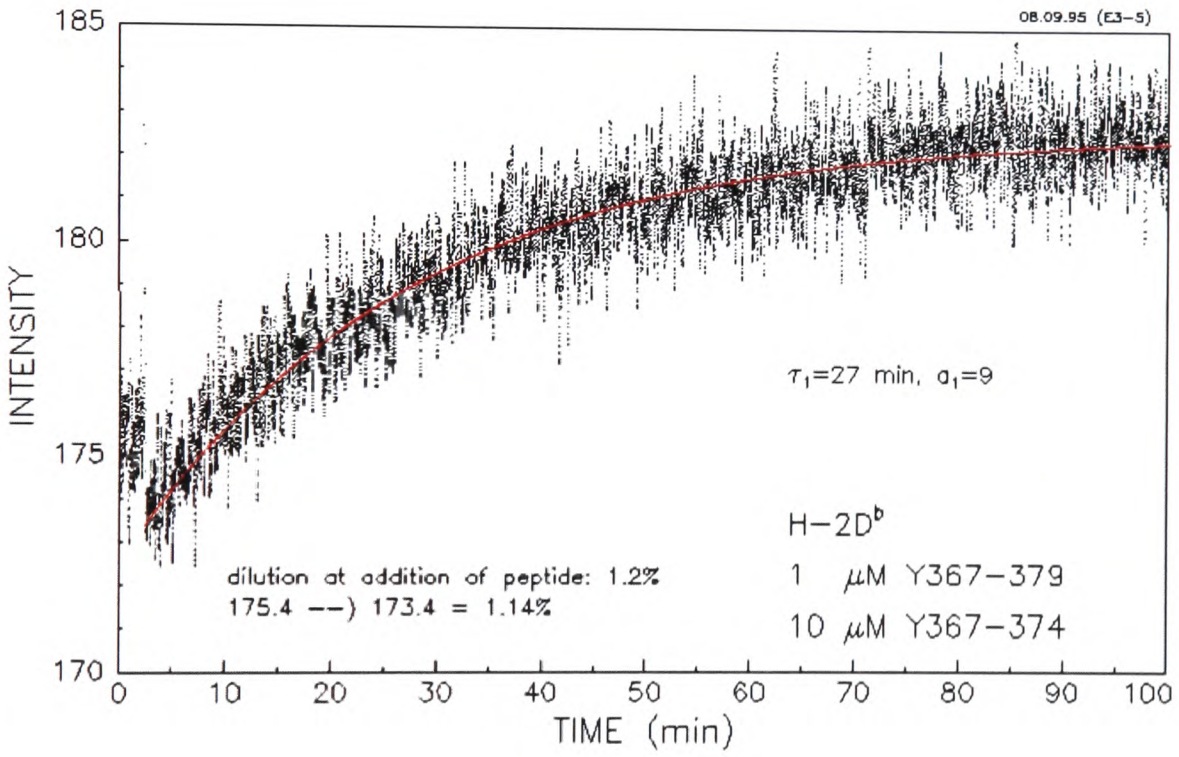

Figure 44: Measurement of the off-rate of NP-Y367-379 by displacement (at room temperature). Top panel, the protein is first incubated with 1 µM Y-367-379; bottom panel, when equilibrium is reached, a ten-fold excess of NP-Y367-374 is added which gives greater fluorescence enhancement. The off-rate of the NP-Y367-379 complex is the time-limiting step for its association. Time constant obtained: $t_{1/2}$ = 27'; k_{off}= $4.28 \cdot 10^{-4}$. Experiment done by Klaus Döring.

6. Summary: Kinetic measurements

The following table 8 puts together the data from binding experiments where on-rate, off-rate, and equilibrium constants were all measured.

peptide	Type of assay	temp. °C	k_{on} ($M^{-1}s^{-1}$)	k_{off} (s^{-1})	k_{on}/k_{off} (M^{-1})	$K_{a.eq.}$ (M^{-1})
NP-Y367-379	A	4	$3.4 \cdot 10^{5}$ (± 0.25)	$7.0 \cdot 10^{-5}$ (± 0.021)	$4.86 \cdot 10^{9}$ (± 0.36)	$4.35 \cdot 10^{6}$ (± 0.69)
	D	4	$6.0 \cdot 10^{2}$	$7.69 \cdot 10^{-5}$	$7.8 \cdot 10^{6}$	$5.8 \cdot 10^{6}$
NP-Y367-374	A	4	$5.41 \cdot 10^{5}$ (± 0.03)	$3.51 \cdot 10^{-7}$ (± 0.53)	$1.54 \cdot 10^{12}$ (± 0.23)	$5.41 \cdot 10^{7}$ (± 0.15)
	D	4	$5.59 \cdot 10^{3}$	$1.24 \cdot 10^{-6}$	$4.51 \cdot 10^{9}$	$2.3 \cdot 10^{7}$
SV-324-332	B	4	$4.6 \cdot 10^{5}$ (± 0.91)	$7.09 \cdot 10^{-6}$ (± 0.14)	$6.48 \cdot 10^{10}$ (± 1.29)	$9.24 \cdot 10^{7}$ (± 1.86)
	B	20	$1.8 \cdot 10^{6}$ (± 0.24)	$3.51 \cdot 10^{-5}$ (± 0.18)	$5.14 \cdot 10^{10}$ (± 0.73)	$3.5 \cdot 10^{7}$
	C	4	$9.6 \cdot 10^{4}$ (± 3.18)	$2.22 \cdot 10^{-6}$ (± 0.11)	$4.32 \cdot 10^{10}$ (± 1.4)	$3.5 \cdot 10^{7}$

Table 8: Comparison of kinetic and equilibrium data. Types of assay: A, recombinant protein, iodinated peptide, no detergent (on-rate by stopped-flow); B, recombinant protein, tritiated peptide, no detergent (on-rates at 16.5 °C); C, recombinant protein (from $T2D^b$ for off-rate measurements), tritiated peptide, in detergent; D, cellular protein, iodinated peptide, in detergent lysate (data taken from [208]). The exponents are also applicable to the standard errors. Standard errors for k_{on}/k_{off} calculated from the law of error propagation.

It is immediately evident that now the difference between the k_{on}/k_{off} ratio and the measured equilibrium K_a is at least three orders of magnitude. This is of course due to the

faster on-rates that were measured with the recombinant protein, putting the predicted affinity constants now in the range of $10^{10} - 10^{11}$ M^{-1}.

The interpretation of these data must lead to the suggestion that a more complex binding process underlies the observations. The confidence with which another model than simple Langmuir binding can be proposed critically depends on the accuracy of the measurements. The following section therefore deals with the usual artefacts in binding studies (in bold; taken from [21] and [22]) and how I have attempted to avoid them. It is important to keep in mind that the discrepancy measured consists of affinity constants (K_a) that are comparatively too low, or on-rates (k_{on} or k_1) that are comparatively too high, and that it is therefore important to obtain good <u>maximum</u> estimates of K_a and <u>minimum</u> estimates for k_{on}.

The tracer ligand in the radioligand binding assay is impure ($L = L_0 - RL$ is invalid). If the impurities have a lower binding affinity for D^b, this would lead to an <u>over</u>estimation of the specific activity, therefore an <u>under</u>estimation of the concentration of ligand bound ([RL]), and an <u>over</u>estimation of the affinity constant. This is a valid caveat for the iodinated (unpurified) but not the tritiated peptide. On HPLC analysis, several radioactive peaks were seen in the iodinated peptide preparation, some of which apparently came from oxidised peptide. On comparison, however, results with HPLC-purified pure iodinated peptide have given the same affinity data as with the unpurified peptide material used in [15]. For example, the binding assay in figure 18 was done with pure tracer ligand, diluted with unlabelled peptide. This and similar criticisms do not apply to the fluorescence experiments, where no tracer ligand was used.

Tracer and unlabeled ligand do not have the same affinity. If the affinity of the tracer ligand for the receptor is less, the specific activity of the bound ligand is less than the overall specific activity: therefore [RL] is <u>under</u>- and Ka <u>over</u>estimated. Instead, I find the K_a to be <u>lower</u> in experiments with iodinated as opposed to tritiated SV-324-

332 peptide, indicating that the affinity of the iodinated peptide might be higher! This could be conclusively demonstrated in an assay using cold iodinated peptide. For the NP peptides, this comparison has not been possible; but for the tritiated SV-324-332, the mismatch kinetics persist.

The specific activity of the tracer ligand is wrong, or counting is erroneous. For iodinated peptide, this is a potential problem due to tracer impurity. Again, HPLC-purified material radioactive material was added to a peptide solution of known concentration (by E_{275}) to circumvent this. The γ-counting of ^{125}I usually poses no technical problems. For tritium, however, scintillation counting is not easy due to the contribution of chemiluminescence which I have controlled for by counting dilutions of pure radioligand under experimental conditions.

Ligand is lost due to adsorption. This tends to be a problem with peptides. If it occurs, it should steepen the binding curve and increase the K_a artificially; it is a potential artefact in the fluorescence experiment in fig. 40. To prevent adsorption, peptide solutions were kept at the highest possible concentration during dilution (100-1000 fold the final concentrations), and buffers of high ionic strength (150 mM NaCl in both PBS and lysis buffer) were used. BSA was not normally added to the binding assays. In kinetics experiments, ligand absorption (like depletion) should lead to an overestimation of the on-rate constants, but only at low concentrations of peptide. I tried to avoid this by measuring on-rates at different concentrations where possible (see figure 39). In the stopped-flow experiments, effects of depletion or adsorption are unlikely as the peptide was always kept in large excess to allow simple curve fitting.

The receptor is unstable. In detergent, empty class I - peptide complexes dissociate overnight. This could have an effect on the on-rate experiments, as the receptor concentration decreases steadily; it was tried to counteract this effect by the inclusion of 1 μM β_2m in the cell lysate. The recombinant D^b-His_6·β2m is stable in PBS over several

weeks.

The accessibility of the receptor limits the on-rate: mass-transport artefacts pose a problem with surface-coupled receptors [213]. They do not trouble the stopped-flow fluorescence as this is done entirely in solution.

The assay method does not separate bound from free. On immuno- or Nickel beads precipitations, sometimes not all of the receptor is bound, although I took care to use the precipitating agent in at least tenfold excess. The error should not be more than 1%, and should mainly reduce the number of binding sites calculated. In the fluorescence method, no separation of bound from free is necessary.

The assay method permits dissociation of an unstable intermediate. In the filtration assay with a separation time of approx. 20 seconds, the off-rate must not be higher than $5.25 \cdot 10^{-3}\ s^{-1}(0.105/\tau)$ if 90% of the ligand should be retained on the beads [21]. For the immunoprecipitation assay (5 minutes), the maximum detectable rate thus calculated is $3.5 \cdot 10^{-4}\ s^{-1}$. It is conceivable that an intermediate with an off-rate faster than these numbers could have been missed in the assay. In a controlled experiment, I compared two on-rate time-courses, one washing the filters (after application of the sample suspension) for the shortest possible time (five seconds), the other washing for five minutes. The result was a nearly constant difference in the counts between the two curves, attributable to higher background binding in the shorter wash; and both curves reached saturation at about the same time. This was taken as an argument against the presence of an intermediate state with life-times longer than ten seconds ($k_{off} < 7 \cdot 10^{-2}\ s^{-1}$). Any intermediate that dissociates faster will not be detectable with biochemical methods; but it would also make the initial equilibrium unfavorable for a binding reaction (see below).

As the fluorescence measurement does not dissociate bound from free ligand, [RL] should be higher in a fluorescence measurement, resulting in a higher affinity constant.

The constant measured in figure 40 ($1.5 \pm 0.6 \cdot 10^7$ M^{-1})does not justify this statement when compared to the binding constant measured biochemically ($1.48 \pm 0.37 \cdot 10^7$ M^{-1}; see table 6). This is assuming that the 'intermediate' would give a fluorescence signal. Along these lines, a triple-syringe stopped-flow experiment, where D^b-His_6·β2m is first mixed with (fluorescence-reducing) GP-92-101 peptide and allowed to associate, then with a large excess of NP-Y367-374 to see if any of the protein is now available for a rapid peptide exchange, would give more evidence.

Background binding provides for artificially fast on-rates in the filtration assay. To avoid non-specific binding, the filters were pre-treated with Western blot blocking buffer (skimmed milk and detergent) overnight. Background binding to the Nickel beads or to protein A sepharose was negligible.

The assay time is not long enough to reach equilibrium. Usually, the time needed for the full equilibration of a system is five times the half-time of the slowest dissociation process in the system [21]; this leads to incubation times of up to 114 days in this system (NP-Y367-374: off-rate $3.51 \cdot 10^{-7}$ s^{-1} at 4 °C, half-time 549 hours)! This is highly impractical, especially in detergent where the empty complexes will dissociate, leading to a continuous depletion of receptor. After overnight incubations, however, no more significant change in [RL] was visible. If the system had not equilibrated at this time, [RL] would have been estimated too high, leading to an overestimated K_a. A limitation of stopped-flow fluorescence experiments is that the instrument baseline is not very stable so that measurements for longer than a few seconds are not possible. Steady-state fluorescence measurements will satisfactorily hold a stable baseline for a few hours if the protein concentration is high enough; unfortunately, it had to be kept low in the binding experiments to minimise ligand depletion (see figure 40).

There is undetected ligand depletion. This will lead - slightly counterintuitively - to an initial steepening of the equilibrium binding curve and an overestimation of the rate

constant [21]. In the radioligand equilibrium binding curves, depletion was taken into account wherever possible by either plotting the data in the Scatchard diagram, or by fitting the full binding function including ligand depletion, and not the simple Langmuir isotherm. In the kinetic radioligand assays, ligand depletion was controlled for by fitting the full on-rate function, including depletion, to the data wherever necessary (see fig. 39). In the stopped-flow experiments, at least tenfold excess of peptide over D^b was used at all times to obtain a strong signal and to allow for easy fitting of the on-rate curves.

Systematic deviations are overlooked in the fitting procedures, or numerical artefacts are introduced in the fitting routine. Wherever possible, the data where linearised to assess deviations from the proposed model. However, the fit was usually performed via a least-squares algorithm directly to the proposed equation, and the standard errors of the original points were taken into account in the fitting routine. If no standard errors were available, a fixed percentage of the value (5%) was assumed as the standard error to avoid an overweighting of the initial points.

The kinetic data are discussed further in the chapter about modelling.

7. Evidence for conformational alterations of the class I molecule upon peptide binding

A second branch of the investigation of the class I - peptide interaction was the attempt to directly investigate the alteration of the class I structure upon the binding of peptide. The most frequently used biophysical methods that are sensitive for conformational parameters are the determination of circular dichroism; ultra-violet, infra-red, fluorescence / fluorescence anisotropy, and Raman spectroscopies; the determination of the energetic parameters of a reaction via isothermal and differential scanning calorimetry or the temperature dependence of the reaction constants; nuclear magnetic resonance (NMR); deuterium exchange mass spectroscopy; and, finally, crystallographic or NMR determination of the full structure of the protein.

Samples of sufficient purity for crystallography, NMR, mass spectroscopy, and calorimetry were only available at the end of this work; these investigations are now being carried out. In the following, work on thermodynamic parameters, fluorescence quenching, CD, and fluorescence anisotropy is reported.

7.1. Thermodynamic analysis of equilibrium and rate constants

Analysis of the thermodynamics of the class I - peptide interaction has not been performed to date; however, the method has added significantly to the understanding of other systems (see below). The theoretical derivations in the following have been taken from the reviews: [282-286].

7.1.1. Equilibrium thermodynamics

The relationship between changes in free energy ($\Delta G°$), enthalpy ($\Delta H°$), temperature (T), and entropy ($\Delta S°$) in the course of a reaction is as follows:

$$\Delta G^\circ = \Delta H^\circ - T \cdot \Delta S^\circ$$

At conditions different from the standard state (where all components are at unit concentration), the net free energy change is defined as

$$\Delta G = \Delta G^\circ + R \cdot T \cdot \ln K_a,$$

where Ka is the association constant of the reaction, and R the universal gas constant (8.314510 $J \cdot mol^{-1}K^{-1}$) . At equilibrium, when the system cannot perform work, ΔG becomes zero, and therefore

$$\Delta G^\circ = - R \cdot T \cdot \ln K_a.$$

Inserting the above relation gives

$$\Delta H^\circ - T \cdot \Delta S^\circ = - R \cdot T \cdot \ln K_a$$

$$\ln K_a = \frac{\Delta S^\circ}{R} - \frac{\Delta H^\circ}{R} \cdot \frac{1}{T} \text{ (van t'Hoff equation).}$$

For a small temperature interval where both ΔH° and ΔS° do not depend on the temperature, plotting $\ln K_a$ against 1/T will give a straight line with a slope of $-\frac{\Delta H^\circ}{R}$ and a y-intersection of $\frac{\Delta S^\circ}{R}$ (van t'Hoff plot). Alternatively, the van t'Hoff equation can be fitted directly to the data.

For the binding of the iodinated peptide, NP-Y367-374, to D^b, the following binding constants were taken from table 6:

temperature	K_a (M^{-1})	s. dev.
4 °C	$5{,}41 \cdot 10^7$	$1.5 \cdot 10^6$
25 °C	$1.48 \cdot 10^7$	$3.7 \cdot 10^6$
37 °C	$5.50 \cdot 10^6$	$7.5 \cdot 10^5$

The van't Hoff plot, and a direct fit, for these data are given in figure 45.

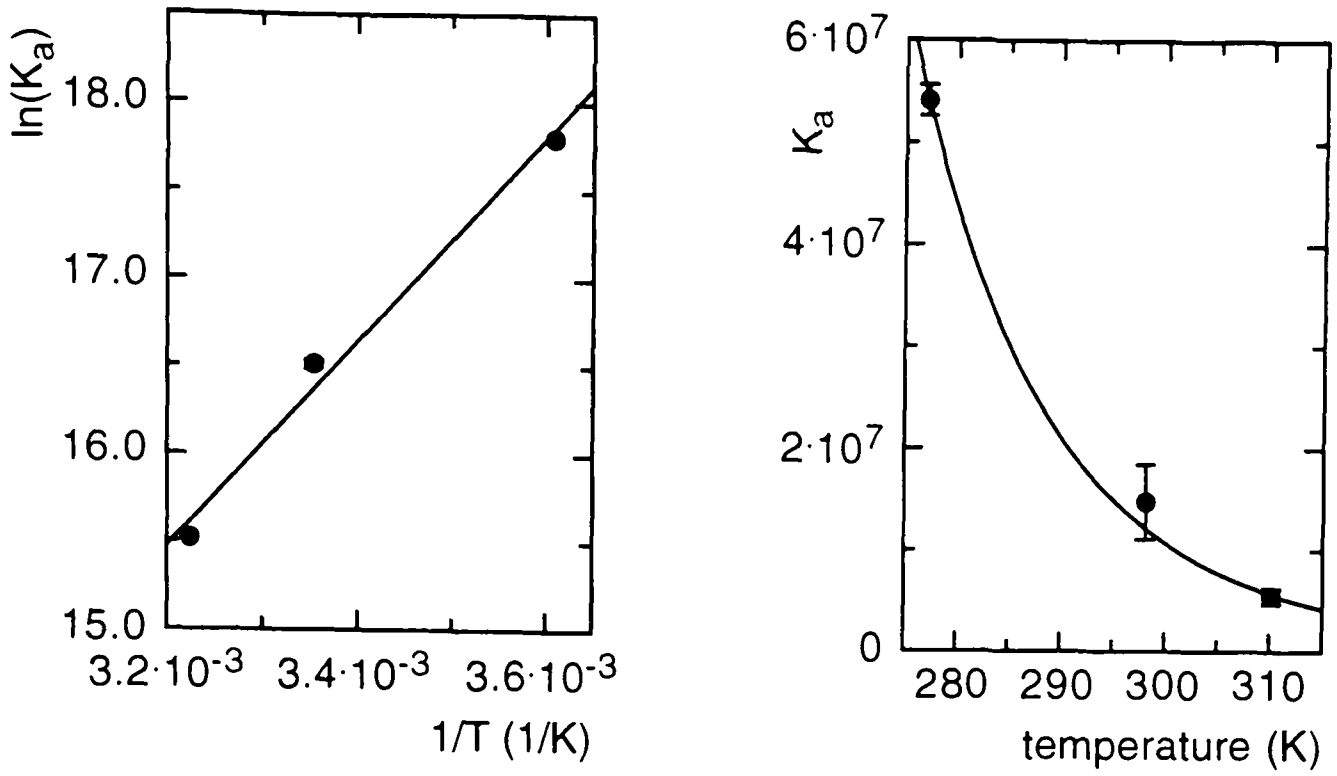

Figure 45: Thermodynamics of equilibrium binding of NP-Y367-374 (iodinated) to D^b. Left panel, van t'Hoff plot; right panel, direct fit. The thermodynamic constants result as follows:

fit:	van t'Hoff plot	direct fit (±SD)
$\Delta G°$ (J/mol, at 300 K)	$-4.10 \cdot 10^4$	$-4.05 \cdot 10^4$
$\Delta S°$ (J/[mol·K])	-26.7	-28.5 (±10)
$\Delta H°$ (J/mol)	$-4.9 \cdot 10^4$	$-4.9\ (\pm 0.28) \cdot 10^4$

The reaction occurs spontaneously because $\Delta G°$ is negative. A negative free energy change during a binding reaction can come from two directions: either a positive entropic contribution (the introduction of more 'molecular disorder' due to the introduction of more translational [= more molecules, e.g. dissociation of hydration shells] or rotational degrees of freedom), or a negative enthalpic contribution (an increase in the heat content per unit mass due to more intramolecular interactions like hydrogen bonds or van der Waals forces), or both. The most important factor is the temperature dependence of $\Delta S°$: if $\Delta S°$ is negative, it must be compensated for by a large negative enthalpic contribution for binding to occur [286].

In an example, Weiland et al. [287] show that the binding of agonists to the β-adrenergic receptor leads to a decrease in entropy (-50 to -150 $J \cdot mol^{-1}K^{-1}$) which is compensated for by a negative enthalpic contribution (-56 to -79 kJ/mol, RT). The binding of antagonists, however was shown to be fully entropy-driven ($\Delta S° = +54$ to $+177$ $J \cdot mol^{-1}K^{-1}$). In their interpretation, binding processes which do not involve 'information transfer' to the receptor are characterised by positive entropies due to the liberation of water molecules from the binding sites, as in the binding of ovalbumin by an antibody ($\Delta S° = +84$ $J \cdot mol^{-1}K^{-1}$) or of organic ions by bovine serum albumin ($\Delta S° = +60$ to $+70$ $J \cdot mol^{-1}K^{-1}$). In these reactions, large enthalpy changes do not occur because all hydrophilic and hydrophobic interactions between ligand and receptor replace similar ones with water molecules. The interaction between receptors and agonists should also involve an increase in entropy as similar numbers of water molecules are displaced. The overall negative entropy change must therefore originate from the introduction of molecular order in a second step, most likely a conformational rearrangement leading to a more rigid structure of the complex. The authors propose a two-step model that includes an initial encounter step with a small (positive or negative) enthalpy and a positive entropy change, and a rearrangement with a large negative entropy contribution, and a large negative enthalpy change to compensate. This interpretation has become widely accepted, although occasional exceptions have led to reservations ([288]; for full review see [286]).

The data obtained here for D^b and NP-Y367-374 show a very clear decrease of the affinity constant with temperature, and therefore a negative entropic contribution. Following the interpretation above, an additional step in the binding process needs to be postulated that involves loss of entropy. This finding is in agreement with a conformational change upon peptide binding, and it might - more specifically - originate from the fixation of the positions of the α-helices by the interactions with the peptide, or the formation of the hydrogen bond networks between peptide, α-helices, and the β-sheet floor at the N and C termini that are an important structural element (see

introduction). The nature of this conformational change could be evaluated using different peptides for the thermodynamic analysis, especially those with modified or elongated termini or changed anchor residues. For greater accuracy of measurement, equilibrium thermodynamic parameters should be derived via isothermal calorimetry, as determination of affinity constants at different temperatures is only the second best method [289].

7.1.2. Transition state thermodynamics

If the temperature dependence of a reaction constant is known, quantitative information can be derived about $\Delta G^{\ddagger}$, the transition state free energy change.

$\Delta G^{\ddagger}$ in an ideal gas has enthalpy and entropy components:

$$\Delta G^{\ddagger} = \Delta H^{\ddagger} - T \cdot \Delta S^{\ddagger}$$

(T = temperature in Kelvin). If concentrations are to be expressed as molar fractions and not as partial pressures, the following equation has to be used instead [290]:

$$\Delta G^{\ddagger} = E_A - T \cdot \Delta S^{\ddagger}$$

E_A, the 'energy of activation', relates to the transition state enthalpy via:

$$\Delta H^{\ddagger} = EA - (1 - \Delta n^{\ddagger}) \cdot RT,$$

with $\Delta n^{\ddagger}$= the difference between the number of molecules after and before the reaction.

This is -1 for a binding reaction, so that here

$$\Delta H^{\ddagger} = EA - 2 \cdot RT.$$

(For T, the mean temperature of the measurements can be used here.)

$\Delta G^{\ddagger}$ is related to the rate constant, k_r, by the Arrhenius equation [291]:

$$k_r = \frac{k \cdot T}{h} \cdot e^{-\Delta G^{\ddagger}/RT}$$

with k: Boltzmann's constant, $1.380658 \cdot 10^{-23}$ J/K,

h: Planck's constant, $6.6260755 \cdot 10^{-34}$ J·s.

Rearrange:

$$\ln (k_r) = \left(\frac{\Delta S^{\ddagger}}{R} + \ln \frac{k \cdot T}{h} \right) - \frac{E_A}{R} \cdot \frac{1}{T}$$

Therefore, a plot of $\ln (k_r)$ against $1/T$ has $-\frac{E_A}{R}$ as the slope of the resulting straight line, and $\left(\frac{\Delta S^{\ddagger}}{R} + \ln \frac{k \cdot T}{h} \right)$ as its y intercept. Alternatively, the curve can be fitted directly.

For the binding of the peptide, NP-Y367-374, to the D^b-His_6·β_2m complex, the following rate constants at different temperatures were measured (see table 3):

temperature	k_{on}	s. dev.
4 °C	$5.41 \cdot 10^5$	300
16.5 °C	$1.81 \cdot 10^6$	$2.4 \cdot 10^5$
25 °C	$3.02 \cdot 10^6$	$6.04 \cdot 10^4$

The Arrhenius plot, and a direct fit, for these data are given in figure 46.

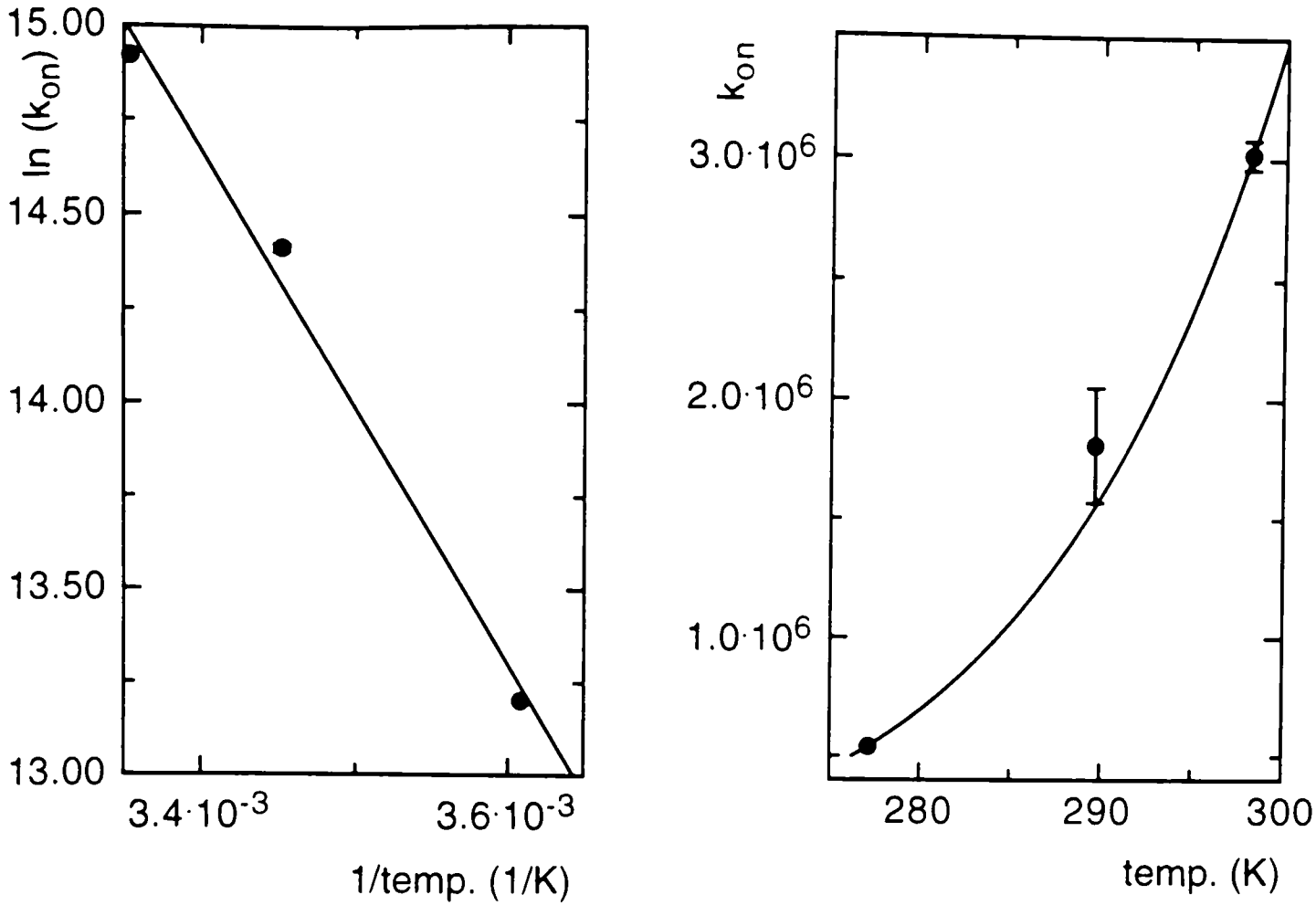

Figure 46: Thermodynamics of the binding of NP-Y367-374 to D^b.

Left panel, Arrhenius plot. Right panel, direct fit. The thermodynamic constants result from the fits as follows:

fit:	Arrhenius plot	direct fit
E_A (J/mol)	$5.70\ (\pm 0.57) \cdot 10^4$	$5.39\ (\pm 0.65) \cdot 10^4$
$\Delta H^{\ddagger}$ (J/mol)	$5.22 \cdot 10^4$	$4.91 \cdot 10^4$
$\Delta S^{\ddagger}$ (J/[mol·K])	70.8263	60.01 (±2.3)
$\Delta G^{\ddagger}$ (J/mol) at 300 K	$3.09 \cdot 10^4$	$3.59 \cdot 10^4$

(Standard deviations are only given where meaningful.)

The transition state has positive entropy and enthalpy changes associated, as opposed to the negative values at equilibrium. This leads to a significant energy barrier ($\Delta G^{\ddagger} > 0$). The activated state fulfils the prediction made from the equilibrium measurements that there must be an initial step with a positive association entropy (see above). Following the activated state, there must be a strong decrease in entropy (while now the driving force for the reaction is provided by the negative enthalpy), best explained with a

conformational rearrangement (see above).

The temperature dependence of a process is often expressed as the ratio of the rate constants measured at 10 K apart, the so-called Q_{10} value. The Q_{10} value of 2, shared by most reactions involving proteins, corresponds to an E_A of 49 kJ/mol [22]. The initial binding of class I and peptide can therefore be said to lie within the common values for protein-ligand encounters. Reactions that are entirely diffusion-controlled usually have energy barriers between 20 and 40 kJ/mol, whereas reactions that involve changes in protein conformation have higher values, up to 100 - 200 kJ/mol. Comparing different classes of antibodies, Foote and Milstein [264] attribute 20 kJ/mol to diffusion control, and 40 kJ/mol to a conformational change of the binding site. The values found here lie higher than that, and it can be suggested that while the initial association does not involve great structural changes in the protein, some rearrangements have to be made to accommodate the peptide. It could be said that he peptide itself will lose a large amount of entropy when immobilised onto the class I molecule; the size of this contribution is difficult to estimate, but the activated complex, where the peptide is already immobilised at least in translational terms, goes along with a large increase in overall entropy (see above). For a tentative scheme of the whole process, see figure 57 below.

More detailed measurements of the on-rate constant might make it possible to detect a multistep mechanism, as these frequently give curved Arrhenius plots [22].

7.2. Circular dichroism (CD) measurements

7.2.1. Circular dichroism

The property of chiral molecules to interact differently with right and left circularly polarized light is called circular dichroism (CD; see review by Woody [292], and [293], and references therein). Proteins are built from chiral amino acids whose CD is strongly influenced by the conformation of the peptide backbone. The CD signal of the latter can

be recorded between 180 and 240 nm (far ultra-violet (UV): the absorption bands of the peptide bonds) to determine the overall conformation of the protein as percentages of α-helix, β-sheet, β-turn, and 'random' coil in its structure; whereas conformations of side chains can be recorded in the near UV (250-350 nm; absorption of aromatic residues and cysteine).

Dynamically, CD measurements can be used to monitor conformational changes in a protein. This approach has been used by Fahnestock and collaborators [219] to look at the thermal stability of the K^d molecule, and by Bouvier and Wiley [141] to estimate the stabilisation energies of different peptides in the complex with HLA-A2. However, the far UV CD signal of a protein mainly allows an estimate of the percentage of the structural elements, and not a complete structural description; minor changes in flexible loops, or shifts of structural elements relative to each other, do not necessarily give a CD signal.

Near-UV (240-300 nm) measurements give no information about protein secondary structures. They can, however, be used to look at protein-ligand binding, and again this was used by Bjorkman and collaborators.

It seemed therefore a good idea to test whether D^b HC·β_2m would exhibit CD changes upon peptide binding.

7.2.2. CD measurements on D^b-His_6·β2m

Two CD spectra of D^b before and after the addition of NP-366-374 peptide were carried out (figure 47). In neither of these experiments was a change visible in the far UV region. This result excludes far-reaching rearrangements of the class I (and peptide!) structure upon the binding of peptide, for example the making and breaking of α-helices or β-sheets, but it certainly does not rule out small alterations e.g. in the position of a helix, or changes in the position or structure of free loops. It is conceivable that the change in conformation is in this range. The difference to Fahnestock et al.'s data could be due to

the specificities of the K^d protein, or to differences in the experimental set-up.

In the same experiments, however, changes in the near UV region were found with a maximum at 295 nm, the main absorption band of tryptophan (see above). This shows that the peptide has indeed bound, and confirms the fluorescence enhancement as an indicator for interactions of the peptide with tryptophans in the protein. However, no further inferences as to conformational alterations are possible from these data.

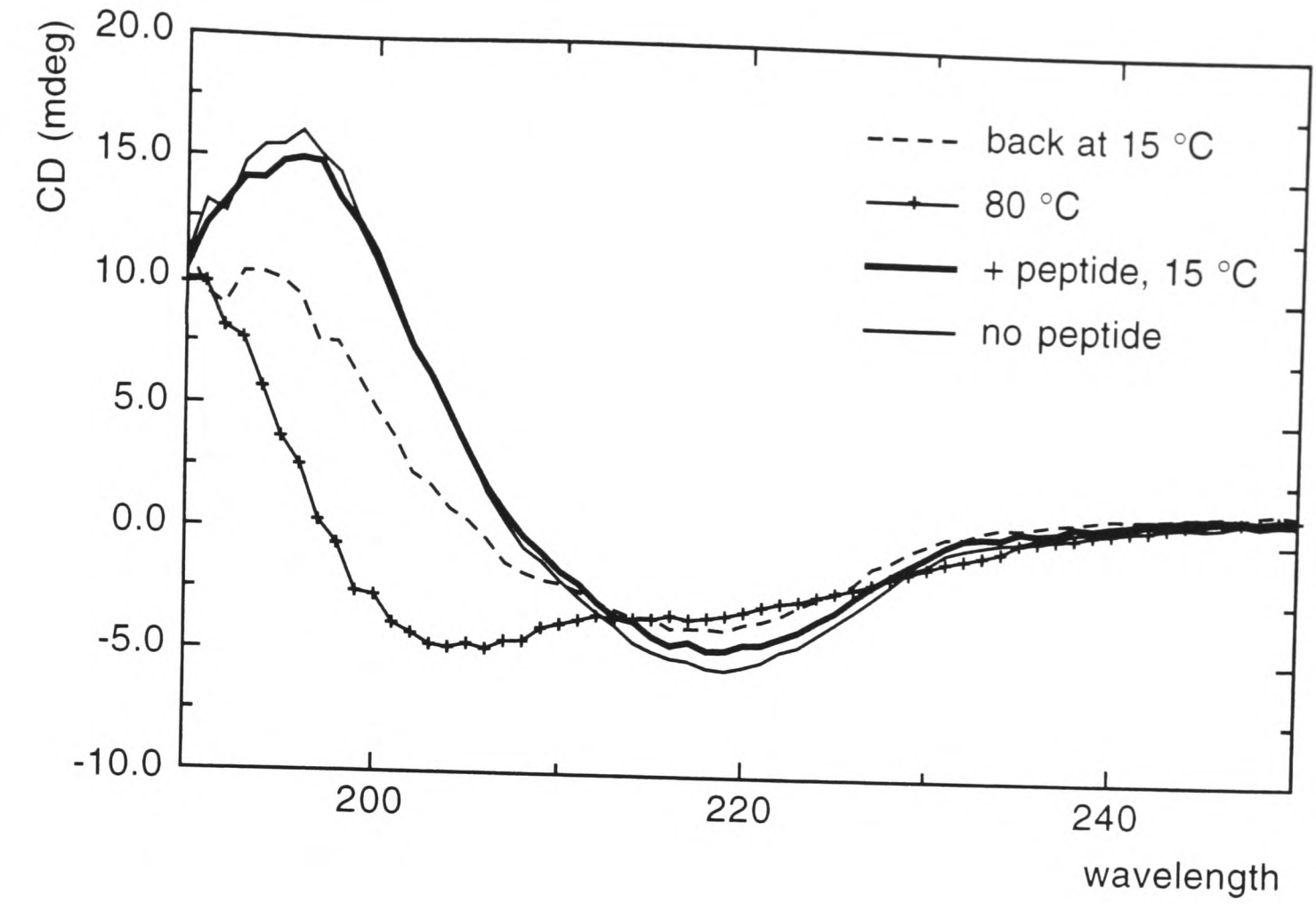

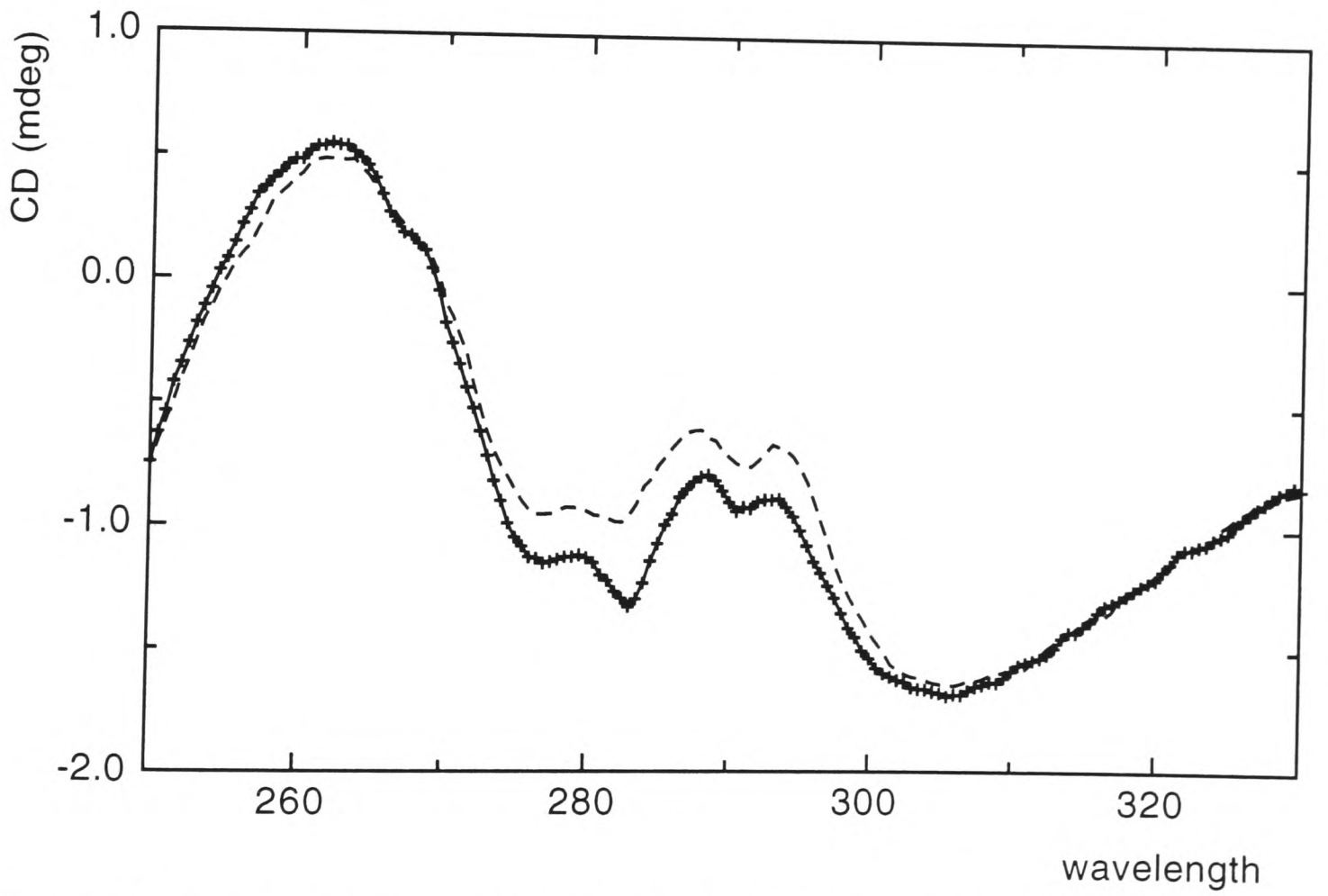

Figure 47: Effects of peptide on near/far UV spectra, and heat denaturation of D^b. Top panel, far UV: curves as in caption; concentration of D^b, 1.9 µM; 1 mm cuvette. Bottom panel, near UV CD of peptide-treated (upper, dashed curve) and untreated material (lower curve): concentration of D^b, 1.9 µM, 10 mm cuvette.

There is a clear effect of peptide on the near UV spectrum but not on the far UV spectrum.

Heating to 80 °C destroys part of the structure irreversibly. Details see text.

I also attempted to measure by CD the thermal stabilisation of the D^b-$His_6 \cdot \beta_2 m$ complexes by peptide, as has been done for K^d by Fahnestock et al, and for HLA-A2 by Bouvier and Wiley [141]. Samples with and without NP-Y366-374 peptide were slowly (1 K / 3 minutes) heated from 20 to 80 °C, and CD at 219 nm recorded (figure 48). The changes in the CD effect upon melting (approx. 1.5 mdeg·l/mol) are approximately threefold higher than observed by these two groups. However, in both studies the authors used the calculated extinction coefficients for the determination of protein concentration; as outlined above, this gives a threefold overestimate of the protein concentration in our hands; therefore, the results can be said to coincide.

The differences between the curves with and without peptide were not as pronounced as in the cited studies, but they invite comparison with figure 3A of the Fahnestock *et al.* paper as especially the curve without peptide is difficult to interpret. The authors in both papers use a fitting algorithm which needs input parameters about the background change in the CD effect (the parts of the curve before and after the steep incline). These parameters, being entirely artificial, profoundly influence the curve fit (especially when several transitions are fitted to one curve). In the instance of the Fahnestock paper, the initial CD change for the empty molecule is seen as part of the melting curve, putting the midpoint of transition (T_m) to 45 °C, whereas for the occupied K^d, this part of the curve is disregarded in the fit, resulting in a T_m of 57 °C. The data shown here for D^b remarkably resemble these two curves in shape. Due to the great number of points measured here, however, this measurement allows for the generation of a first-derivative plot. If the region of steepest incline in this plot is being taken to represent the T_m, then values of 32 °C (empty) and 42 °C (full, midrange) can be assumed. This would make D^b significantly less stable than K^d (45 → 57 °C). An alternative, and more cautious, interpretation would assume that both empty and peptide-filled molecules experience transitions between 30 and 55 °C, and that there is an additional process in the empty molecule between 25 and 30 °C (where the curve for the occupied is flat). This

observation would coincide with the melting point of 28 °C observed in the fluorescence melting experiments described above.

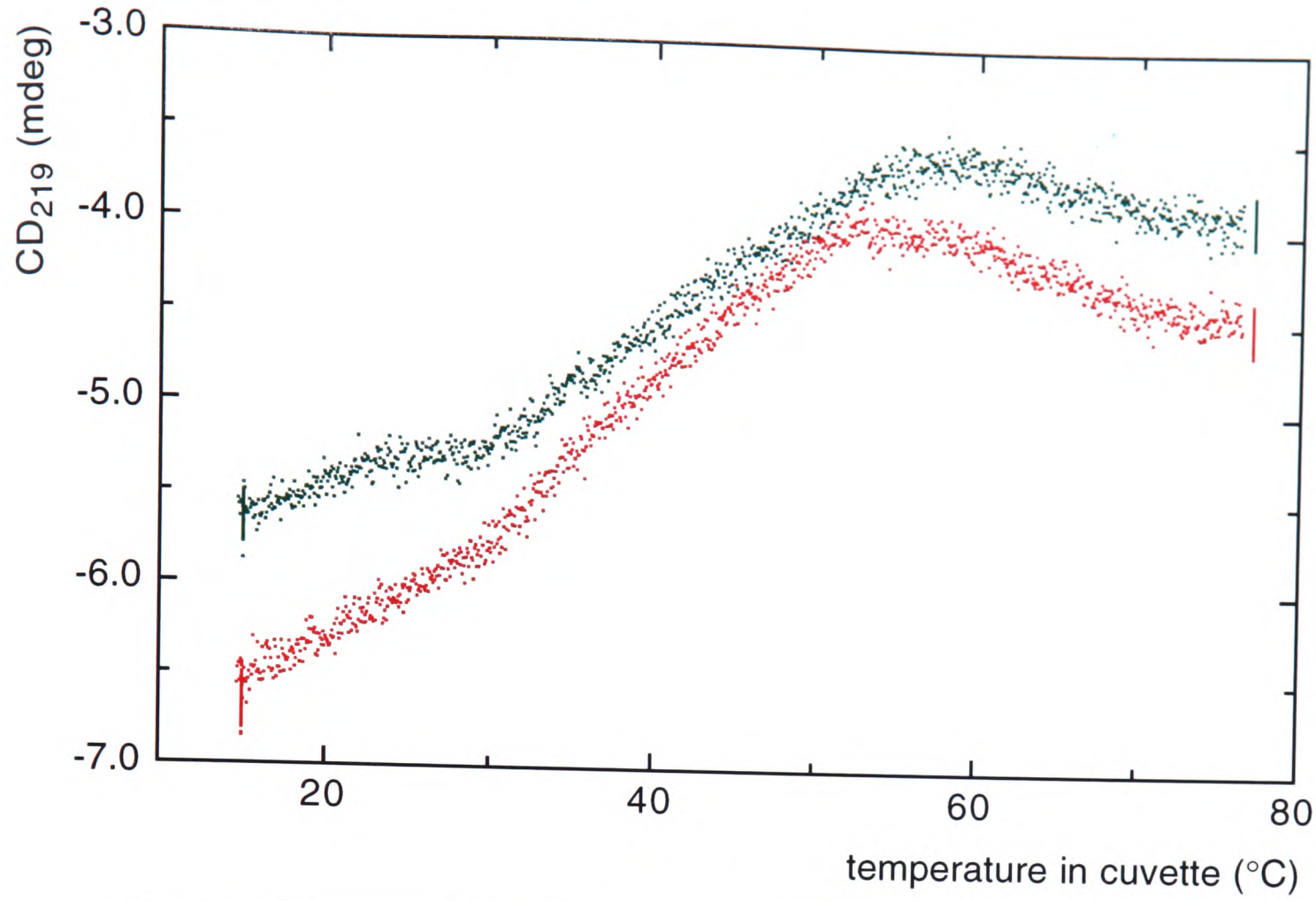

Figure 48: CD gives no clear indication of the melting temperature. CD effect at 219 nm of Db with (green) and without (red) NP-366-374 peptide on heating from 15 °C to 75 °C.

Top panel, CD readings; bottom panel, first derivative (smoothed).

No clear transition midpoints for the protein can be seen in either curve. The CD of the peptide-untreated material seems to increase faster between 20 and 40 °C, possibly indicating denaturation.

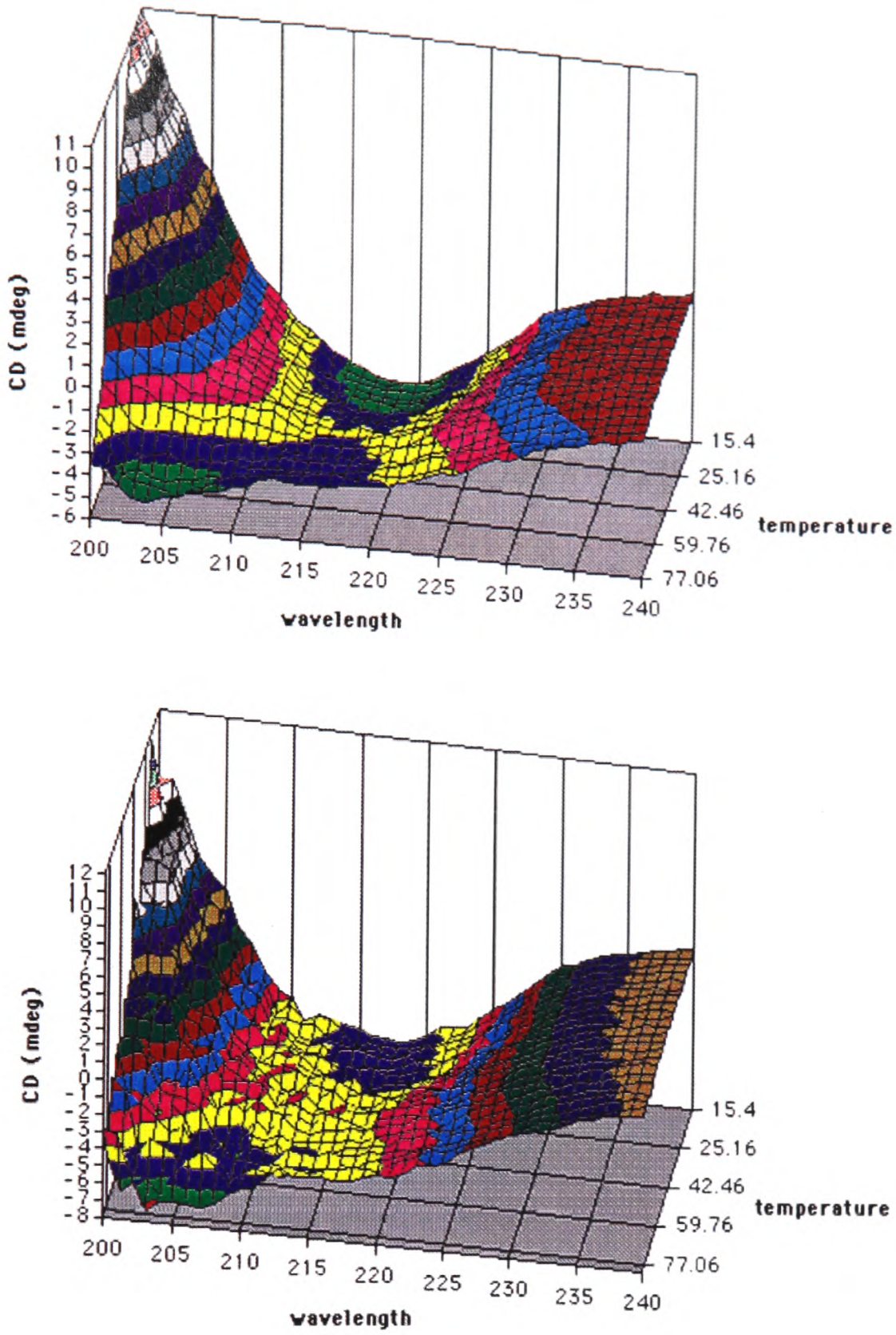

Figure 49: CD scans at different temperatures of D^b-His_6·β_2m in the empty state (bottom panel) and loaded with NP-366-374 peptide (top panel). In the area between 215 and 220 nm, the peptide-loaded material shows more pronounced changes in the CD effect; this could be due to a greater stabilisation of the complex by the peptide.

In an extension of this experiment, samples with and without peptide were heated to 80 °C while full far-UV CD scans were continuously performed. Figure 49 shows the three-dimensional plots arising from this experiment. While it may be noted that in the range around 215-225 nm, where contributions from both helix and sheet are expected, there is generally a more pronounced transition to higher temperatures, systematic analysis of views in the CD/temperature plane (looking at 'melting curves' at different wavelengths) did not reveal an observation wavelength better suited to meaningful analysis.

In accordance with earlier observations is, however, the observation that D^b can be destroyed by heating it to 80 °C - with or without peptide. The molecule exhibited an entirely different CD spectrum after recooling to room temperature (figure 50), and did not bind any peptide in a subsequent fluorescence assay (data not shown).

It can be concluded that CD spectroscopy is not an ideal tool for the observation of conformational changes in class I, and that for the determination of the melting points of different peptide complexes fluorescence (see above) or absorption spectroscopy (as indeed performed by Fahnestock et al.) appears far superior. If one subscribes to the interpretations of Fahnestock *et al.* and Bouvier and Wiley, D^b would have a T_m circa 10 K lower in both the peptide-loaded and unloaded states.

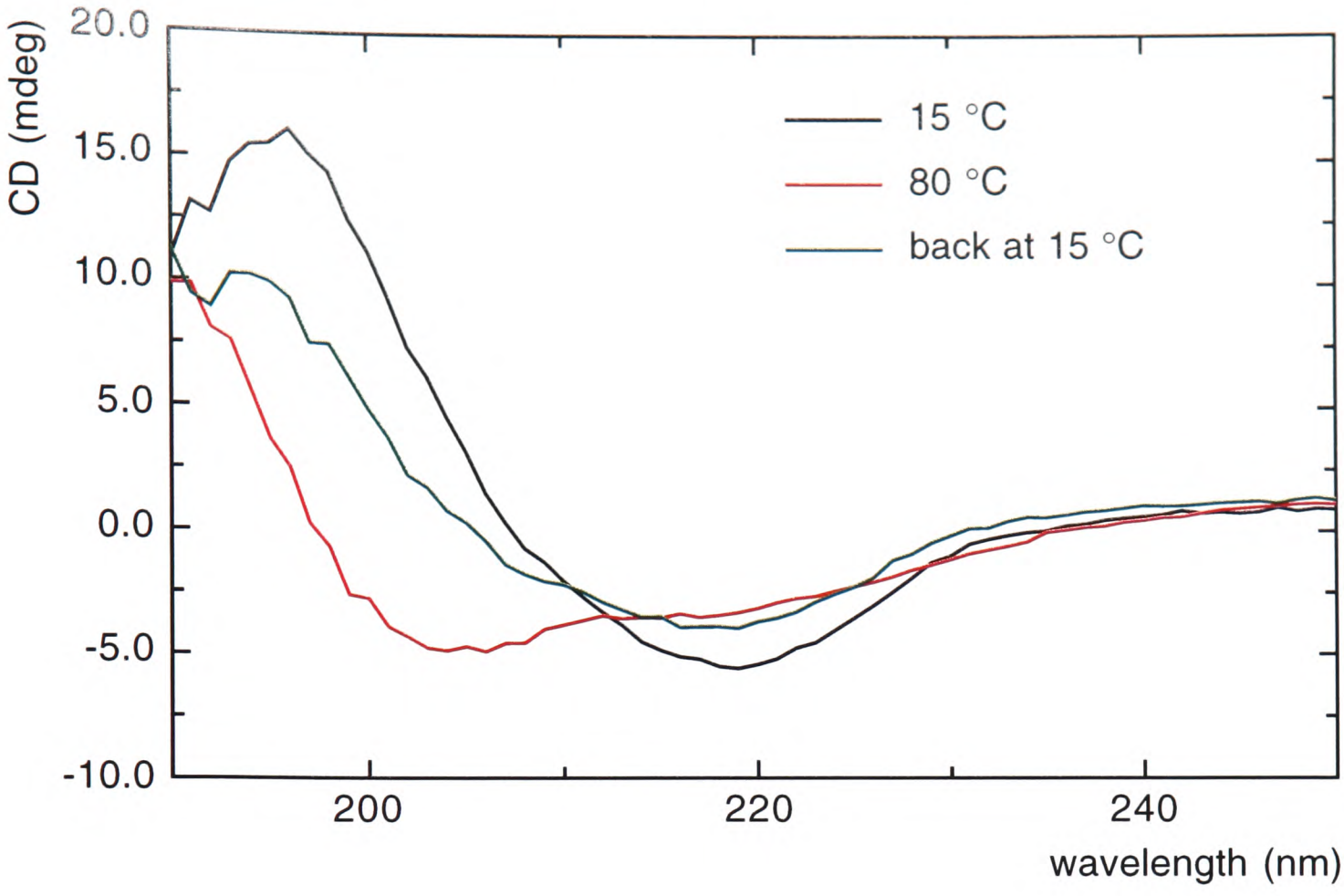

Figure 50: Heat denaturation of empty D^b-His_6·β_2m measured by CD. After heating to 80 °C (red) and recooling to 15 °C, the protein is permanently denatured (green) as compared to the start of the experiment (black). The recooled material does not bind peptide in the fluorescence assay.

7.3. Fluorescence quenching

7.3.1. Principles

A more sensitive way than CD to look at the conformation of flexible regions in a protein is fluorescence quenching. (General reviews: [294, 295].) The method is based on the ability of solutes like molecular oxygen, iodide ion, and acrylamide, to dissipate the energy of the excited state of a fluorophore as heat upon collision. This leads to a decrease (quenching) of the fluorescence emission. As a close steric proximity is necessary for an efficient quenching process, the magnitude of quenching depends strongly on the accessibility of the fluorophores. Quenching studies therefore can be used to derive information about protein conformation, especially when non-polar quenchers, which will have access to most protein interiors, are compared with polar quenchers which can only sample the protein surface.

The effect of the concentration of the quencher on the steady-state fluorescence of a sample is described by the Stern-Volmer equation:

$$\frac{I_0}{I} = 1 + K_{sv} \cdot [Q]$$

with I fluorescence intensity (I_0 in the absence of quencher)

K_{sv} Stern-Volmer constant, $K_{sv} = k_q \cdot \tau_0$

with k_q = quenching rate constant

$[Q]$ concentration of quenching agent

τ fluorescence lifetime (τ_0 in the absence of quencher).

The Stern-Volmer constant is a measure of the quencher's ability to quench the fluorescence of the fluorophore. The higher K_{sv}, the more efficient the quenching process.

7.3.2. Quenching measurements on D^b-His_6·β2m

I have performed quenching experiments with the hydrophilic quencher iodide and the hydrophobic quencher acrylamide and 100 nM D^b complexes in the presence and absence of peptides. Figure 51 shows the fluorescence intensities in relation to the quencher concentration, and the resulting curve fits; table 9 gives the resulting numbers.

Remarkably, the quenching plots for iodide are curved upwards, especially the -peptide curve. This is could be due to several factors (reviewed in [294]): static quenching (due to pre-existing complexes of quencher and fluorophore, e.g. ionic interaction of the iodide ion with the protein surface); nonexponential fluorescence decay due to various reasons, leading to a time-dependent term in the Smoluchowski equation; and also the fact that the 13 tryptophans in the class I molecule have different contributions towards the final fluorescence effect. Because of the latter reason, it is not feasible to deconvolute this curved plot; however, initial fits can be performed with sufficient accuracy to give an estimate for K_{SV} (see figure 51, lower panel).

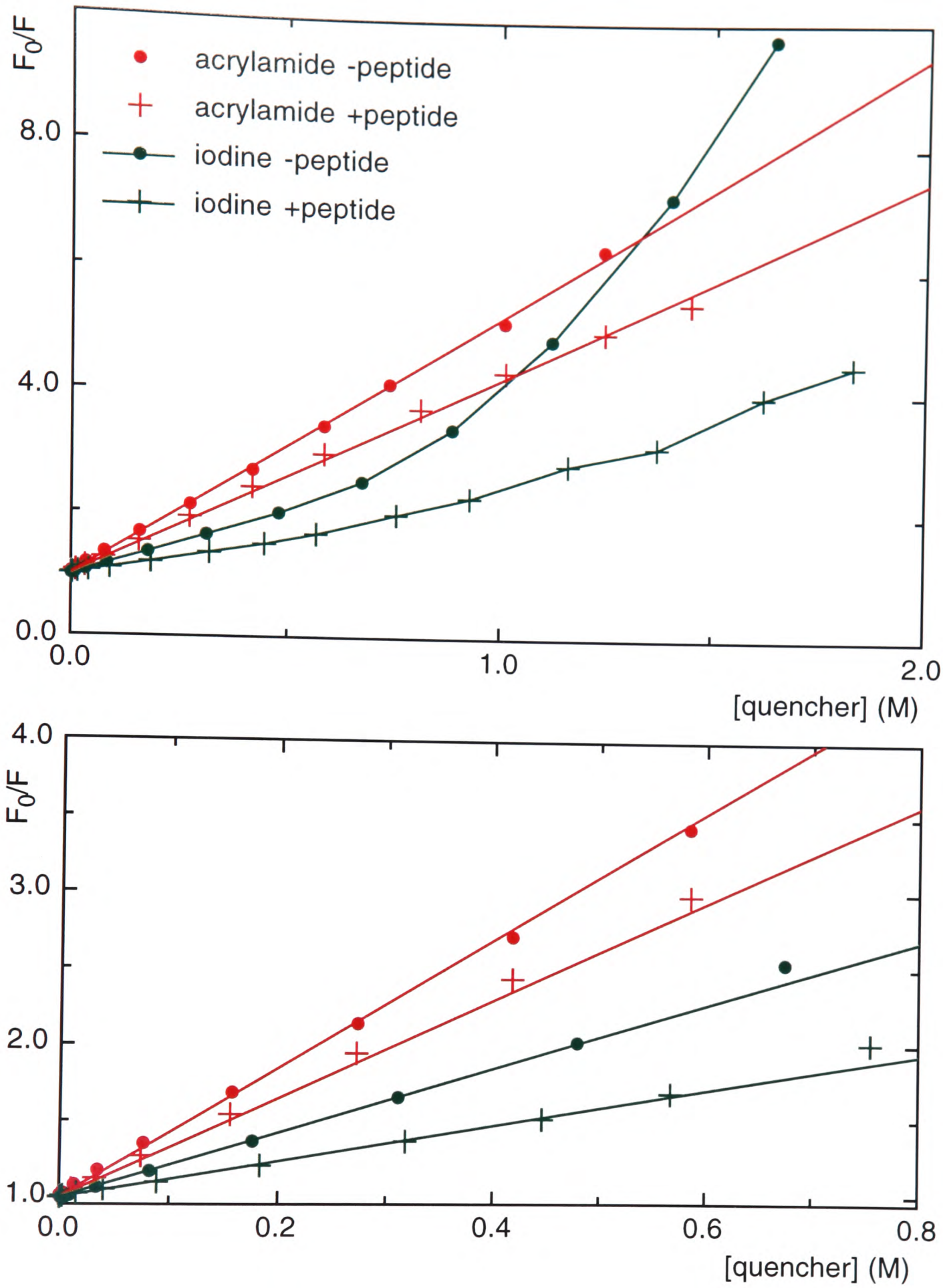

Figure 51: Fluorescence quenching of D^b-His_6·β_2m with (crosses) and without (dots) NP-Y367-374 peptide, by acrylamide (red) and iodide (green). Upper panel: full range plot showing the curvature of the iodide quenching curves, and the full-range fits for the acrylamide quenching curves. Lower panel: partial view, showing the full-range fits for the acrylamide, and the initial range fits for the iodide quenching curves.

	iodide	acrylamide
K_{SV}, no peptide (M^{-1})	2.11 ± 0.013	4.22 ± 0.027
K_{SV}, 1 µM Y367-74 (M^{-1})	1.17 ± 0.011	3.23 ± 0.036
decrease %	**44.5**	**23.4**

Table 9: Stern-Volmer constants for the iodide and acrylamide fluorescence quenching of 100 nM D^b-His_6·β2m complex, and their decrease upon addition of peptide. The decrease in iodide quenching is greater than for acrylamide.

Upon addition of peptide, both acrylamide and iodide quenching are reduced. This agrees with the notion that the peptide molecule is shielding some tryptophan residues from the surrounding water, making them less accessible to the solute quenchers. Interestingly, the reduction is much greater for the charged iodide than for the uncharged acrylamide which is able - to a certain extent - to diffuse into folded proteins, confirming the hypothesis that these tryptophan residues are now removed from the water-accessible surface of the protein.

It is difficult to distinguish this effect from a true conformational change of the protein which could bury tryptophan residues away from the binding groove and make them less accessible to quenchers. If the contribution to the fluorescence of the tryptophan residues in the binding groove could be suppressed, an estimate of the influence of peptide binding on residues outside the groove would become possible. It would be a good idea, in this context, to test various peptides with different influences on the D^b fluorescence (see above).

I therefore tested, in another experiment, the GP-92-101 peptide (CSANNSHHYI) that gave a decrease in the D^b fluorescence upon binding (see above). It showed a K_{SV} of 1.15 (±0.026) with iodide, very close to the NP-Y367-374 peptide (in this experiment 1.03 ± 0.072). This result suggests that the average tryptophan in D^b is about as

accessible to iodine as the ones in the binding groove (believed to be 'switched off' by the GP peptide); if there were more tryptophan residues accessible, the quenching constant with the GP peptide would have to be higher than with the NP peptide. Therefore, in the peptide-bound state, most tryptophan residues seem inaccessible. However, the Stern-Volmer constant in the empty state of the protein is much higher, implying that considerably more tryptophans are exposed. Further experimentation, using different peptides, could aim to explore whether the 50% decrease of K_{SV} can be due to the covering of only three tryptophans, or whether a conformational change that buries others can be implied.

7.4. Fluorescence anisotropy measurements

7.4.1. Principles and use

Looking at the fluorescence anisotropy (FA) of a protein provides a measure of the overall motility of the fluorophores (usually tryptophan residues; general reviews: [256, 296-298] and references therein). The principle of an FA experiment is outlined in figure 52: The sample is irradiated with a beam of polarised light. Only those fluorophores in the sample molecule are excited whose transition moments have a component in the plane of polarisation (photoselective excitation); thus, the emitted fluorescence is polarised in the same manner, and this signal (the parallel intensity) is detected by a photomultiplier through a polariser parallel to the plane of polarisation of the incident beam.

During the very short (tens of nanoseconds) life-time of the excited electronic state, the fluorophore can alter its orientation in space, via Brownian rotational diffusion, according to different modes. (The life-time of the fluorescence itself also depends on the chemical environment and can be used for probing it; see [256-258].) In the case of a tryptophan residue in a protein, in order of ascending half-time of the movement, the side-chain can rotate or flip; the protein backbone can oscillate; structural elements or subunits of the

protein can move against each other; or the whole protein can rotate in solution. At the time of fluorescence emission, therefore, any of these movements will have caused an altered orientation of the fluorophore, and the emitted light will be in a different plane of polarisation. Seen over the multitude of fluorophore molecules in the sample solution, this will lead to a summary depolarisation of the fluorescence signal, so that the parallel intensity will decrease, but some emission can now be detected through a polariser oriented at a right angle, along the y axis in figure 52 (the orthogonal intensity).

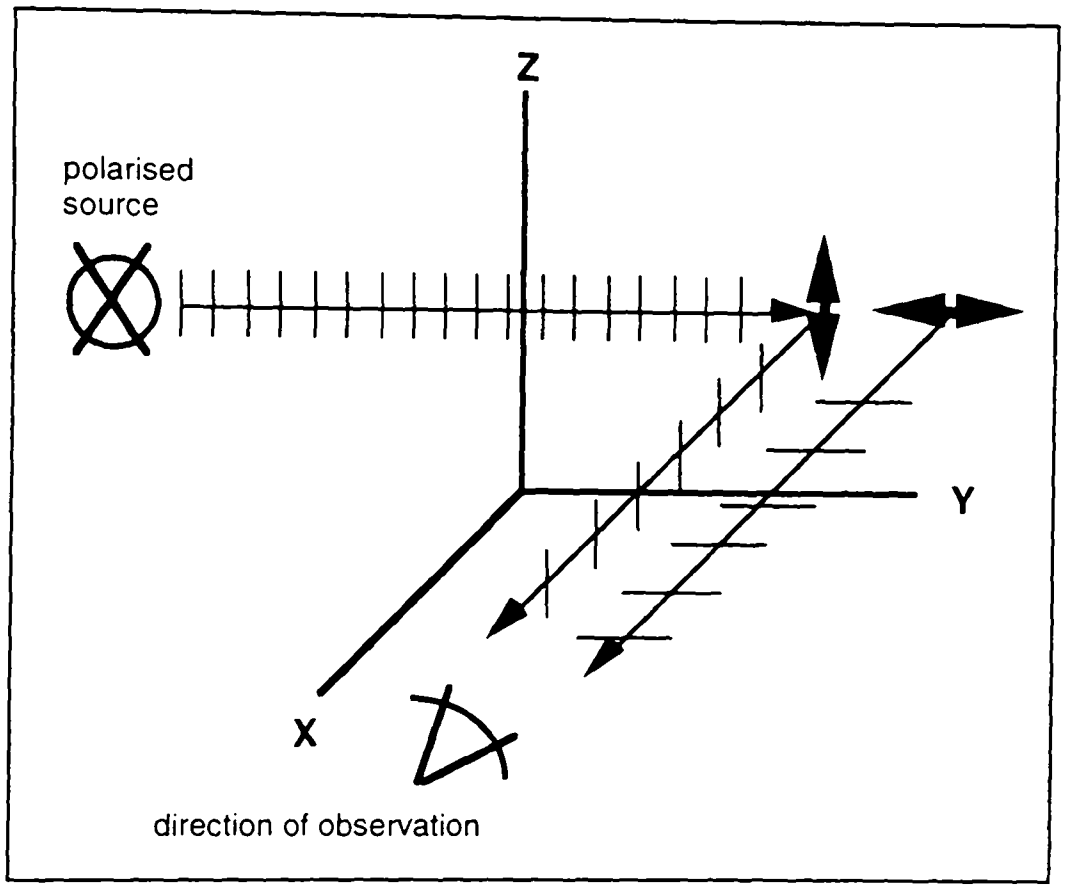

Figure 52: principle of fluorescence polarisation / anisotropy (adapted from [297]): The incident beam (from -y) is polarised in the z direction (vertical lines), and the fluorophore in the sample (left double-arrow) is excited in this direction. Fluorescence is observed from the x direction. If any rotation of the fluorophore in the z/y plane occurs during the lifetime of the fluorescence effect, a y-polarised fluorescence signal (horizontal lines) will be seen in addition to the main, z-polarised signal. From these two signals the anisotropy value is calculated (see text).

Fluorescence anisotropy (R) is defined as follows:

$$R := \frac{I_z - I_y}{I_z + 2 \cdot I_y} = \frac{I_p - I_o}{I_p + 2 \cdot I_o}$$

with $I_{z,y}$:= intensities along the coordinate axes z and y (see figure 52), or parallel (p) and orthogonal (o). An older formulation, sometimes seen in the literature, uses fluorescence polarisation P:

$$P := \frac{I_z - I_y}{I_z + I_y}.$$

Anisotropy is a measure of order (the smaller I_y, the higher R); therefore, the higher the value of anisotropy, the lower the ability of the protein to randomise the plane of polarised light, and the lower the overall rotational diffusion of its fluorophores.

Fluorescence anisotropy can be measured in a time-resolved set-up (see below), and in a steady-state assay looking at the summary effects of all the motions mentioned above. To do the latter in the Perkin-Elmer LS-50B spectrofluorimeter, vertical and horizontal polarisers in the excitation and emission path are switched every 15 seconds to measure fluorescence intensity (I) in all four possible combinations: I_{vh}, I_{vv}, I_{hv}, and I_{hh} (where v,h:= direction of polariser; first index: excitation, second index: emission polariser), from which the machine calculates the anisotropy value of the sample.

All fluorescence anisotropy and anisotropy decay measurements were performed by Klaus Döring in Tübingen.

7.4.2. Anisotropy changes during peptide binding

Figure 53 shows a time-drive measurement, where anisotropy of a 100 nM solution of D^b-His_6·β2m was measured in 15-second intervals before and after the addition of NP-Y367-374 peptide. On exposure to the peptide, the anisotropy value of the protein decreases significantly, but not to a large extent, with a half-time of a minute or less. The experiment was repeated twice and gave consistent results (data not shown).

As the anisotropy value decreases, it can be concluded that the fluorophoric tryptophans

in the protein are less restricted in their movement, either because of a size decrease (dissociation of oligomers) of the protein on peptide binding, or due to the loosening of conformational constraints following the binding of peptide. The latter would be an unexpected result, as the binding of the peptide is likely to result in a more ordered state of the protein (see the thermodynamical measurements above). The D^b-His_6·β2m complexes were dimeric in this preparation, and it was important to control by fluorescence anisotropy decay (see below) that this did not change upon the binding of peptide. If dissociation of class I dimers upon peptide binding cannot be securely excluded, the results of the steady-state anisotropy are difficult to interpret.

It was attempted to extend these measurements in two directions: first, to increase the time resolution of the measurement. A rotating 'fast filter accessory' should allow for rapid polarisation measurements (50 time-points per second). This accessory is installed in the LS-50B machine in Oxford, but experiments that I carried out with it gave a high background noise and no clear signal (data not shown). Later, the polarisers used in this wheel were found to be of inferior quality compared to those in the slow exchange apparatus, and error-prone due to optical distortions. There is no adequate machine available from another supplier. A higher time-resolution of the process could, therefore, not be achieved.

The second extension of this experiment was the measurement of fluorescence anisotropy decay (FAD, see below).

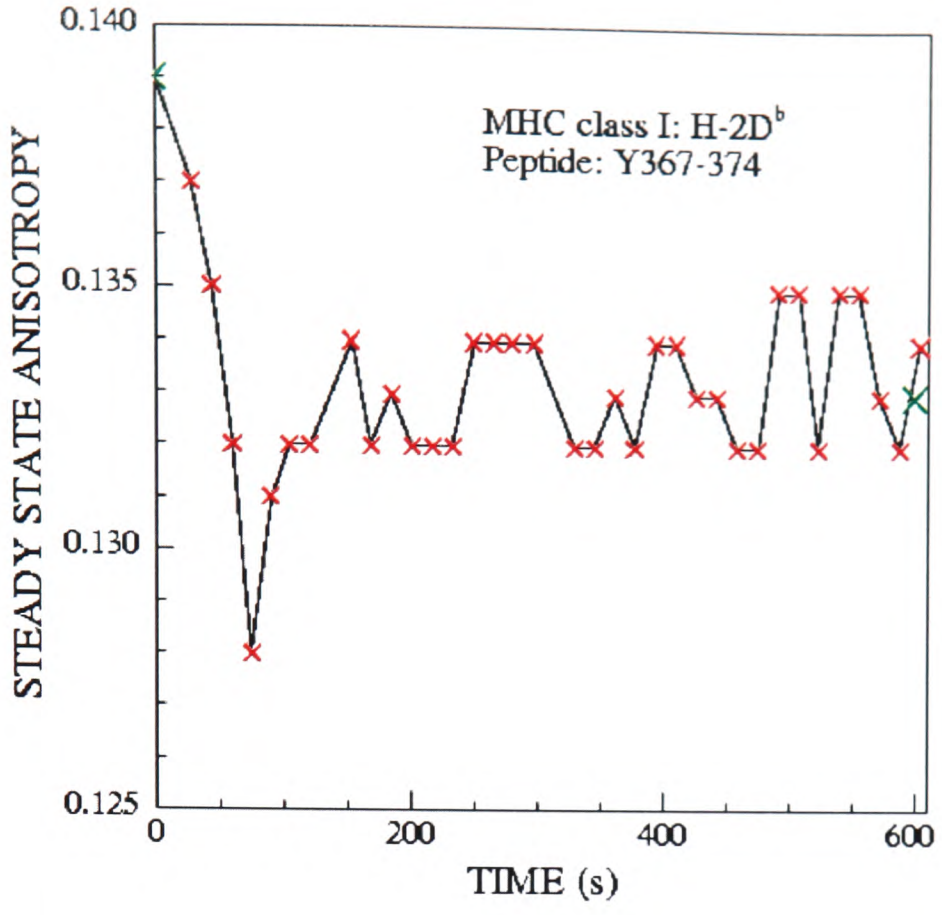

Figure 53: Results of the steady-state anisotropy experiment (done by Klaus Döring): time-drive, emission 300 nm, excitation 350 nm. The green crosses mark the values before (left) and after (right) the addition of peptide, averaged over 1000 seconds. 1 µM NP-Y367-374 peptide is added at t=0, and anisotropy measured in 15 second intervals. Discussion see text.

7.5. Fluorescence anisotropy decay measurements

7.5.1. Fluorescence anisotropy decay

Extending the possibilities of steady-state fluorescence anisotropy, fluorescence anisotropy decay (FAD) allows the observation of the individual modes of internal and external rotation (reviews: [296, 297]; for a description of the experimental set-up, see the materials and methods section, and [16]). The sample is excited by a picosecond laser pulse and the fluorescence emission is detected through a polariser (set in parallel to the plane of polarisation of the incident beam for half of the experiment, and in the orthogonal plane for the other half) and a monochromator by a photomultiplier, followed by single-photon counting equipment. The data are sampled in a multichannel analyser, set to a time window of several tens of nanoseconds, until approx. 10^6 counts in the maximum channel are reached. This procedure results in the time course of the two intensity decays $i_p(t)$ (parallel intensity) and $i_o(t)$ (orthogonal intensity) from which the anisotropy decay r(t) can be deduced.

Calculation then gives a time-course of the 'decay' of fluorescence anisotropy: in the early channels, most fluorescence events will be highly polarised as only some very fast movements will have taken place; in the late channels, slow events such as rotation will have contributed additional randomisation. The resulting curve represents an integration over all polarisation-randomising (anisotropy-decreasing) processes within the sample.

One observes in such experiments (see figure 54 for an example) that the anisotropy decays fast during the first ten nanoseconds, and more slowly later. It is usually possible to deconvolute the decay curve into two to four significant component exponentials; these components represent different rotational modes of the fluorophores with different half-times, averaged over the contributions from different fluorophores. The slowest of these anisotropy decay components can usually be assigned with more or less security to the

overall rotation of the protein (this is dependent on the viscosity of the medium, and the size of the protein, and can be efficiently predicted from the sedimentation constant [296]). Other processes that contribute to the overall decay are short-range non-radiative energy transfer [299] (this is not usually visible as a curve because it happens too fast); localised movements of tryptophan side-chains relative to the protein backbone; and peptide backbone or domain movements.

Being able to distinguish the contributions of the different rotational modes to the overall anisotropy effect makes FAD experiments far more powerful than the steady-state fluorescence anisotropy measurements described above. However, a single experiment ideally takes several hours, so that changes of anisotropy in time cannot be followed with the highest accuracy.

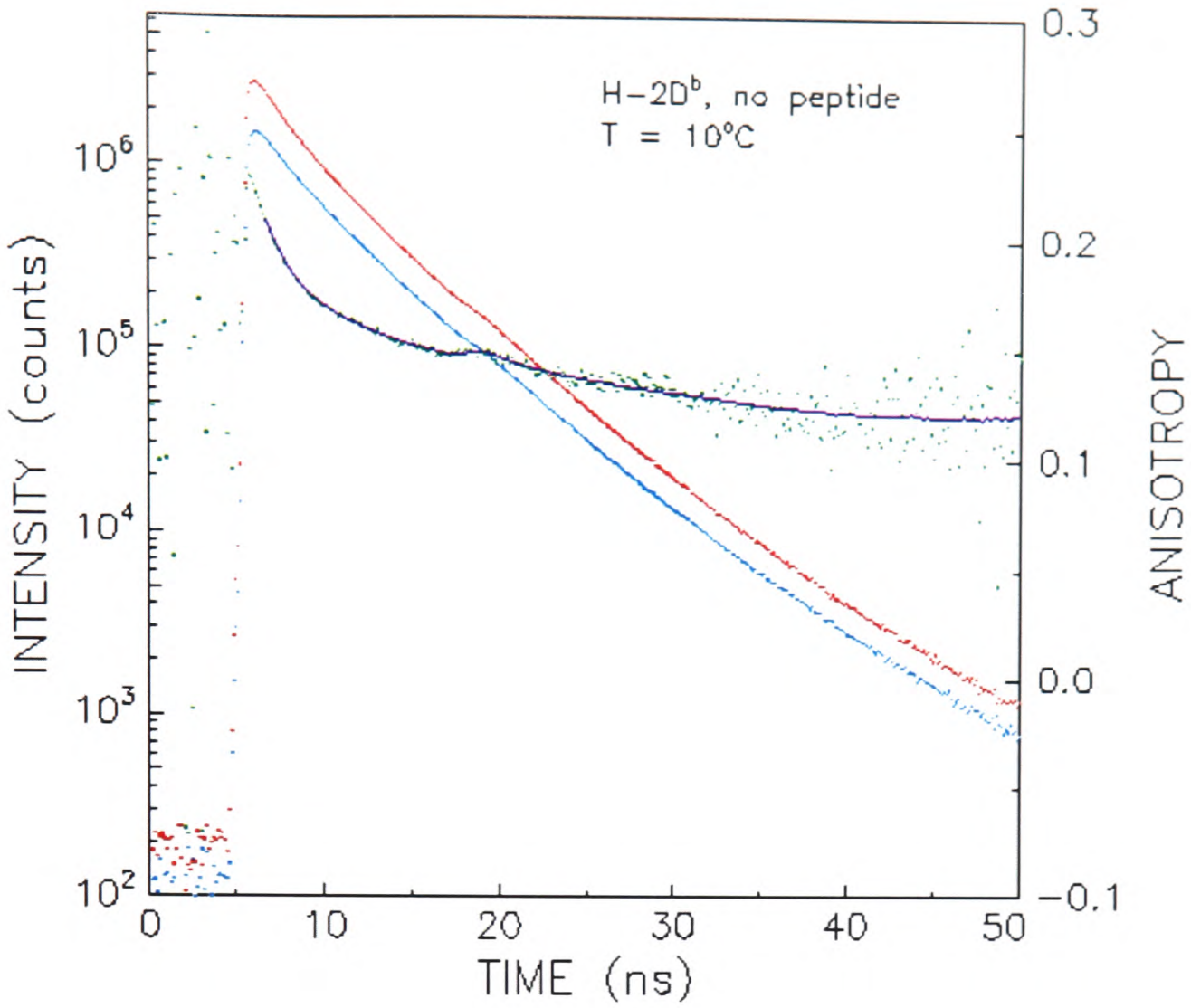

Figure 54: Fluorescence anisotropy decay. Primary diagram of the parallel (red, I_z) and orthogonal (cyan, I_y) polarised fluorescence emission (left y axis), and of the anisotropy (data points: green, fitted curve: blue; right y axis) against time in nanoseconds after the excitation pulse.

Sample: D^b protein without peptide.

Experiment and evaluation done by Klaus Döring.

FAD has been used by Pecht, Kourilsky, and collaborators to look for conformational alterations in a single-chain H-2K^d (sc-K^d) molecule [300] upon peptide binding. They find a faster overall fluorescence anisotropy decay in what they call the 'unloaded state' of the molecule and interprete this as a higher rigidity, or a greater compactness, of the protein after peptide binding. However, they are unable to explain conclusively what the rotational mode in the range of several nanoseconds represents, ascribing much of it to 'Foerster' long-range nonradiative energy transfer (see ref. 26 in this paper); furthermore, their 'unloaded state' of sc-K^d molecules has been shown by Ojcius *et al.* [217] to be not peptide-free but preloaded with cellular peptides, calling the results of the study in question. (There are also problems with the theoretical considerations in this article as many of the Greek characters have not printed!)

Pecht, Strominger, and collaborators try to expand on these studies using bacterial recombinant HLA-A2 [301]. In this paper, their conclusions are fairly limited, due again to a lack of an 'empty class I' control. They are able to say that the mobility of the tryptophan residues is 'not significant', and that their protein might be dimerised in solution (see my own results above).

7.5.2. Experiments on empty, full, and transitory molecules

Klaus Döring has performed several fluorescence anisotropy decay experiments with the D^b-His$_6$·β2m complex; one, with representative results, is shown in figure 55; the data are summarised in table 10.

Analysis of the raw data is described in [16]. Briefly, a multi-exponential decay was assumed for the fluorescence signal S,

$$S(t) = \sum_{i=1}^{N} a_i \cdot \exp(-t/t_i)$$

and for the anisotropy (R) a multi-exponential decay plus a residual anisotropy at long times (R_∞):

$$R(t) = \sum_{j=1}^{M} b_j \cdot \exp(-t/\phi_j) + R_\infty$$

(with a_i and b_j being the amplitudes, and τ_i and ϕ_j the life-times, of fluorescence and anisotropy, respectively). Taking into account the background signal and the apparatus response curve (eliminating the characteristics of the detection system), anisotropy and intensity values were calculated from the parallel (i_p) and orthogonal (i_o) intensities in the time channels, and non-linear least-square fit analysis performed by varying a_i, τ_i, b_i, ϕ_i, and R_∞ in the equations above, using visual rating of the residuals and a χ^2 test as criteria. Fitting was started with a monoexponential decay in both cases, and further exponential functions were introduced until no further components were resolved.

Partial fluorescence amplitudes were calculated according to

$$\alpha_i = a_i \,/\, \sum_j a_j \,.$$

Parameters derived from the data are $\mathbf{\langle P_2 \rangle_i}$, the orientational order parameter of the fluorophore, and $\mathbf{D_{o,i}}$, the rotational diffusion coefficient (derivations in [16]).

$\langle P_2 \rangle_i$ is a measure of the amplitude of the rotational oscillation that results in the anisotropy exponential function i (the total anisotropy seen as a sum of exponential functions, see above), or for the width of distribution of the angles of the fluorophores relative to their averaged orientation. The greater $\langle P_2 \rangle_i$, the greater the 'order' = the smaller the movement of the tryptophan residue(s) in the rotational mode i. The root of mean square of the angles of deviation of the fluorophores, ϑ_{rms}, can be calculated from $\langle P_2 \rangle$, and it is an easily accessible measure of the motion which they experience.

$D_{o,i}$ is a measure of the mobility of the fluorophores, the inverse of the 'viscosity' of the surrounding medium that a tryptophan side-chain experiences in the rotational mode i. (It also depends, as every diffusion coefficient, on the shape and the volume of the rotating species.) High values of D_o mean that it is easy for the residue to move, low values mean

that movement is difficult.

Four different time-points were taken from one sample: the first on the empty molecule before the addition of peptide (for 2500 seconds), the second directly after peptide addition for 8 minutes, and then two further points from 9 to 25 and from 25 to 65 minutes.

In all of these experiments, three anisotropy correlation times could be fitted: a very short one (ϕ_1) of 1.2 to 1.7 ns, a medium one (ϕ_2, 2.9 to 3.4 ns), and a long half-time (ϕ_3, 42 to 47 ns) which gave the highest anisotropy contribution in all time points.

The longest correlation time should allow conclusions as to the overall size of the protein, as it is most likely to represent the rotation of the whole protein in solution (rotational correlation time). A theoretical value for the total rotational correlation time can be calculated according to the Stokes-Einstein formula:

$$\phi = \eta V/kT$$

where ϕ: rotational correlation time

V: volume of the protein

η: viscosity of the medium

k: Boltzmann's constant

T: absolute temperature.

For aqueous media at room temperature, η/kT is approx. $2.42 \cdot 10^{11}$ s/cm^3 [273]; the question in the case of D^b is how the volume of the protein should be calculated. The best way is to calculate the effective radius in solution from sedimentation equilibrium or velocity data (see [296] for a description of the method, and comparisons). The sedimentation constant for class I molecules has unfortunately not been determined. The volume can be estimated from the dimensions of the protein, but this regularly gives values that are too small by a factor of 1.4 to 2.4 (rule of thumb: factor 2) because the hydration shell is <u>not</u> taken into account [296]. An estimate using 70 x 40 x 40 Å [122] =

$1.12 \cdot 10^{-19}$ cm^3 for the molecular volume gives 27.3 nanoseconds rotational correlation time. However, in this calculation, the density of the protein comes to

$$\frac{\text{mass}}{\text{volume}} = \frac{55000 \,/\, 6.023 \cdot 10^{23}}{1.12 \cdot 10^{-19}} = 0.82;$$

the density of a folded protein is always found to be greater than 1, and usually between 1.3 and 1.4 (Klaus Döring, pers. comm.; see [302] for review). It seems, therefore, that Bjorkman's dimensions are not appropriate to estimate a volume. Instead, the volume, when calculated back from the molecular weight and a density of 1.35, comes to $6.76 \cdot 10^{-20}$ cm^3 (radius 25.3 Å); recalculating the volume including a 5 Å hydration shell (a common estimate) gives $1.16 \cdot 10^{-19}$ cm^3, and 28 ns as overall rotational correlation time.

The ϕ_3 value observed here, 45.4 ns (in average), is larger than the theoretical result by a factor of 1.62. This makes a strong point for the presence of D^b dimers in this experiment. The ϕ_3 value also does not change during the experiment, which provides an indication that there is no dissociation of the aggregates as a result of or in parallel to peptide binding, making the other data (and eventual steady-state anisotropy data when obtained with the same protein preparation) easier to interpret. (The hydrated volume of the whole complex then calculates as $1.9 \cdot 10^{-19}$ cm^{-3}, and its radius as 35.5 Å).

Looking at the relative amplitudes of the anisotropy decay functions, it appears that the relative contribution of ϕ_3 remains constant. In contrast, there is a strong increase in b_1, and a corresponding strong decrease in b_2, at the time-point just after the addition of the peptide, with a return to the previous values from the 9-25 minute time-point on. This manifests itself in a decrease in $\langle P_2 \rangle_1$ (0.92 to 0.83) and an increase in $\langle P_2 \rangle_2$ (0.88 to 0.95). The effects on the rotational diffusion coefficients are: $D_{o,1}$ increases from 22.1 to 32.6, and returns to 24.4 μs^{-1}, while $D_{o,2}$ decreases from 13.8 to 4.9, and returns to 9.7 μs^{-1}. The following figure shows the development of the root of mean square of the angular distributions of the fluorophores in the modes 1 and 2:

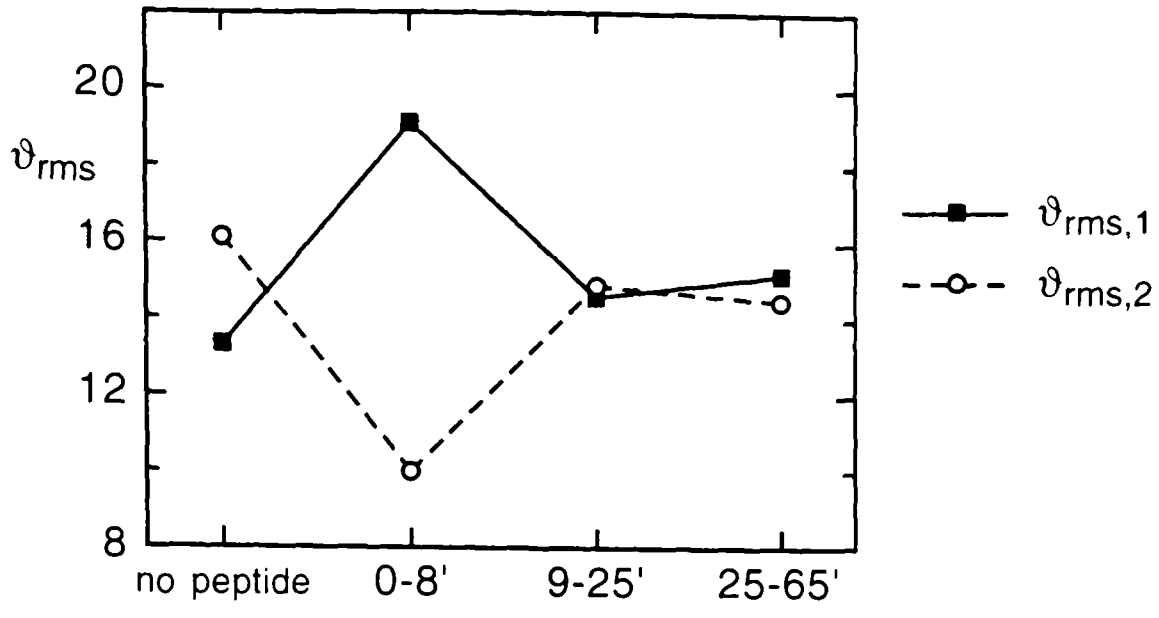

Figure 56: ϑ_{rms} values in the course of the peptide binding reaction.

Data taken from table 10.

These results suggest that the protein is in a different dynamic state during the first minutes after peptide addition. The fastest rotational movement, ϕ_1, sees a more flexible environment and also increases in amplitude, while the middle movement, ϕ_2, sees a far more restrictive environment, and moves with a lesser amplitude.

From comparisons to the rotational modes in other proteins, the rotational lifetimes ϕ_n can be - highly tentatively! - assigned to different modes of movement in the protein: ϕ_3 to the rotation of the whole protein in solution (as seen above), ϕ_1 to movements of the tryptophan side-chains, and ϕ_2 to movements of the protein backbone and/or protein domains against each other. This assignation, if justifiable in further experiments, would allow us to propose a dynamic picture of the D^b molecule as it binds peptide: in a transitory period, there is much more mobility in the side-chains, but the frame of the protein is more restricted in its movement. This dynamic intermediate might represent the 'searching' of the peptide for its final, stable conformation in the binding site and the movements of side chains to accommodate it; in this case, the change in β_1 would stem mostly from the tryptophan residues in the binding groove.

Once the peptide is bound, the picture changes: the protein backbone again becomes more flexible, but not as flexible as in the empty state; the side-chains become more rigid again as the peptide is 'locked' into a bound conformation.

The time-frame within which this reaction proceeds is difficult to describe more accurately, because the time resolution of the FAD experiment cannot be increased. It seems that several minutes is a long time for a protein to bind a ligand; this time-scale clearly reminds more of protein folding events. Very slow binding to class I was demonstrated in the 37 °C fluorescence binding experiment (see above), where almost certainly a refolding process of the 'melted' binding site is involved. An experiment that gave limited indications is the steady-state anisotropy measurement demonstrated above: it was done with the same preparation of protein as this FAD experiment, therefore the continuous dimeric state of the molecules was clearly defined. The main change in anisotropy was over after one minute; therefore it can be assumed that the life-time of the FAD intermediate will be in the same range. It is important to note that this FAD experiment is an integration over a long dynamic process with probably many different conformational substates; it is therefore impossible to say even whether the state with a high $\vartheta_{rms,1}$ is the same then the one with the low $\vartheta_{rms,2}$! The above interpretation of the binding process is therefore highly conjectural, and all that can be said with certainty is that a dynamic intermediate exists that has dramatically different dynamic properties from initial and final form. This is most easily envisaged in figure 55: the curve for the 0-8' time is clearly below that for the initial (or final) time from a very early time, whereas later they run in parallel (as much as can be said). Therefore, the protein in the intermediate form has a fast mode of movement that contributes much more strongly to the decay of anisotropy.

In another experiment (the details of which are not given here), it was shown that the elongated peptide NP-Y367-379 has the ability to evoke this conformational change; but, as both peptides were added to saturating concentrations (10 µM) the effect was less pronounced with the long peptide. The simplest interpretation of this finding is that the long peptide binds D^b in a different way.

While - at this point in time - an interpretation of these data must remain tentative, they clearly demonstrate that there is an intermediate in the class I - peptide binding process, and that conformational rearrangements are necessary to bind peptide. These conformational changes probably involve the amino acid side-chains of the class I molecule; this would be expected from the extensive contacts that they make with the peptide. More interesting is whether the backbone of the protein will be altered in its conformation. The differences in the position of the N-terminus of the α–helix of the α2 domain between complexes with different peptides, both in HLA-A2 [144] and in H-2K^b [138] provide evidence that this helix might be flexible, and reactive to the binding of peptide. The above interpretation of the FAD experiment suggests that indeed a dynamic change is taking place that involves rearrangement of the protein backbone, and that three different states are discernible, only the last of which is structurally known by protein crystallography.

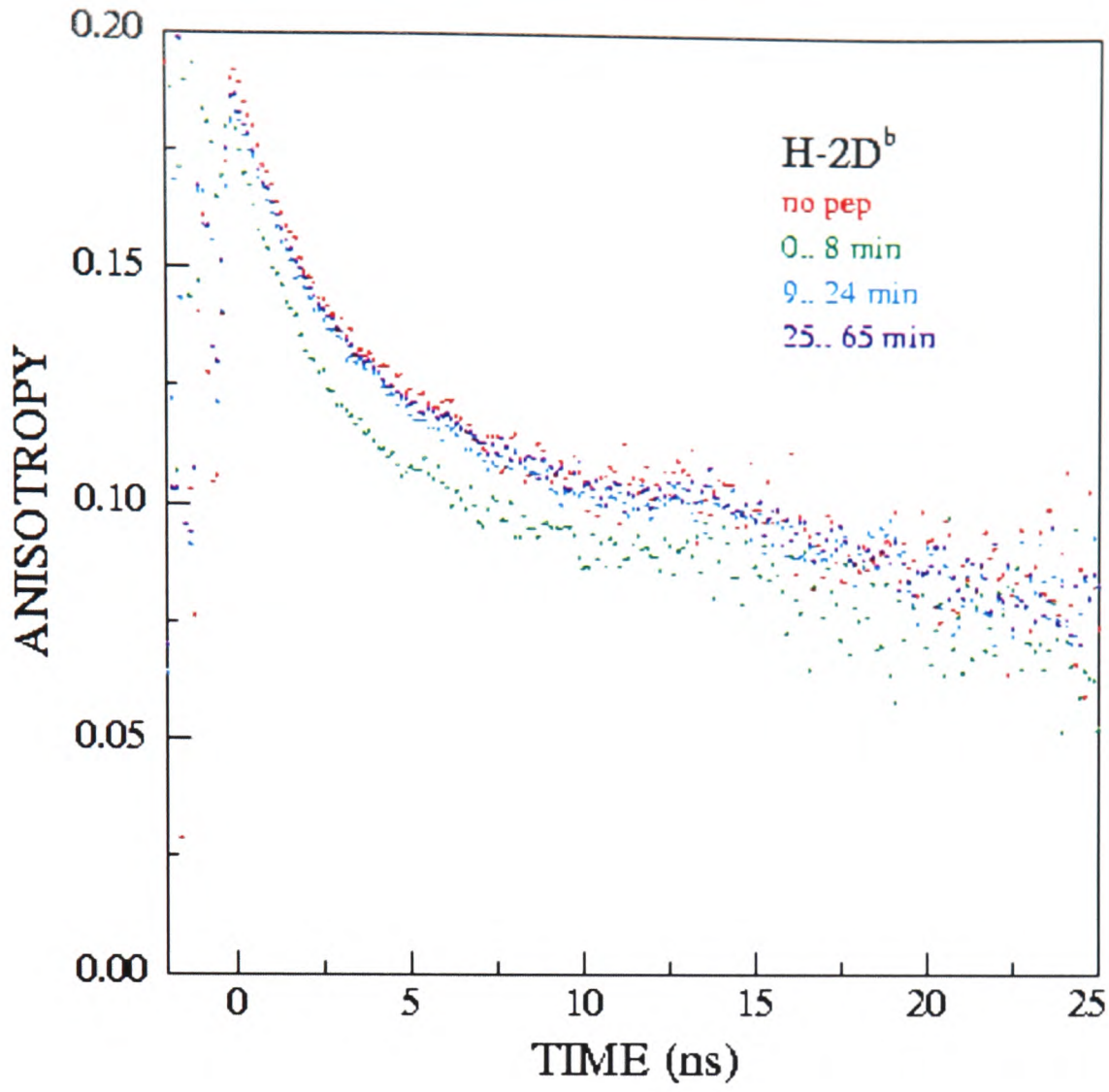

Figure 55: fluorescence anisotropy decay of D^b at different times before and after the addition of 1 µM NP-Y367-374 peptide. Temperature 10 °C, excitation 300 nm, emission 350 nm.

Experiment and evaluation done by Klaus Döring.

The state of faster anisotropy decay at the shortest time (0-8 min) is clearly visible. Discussion see text.

	no peptide	t= 0...8 min	t= 9...25 min	t= 25...65 min
τ_1 (ns)	1.0	0.7	0.7	1.0
τ_2	3.0	2.8	2.9	3.0
τ_3	5.3	4.8	5.0	5.0
τ_4	13.6	13.9	18.0	19.6
α_1	0.23	0.18	0.18	0.15
α_2	0.42	0.35	0.41	0.44
α_3	0.34	0.46	0.41	0.41
α_4	0.005	0.007	0.004	0.003
$<\tau>$ (ns)	3.0	3.4	3.4	3.5
ϕ_1 (ns)	1.2	1.7	1.3	1.5
ϕ_2	2.9	3.2	3.4	3.3
ϕ_3	47.2	42.4	45.9	46.2
b_1	0.033	0.054	0.035	0.040
b_2	0.039	0.011	0.030	0.029
b_3	0.137	0.113	0.124	0.129
b_4	0.000	0.000	0.000	0.000
R_0	0.21	0.18	0.19	0.20
R_∞	0.000	0.000	0.000	0.000
χ^2	3.3	1.1	1.4	2.1
$<P_2>_1$	0.92	0.83	0.90	0.89
$<P_2>_2$	0.88	0.95	0.90	0.90
$\vartheta_{rms,1}$ (°)	13.3	19.1	14.6	15.2
$\vartheta_{rms,2}$	16.1	10.0	14.9	14.5
$D_{o,1}$ (μs^{-1})	22.1	32.6	24.7	24.4
$D_{o,2}$	13.8	4.9	10.0	9.7

Table 10: (see legend on next page)

Table 10: Table of fluorescence anisotropy decay data: parameters of the fits to the data from the experiment shown in figure 55. Numbers are shown to the last significant digit.

Meaning of the symbols:

α_i and τ_i , the partial amplitude and the fluorescence life-time (time constant, in nanoseconds)of the fluorescence exponential function i (see expression for S(t) above);

b_j and ϕ_j, the amplitude and the life-time of the anisotropy exponential function j (see expression for R(t) above);

$\langle\tau\rangle$, the mean fluorescence lifetime (in nanoseconds);

R_0, initial anisotropy at time zero (starting value); R_∞, residual anisotropy at long times; χ^2, the χ^2 value of the underlying fit;

$\langle P_2\rangle_j$, the orientational order parameter of the fluorophore;

$\vartheta_{rms,j}$, the root mean square of the distribution of the fluorophore axis relative to its mean orientation regarding the anisotropy exponential function j;

$D_{o,j}$, the orthogonal diffusion coefficient regarding the anisotropy exponential function j.

7.6. Summary: Biophysical measurements of peptide binding

In this chapter, several attempts have been outlined to directly investigate the alteration of the structure of D^b-His_6·β2m upon the binding of peptide. The experiments measuring far-UV circular dichroism have not revealed a major structural change. It seems unlikely that the binding of peptide would go along with a complete reorganisation of the 'core' structural elements of the class I molecule, the immunoglobulin domains α_3 and β_2m, and the β-sheet and α-helices that make up the peptide binding site; but if changes in loops between such structural elements or positional shifts of structural elements against each other occurred, the CD signal of the protein would not necessarily change very much. It is also important to keep in mind that the α-helices are bent in the crystal structure, and that again changes in the bending angles would be very difficult to detect in a CD experiment. It would be interesting to see in a direct experiment, in this context, whether addition of the peptide to the 'melted' binding site at > 30 °C has a strong influence on the CD signal. Comparison of the two heating experiments performed with and without peptide (figure 48) do not suggest a considerable drop in the CD signal on

the addition and the (slow) binding of peptide at 30 °C; this would imply that not even the 'melting' of the binding site involves a detectable change in the overall content of helical or sheet structure! The best estimate is, therefore, a limited rearrangement of side-chains, and possibly adjustments in the positioning of the α-helices against each other, or the β-sheet. In this context, it is interesting to see that in the neonatal Fc receptor (FcRn), closely related to class I in structure, the α_2 helix is tilted towards the α_1 helix to seal what is the peptide binding site in class I molecules [303, 304]. Could the structure of the empty class I molecule in solution be similar to this? It would be interesting to perform comparative CD measurements on FcRn.

Support for a side-chain readjustment also comes from the FAD measurements which finds a far greater rotational diffusion coefficient for the fastest mode of movement, tentatively assigned to the side-chain movements of the tryptophans, in the transitory state while the protein is seeking to accommodate the peptide molecule. This flexibility disappears at longer times when the peptide is bound. In agreement with the CD, FAD clearly sees a firm state of the D^b-His_6·β2m complex before the binding of peptide; but it is not possible to say whether this state represents one 'structure of an empty class I molecule' or an integral over several substates. The latter might make the empty D^b-His_6·β2m complex difficult to crystallise; but even a crystal structure determination would not prove that this was the predominant structure. There are now interesting examples of crystallographic structures that have not been confirmed by NMR experiments in solution [305], and one might expect this to be the case especially with very flexible proteins or domains.

FAD measurements also give an indication of the time-scale of the conformational changes. Within eight minutes, the final structure seems to have been reached, and no further changes are observed. To cause noticeable changes in the FAD signal integrated over minutes 1 to 8 after peptide addition, the transitional state of the molecule must have been present for a time in the upper seconds range at least (Klaus Döring, pers. comm.).

This puts the lifetime for the conformational intermediate to between 0.1 and 2 minutes: this is a long time, even for a conformational transition, but conceivable as it involves the complex binding process of a large ligand, and interactions at many different sites (ca. 100 van der Waals contacts, and 30 hydrogen bonds; see introduction) that have to be established. Changes in the near-UV CD signal upon the addition of peptide, indicating an interaction of tryptophan side-chains with the peptide, were observed in the same time-range in preliminary experiments (data not shown). The unexplored second, slower rate constant in the change of the tryptophan fluorescence, with a half-time in the range of minutes, could also be implicated in this process. Measurements of the steady-state anisotropy with time can provide more exact estimates, if the sample is also investigated with FAD spectroscopy.

If the transitional state of the molecule, as defined by the FAD experiment, indeed lasts for seconds, then the peptide must be tightly bound by this time already. Association as defined by stopped-flow fluorescence is a fast process, and no intermediate with a fast off-rate in the seconds or minutes range could be detected shortly after the addition of peptide. The fact that tryptophans in the binding groove interact with the peptide very shortly after binding, and that the fast binding process measured in the stopped-flow experiment is already peptide-specific, shows that the FAD 'intermediate' must be a more subtle slow adaptation of the complex.

The notion of an intermediate in the binding process also receives strong support from the thermodynamical evaluation of the temperature dependence of the equilibrium and the on-rate constant. It seems that there is a gain of entropy in the first binding step (= increase in the rate constant with temperature), probably due to the displacement of water molecules from peptide and binding site. The complex at dynamic equilibrium, however, has considerably less entropy than the empty D^b-His_6·β2m (decrease of the equilibrium constant with temperature), suggesting that the structure is now more highly ordered.

The resulting picture is that upon initial contact, peptide and class I molecule form an 'encounter' or activated complex which is energetically unfavorable (positive $\Delta H^{\ddagger}$), but driven by the liberation of water molecules (positive $\Delta S^{\ddagger}$). At an early stage in the binding process, peptide side chains already interact with tryptophan residues in the binding groove, and anchor residues and peptide length are both important at this stage (stopped-flow results). The side-chains of the class I molecule then become more flexible (increase in $D_{o,1}$) as it seeks to accommodate the peptide and establish van der Waals and hydrogen bonding interactions, while the flexibility of the backbone is limited (decrease in $D_{o,2}$), possibly due to the establishment of initial contacts that involve the peptide and different structural domains of the heavy chain. To reach this state, no dramatic alterations in the overall structure take place; instead, slight movements of the structural domains against each other, or changes in flexible loops, enable the initial binding of peptide. It seems, therefore, that the peptide binds to a site that is generally preformed but must find the 'fine tuning' of the interaction through a long process. The transitory state of the class I - peptide complex gives rise to the stable end-product with a half-time between 0.1 and 2 minutes (FAD experiments) which is reminiscent of a multistep folding event. During this process, entropy is consumed to reach a state of higher order (negative $\Delta S°$), compensated for by the final establishment of tight binding between the heavy chain and the peptide (negative $\Delta H°$). Due to this tight binding, the side chains of the class I molecule become immobilised again (decrease in $D_{o,1}$), and the backbone is also more rigid than in the empty state ($D_{o,2}$); it seems that during most of the reorganisation process, the complex already has a very small off-rate (radioligand binding experiments). The final product of the binding process has an overall structure not much changed from the empty molecule (CD results), but with a higher rigidity in its backbone (decrease in $D_{o,2}$). It is possible that limited conformational changes involving tryptophan residues have also taken place elsewhere in the molecule (fluorescence quenching results).

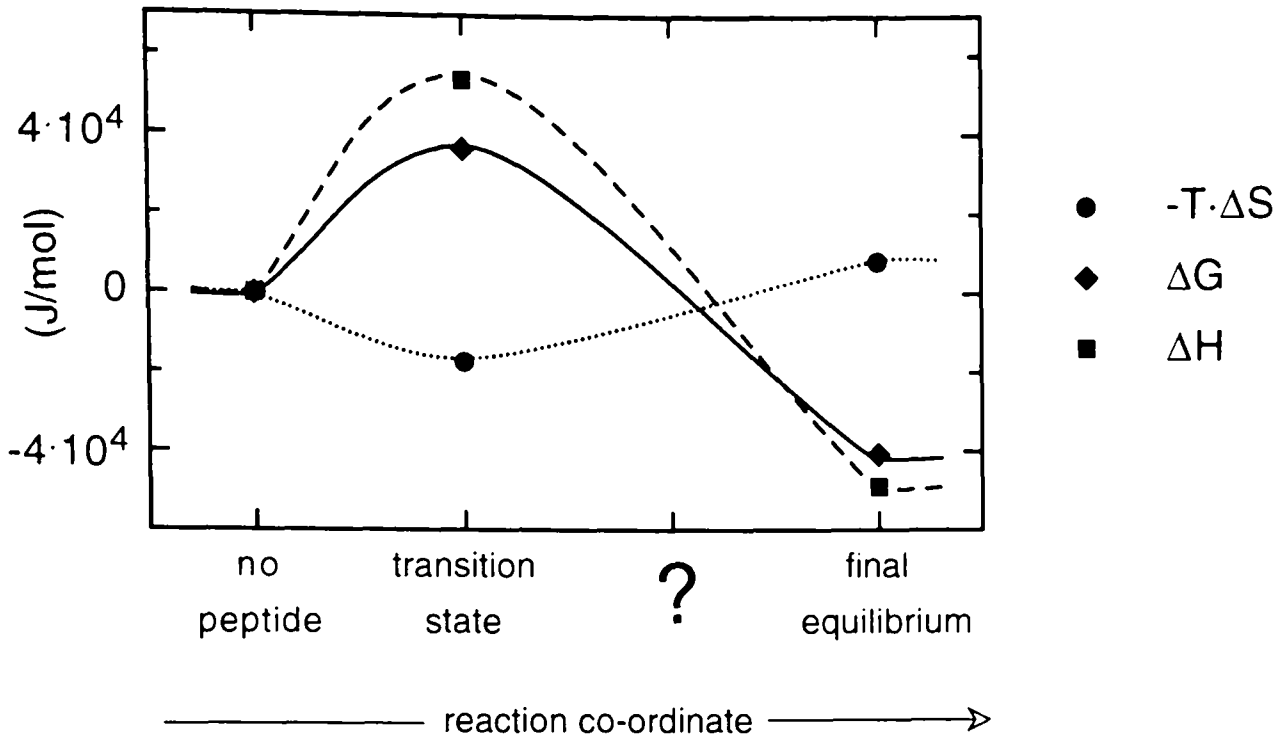

Figure 57: Plot of the progress of the peptide-binding reaction, with thermodynamical parameters on the y axis. 'Transition state' is the transition state as defined by the fluorescence thermodynamics. The state labelled '?' could correspond to the intermediate defined by FAD.

8. Models for class I - peptide binding

8.1. Initial considerations

In this chapter I will try to base upon the kinetic and biophysical measurements a mathematical treatment to describe them. A mathematical model of class I - peptide binding would be useful in predicting features of the system (to be tested in future experiments), and to provide an indication about the mechanism of the reaction. I will begin with some initial considerations, derived from the theory of binding reactions.

In the last few years, NMR analysis has shown that proteins in solution are not the rigid structures seen in crystallisation studies [22]. Instead, they exist in a large number of conformational substates in equilibrium [261]. If environmental parameters are changed (temperature, pH; addition of ligand), each of these substates reacts in a specific way. Kinetics of change are therefore always a weighted average over a spectrum of responses.

Similarly, the binding of a ligand to a receptor consists of many steps in molecular terms. Taking the protein as immobile (see below), the ligand will diffuse according to the 'random walk' theory [306], searching mainly the local space around itself, rotating and diffusing for very small distances, until the rare event of a significant departure in one direction occurs [307]. It will therefore stay close to the protein for a while once it has encountered it, and the actual frequency with which binding occurs depends on the rotational diffusion of the receptor allowing the ligand to sample larger areas of its surface [22]. This process can be intensified and accelerated by long-distance electrostatic interactions between receptor and ligand (as has been shown for DNA-binding proteins, [273]); it can also be treated mathematically as a reduction in the dimensionality of the search (one-dimensional on DNA, two-dimensional on protein surfaces; see [308]). The initial encounter will depend on diffusion alone, and it will be the only second-order reaction in the binding process. Its magnitude can be estimated from the Smoluchowski equation [274, 22] which gives $7 \cdot 10^9\ M^{-1}s^{-1}$ as $k_{encounter}$ for two molecules of the same

size, irrespective of their size [267]; and $1.2 \cdot 10^9$ $M^{-1}s^{-1}$ for $k_{encounter}$ of class I and a peptide molecule (see above). The rate of the next, the first productive, binding step is difficult to estimate; it will depend on the rotational diffusion of the receptor and the 'microdiffusion' of the ligand. (From the FAD experiments, we know the rotational correlation time of the class I molecule, 45 nanoseconds, giving a rotational rate-constant of $1.54 \cdot 10^7$ s^{-1}.) Overall, the initial association rate constants for receptors and ligands, or for enzymes and substrates, are usually in the range of 10^6 - 10^8 $M^{-1}s^{-1}$ [267]; the value at 16.5 °C that I have measured for two peptides, $2 \cdot 10^6$ $M^{-1}s^{-1}$, is at the lower end of this range. This could be because the first binding step will already involve some orientation of the peptide which is conformationally even less restricted than the class I molecule as it has no long protein backbone that is folded into a particular conformation. Once an initial association is achieved, both molecules will have to desolvatise (remove the water molecules from) their binding sites to allow direct interaction. With the highly hydrophobic binding sites of class I molecules that hold many water molecules bound in an ordered state, it is no wonder that this seems to be accompanied by a large increase in entropy. This period will see the greatest reorganisation in molecular interactions, and it will be close to the thermodynamic intermediate with a positive $\Delta H^{\ddagger}$ (high energy barrier).

The following depends very strongly on the nature of the protein and ligand. In many systems, stable binding is reached soon after the thermodynamic intermediate; in others, conformational rearrangements take place. Numerous claims of their detection exist; but their published rate constants of 10 to 10^4 s^{-1} (or half-lives, from 10 µs to 100 ms; see [267, 22]) almost always seem to depend on other steps, and so have to be taken *cum grano salis*. In fact, kinetic intermediates almost always decay far more slowly (see table below). The caveat about conformational substates especially applies, of course, to the concept of a conformational change; here, a 'conformational change' might be a sequence of many different steps, and different protein molecules might reach a given final state in different, parallel pathways.

It is impossible to derive complete information about all these processes in a simple course of experimentation. However, as Gutfreund ([22] p.245) points out, there is nothing wrong with conceptually reducing this complexity: 'What is to a biochemist a single step in a reaction is a sequence of events to a physical-organic chemist and in turn the latter's single step is a sequence of events to a physicist'. In biochemistry, a model needs to be related to and testable in the system under experimental investigation. Therefore, Ockham's razor 'non est ponenda pluralitas sine necessitate' can be applied, and the model with the minimum number of steps that will explain the data must be suggested. However, it is important to keep in mind that the double arrows of a kinetic scheme do not *per se* make any statements about biophysical reality; thus, that these calculations can be much more easily used to disprove a mechanism than to demonstrate one.

Fersht [267] reminds the reader of another two important rules used in the building of kinetic models: Firstly, the principle of microscopic reversibility: 'The transition between any two states takes place with equal frequency in either direction at equilibrium'. This states that the reaction pathway for the reverse of a reaction at equilibrium is the exact opposite of the pathway for the forward direction, and that the transition states for the forward and backward reactions are identical. In a kinetical scheme, equilibrium cannot be maintained by a cyclic process $a \rightarrow b \rightarrow c \rightarrow a$.

Secondly, to 'prove' the involvement of an intermediate, it must 1) have been observed and characterised; 2) form sufficiently rapidly to be on the reaction pathway; and 3) react sufficiently rapidly to be on the reaction pathway. These rules were originally designed for enzymes where the biochemical isolation of reaction intermediates is often possible; however, it does apply to receptor-ligand reactions in the same stringency.

8.2. A simple model of rearrangement

From the radioligand binding, the fluorescence, and the other biophysical experiments, I

have already drawn a crude picture of the class I - peptide binding process (see above). In short, the first detectable process is a change in the fluorescence of the tryptophans at about $2 \cdot 10^6$ $M^{-1}s^{-1}$ at 16.5 °C; it is possible that the thermodynamical 'intermediate' or 'transition state' that has already seen the liberation of water molecules precedes it. The 'transitory state' in FAD spectroscopy would probably come after the fluorescence change, and might last into the minutes range, during which time there could be a slow multi-step rearrangement to form the stable complex.

Independent evidence for a conformational change comes from theoretical considerations. The main finding that a kinetic model of class I - peptide interaction will have to explain is the relatively low affinity for the ligand at fast on- and slow off-rates. To this, Chothia [139] and Franklin [309] have stated that receptors will often 'use up' part of the primary binding energy of the ligand for a subsequent conformational change, thus lowering the apparent binding affinity. Fersht [267] has extended this theory to state that enzymes will use up some of the binding energy to hold the ligand in a distorted conformation which enables the subsequent catalytic step. Every low-affinity / high-specificity interaction can be suspected of similar processes.

In the following, I will use the word 'system' for a particular arrangement of reaction pathways, and 'model' for a mechanistic proposal that is based on a system and contains other assumptions (e.g. values for rate constants or ratios of rate constants). Systems can be dealt with theoretically, while models can be calculated.

Apart from the basic Langmuir binding equation, which has given rise to the 'kinetics mismatch', the simplest system ('system 1' in the following) is obtained if one assumes a fast initial binding step, and a subsequent conformational change:

$$\mathbf{R+L} \underset{k_{-1}}{\overset{k_1}{\rightleftharpoons}} \mathbf{RL} \underset{k_{-2}}{\overset{k_2}{\rightleftharpoons}} \mathbf{R'L}$$

where R'L is the complex with the receptor in an altered conformation, k_1 and k_2 are the

forward rate constants, and k_{-1} and k_{-2} the backward rate constants. This scheme has two partial equilibrium association constants, $K_1 = k_1/k_{-1}$, and $K_2 = k_2/k_{-2}$. The overall equilibrium constants in this system are:

$$K_{a,R'L} := \frac{R'L}{R \cdot L} = \frac{k_1 \cdot k_2}{k_{-1} \cdot k_{-2}} = K_1 \cdot K_2$$

$$K_{a,total} := \frac{RL + R'L}{R \cdot L} = \frac{k1}{k\text{-}1} + \frac{k_1 \cdot k_2}{k_{-1} \cdot k_{-2}} = K_1 (1 + K_2)$$

depending on whether the method used will see R'L only, or both forms of the complex. (In our case, K_2 is generally >>1, therefore the two constants are equal.)

The following model is an actual calculation with data from the SV-324-332 peptide at 4 °C (the data are from table 8). Because the radioligand binding experiments have shown a mono-exponential off-rate, I assume that they do not see significant amounts of RL (either because there is very little there at equilibrium, or because it dissociates too quickly.) I therefore assume that the equilibrium constant from the table, $9.2 \cdot 10^7\ M^{-1}$, is equivalent to $K_{a,R'L}$. The off-rate measured in the radioligand experiments would be k_{-2} at $7.1 \cdot 10^{-6}\ s^{-1}$ (assuming that $k_{-2} \ll k_{-1}$, so that the dissociation of the intermediate never becomes rate-limiting), and the fast on-rate measured in radioligand binding and stopped-flow would be k_1 at $4.6 \cdot 10^5\ M^{-1}s^{-1}$. Therefore, inserting this in the equation above one obtains

$$9.2 \cdot 10^7 = \frac{4.6 \cdot 10^5 \cdot k_2}{k_{-1} \cdot 7.1 \cdot 10^{-6}} ,$$

and $k_2/k_{-1} = 1.4\ (\pm 0.40) \cdot 10^{-3}$. This is the ratio between the reaction rates of both ways in which the intermediate can react; here, the probability for it to decay back to the initial state is 700 times higher, than to react on along k_2 to form the final product.

It is more difficult to determine the exact values of the constants k_2 and k_{-1}.

If it is assumed that k_{-1} is too fast to be detected with the radioligand binding procedure, it should be $> 7 \cdot 10^{-2}\ s^{-1}$. As the number of binding sites per molecule of protein is close to unity (figure 18), it can be concluded that almost all of the peptide-D^b complex at

equilibrium is in a form that can be detected in the assay. Therefore, at equilibrium, there must be little RL, so that $K_2 = k_2/k_{-2}$ must be at least 10. This gives a minimum estimate for k_2 as $7 \cdot 10^{-5}$ s^{-1}, but it could easily be far higher.

If RL is the kinetic intermediate observed in the FAD experiment, its half-life would be between 0.1 and 2 minutes, but probably closer to 0.1 minutes because of the results of the steady-state anisotropy experiment where the two states of the protein interconverted within about 30 to 60 seconds. The following sets of parameters are all possible under these assumptions (the last column gives the half-time of the dissociation of RL via the k_{-1} way):

assumed half-life of RL along k_2 (minutes)	k_2 (s^{-1})	k_{-1} (s^{-1})	$\ln(2)/k_{-1}$ (seconds)
0.2	$5.8 \cdot 10^{-2}$	41.5	0.017
0.5	$2.3 \cdot 10^{-2}$	16.5	0.042
2	$5.8 \cdot 10^{-3}$	4.1	0.17
10	$1.5 \cdot 10^{-3}$	0.82	0.84

The basis of this model is that (fast) binding and (slow) dissociation of the peptide involve different forms of the complex. For this to be true, the fluorescence (very fast binding) and the radioligand (stable binding) on-rates have to describe consecutive reactions. The on-rate constants detected in the radioligand binding assays are in the same range as those seen in the stopped-flow experiments, possibly slightly slower (the stopped-flow on-rates for SV-324-332 and NP-Y367-374 seem identical (table 3); stopped-flow at 4 °C gives k_{on}= 5.41 (±0.03) $\cdot 10^5$ $M^{-1}s^{-1}$ for NP-Y367-374, while radioligand binding gives k_{on}= 4.6 (±0.91) $\cdot 10^5$ $M^{-1}s^{-1}$ for SV-324-332). Therefore, this model is only valid if the interconversion RL $\rightarrow$ R'L happens fast, so that the apparent on-rate for the stable complex R'L is not much less than the one for the intermediate RL.

Another indication for a fast rate of conversion from RL to R'L comes from a prediction

that this model makes about rate-limiting steps at different ligand concentrations ([269]; derived in [310]): at low concentrations of ligand (L_0), availability of ligand and therefore the first reaction (k_1) will limit the rate of formation of R'L; if the concentration of L_0 is increased, however, there will be a point when the reaction to the intermediate (k_1) proceeds faster than the conformational change (k_2), and no further acceleration is possible, no matter how much more ligand is added. If the formation of R'L is observed (and k_{-1} is taken to be >> k_2), the <u>observed</u> forward rate constant k_{obs} is

$$k_{obs} = \frac{d(R'L)}{dt} = \frac{k_1 \cdot k_2 \cdot L_0}{k_1 \cdot L_0 + k_{-1}}.$$

Under conditions of very high [L_0], when $k_1 \cdot L_0 >> k_{-1}$, this expression simplifies to $k_{obs} = k_2$. The plot of k_{obs} against [L_0] should therefore be curved above a certain [L_0], and reach $k_{obs} = k_2$ as its maximum value. In the radioligand binding experiments, k_{obs} of up to 1.25 ($\pm$0.08) $\cdot 10^{-2}$ s^{-1} was seen (table 5). As this value was observed at [L] = 25 nM without any visible saturation of k_{obs}, the value of k_2 must lie <u>above</u> that number, making the possible half-life of RL along k_2 equal to or shorter than one minute to be consistent with this model.

However, it can be shown that the model is unable to accommodate a k_{obs} constant of this magnitude. I will use an estimate of the maximum possible k_{obs} to demonstrate this. For the steady-state concentration of RL (RL_{ss}), Strickland *et al.* [310] give :

$$RL_{ss} = \frac{k_1 \cdot R \cdot L + k_{-2} \cdot R'L}{k_{-1} + k_2}.$$

It can be assumed that $L=L_0$ (no ligand depletion), $R=R_0$ (this will not pose a problem as we are undertaking a maximum estimate), $k_{-2} \cdot R'L$ negligible (both very small numbers at the start of the reaction), and $k_{-1} >> k_2$ (see above); then the equation simplifies to

$$RL_{ss} = \frac{k_1}{k_{-1}} \cdot R_0 \cdot L_0$$

(which is in fact an equilibrium assumption for RL if R'L is completely disregarded). The maximum decay constant for RL along k_2 is $k_{obs.max} = (RL_{ss}/R_0) \cdot k_2$.

To define RL_{ss} further, we use from above:

$$K_{a,R'L} := \frac{R'L}{R \cdot L} = \frac{k_1 \cdot k_2}{k_{-1} \cdot k_{-2}},$$

and rearrange:

$$\frac{k_1}{k_{-1}} = \frac{k_{-2}}{k_2} \cdot K_{a,R'L},$$

so that

$$RL_{ss} = \frac{k_{-2}}{k_2} \cdot K_{a,R'L} \cdot R_0 \cdot L_0.$$

If this, and RL_{ss}, are inserted into the equation for $k_{obs,max}$ above, k_2 cancels:

$$k_{obs,max} = k_{-2} \cdot K_{a,R'L} \cdot L_0.$$

In the system above (SV-324-332 peptide, 4 °C), k_{-2} is $7.1 \cdot 10^{-6}$ s^{-1} and $K_{a,R'L} = 9.2 \cdot 10^{7}$ M^{-1} therefore, $k_{obs,max} = 653 \cdot R_0 \cdot L_0$. Therefore, this system will only reach k_{obs} values of $1.25 \cdot 10^{-2}$ s^{-1} if the initial concentration of ligand is equal to or greater than $1.9 \cdot 10^{-5}$ M. As the ligand concentration was $2.5 \cdot 10^{-8}$ M, the observed velocities could not have been reached. The above calculation is independent of the particular choice of k_2, k_1, and k_{-1}; it only depends on the off-rate k_{-2}, and on the equilibrium constant $K_{a,R'L}$ both of which we have measured.

Speaking in descriptive terms: as k_{-2} is very low, any k_2 that will lead to a substantial progress of the reaction will cause K_2 to be large, typically in the order of magnitude of $K_{a,R'L}$ or even greater. Therefore, k_1/k_{-1} will have to be close to unity in order to maintain the overall $K_{a,R'L}$. However, the distribution of receptor between R and R'L is described by $k_1 \bullet L/k_{-1}$; this number will therefore be in the same range as L, which means that only a very small fraction of receptor will be in the state RL (at 1 µM ligand, 0.0004%), and very little will react further to give R'L. If k_2 is increased to compensate for this, RL_{ss} is decreased further. This model must therefore be considered inappropriate to describe the fast on-rate from the radioligand binding experiments.

(One assumption made above is that the intermediate, RL, is not being detected by the

radioligand binding assay. It is easy to dismiss the opposite: If RL was detected by the assay, only little RL could be present at equilibrium, because a two-slope off-rate is not seen, and the binding at equilibrium is close to unity. This, again, makes $K_2 \geq 10$, and $k_2 \geq 7 \cdot 10^{-5}\ s^{-1}$. As we have assumed above that $k_{-1}/k_2 \approx 714$, this gives $k_{-1} = 0.05\ s^{-1}$ and a half-time of 14 seconds, making it too fast to be detected.)

Another model based on this system could postulate that stopped-flow fluorescence and radioligand binding are both observing the same forward reaction, namely the isomerisation of the intermediate to give the stable product. This is a legitimate assumption, as I have nowhere been able to demonstrate that the fluorescence-enhancing process lies before a conformational change, or that it leads to a rapidly dissociating intermediate. For this model, k_{-2} at $7.1 \cdot 10^{-6}\ s^{-1}$ and $K_{a,R'L} = 9.2 \cdot 10^7\ M^{-1}$ can still be assumed, but now the observed on-rate is along the k_2 arrow, the k_1 assumption is no longer valid, and the rate constants have to be derived from k_{obs} in a different way.

Unfortunately, this model falls victim to the same consideration as above. If the series of stopped-flow experiments with the NP-Y367-374 at 4 °C are used as an example, k_{obs} values of up to $1.2\ s^{-1}$ (at 2 µM peptide) have been observed; $K_{a,R'L}$ is $5.4 \cdot 10^7\ M^{-1}$, and k_{-2} is $3.5 \cdot 10^{-7}\ s^{-1}$. This leads to $k_{obs,max} = 19 \cdot L_0\ s^{-1}$, and $L_0 = 6.3 \cdot 10^{-2}\ M^{-1}$.
This result was derived making the above assumption that $k_{-1} >> k_2$; if this is not the case and $k_2 >> k_{-1}$, the equation for RL_{ss} above simplifies to

$$RL_{ss} = \frac{k_1}{k_2} \cdot R_0 \cdot L_0$$

and $k_{obs,max} = k_1 \cdot L_0$. This seems to be the only case when k_{obs} can remotely be matched by the model; however, here, limits on k_1 are set; namely, as k_2 needs to be at least 1, and $k_2 >> k_{-1}$, K_2 will be at least $3 \cdot 10^6$ which again gives $k_1/k_{-1} = 10$, and as $k_{-1} << k_2$, k_1 cannot be larger than 1 instead of the 10^6 which would have been necessary.

Although the occupation with this system has proven somewhat frustrating, it provides a

different way of obtaining rate constants from the data, namely by fitting the k_{obs}/L_0 pairs directly to the k_{obs} equation (see [310] for detailed discussion). As above, under steady-state condition, and assuming that $k_{-1} >> k_2$:

$$k_{obs} = \frac{k_1 \cdot k_2 \cdot L_0}{k_1 \cdot L_0 + k_{-1}} + k_{-2}.$$

Rearrangement gives:

$$k_{obs} = \frac{k_2}{1 + \frac{1}{K_1 \cdot L_0}} + k_{-2},$$

which can be used to fit the data directly, or in its linearised form (assuming that $k_{-2} = 0$):

$$\frac{1}{k_{obs}} = \frac{1}{k_2} + \frac{1}{L_0} \cdot \frac{1}{K_1 \cdot k_2}$$

Therefore, in a plot of $1/k_{obs}$ against $1/L_0$, $1/k_2$ should be the y intercept, and $1/K_1k_2$ the slope of the straight line through the data. Figure 58 gives direct fits and linearisation for two groups of k_{obs}/L_0 data: the association of NP-Y367-374 at 16.5 °C as measured by stopped-flow (panels C and D); and a combined dataset of the on-rates for tritiated SV-324-332 by radioligand binding (15 and 25 nM peptide), and the stopped-flow data for NP-Y367-374, both at 4 °C (panels A,B). I combined the latter two datasets because I found that with data spanning only a narrow range of concentration, or with less than 6 points, no satisfactory non-linear fit could be achieved. The combination should be legitimate as the SV and NP peptides have behaved very similar in all respects otherwise. The results of this fit are very interesting: they provide the first direct estimate of k_2 constants, giving about 9 s^{-1} at 4 °C, and 130 s^{-1} (albeit with a large error) at 16.5 °C. If this strong increase with temperature was true it would stand for a remarkable gain of entropy in this step (see discussion above). The equilibrium constant of the first step, K_1, seems to decrease with temperature instead. Of course, the data thus obtained do not fit with the off-rate measurements. If $K_1 \cdot k_2$ is $5 \cdot 10^5$ $M^{-1}s^{-1}$ then this leaves k_{-2} at ca. 0.01 s^{-1} if K_a is to be $5 \cdot 10^7$ M^{-1}.

This fit was undertaken under the assumption that the dissociation rate of the initial complex was far higher than the rate of rearrangement (k_2). If the opposite is assumed,

the k_{obs} equation develops into

$$\frac{1}{k_{obs}} = \frac{1}{k_2} + \frac{1}{L_0} \cdot \frac{1}{k_1} .$$

In this case, the fits below are just as valid, but instead of '$K_1 \cdot k_2$' in the table, read 'k_1'. Naturally, the results for k_1 are in agreement with the k_{on} values derived from the same data earlier (see tables 3 and 4). The estimate for k_2 obtained in the fits is still valid, however, because it does not depend on the magnitude of k_{-1}.

Unfortunately, this fit can only be considered significant *per se* if it can be demonstrated that at high $[L_0]$ the k_{obs} values will approach a constant, k_2. The datasets shown here can be fitted with straight lines at similar χ^2 values (see above). Therefore, these fits in themselves provide no indication for the mechanism, but they give a likely number for k_2 should this - or a very similar - mechanism be appropriate. One experimental approach to this problem would be to study lower-affinity ligands, for example extended peptides, at high ligand concentrations in a stopped-flow fluorescence study.

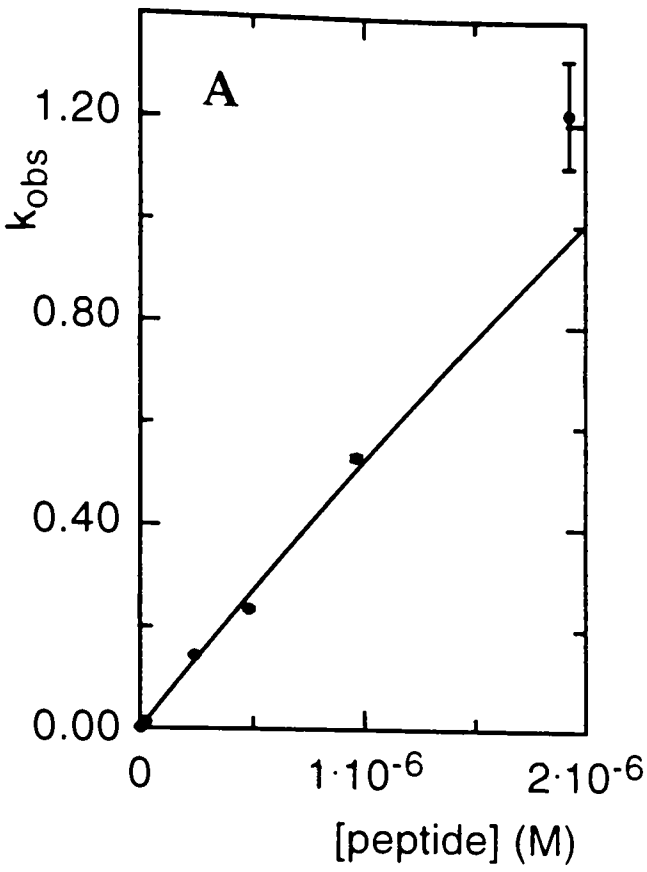

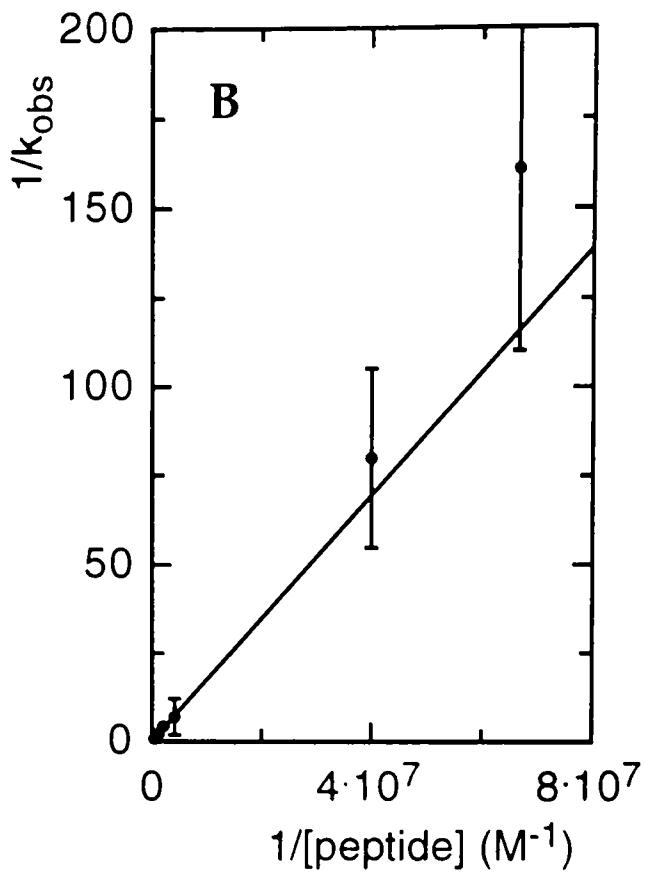

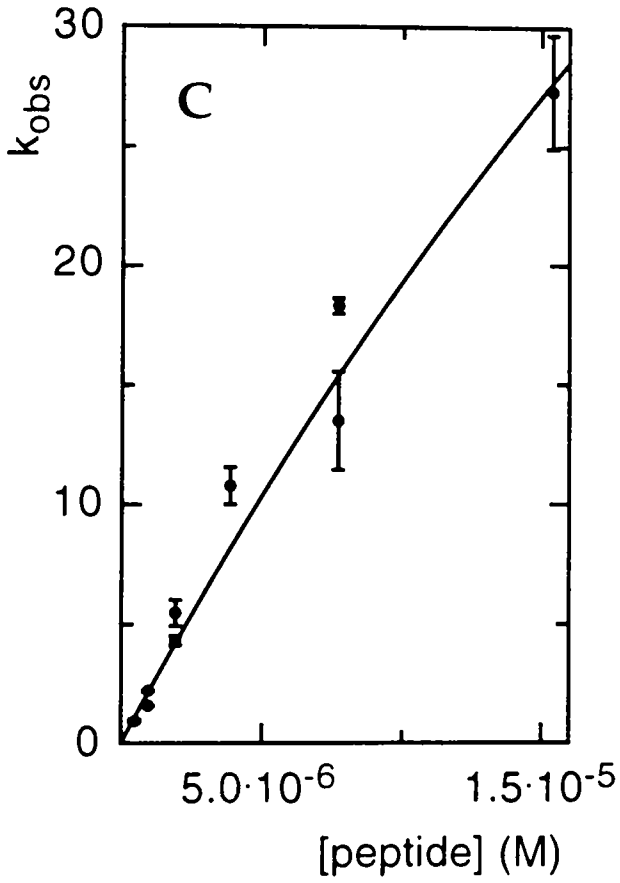

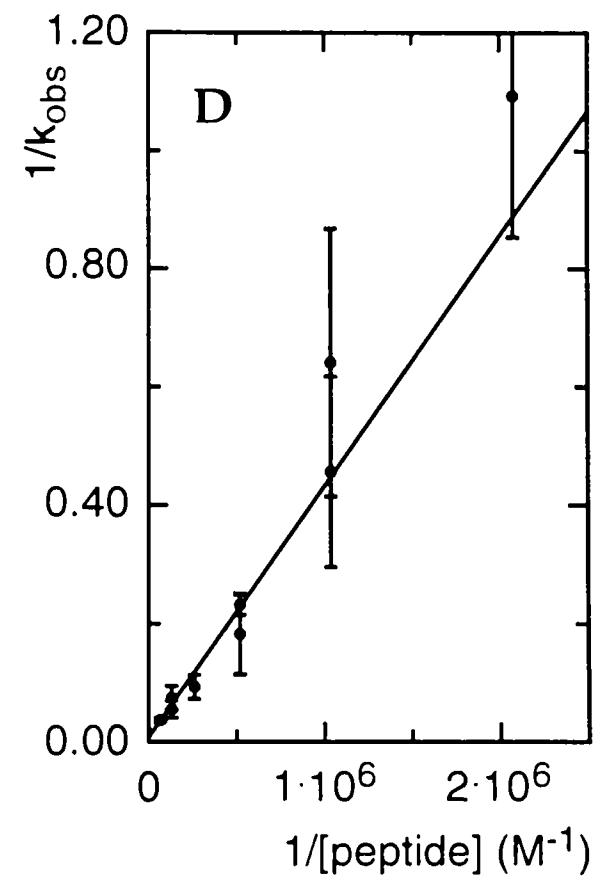

peptide, temp.	panel (fit)	$K_1 \cdot k_2$ (M^{-1} s^{-1})	K_1 (M^{-1})	k_2 (s^{-1})
NP-Y367-374, 4° / SV-324-332, 4°	A (direct)	*5.6 ± 2.7 ·10^5*	5.9 ± 2.0 ·10^4	9.5 ± 3.2
	B (linearised)	5.8 ± 0.06 ·10^5	*6.9 ± 1.8 ·10^4*	8.3 ± 2.2
NP-Y367-374, 16.5 °	C (direct)	*2.2 ± 2.0 ·10^6*	1.6 ± 1.1 ·10^4	138 ± 85
	D (linearised)	2.4 ± 0.19 ·10^6	*2.0 ± 1.1 ·10^4*	120 ± 66

Figure 58: direct fits (A, C) and linearisations (B, D) of k_{obs} / L_0 datasets, and tabulation of the fitting results (deduced parameters in italics).

For discussion, see the text.

Initial diffusion-limited association (10^6 to 10^8 $M^{-1}s^{-1}$) and subsequent conformational change (10 to 10^4 s^{-1}) have been used to explain many binding processes (see references in [310, 267, 22]). The following table shows a selection with fairly well-established rate (or equilibrium) constants:

ref.	protein	k_1 ($M^{-1}s^{-1}$)	k_{-1} (s^{-1})	k_2 (s^{-1})	k_{-2} (s^{-1})
1	Glu-plasminogen	K_1= 22.5 M^{-1}		69	3
2	Fc_ε receptor	$3 \cdot 10^5$	$1 \cdot 10^{-2}$	$8 \cdot 10^{-4}$	$1 \cdot 10^{-3}$
3	muscarinic receptor	$K_1 = 5.6 \cdot 10^8$		$5.5 \cdot 10^{-3}$	$3.3 \cdot 10^{-4}$
4	muscarinic receptor	$K_1 = 3.7 \cdot 10^8$		$1.7 \cdot 10^{-3}$	$2.8 \cdot 10^{-4}$
	(different ligands)	$K_1 = 1.51 \cdot 10^8$		$8.8 \cdot 10^{-3}$	$1.2 \cdot 10^{-3}$
5	bact. binding proteins	$K_1 \cdot k_2 = 10^7$ $M^{-1}s^{-1}$			1-100
6	monocl. antibody	$9.2 \cdot 10^4$	$7.9 \cdot 10^{-3}$	$5.4 \cdot 10^{-3}$	$3.3 \cdot 10^{-3}$

(the references are: 1, [271]; 2, [311, 312]; 3, [313]; 4, [314]; 5, [260]; 6,[315]. More examples are found in the references of [310], and a large review of antibody binding constants is in [278].)

It can be seen that the equilibrium constants for the first step are generally in the 10^7 to 10^8 range (apart from Glu-plasminogen which has a very low substrate affinity), and that the subsequent steps seem to proceed fairly slowly. It is interesting to note that the equilibrium constant for the second step, $K_2 = k_2/k_{-2}$ is between 1 and 10 for all these cases. If a two-step model could be confirmed in our case, the data would clearly look different from this table (see figure 58): $K_1 \cdot k_2$ would be only 10^6 and not 10^8 $M^{-1}s^{-1}$ with an estimate of k_1 of 10^6 $M^{-1}s^{-1}$ and k_{-1} of 1 s^{-1}; k_2 would certainly be much larger than in these cases, certainly in the range of 10-100 s^{-1}. Also, of course, k_{-2} would be far less (as measured)!

To conclude, it can be said that this model will not fit the data and can therefore be refuted. Additionally, trying to approximate values for k_1, k_{-1}, and k_2, which is possible

entirely without equilibrium or dissociation considerations, it seems that very different values from the ones observed in other ligand-receptor systems are obtained.

8.3. Other models and considerations

Another assumption that has often been made in ligand binding studies provides an alternative system to system 1 above. If the receptor isomerises not in the presence but in the absence of ligand [267, 22], one could assume that the ligand can only bind to one of the states of the receptor (**system 2**):

$$\mathbf{R} \underset{k_{-1}}{\overset{k_1}{\rightleftarrows}} \mathbf{R'} \qquad\qquad \mathbf{R' + L} \underset{k_{-2}}{\overset{k_2}{\rightleftarrows}} \mathbf{R'L}$$

The constants are

$$K1 = \frac{R'}{R} = \frac{k1}{k\text{-}1} \; ; \; K2 = \frac{R'L}{R' \cdot L} = \frac{k2}{k\text{-}2} \; ; \text{ and } KR'L = \frac{R'L}{R \cdot L} = K1 \cdot K2 \, .$$

Here again, a fast k_{on} and a slow k_{off} can be reconciled with an overall small $K_{R'L}$ in the same way as above (the same equations apply).

Strickland [310] gives a valuable toolkit to distinguish between systems 1 and 2. Firstly, if the conformational change is taken to be rate-limiting at high $[L_0]$, the maximum reaction velocity should be the same for all ligands. Secondly, if the concentration of R' in the absence of L at equilibrium, R'_{eq}, is >10% of R_0 (that is to say, if $K_1 > 0.1$), an initial 'burst' of generation of R'L will be observed, followed by a slower reaction proceeding at k_1. Thirdly, if a property of R' or R'L can be followed in real-time, the onset of the reaction should be slow in this system (determined by k_1), and it should be independent of the concentration of substrate added.

Again modelling the data from the SV-324-332 peptide at 4 °C ($K_{R'L} = 9.2 \cdot 10^7\ M^{-1}$; $k_{-2} = 7.1 \cdot 10^{-6}\ s^{-1}$; $k_2 = 4.6 \cdot 10^5\ M^{-1}s^{-1}$), I obtain by inserting into the $K_{R'L}$ equation:

$$9.2 \cdot 10^7 = \frac{k1 \cdot 4.6 \cdot 10^5}{k_{-1} \cdot 7.1 \cdot 10^{-6}} \, ,$$

and $K_1 = k_1/k_{-1} = 1.4\ (\pm 0.40)\cdot 10^{-3}$. Therefore, if no ligand is present, R' is just 0.1% of R_0.

This system can be excluded through a consideration similar to the one above for system 1. The maximum forward rate constant must be $k_{obs,max} = K_1 \cdot k_2 \cdot L_0$. From the $K_{R'L}$ equation, $K_{R'L} = K_1 \cdot k_2/k_{-2}$, and therefore $K_1 = K_{R'L} \cdot k_{-2}/k_2$. Inserting this in the $k_{obs,max}$ equation, I obtain

$$k_{obs,max} = K_{R'L} \cdot k_{-2} \cdot L_0 = 653 \cdot L_0.$$

A forward rate constant of 0.0125 would only be possible at a ligand concentration of 19 µM, and not 25 nM, where it was observed.

Foote and Milstein [316] show that this mechanism holds true for two different monoclonal antibodies. They prove it by observing two on-rate constants, and the slower decreasing with increasing $[L_0]$.

For antibody-antigen interactions, a combination of system 1 and system 2 has been found independently in two cases and thoroughly investigated [317, 278, 316]: the receptor can change conformation in the presence and absence of ligand, leading to a circular four-state mechanism. However, in both cases, biexponential dissociation kinetics are observed, and they are necessary to make a significant assignment to this mechanism; also, this system has similar problems to system 2 to accommodate the 'mismatch kinetics'. The equilibrium constants for the conformational changes in these measurements are again between 0.3 and 10.

A model that specifically addresses the question why the affinity constant can be relatively low at high on- and low off-rates was proposed by Alain Townsend, and I have found no references in the literature to anything similar (**system 3**). It suggests that there are two forms of the empty receptor, R and R", and that both of them equilibrate with the intermediate RL, but only one of them, R, is present at t=0:

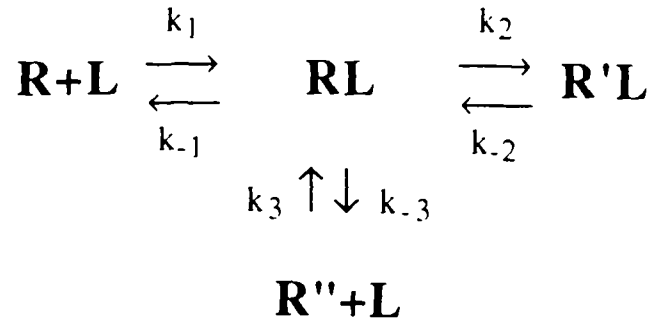

If all the rate constant equations

$$K_1 = k_1/k_{-1};\ K_2 = k_2/k_{-2};\ K_3 = k_3/k_{-3}$$

are written out as products of their respective species, and these inserted into the law of mass conservation

$$R_0 = R + R'' + RL + R'L\ ,$$

one obtains for the concentration of the intermediate <u>at equilibrium</u>:

$$RL_{eq} = R_0 \cdot \left(1 + \frac{1}{K_1 \cdot L} + \frac{K_3}{L} + K_2\right)^{-1};$$

and, using the relation $R'L = K_2 \cdot RL$:

$$R'L_{eq} = R_0 \cdot \left(1 + \frac{1}{K_2} \cdot \left(1 + \frac{1}{K_1 \cdot L} + \frac{K_3}{L}\right)\right)^{-1};$$

if $R'L_{eq}$ is set to $R_0/2$, the value of L (where apparent binding is half-maximal) gives after rearrangement the inverse of the apparent affinity constant K_{app}:

$$L_{50\%} = \frac{1/K_1 + K_3}{K_2 - 1}\ , \text{and}$$

$$K_{app} = \frac{K_2 - 1}{1/K_1 + K_3}\ .$$

This system has many interesting features. It is too complicated to deal with summarily, but one major shortfall can be demonstrated briefly. In the process of a binding reaction, RL will be formed first and decay along k_2 and k_3 according to the ration of these affinity constants. Therefore, under kinetic conditions (as long as there is no back-reaction), the ratio R'L/R'' will be k_2/k_3. In the second phase of the reaction, when R is exhausted, slow reactions begin along k_{-2} and k_{-3} to establish the proper equilibrium between R'L and R'' which is

$$\frac{R'L}{R''} = \frac{R'L}{RL} \cdot \frac{RL}{R''} = K_2 \cdot \frac{L}{K_3} .$$

If there has been an overshoot in R'L, equilibrium will take a very long time to reach because it will proceed with the slow rate k_{-2}. If the overshoot is into R", equilibration will also be slow as k_{-3} cannot be very fast (if k_{-3} was as fast as k_1, no accumulation of R" would take place, and the model would approximate system 1). Such 'creeping' equilibrations have never been seen in our experiments, but maybe they are very slow, and the binding assays are not sensitive enough over a long time.

Another grave problem with system 3 is that it does not allow for another rapid increase in R'L upon the addition of a second bolus of peptide. Instead it predicts that most of R will be altered into slow-binding R" in the course of the reaction, even if very little peptide is present. The hypothesis, of course, is eminently testable: however, it seems unlikely as (for example in the fluorescence step-titration experiment) fast binding has been observed upon addition of more ligand.

8.4. Summary, and comparison with results from others

None of the simple models discussed above will fit the data, and the basic enigma of a low K_a in a system with high k_{on} and (especially) low k_{off} remains. As only monophasic on- and off-rates are seen in the system (the exception being the slow on-rate in the fluorescence experiment), independently demonstrating a complicated mechanism is and will be difficult. One possibility to do this are k_{obs} / L_0 plots at high concentrations of ligand, hoping that a limiting $k_{on,max}$ exists which could 'prove' system 1. This would also generate independent data about K_1 and k_2 which are now only tentative (see figure 58); but even now it can be said that if there is a further reaction after the initial binding step, which leads to the stable complex, its rate constant must be ≥ 10. Similarly, if k_2 is assumed to be small against k_{-1}, $K_1 \cdot k_2$ comes out as approximately 10^6 $M^{-1}s^{-1}$. However, these data do not agree with the extremely low off-rates that represent some of the slowest that I have seen for any system.

It is interesting to compare my measurements with the data obtained by others (see introduction, table 1). While the affinity constants for the optimal-length and the longer peptides fall well into the general range, the on-rates I have seen (up to $2 \cdot 10^6$ $M^{-1}s^{-1}$ at 25 °C) are much faster than anything described previously (with the exception of a single paper where association onto cells is measured, [133]). The fast on-rates I have first observed with stopped-flow spectroscopy, and later confirmed with radioligand binding experiments; furthermore, I have shown that iodination of the peptide, detergent, and the presence of cell lysate all slow down the rate of peptide binding. These observations, together with the fact that class I molecules isolated from peptide transport-competent cells might be empty for a good reason - because many of them are unable to bind peptide properly - could well account for the slowness of the on-rates in the literature. In addition, Margulies' on-rates could be low because of the common mass-transport problem with surface measurements [213], or the immobilisation of the peptide having other effects.

It is conceivable that a system can be found to explain these data, although we have been at a loss so far. Trying to correlate the biophysical measurement to the kinetics, it would be tempting to assume a half-time for a conformational rearrangement in the upper seconds range or even slower, leading to 0.01-0.1 $M^{-1}s^{-1}$ as the forward rate constant for this step. This agrees roughly with the k_2s for conformational change above, but it would mean that this step is different from the k_2 in system 1 above. Maybe it is somewhere later on the reaction coordinate, and the answer is indeed a multistage progression to a stable endproduct, with many different states along the way.

9. General summary, and outlook

9.1. What has been shown

I consider the main points of this thesis to be: Firstly, the cloning and production of a soluble D^b-His_6·β2m complex to study the properties of the empty and the occupied molecule in a detergent-free controlled *in vitro* system. Secondly, the development of a novel fluorescence assay to look at the binding of peptide; this assay allows the determination of on-rates by the stopped-flow method, and of the thermal stability of D^b-peptide complexes. Thirdly, the establishment of a fast on-rate for the binding of peptide to D^b-His_6·β2m, faster than any of the rate constants seen previously by this laboratory or other researchers. Fourthly, the demonstration of a kinetic intermediate of high mobility in class I - peptide binding by fluorescence anisotropy decay spectroscopy.

9.2. Consequences for the *in vivo* situation

Which kinetic parameters are important for class I - peptide binding in cells? For antibodies, this question has been asked in various experimental settings. Mason and Williams [276] studied the binding of antibodies to cell surfaces. They find fairly uniform association constants (around 10^6 $M^{-1}s^{-1}$) and conclude that the affinity of an antibody is mainly determined by its off-rate (they find k_{off}= 10^{-5} to 10^{-3} s^{-1}). Theoretically, in this assay, the on-rates could have been determined by the diffusion of the antibody to the cell surface; the authors have shown by calculations that this is not so (Don Mason, pers. comm.). Foote and Milstein [264] compare rate and equilibrium constants of 31 species of antibody derived form different stages of an immune response. They see a uniform shift towards lower k_{off} values in the course of affinity maturation; of different V gene family products, the one that is capable of a higher on-rate clearly predominates at later time-points, although its initial affinity is even less; the on-rates themselves do not seem to change much in the course of the maturation. This suggests an important role for the

on-rate constant in the selection of B cells.

For class I molecules, the most distinctive feature is the slow off-rate. This makes biological sense, as the class I - peptide complexes have to reach the cell surface and stay there without losing their peptide cargo. If peptides were to dissociate from class I molecules during their life-time, large amount of empty class I molecules on the surface would make cells vulnerable to CTL destruction specific for peptides from neighbouring, virus-infected cells.

Thinking about the role of the on-rate is more difficult. A fast k_{on} might give a peptide an advantage in the competition for class I binding sites in the ER; however, the initial on-rates all seem fairly similar (see figure 3), and they cannot be the only means of distinction between peptides of different ability to be presented. However, even with the elongated peptide, the radioligand off-rates would be slow enough to allow egress of the D^b molecules out of the ER with this peptide on. Therefore, selection of peptides cannot be based upon this off-rate; it must be the fast dissociation rate of an initial complex (k_{-1} in system 1?) that allows exchange of the longer peptide against one that fits better. If one assumes that this is not the case, a mechanism must be postulated that retains class I molecules with suboptimal peptides in the endoplasmic reticulum; there is no evidence to this date for such a factor. A cautious assessment therefore comes to the conclusion that peptide selection will most likely be exercised at the stage of the intermediate; and indeed, the fluorescence enhancement, the fastest measure of binding that we have, is already fully peptide-specific.

One interesting point in this context is the slow on-rate at 37 °C which would completely alter the picture if the same kinetics ($t_{1/2}$ = 60 minutes) applied in the cell (murine body temperature is even slightly above this) There are two obvious answers to this. Firstly, the overall conditions in the endoplasmic reticulum could be very different from those in the *in vitro* assay. Primarily, the concentration of background solutes (especially of those with a high molecular weight, such as proteins) has a strong effect on the thermodynamical activities of protein and ligand (especially with large ligands such as peptides!) [318, 302]. The net protein content of a mammalian cell is 18% = 180 mg/ml,

and this number may be twice as high in the ER [319]). As all law of mass action equations are only valid for activities, concentrations have to be corrected by an activity coefficient; this can easily mean an increase in the equilibrium constant by a factor of 10, and accelerate or decelerate rate constants depending on the special conditions. Secondly, class I molecules might interact with proteins that hold their binding site 'in shape' and enable fast association with (selected? delivered?) peptides; the various chaperones that have been seen to bind class I molecules (see introduction) are obvious candidates.

9.3. Perspectives

The greatest challenge in this area of study is still to find a convincing model for the kinetics of interaction of class I molecule and peptide. To this end, careful observations of binding reactions with stopped-flow fluorimetry could provide definitive evidence for a two-step model, and supply rate constants. Both these and FAD measurements could then be carried out with a variety of peptides to establish which of these parameters depends on which features of the peptide; the study should also be extended to different class I molecules and/or mutants of the D^b molecule to assess the effect of changes in the sequence of the protein and come to a full picture of the process. The empty D^b-His_6·β2m molecules can be investigated with a variety of other methods, the most important of which is certainly calorimetry, the 'gold standard' of interaction analyses, to fully describe the energetics of binding. Crystallisation of the empty complex to understand the state of the binding site, and investigations via mass spectroscopy and nuclear magnetic resonance (which are just beginning) will obtain further information directly from the protein.

Appendix A. The theory of binding reactions

The following appendix gives some basic binding theory, and deviations of the most common equations [21, 22]. Others are found in the text of the results section.

For concentrations of reactants, the letters themselves are often used in formulas (to simplify) instead of square brackets, e.g. X for [X]. (In the text, [X] is always used for 'concentration of X'.)

In equilibrium equations, X (without index, or X_{eq}) denotes concentration of X at equilibrium. For kinetical equations, X (without index) denotes concentration of X at time=t. X_0 always means the concentration of X at time 0, or 'added X'.

The saturation function Y is defined as $Y := \frac{RL}{R_0}$.

k_{obs} is an observed rate constant (most frequently the on-rate) as measured; it depends on [L]. k_{on} and k_{off} are concentration-independent absolute rate constants. k_n (n=number) are rate constants from a theoretical model.

The inverse of a rate constant is called the life-time (τ) or relaxation time of the reaction; ln(2) divided by a rate constant is called the half-time ($t_{1/2}$).

In models, the double-headed arrow <=> is sometimes used instead of the 'reversible' double-arrow $\underset{\leftarrow}{\overset{\rightarrow}{}}$ due to type-setting limitations.

A.1. classical binding reaction:

The simple binding reaction

$$R + L \underset{k_{-1}}{\overset{k_1}{\rightleftarrows}} RL$$

is described in kinetical terms as

$$\frac{dRL}{dt} = -\frac{dL}{dt} = -\frac{dR}{dt} = k_1 \cdot L \cdot R - k_{-1} \cdot RL. \qquad (1)$$

The equilibrium affinity constant K_a is defined as

$$K_a = \frac{RL}{R \cdot L} = \frac{k_1}{k_{-1}} \qquad (2)$$

A.1.1. Binding isotherm without ligand depletion

In the simplest case, when the depletion of ligand is not taken into account ($L = L_0 =$ constant), the calculation of equilibrium binding uses the classical Langmuir isotherm The equilibrium constant equation can be written as:

$$K_a = \frac{RL}{R \cdot L} \text{ or } LR = K_a \cdot L \cdot R \qquad (3)$$

The law of mass conservation states for the different forms of receptor:

$$R_0 = R + RL \qquad (4)$$

Now set $L = L_0$, and insert (4) into (3):

$$K_a = \frac{RL}{L_0 \cdot (R_0 - RL)}$$

$$K_a = \frac{1}{\frac{L_0 \cdot R_0}{RL} - L_0}$$

$$RL = \frac{L_0 \cdot R_0}{L_0 + 1/K_a} \qquad (5)$$

A.1.2. Isotherm with ligand depletion

If ligand depletion is taken into account, L in (3) has to be substituted by $(L_0 - RL)$:

$$K_a = \frac{RL}{(L_0 - RL) \cdot (R_0 - RL)}$$

$$K_a = \frac{L}{R_0 \cdot L_0 - RL \cdot (R_0 + L_0) + RL^2}$$

$RL^2 - RL \cdot (R_0 + L_0 + 1/K_a) + R_0 \cdot L_0 = 0$, and

$$RL = \frac{R_0 + L_0 + 1/K_a}{2} - \sqrt{\frac{(R_0 + L_0 + 1/K_a)2}{4} - R_0 \cdot L_0}\,, \qquad (6)$$

and this equation can be used to directly fit binding data where the signal to concentration relation is known.

A.1.3. Kinetics

In the simple case, the backward reaction along k_{-1} is negligible, and the system simplifies to $R + L \rightarrow RL$.

From equation (1) above can be derived:

$$\frac{dRL}{dt} = -\frac{dR}{dt} = k_1 \cdot L \cdot R = k1 \cdot L_0 \cdot R \qquad (7)$$

(again assuming that no ligand depletion takes place, e.g. that $L = L_{0)}$; and

$$d\ln R = -k_1 \cdot L_0\, dt$$

$$R = R_0 \cdot e^{-k_1 \cdot L_0 \cdot t}$$

now as $RL = R_0 - R$,

$$RL = R_0 \cdot (1 - e^{-k_1 \cdot L_0 \cdot t}). \qquad (8)$$

A.1.4. Full reaction kinetics: integrating the law of mass action

If the backward reaction is taken into account, the basic equation is derived using equation (1), setting $L = L_0$ (no ligand depletion), and inserting $(R_0 - RL)$ for R:

$$\frac{dRL}{dt} = k_1 \cdot L_0 \cdot (R_0 - RL) - k_{-1} \cdot RL.$$

$$\frac{dRL}{dt} = k_1 \cdot L_0 \cdot R_0 - (k_1 \cdot L_0 + k_{-1}) \cdot RL \qquad (9)$$

This is solved via the comparison of coefficients: one assumes that the system will behave like

$$y = a_1 + a_2 \cdot (1 - e^{-a_3 \cdot x}). \qquad (10)$$

a_1 is bound to be = 0 because $RL_0 = 0$.
Now we shall try to express $\frac{dy}{dx}$ in terms of y, and compare with $\frac{dRL}{dt}$.

$$\frac{dy}{dx} = \frac{da_2}{dx} - \frac{d(a_2 \cdot e^{-a_3 \cdot x})}{dx}$$

$$\frac{dy}{dx} = 0 + a_2 \cdot a_3 \cdot e^{-a_3 \cdot x} \qquad (11)$$

compare (from 10): $y = a_2 - a_2 \cdot e^{-a_3 \cdot x}$

rearrange: $$-(y - a_2) \cdot a_3 = a_2 \cdot a_3 \cdot e^{-a_3 \cdot x} \qquad (12)$$

from the comparison of (11) and (12) it follows that

$$\frac{dy}{dx} = -(y - a_2) \cdot a_3 = a_2 \cdot a_3 - a_3 \cdot y \qquad (13)$$

compare (9) and (13):

$\frac{dy}{dx} = a_2 \cdot a_3 - a_3 \cdot y$	$\frac{dRL}{dt} = k_1 \cdot L_0 \cdot R_0 - (k_1 \cdot L_0 + k_{-1}) \cdot RL$
a_3	$(k_1 \cdot L_0 + k_{-1})$
a_2	$\frac{k_1 \cdot L_0 \cdot R_0}{a_3} = \frac{L_0 \cdot R_0}{L_0 + 1/K_a}$

so that now

$$RL = \frac{L_0 \cdot R_0}{L_0 + 1/K_a} \cdot (1 - e^{-(k_1 \cdot L_0 + k_{-1}) \cdot t}) \qquad (14).$$

The expression $\frac{L_0 \cdot R_0}{L_0 + 1/K_a}$ describes RL_{eq}, the concentration of the complex at equilibrium, and $(k_1 \cdot L_0 + k_{-1})$ describes k_{obs}, the observed total on-rate constant, so that

$$RL = RL_{eq} \cdot (1 - e^{-k_{obs} \cdot t}) \qquad (15)$$

An equation for association kinetics that respects ligand depletion is given in [21], p.70.

A.2. More complicated models

are dealt with in the section about modelling, and the most important equations derived. They can also be found in most of the cited papers which have a theoretical section.

Appendix B. The mathematical fitting of binding data

Deriving rate constant information from binding data is not always easy. The following section covers the main approaches. Sometimes, more details are given in the text. General reviews about the topic are [21, 23].

B.1. Fitting equilibrium constants

For equilibrium binding studies, it is useful to distinguish titration curve (bound plotted against added ligand) from binding curve (bound against free ligand).

The direct plot of a **titration curve** enables one to establish that the binding process is saturable, and to get an idea of the maximum number of binding sites. The following picture is a titration curve with computer-generated data (Ka= $5 \cdot 10^7$, $2 \cdot 10^{-9}$ M binding sites, errors 5%; the same in the following):

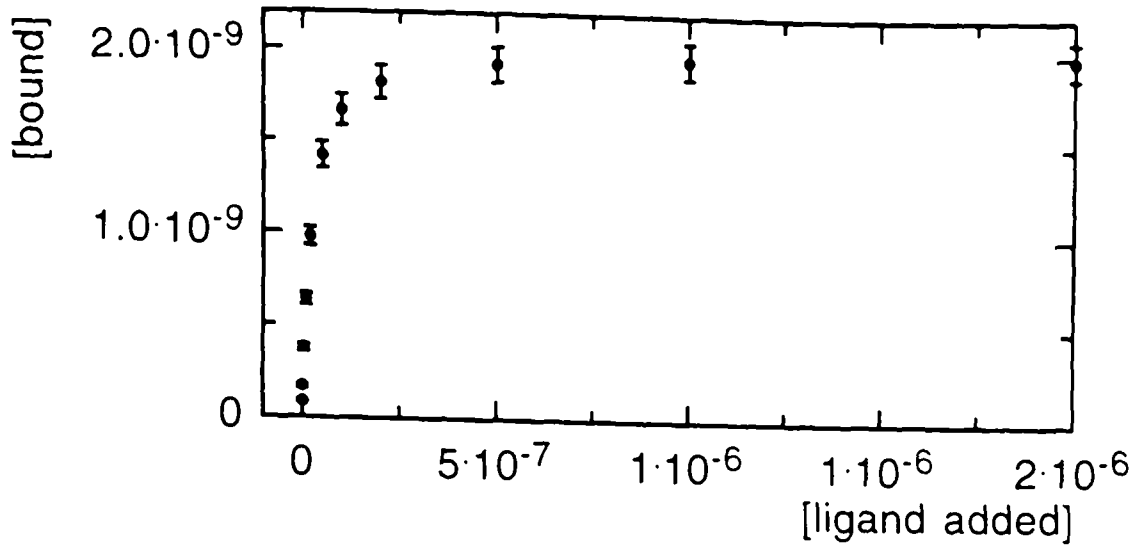

The **semilogarithmic plot** of the titration curve allows the direct estimation of the affinity constant from the plot. As it gives a sigmoid curve and not a straight line, only non-linear least-square fits are possible. It is more difficult to recognise systematic deviations from simple binding with this model; an especially dangerous situation is when $R_0 \geq 1/K_a$; in that case, all of the ligand will bind at the lower concentrations, giving a wrong estimate of $K_{a,app.} = 2/R_0$. The following picture shows a semilogarithmic titration curve:

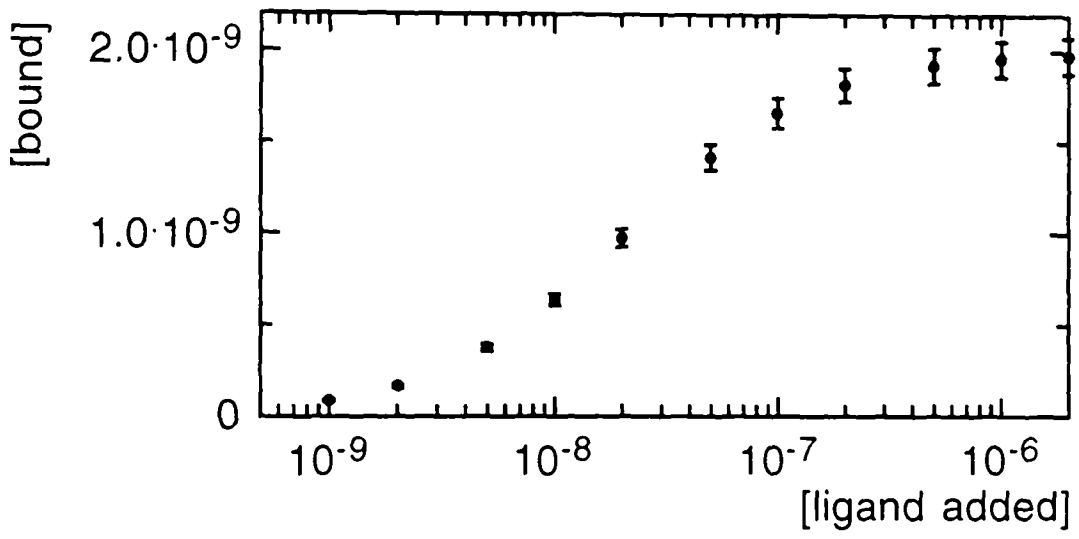

For a least-squares fit, one can use either a simple fit that does not take ligand depletion into account, or full fit with ligand depletion. This was usually done with the following Pascal routine:

```
function  equilibrium_directfit;

description
 'bimolecular binding reaction R+L <=> RL, with ligand depletion',
 '[ligand bound] (M) against [ligand added] (M)';

parameters  2;

defaults
  a[1]:=1e-7,  active,  'sites',  0,  INF;
  a[2]:=1e+10,  active,  'Ka',  0,  INF;

var
 bound:extended;

begin
   bound:=   (a[1]+x+1/a[2])/2-sqrt((a[1]+x+1/a[2])^2/4-a[1]*x);
 y:=bound;

end;
```

This fit needs no correlation between signal and concentration; it usually compares well with the Scatchard plot.

If the relation between signal and concentration of bound ligand is unknown, one can use a **direct linearisation** of the titration curve to detect systematic deviations, for example the Heyn-Weischet plot [24]:

$$\frac{1}{1 - Y} = K_a \cdot \frac{L_0}{Y} - K_a \cdot R_0$$

(with Y= 'fraction of receptor occupied' = RL/RL_0); therefore, a plot of $\frac{1}{1 - Y}$ against $\frac{L_0}{Y}$ has the slope K_a , and an x intercept = R_0. The following shows a Heyn-Weischet plot, with the last five points of the above dataset removed because of the very large errors. These plots need especially many data in the low concentration range.

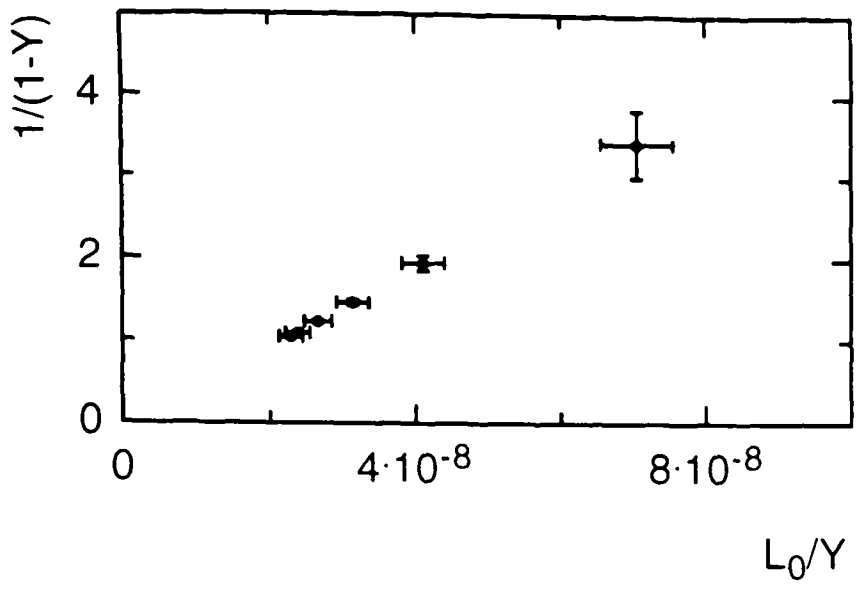

If the concentration of bound ligand can be determined, **Scatchard** fitting is the usual way to linearise. It is the only satisfactory way to plot binding (as opposed to titration) curves. Problems with this plot are no real separation of variables, uneven weighting of data, and the difficulty to see several binding constants if they are far apart. It is very good for the determination of the number of binding sites. Starting with

$$RL = \frac{R_0 \cdot L}{1/K_a + L}$$

as in (5) - but here L is the free ligand and not L_0 as simplified above -

we invert:
$$\frac{1}{RL} = \frac{1}{K_a \cdot R_0 \cdot L} + \frac{1}{R_0}$$

and multiply by $K_a \cdot RL \cdot R_0$:

$$\frac{RL}{L} = K_a \cdot R_0 - K_a \cdot RL\ ;$$

if $\frac{RL}{L}$ are plotted against RL, the slope is $-K_a$, and the x-intercept R_0.

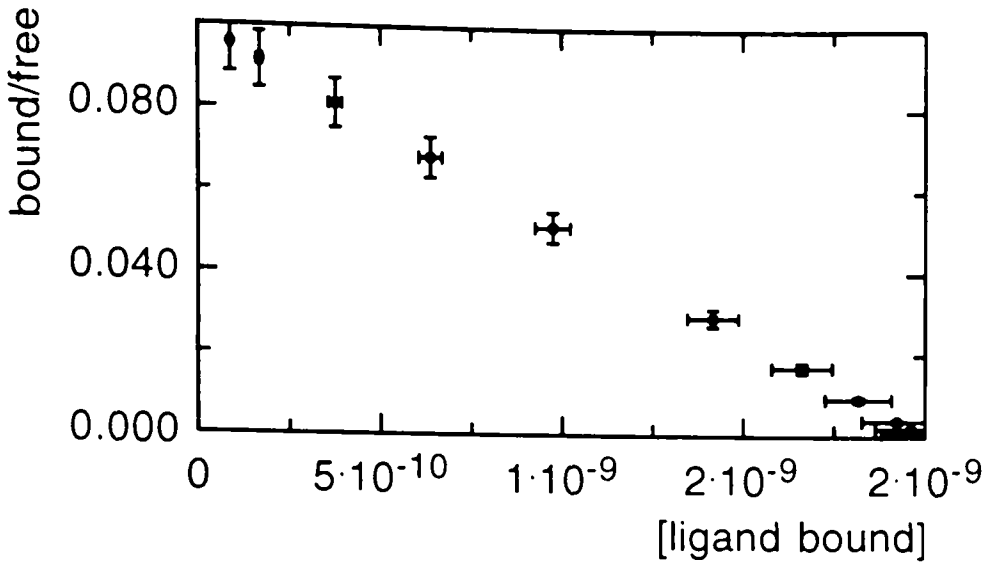

B.2. Fitting off-rates

In the presence of excess unlabeled competitor, or the constant removal of ligand, a dissociation process follows simple first-order kinetics.

For the reaction RL $\rightarrow$ R + L, the decay equation is $RL = RL_0 \cdot e^{-k_{off} \cdot t}$; this equation can be fitted to the data as least-squares fit. Linearisation is in a semilogarithmic plot: ln $(\frac{RL}{RL_0}) = -k_{off} \cdot t$, so that in a plot of ln $(\frac{RL}{RL_0})$ against t, $-k_{off}$ is the slope of the straight line through the data.

B.3. Fitting on-rates

The simplest fitting routines assume that no further reaction takes place after the initial binding, or that it is too slow to play a role in the time-scale of the experiment. If that is not the case, more complicated models apply (see below).

If the correlation between signal S and the concentration of bound ligand is unknown (for example in stopped-flow fluorescence experiments), a direct least-squares fit to the **simple binding function** is the method of choice. Equation (15) from above gives:

$$RL = RL_{eq} \cdot (1 - e^{-k_{obs} \cdot t}) \qquad (15)$$

Substituting S (signal) for RL (so that S equals RL times the unknown correlation factor) and S_0 for RL_0, this becomes

$$S = S_{eq} \cdot (1 - e^{-k_{obs} \cdot t}) \qquad (16)$$

Then, in a secondary plot of k_{obs} against L_0, k_1 and k_{-1} can be determined:

$$k_{obs} = k_1 \cdot L_0 + k_{-1}$$

Here, ligand depletion cannot be taken into account; therefore the experiment must be designed so that ligand depletion does not play a role ($R_0 << L_0$). The k_{obs}/L_0 plot is easiest to interpret if $k_1 \cdot L_0$ and k_{-1} are in the same order of magnitude.

If a final value of RL can be approximated correctly (for example in stopped-flow experiments by fitting a straight line through the last portion of the binding curve), then **initial rate fits** can be used. They are very sensitive towards errors in the final value determination, but give good estimates of the initial on-rate.

Rearrange (16): $1 - \frac{S}{S_{eq}} = e^{-k_{obs} \cdot t}$, and

$$\ln\left(1 - \frac{S}{S_{eq}}\right) = -k_{obs} \cdot t.$$

Therefore, a plot of $\ln\left(1 - \frac{S}{S_{eq}}\right)$ against t has a slope of $-k_{obs}$.

If the signal-concentration correlation exists, a **full least-squares fit with ligand depletion** to the equation given in [21], p.70, is possible (and necessary for radioactivity binding experiments). This fit requires the input of an equilibrium constant (K_a). If a multistep reaction is suspected, it cannot be assumed that the K_a for the initial reaction will be the equilibrium K_a. It is possible to fit all k_{on}, k_{off}, and K_a; this is only meaningfully possible if $k_{on} \cdot L_0$ is in the same order of magnitude than k_{off}. (When ligand depletion is not taking place, a fit to equation 14 can be done instead.)

For the on-rate fitting in the tritium peptide binding experiments, a **compromise method** was used. After subtraction of the background (never more than 5%), the concentration of bound ligand was calculated from the number of bound cpm and the specific activity of the peptide; this was then plotted against the concentration of bound ligand. Fitting was with the full binding curve, including ligand depletion, according to the following Pascal routine:

```
function  full_onratefit;

description
 'simple bimolecular receptor-ligand interaction with ligand depletion',

parameters  5;

defaults
   a[1]:=5e+5,active,'k1',0,inf;
   a[2]:=1e-5,active,'k-1',0,inf;
   a[3]:=1e-5,inactive,'Lo',0,inf;
   a[4]:=1e-7,inactive,'Ro',0,inf;
   a[7]:=2e+6,   active,'factor',0,inf;

var
 RLeq:extended;
 b:extended;
 Kd:extended;
 c:extended;
 signal_factor:extended;

begin
   Kd:=a[2]/a[1];
    RLeq:=0.5*((a[3]+a[4]+Kd)-sqrt(sqr(a[3]+a[4]+Kd)-4*a[4]*a[3]));
   b:=a[4]*a[3]/RLeq;
   c:=exp((RLeq-b)*a[1]*x);
    y:=a[7]*(RLeq*b*(c-1))/(RLeq*c-b);

end;
```

The 'factor' was allowed to float free to avoid a distortion of the rate constants due to errors in the determination of the specific activity, R_0, or RL (counting errors are familiar with tritium). 'factor' was always between 0.75 and 1.6 (see results section). It was not possible by this, or any other, method to obtain meaningful values for k_{off} (see results section).

Notes on on-rates assuming more complicated models:

· if there is an initial first-order reaction that is faster than everything else, it can be neglected.

· if there is an initial first-order reaction that is rate-limiting, only this reaction will be seen and the k_{obs} will be independent of L_0.

· if there is an initial second-order reaction, the intermediate is being observed, and everything else is slower, the rest can be neglected.

· if there is an initial second-order reaction, the final product is being observed, and everything else is slower, the k_{obs} will depend on L_0 (like in a second-order reaction) at low L_0, and be independent of L_0 (like in a first-order reaction) at high L_0.

· if there is an initial second-order reaction, the intermediate is being observed, and the following reaction is faster, there will be very little intermediate to observe.

· if there is an initial second-order reaction, the intermediate is being observed, and the following reaction is slower, then the observed species will go through a maximum.

A description of some of these systems can be found in [21].

Abbreviations and symbols

Standard three- and single-letter codes for amino acids and single-letter codes for nucleotides are as in [Sambrook, 1989 #990]. Abbreviations of sizes and units of the SI system, and symbols that occur only once, are not listed here. All abbreviations and symbols are defined when they first appear.

' (or min.)	minutes
" (or sec.)	seconds
:=	is defined as (mathematical sign)
°	degrees (Celsius or angular),
	or: denotes equilibrium (in $\Delta G°$, $\Delta S°$, $\Delta H°$)
‡	denotes the transition state (in $\Delta G^{‡}$, etc.)
[L] (or L)	concentration of L
AU	artificial units (of fluorescence)
aq.dest.	double distilled or ion-exchange purified (Millipore) water
BSA	bovine serum albumin
ccc	covalently closed circular (of DNA)
CD	circular dichroism
CHO	chinese hamster ovary (cells)
CIP	calf intestinal phosphatase (removes 3' phosphates from DNA)
cpm	counts per minute
Da	dalton (unit of molecular weight)
DEPC	diethyl pyrocarbonate
DMEM	Dulbecco's modified Eagle's medium
dNTP	deoxynucleoside triphosphate
DTT	dithiothreitol
e	2.71828
FA	fluorescence anisotropy

FAD	fluorescence anisotropy decay
FCS	fetal calf serum
GuaHCl	guanidinium hydrochloride
h	Schrödinger's constant (6.6260755e-34 J·s)
$h\beta_2m$	human beta-2 microglobulin
HEPES	4-(2-Hydroxyethyl)piperazine-1-ethanesulfonic acid (buffer)
HPLC	high pressure liquid chromatography
hr(s)	hour(s)
IEF	isoelectric focusing
I_z	intensity of fluorescence polarised in the z direction
k or k_B	Boltzmann's constant (1.380658e-23 J/K)
k	kinetic constant (when with index):
k_x	forward reaction constant
k_{-x}	backward reaction constant
K	equilibrium constant
K_a	equilibrium association constant, $\frac{k_{on}}{k_{off}}$
K_d	equlilibrium dissociation constant, $\frac{k_{off}}{k_{on}}$
k_{obs}	apparent on-rate constant ('observed')
k_{off}	kinetic dissociation constant
k_{on}	kinetic association constant
L	ligand (for peptide in kinetic equations)
LB	Luria-Bertani broth (for bacteria)
LRB	Laemmli running buffer for SDS-PAGE
LSB	Laemmli sample buffer for SDS-PAGE
MEGA-9	Nonanoyl methyl glucanamide (detergent)
MHC	major histocompatibility complex
MW	molecular weight
N_A	Avogadro's number ($6.023 \cdot 10^{23}$ mol^{-1})
n_D	refractive index at 20 °C

NP-40	Nonidet P-40 (detergent)
NTP	nucleoside triphosphate
o/n	overnight
OD_n	optical density or extinction of solution at RT, wavelength n, light path length 10 mm.
PAGE	polyacrylamide gel electrophoresis
PCR	polymerase chain reaction
R	universal gas constant (8.314510 J/(mol·K))
R, R', R''	receptor (for class I in kinetic equations; in different states)
R	fluorescence anisotropy ($R:=\frac{I_z - I_y}{I_z + 2 \cdot I_y}$)
RL, R'L	receptor-ligand complex (in different states)
rpm	revolutions per minute
RPMI	Roswell Park Memorial Institute Medium
RT	room temperature
S	signal (dimensionless)
SDS	sodium dodecyl (or lauryl) sulfate (detergent)
STI	trypsin inhibitor from Soybean
TCR	T cell receptor
Tris•Cl	Tris(hydroxymethyl)aminomethane hydrochloride (buffer)
Tween-20	polyoxyethylene sorbitan monolaurate (detergent)
U	unit (of enzyme activity)
v/v	volume of volume (of percentages) 1%(v/v) = 1 ml/100 ml
w/v	weight of volume (of percentages) 1%(w/v) = 1 g/100 ml
Y	fraction of receptor occupied, $Y:=\frac{RL}{R_0}$

Names, origins, and sequences of the peptides mentioned in this thesis

designation	originally derived from	sequence	binds
GP-92-101 (also JEG#4)	lymphocytic choriomeningitis virus glycoprotein	CSANNSHHYI	D^b
MCMV-168-176	murine cytomegalovirus pp89 early regulatory protein	YPHFMPTNL	L^d
NP-91-99	influenza nucleoprotein	KTGGPIYKR	A*6801
NP-147-155	influenza nucleoprotein	TYQRTRALV	K^d
NP-366-374	influenza nucleoprotein (1968 strain)	ASNENMDAM	D^b
NP-C365-374	influenza nucleoprotein (1968 strain)	CSNENMDAM	D^b
NP-Y365-374	influenza nucleoprotein (1968 strain)	YSNENMDAM	D^b
NP-Y365-374G9	influenza nucleoprotein (1968 strain)	YSNENMDAG	D^b
NP-50-63	influenza nucleoprotein (1934 strain)	SDYEGRLIQNSLTI	D^b
OVA-55-62C6	chicken ovalbumin	KVVRFCKL	K^b
OVA-257-264	chicken ovalbumin	SIINFEKL	K^b
SV-324-332	Sendai virus nucleoprotein	FAPGNYPAL	K^b, D^b
OVA-257-264C6	chicken ovalbumin	SIINFCKL	K^b
VSV-8	vesicular stomatitis virus nucleoprotein	RGYVYQGL	K^b

References

1. Sambrook, J., E.F. Fritsch, and T. Maniatis, *Molecular Cloning - A Laboratory Manual*. 1989, Cold Spring Harbor: Cold Spring Harbor Laboratory Press.

2. Barnstable, C.J., *et al.*, *Production of monoclonal antibodies to group A erythrocytes, HLA and other human cell surface antigens- new tools for genetic analysis.* Cell **14** (1978) 9-20.

3. Ozato, K. and D.H. Sachs, *Monoclonal antibodies to mouse MHC antigens. Hybridoma antibodies reacting to antigens of the H-2b haplotype reveal genetic control of isotype expression.* J. Immunol. **126** (1980) 317-321.

4. Allen, H., D. Wraith, P. Pala, B. Askonas, and R.A. Flavell, *Domain interactions of H-2 class I antigens alter cytotoxic T-cell recognition sites.* Nature **309** (1984) 279-282.

5. Allen, H., J. Fraser, D. Flyer, S. Calvin, and R. Flavell, *Beta-2 microglobulin is not required for cell surface expression of the murine class I histocompatibility antigen H-2D^b or a truncated D^b.* Proc. Natl. Acad. Sci. USA **83** (1986) 7447-7451.

6. Hämmerling, G.J., U. Hämmerling, and H. Lemke, *Isolation of twelve monoclonal antibodies against Ia and H-2 antigens. Serological characterization and reactivity with B and T lymphocytes.* Immunogenetics **8** (1979) 433-445.

7. Ey, P.L., S.J. Prowse, and C.R. Jenkin, *Isolation of pure IgGI, IgG2a and IgG2b immunoglobulin from mouse serum using protein A-sepharose.* Immunochem. **15** (1978) 429-436.

8. Harlow, E. and D. Lane, *Antibodies - a laboratory manual.* 1988, Cold Spring Harbor: Cold Spring Harbor Laboratory Press.

9. Dawson, R.M.C., D.C. Elliott, W.H. Elliott, and K.M. Jones, *Data for biochemical research.* Third ed. 1984, Oxford: Clarendon Press.

10. Gill, S.C. and P.H. von Hippel, *Calculation of protein extinction coefficients from amino acid sequence data.* Anal Biochem **182** (1989) 319-326.

11. Genetics Computer Group, *Program manual for the Wisconsin package.* 8th ed. 1994, Madison, Wisconsin: GCG.

12. Laemmli, U.K., *Cleavage of stuctural proteins during assembly of the head of bacteiphage T4.* Nature **227** (1970) 680-685.

13. Edelhoch, H., *Spectroscopic determination of tryptophan and tyrosine in proteins.* Biochemistry **6** (1967) 1948-1954.

14. Townsend, A., *et al.*, *Assembly of MHC class I molecules analyzed in vitro.* Cell **62** (1990) 285-95.

15. Cerundolo, V., *et al.*, *The binding affinity and dissociation rates of peptides for class I histocompatibility complex molecules.* Eur. J. Immunol. **21** (1991) 2069-2075.

16. Döring, K., W. Beck, L. Konermann, and F. Jähnig, *The use of a long lifetime component of tryptophan to detect slow orientational fluctuations of proteins.* Eur. Biophys. J. **submitted** (1996) .

17. Döring, K., L. Konermann, T. Surrey, and F. Jähnig, *A long lifetime component in the tryptophan fluorescence of some proteins.* Eur. Biophys. J. **23** (1995) 423-432.

18. Nicholls, A., K.A. Sharp, and B. Honig, *Protein folding and association: Insights from the interfacial and thermodynamic properties of hydrocarbons.* Proteins Structure Function And Genetics **11** (1991) 281-296.

19. Press, W.H., B.P. Flannery, S.A. Teukolsky, and W.T. Vetterling, *Numerical recipes - the art of scientific computing.* 2 ed. 1992, Cambridge: Cambridge University Press.

20. Taylor, J.K., *Statistical techniques for data analysis.* 1990, Chelsea, MI: Lewis Publishers.

21. Hulme, E.C. and N.J.M. Birdsall, *Strategy and tactics in receptor-binding studies,* in *Receptor-Ligand Interactions: A Practical Approach,* E.C. Hulme, Editor. 1992, Oxford University Press: Oxford. p. 63-176.

22. Gutfreund, H., *Kinetics for the life sciences.* 1995, Cambridge (UK): Cambridge University Press.

23. Bisswanger, H., *Theorie und Methoden der Enzymkinetik.* 1979, Weinheim: Verlag Chemie.

24. Heyn, M.P. and W.O. Weischet, *Circular dichroism and fluorescence studies on the binding of ligands to the alpha subunit of tryptophan synthase.* Biochemistry **14** (1975) 2962-2968.

25. Townsend, A. and H. Bodmer, *Antigen recognition by class I -restricted cytotoxic T lymphocytes*. Annu. Rev. Immunol. **7** (1989) 601-624.

26. Elliott, T., M. Smith, P. Driscoll, and A. McMichael, *Peptide selection by class I molecules of the major histocompatibility complex*. Curr. Biol. **3** (1993) 854-866.

27. Germain, R.N. and D.H. Margulies, *The biochemistry and cell biology of antigen processing and presentation*. Annu. Rev. Immunol. **11** (1993) 403-50.

28. Germain, R.N., *MHC-dependent antigen presentation: Providing ligands for T-lymphocyte activation*. Cell **76** (1994) 287-299.

29. Heemels, M.T. and H. Ploegh, *Generation, translocation, and presentation of MHC class I restricted peptides*. Annu. Rev. Biochem. **64** (1995) 463-491.

30. York, I.A. and K. Rock, *Antigen processing and presentation by the class I major histocompatibility complex*. Annu. Rev. Immunol. **14** (1996) 369-96.

31. Cerundolo, V. and V. Braud, *Cell biology of MHC class I molecules*, in *HLA and MHC: genes, molecules and function*, M. Browning and A. McMichael, Editor. 1996, BIOS Scientific Publishers: Oxford. p. 193-223.

32. Zinkernagel, R.M. and P.C. Doherty, *Restriction of in vitro T cell - mediated cytotoxicity in lymphocytic choriomeningitis within a syngeneic or allogeneic system*. Nature **248** (1974) 701-702.

33. Blanden, R.V., *et al.*, *Genes required for cytotoxicity against virus-infected target cells in K and D regions of H-2 complex*. Nature **254** (1975) 269-270.

34. Townsend, A. and J. Skehel, *Influenza A specific cytotoxic T-cell clones that do not recognize viral glycoproteins*. Nature **300** (1982) 655-657.

35. Townsend, A. and J. Skehel, *The influenza A virus nucleoprotein gene controls the induction of both subtype specific and cross-reactive cytotoxic T cells*. J. Exp. Med. **160** (1984) 552-563.

36. Townsend, A., A. McMichael, N. Carter, J. Huddlestone, and G. Brownlee. *Cytotoxic T cell recognition of the influenza nucleoprotein and hemagglutinin in transfected moiuse L cells.* Cell **39** (1984) 13-25.

37. Townsend, A.R.M., F.M. Gotch, and J. Davey. *Cytotoxic T cells recognise fragments of influenza nucleoprotein.* Cell **42** (1985) 457-467.

38. Townsend, A., *et al.*, *The epitopes of influenza nucleoprotein recognized by cytotoxic T lymphocytes can be defined with short synthetic peptides.* Cell **44** (1986) 959-968.

39. Bastin, J., J. Rothbard, J. Davey, I. Jones, and A. Townsend, *Use of synthetic peptides of influenza nucleoprotein to define epitopes recognized by class I-restricted cytotoxic T lymphocytes.* J. Exp. Med. **165** (1987) 1508-1523.

40. Maryanski, J.P., P. Pala, G. Corradin, B.R. Jordan, and J.C. Cerottini, *H-2 restricted cytotoxic T cells specific for HLA can recognise a synthetic HLA peptide.* Nature **324** (1986) 578-579.

41. Townsend, A., J. Bastin, K. Gould, and G. Browlee, *Cytotoxic T lymphocytes recognize influenza haemagglutinin that lacks a signal sequence.* Nature **234** (1986) 575-577.

42. Townsend, A.R.M., A.J. McMichael, and G.G. Brownlee, *Recognition of the viral nucleoprotein by influenza A specific cytotoxic T cells.* Immune Regulation, ed. M. Feldmann and N.A. Mitchison. 1985, London: The Humana Press. 231-241.

43. Townsend, A., *et al.*, *Association of class I major histocompatibility heavy and light chains induced by viral peptides.* Nature **340** (1989) 443-8.

44. Cerundolo, V., *et al.*, *Presentation of viral antigen controlled by a gene in the major histocompatibility complex.* Nature **345** (1990) 449-52.

45. Siliciano, R.F. and M.J. Soloski, *MHC class I - restricted processing of transmembrane proteins - Mechanism and biological significance.* J. Immunol. **155** (1995) 2-5.

46. Morrison, L., A. Lukacker, V. Braciale, D. Fan, and T. Braciale. *Differences in antigen presentation to MHC class I and class II restricted influenza specific cytotoxic T lymphocyte clones.* J. Exp. Med **163** (1986) 903-910.

47. Henderson, R.A., *et al.*, *Direct identification of an endogenous peptide recognized by multiple HLA-A2.1-specific cytotoxic T cells.* Proc. Natl. Aca. Sci. USA **90** (1993) 275-279.

48. Kovacsovics-Bankowski, M. and K. Rock, *A phagosome-to-cytosol pathway for exogenous antigens presented on MHC class I molecules.* Science **267** (1995) 243-246.

49. Stearz, U., H. Karasuyama, and A. Garner, *Cytotoxic T lymphocytes against a soluble protein.* Nature **329** (1988) 449-450.

50. Yide, J., S. Wai-Kuo, and I. Berkower, *Human T cell response to the surface antigen of hepatitis B (HBsAg). Endosomal and non-endosomal processing pathways are accessible to both endogenous and exogenous antigen.* J. Exp. Med. **168** (1988) 293-297.

51. Elliott, T., A. Willis, V. Cerundolo, and A. Townsend, *Processing of major histocompatibility class I-restricted antigens in the endoplasmic reticulum.* J. Exp. Med. **181** (1995) 1481-1491.

52. Snyder, H.L., J.W. Yewdell, and J.R. Bennink, *Trimming of antigenic peptides in an early secretory compartment.* J. Exp. Med. **180** (1994) 2389-94.

53. Peters, J.M., *Proteasomes: protein degradation machines of the cell.* Trends Biochem. Sci. **19** (1994) 377-382.

54. Löwe, J., *et al.*, *Crystal structure of the 20S proteasome from the archeon T. acidophilum at 3.4 Å resolution.* Science **268** (1995) 533-539.

55. Rock, K.L., *et al.*, *Inhibitors of the proteasome block the degradation of most cell proteins and the generation of peptides presented on MHC class I molecules.* Cell **78** (1994) 761-771.

56. Grant, E.P., M.T. Michalek, A.L. Goldberg, and K.L. Rock, *Rate of antigen degradation by the ubiquitin-proteasome pathway influences MHC class I presentation*. J. Immunol. **155** (1995) 3750-3758.

57. Harding, C.V., *et al.*, *Novel dipeptide aldehydes are proteasome inhibitors and block the MHC-I antigen processing pathway*. J. Immunol. **155** (1995) 1767-1775.

58. Brown, M., J. Driscoll, and J. Monaco, *Structural and serological similarity of MHC-linked LMP and proteosome (multicatalytic proteinase) complexes*. Nature **353** (1991) 355-357.

59. Glynne, R., *et al.*, *A proteosome-related gene between the two ABC transporter loci in the class II region of the human MHC*. Nature **353** (1991) 357-360.

60. Ortiz-Navarrete, V., *et al.*, *Subunit of the '20S' proteasome (multicatalytic proteinase) encoded ny the major histocompatibility complex*. Nature **353** (1991) 662-664.

61. Kelly, A., *et al.*, *A second proteasome-related gene in the human MHC class II region*. Nature **353** (1991) 667-668.

62. Früh, K., *et al.*, *Displacement of housekeeping proteasome subunits by MHC-encoded LMPs: a newly discovered mechanism for modulating the multicatalytic proteinase complex*. EMBO J. **13** (1994) 3236-3244.

63. Akiyama, K.-Y., *et al.*, *cDNA cloning and interferon gamma down-regulation of proteasomal subunits X and Y*. Science **265** (1994) 1231-1234.

64. Belich, M., R. Glynne, G. Senger, D. Sheer, and J. Trowsdale, *Proteasome components with reciprocal expression to that of the MHC-encoded LMP proteins*. Curr. Biol. **4** (1994) 0-0.

65. Driscoll, J., M.G. Brown, D. Finley, and J.J. Monaco, *MHC-linked LMP gene products specifically alter peptidase activities of the proteasome [see comments]*. Nature **365** (1993) 262-4.

66. Gaczynska, M., K.L. Rock, and A.L. Goldberg. *Gamma-interferon and expression of MHC genes regulate peptide hydrolysis by proteasomes [see comments]*. Nature **365** (1993) 264-7.

67. Ehring, B., T.H. Meyer, C. Eckerskorn, F. Lottspeich, and R. Tampé. *Effects of MHC-encoded subunits on the peptidase and proteolytic activities of human 20S proteasomes: Cleavage of proteins and antigenic peptides*. Eur. J. Biochem. **in press** (1996) .

68. Ciechanover, A., *The ubiquitin-proteasome proteolytic pathway*. Cell **79** (1994) 13-21.

69. Jennissen, H.P., *Ubiquitin and the enigma of intracellular protein degradation*. Eur. J. Biochem. **231** (1995) 1-30.

70. Bachmair, A., D. Finley, and A. Varshavsky, *In vivo half-life of a protein is a function of its amino-terminal residue*. Science **234** (1986) 179.

71. Townsend, A., *et al.*, *Defective presentation to class I-restricted cytotoxic T lymphocytes in vaccinia-infected cells is overcome by enhanced degradation of antigen*. J. Exp. Med. **168** (1988) 1211-24.

72. Hahn, Y.S., C.S. Hahn, V.L. Braciale, T.J. Braciale, and C.M. Rice, *T cell recognition of an endogenously processed epitope is regulated primarily by residues within the epitope*. J. Exp. Med. **176** (1992) 1335-1341.

73. Eisenlohr, L.C., J.W. Yewdell, and J.R. Bennink, *Flanking sequences influence the presentation of an endogenously synthesized peptide to cytotoxic T lymphocytes*. J. Exp. Med. **175** (1992) 481-7.

74. Niedermann, G., *et al.*, *Contribution of proteasome-mediated proteolysis to the hierarchy of epitopes presented by major histocompatibility complex class I molecules*. Immunity **2** (1995) 289-299.

75. Cerundolo, V., A.G.D. Tse, R.D. Salter, P. Parham, and A. Townsend, *CD8 independence and specificity of cytotoxic T lymphocytes restricted by HLA-Aw68.1*. Proc. R. Soc. Lond. B. **244** (1991) 169-177.

76. Del Val, M., H.J. Schlicht, T. Ruppert, M.J. Reddehase, and U.H. Koszinowski. *Efficient processing of an antigenic sequence for presentation by MHC class I molecules depends on its neighboring residues in the protein.* Cell **66** (1991) 1145-53.

77. Hahn, Y., V. Braciale, and T. Braciale, *Presentation of viral antigen to class I major histocompatibility complex-restricted cytotoxic T lymphocyte. Recognition of an immunodominant influenza hemagglutinin site by cytotoxic T lymphocyte is indepepndent of the position of the site in the hemagglutinin translation product* . J. Exp. Med. **174** (1991) 733-736.

78. Chimini, G., P. Pala, J. Sire, B.R. Jordan, and J.L. Maryanski. *Recognition of oligonucleotide-encoded T cell epitopes introduced into the original antigen.* J. Exp. Med. **169** (1989) 297-302.

79. DeMars, R., *et al.*, *Mutations that impair a posttranscriptional step in the expression of HLA-A and -B antigens.* Proc. Natl. Acad. Sci. USA **82** (1985) 8183-1813.

80. Salter, R.D. and P. Cresswell, *Impaired assembly and transport of HLA-A and -B antigens in a TxB cell hybrid.* EMBO J. **5** (1986) 943-949.

81. Spies, T., *et al.*, *A gene in the human major histocompatibility complex class II region controlling the class I antigen presentation pathway.* Nature **348** (1990) 744-7.

82. Spies, T. and R. DeMars, *Restored expression of major histocompatibility class I molecules by gene transfer of a putative peptide transporter* . Nature **351** (1991) 323-4.

83. Kelly, A., *et al.*, *Assembly and function of the two ABC transporter proteins encoded in the human major histocompatibility complex.* Nature **355** (1992) 641-644.

84. Cerundolo, V., *Antigen processing and presentation : The role of the endoplasmic reticulum.* Subcell. Biochem. **21** (1993) 209-228.

85. Townsend, A. and J. Trowsdale, *The transporters associated with antigen presentation.* Semin. Cell Biol. **4** (1993) 53-61.

86. Yang, Y., *et al.*, *Major histocompatibility complex (MHC) - encoded HAM2 is necessary for antigenic peptide loading onto class I MHC molecules.* J. Biol. Chem. **267** (1992) 11669-11672.

87. Kleijmeer, M., *et al.*, *Location of MHC-encoded transporters in the endoplasmic reticulum and cis-Golgi.* Nature **357** (1992) 342-344.

88. Androlewicz, M. and P. Cresswell, *Human transporters associated with antigen processing possess a promiscuous peptide-binding site.* Immunity **1** (1994) 7-14.

89. Uebel, S., *et al.*, *Requirements for peptide binding to the human transporter associated with antigen processing revealed by peptide scans and complex peptide libraries.* J. Biol. Chem. **270** (1995) 18512-18516.

90. Androlewicz, M., K. Anderson, and P. Cresswell, *Evidence that transporters associated with antigen processing translocate a major histocompatibility complex class I-binding peptide into the endoplasmic reticulum in an ATP-dependent manner.* Proc. Natl. Acad. Sci. USA **90** (1993) 9130-9134.

91. Shepherd, J., *et al.*, *TAP1-dependent peptide translocation in vitro is ATP dependent and peptide selective.* Cell **74** (1993) 577-584.

92. Meyer, T.H., P.M. van Endert, S. Uebel, B. Ehring, and R. Tampé, *Functional expression and purification of the ABC transporter complex associated with antigen processing (TAP) in insect cells.* FEBS Lett. **351** (1994) 443-447.

93. Neefjes, J., F. Momburg, and G. Hämmerling, *Selective and ATP-dependent translocation of peptides by the MHC-encoded transporter.* Science **261** (1993) 769-771.

94. Momburg, F., J. Roelse, G. Hämmerling, and J. Neefjes, *Peptide size selection by the major histocompatibility complex-encoded peptide transporter.* J. Exp. Med. **179** (1994) 1613-1623.

95. Neefjes, J.J., F. Momburg, and G.J. Hämmerling, *Selective and ATP-dependent translocation of peptides by the MHC-encoded transporter.* Science **261** (1993) 769-771.

96. Schumacher, T., *et al.*, *Peptide length and sequence specificity of the mouse TAP1/TAP2 translocator.* J. Exp. Med. **179** (1994) 533:540.

97. Neisig, A., *et al.*, *Major differences in transporter associated with antigen presentation (TAP)-dependent translocation of MHC class I-presentable peptides and the effect of flanking sequences.* J. Immunol. **154** (1995) 1273-1279.

98. Powis, S.J., *et al.*, *Effect of polymorphism of an MHC-linked transporter on the peptides assembled in a class I molecule.* Nature **357** (1992) 211-215.

99. Roelse, J., M. Grommé, F. Momburg, G. Hämmerling, and J. Neefjes, *Trimming of TAP-translocated peptides in the endoplasmic Reticulum and in the cytosol during recycling.* J. Exp. Med. **180** (1994) 1591-1597.

100. Römisch, K. and R. Schekman, *Distinct processes mediate glycoprotein and glycopeptide export from the endoplasmic reticulum in Saccharomyces cerevisiae.* Proc. Natl. Acad. Sci. USA **89** (1992) 7227.

101. Skipper, J.C.A., *et al.*, *An HLA-A2 restricted tyrosinase antigen on melanoma cells results from posttranslational modification and suggests a novel pathway for the processing of membrane proteins.* J. Exp. Med. **183** (1996) 527-534.

102. Tragardh, L., L. Rask, K. Wiman, J. Fohlman, and P.A. Peterson, *Complex amino acid sequence of pooled papain-solubilized HLA-A, -B, and -C antigens: Relatedness to immunoglobulins and internal homologies.* Proc. Natl. Acad. Sci. USA **77** (1980) 1129-1133.

103. Coligan, J.E., T.J. Kindt, H. Uehara, J. Martinko, and S.G. Nathenson, *Primary structure of a murine transplantation antigen.* Nature **291** (1981) 35-39.

104. Strominger, J.L., *et al.*, *Complete primary structure of human histocompatibility antigen HLA-B7: Evolutionary and functional implications.* Curr. Top. Dev. Biol. **14** (1980) 97-113.

105. Ploegh, H.L., H.T. Orr, and J.L. Strominger, *Molecular cloning of a human histocompatibility antigen cDNA fragment.* Proc. Natl. Acad. Sci. USA **77** (1980) 6081-6085.

106. Sood, A.K., D. Pereira, and S.M. Weissman, *Isolation and partial nucleotide sequence of a cDNA clone for human histocompatibility antigen HLA-B by use of a oligodeoxynucleotide primer*. Proc. Natl. Acad. Sci. USA **78** (1981) 616-620.

107. Kvist, S., *et al.*, *cDNA clone coding for part of a mouse H-2^d major histocompatibility antigen*. Proc. Natl.Acad. Sci. USA **78** (1981) 2772-2776.

108. Reyes, A.A., *et al.*, *Identification of an H-2K^b-related molecule by molecular cloning*. Immunogenetics **14** (1981) 383-392.

109. Malissen, M., B. Malissen, and B.R. Jordan, *Exon/intron organisation and complete nucleotide sequence of an HLA gene*. Proc. Natl. Acad. Sci. USA **79** (1982) 893-897.

110. Moore, K.W., B.T. Sher, Y.H. Sun, K.A. Eakle, and L. Hood, *DNA sequence of a gene encoding a BALB/c mouse L^d transplantation antigen*. Science **215** (1982) 679-682.

111. Lippe, R., E. Luke, Y.T. Kuah, C. Lomas, and W.A. Jefferies, *Adenovirus infection inhibits the phosphorylation of major histocompatibility complex class I proteins*. J. Exp. Med. **174** (1991) 1159-66.

112. Eichholtz, T., P. Vossebeld, M. van Overveld, and H.L. Ploegh, *Activation of protein kinase C accelerates internalization of transferrin receptor but not of major histocompatibility complex class I, independent of their phosphorylation status*. J. Biol. Chem. **267** (1992) 22490-22495.

113. Heinrichs, H. and H.T. Orr, *HLA non-A,B,C class I genes: their structure and expression*. Immunol.Res. **9** (1990) 265-74.

114. Shawar, S.M., J.M. Vyas, J.R. Rodgers, and R.M. Rich, *Antigen presentation by major histocompatibility complex class I-B molecules*. Annu. Rev. Immunol. **12** (1994) 839-880.

115. Stiernberg, J., M.G. Low, L. Flaherty, and P.W. Kincade, *Removal of lymphocyte surface molecules with phosphatidylinositol-specific phospholipase C: Effects on mitogen responses and evidence that ThB and certain Qa antigens are membrane-anchored via phosphatidylinositol*. J. Immunol. **138** (1987) 3877-3884.

116. Grey, H.M., *et al.*, *The small subunit of HL-A antigens is beta 2-microglobulin.* J. Exp. Med. **138** (1973) 1608-1612.

117. Cunningham, B.A., J.L. Wang, I. Berggard, and P.A. Peterson, *The complete amino acid sequence of beta-2-microglobulin.* Biochemistry **12** (1973) 4811-4822.

118. Gates, F.T.I., J.E. Coligan, and T.J. Kindt, *Complete amino acid sequence of murine beta 2-microglobulin: Structural evidence for strain-related polymorphism.* Proc. Natl. Acad. Sci. USA **78** (1981) 554-558.

119. Bix, M. and D. Raulet, *Functionally conformed free class I heavy chains exist on the surface of beta-2 microglobulin negative cells.* J. Exp. Med. **176** (1992) 829-834.

120. Bjorkman, P., *et al.*, *Structure of human class I histocompatibility antigen, HLA-A2.* Nature **329** (1987) 506-511.

121. Madden, D.R., *The three-dimensional structure of peptide-MHC complexes.* Annu. Rev. Immunol. **13** (1995) 587-622.

122. Bjorkman, P.J. and P. Parham, *Structure, Function, and diversity of the class I major histocompatibility complex molecules.* Annu. Rev. Biochem. **59** (1990) 253-288.

123. Matsumura, M., D.H. Fremont, P.A. Peterson, and I.A. Wilson, *Emerging principles for the recognition of peptide antigens by MHC class I molecules.* Science **257** (1992) 927-934.

124. Madden, D., J. Gorga, J. Strominger, and D. Wiley, *The structure of HLA-B27 reveals nonamer self-peptides bound in an extended conformation.* Nature **353** (1991) 321-325.

125. Bjorkman, P., *et al.*, *The foreign antigen binding site and T cell recognition regions of class I histocompatibility antigens.* Nature **329** (1987) 512-519.

126. Young, A.C.M., W. Zhang, J.C. Sacchettini, and S.G. Nathenson, *The three-dimensional structure of H-2D^b at 2.4 Å resolution: implications for antigen-determinant selection.* Cell **76** (1994) 39-50.

127. Van Bleek, G.M. and S.G. Nathenson, *Isolation of an endogenously processed immunodominant viral peptide from the class I H-2 Kb molecule.* Nature **348** (1990) 213-216.

128. Rötzschke, O., *et al.*, *Isolation and analysis of naturally processed viral peptides as recognized by cytotoxic T cells.* Nature **348** (1990) 252-4.

129. Falk, K., O. Rötzschke, and H.-G. Rammensee, *Cellular peptide composition governed by major histocompatibility complex class I molecules [see comments].* Nature **348** (1990) 248-51.

130. Falk, K., O. Rötzschke, S. Stevanovic, G. Jung, and H.-G. Rammensee, *Allele-specific motifs revealed by sequencing of self-peptides eluted from MHC molecues.* Nature **351** (1991) 290-296.

131. Rammensee, H.-G., T. Friede, and S. Stevanovic, *MHC ligands and peptide motifs: first listing.* Immunogenetics **41** (1995) 178-228.

132. Saito, Y., P.A. Peterson, and M. Matsumura, *Quantitation of peptide anchor residue contributions to class I major histocompatibility complex molecule binding.* J. Biol. Chem. **268** (1993) 21309-21317.

133. Hudrisier, D., H. Mazarguil, M.B. Oldstone, and J.E. Gairin, *Relative implication of peptide residues in binding to major histocompatibility complex class I H-2D^b: application to the design of high-affinity, allele-specific peptides.* Mol. Immunol. **32** (1995) 895-907.

134. Hudrisier, D., H. Mazarguil, F. Laval, M.B.A. Oldstone, and J.E. Gairin, *Selection and presentation of viral antigens by major histocompatibility complex H-2D^b molecules are restricted by dominant negative elements at peptide non-anchor residues.* submitted (1995) .

135. Wilson, I.A. and D.H. Fremont, *Structural analysis of MHC class I molecules with bound peptide antigens.* Semin. Immunol. **5** (1993) 75-80.

136. Young, A.C., S.G. Nathenson, and J.C. Sachhettini, *Structural studies of class I major histocompatibility complex proteins: insights into antigen presentation.* FASEB J. **9** (1995) 26-36.

137. Stanfield, R.L. and I.A. Wilson, *Protein-peptide interactions*. Curr. Opin. Struct. Biol. **5** (1995) 103-113.

138. Fremont, D.H., M. Matsumura, E.A. Stura, P.A. Peterson, and I.A. Wilson, *Crystal structure of two viral peptides in complex with murine MHC class I H-2K^b*. Science **257** (1992) 919-927.

139. Chothia, C. and J. Janin, *Principles of protein-protein recognition*. Nature **256** (1975) 705-708.

140. Garrett, T., M. Saper, P. Bjorkman, J. Strominger, and D. Wiley, *Specificity pockets for the side chains of peptide antigens in HLA-Aw68*. Nature **342** (1989) 692-696.

141. Bouvier, M. and D.C. Wiley, *Importance of peptide amino and carboxyl termini to the stability of MHC class I molecules*. Science **265** (1994) 398-402.

142. Madden, D.R., J.C. Gorga, J.L. Strominger, and D.C. Wiley, *The three-dimensional structure of HLA-B27 at 2.1 Å resolution suggests a general mechanism for tight peptide binding to MHC*. Cell **70** (1992) 1035-1048.

143. Elliott, T., J. Elvin, V. Cerundolo, H. Allen, and A. Townsend, *Structural requirements for the peptide induced conformational change of free MHC class I heavy chains*. Eur. J. Immunol. **22** (1992) 2085-2091.

144. Madden, D.R., J.C. Gorga, J.L. Strominger, and D.C. Wiley, *The antigenic identity of peptide/MHC complexes: a comparison of the conformations of five viral peptides presented by HLA-A2*. Cell **75** (1993) 693-708.

145. Jardetzky, T., W. Lan, R. Robinson, D. Madden, and D. Wiley, *Identification of self-peptides bound to purified HLA-B27*. Nature **353** (1991) 326-329.

146. Ruppert, J., *et al.*, *Prominent role of secondary anchor residues in peptide binding to HLA-A2.1 molecules*. Cell **74** (1993) 929-937.

147. Parker, K.C., M.A. Bednarek, and J.E. Coligan, *Scheme for ranking potential HLA-A2 binding peptides based on independent binding of individual peptide side-chains*. J. Immunol. **152** (1994) 163-175.

148. Chen, Y., *et al.*, *Naturally processed peptides longer than nine amino acid residues bind to the class I MHC molecule HLA-A2.1 with high affinity and with different conformations*. J. Immunol. **152** (1994) 2874-2881.

149. Collins, E.J., D.N. Garboczi, and D.C. Wiley, *Three-dimensional structure of a peptide extending from one end of a class I MHC binding site*. Nature **371** (1994) 626-629.

150. Guo, H.-C., Jardetzky, T.S., Garrett, T.P., Lane, W., Strominger, J., Wiley, D., *Different length peptides bind to HLA-Aw68 similarly at their ends but buldge out in the middle*. Nature **360** (1992) 364:366.

151. Engelhard, V.H., *Structure of peptides associated with MHC class I molecules*. Curr. Opin. Immunol. **6** (1994) 13-23.

152. Utz, U., S. Koenig, J.E. Coligan, and W.E. Biddison, *Presentation of 3 different viral peptides, HTLV-1 TAX, HCMV gB, and influenza virus M1 is determined by common structural features of the HLA-A2.1 molecule*. J. Immunol. **149** (1992) 214-221.

153. Elliott, T., V. Cerundolo, J. Elvin, and A. Townsend, *Peptide-induced conformational change of the class I heavy chain*. Nature **351** (1991) 402-6.

154. Allen, H., J. Fraser, S. Flyer, S. calvin, and R. Flavell, *β-2 microglobulin is not required for cell surface expression of the murine class I histocompatibility antigen H-2Db or of a truncated H-2Db*. Proc. Natl. Acad. Sci. USA **79** (1988) 7447-7451.

155. Wang, H., R.G. Chapps, B.E. Robinson, and M.C. Zuniga, *Ab initio association with beta 2-microglobulin during biosynthesis of the H-2L^d class I major histocompatibility complex heavy chain promotes proper disulfide bond formation and stable peptide binding*. J. Biol. Chem. **269** (1994) 22276-22281.

156. Neefjes, J., G. Hämmerling, and F. Momburg, *Folding and assembly of major histocompatibility complex class I heterodimers in the endoplasmic reticulum of intact cells precedes the binding of peptide*. J. Exp. Med. **178** (1993) 1971-1980.

157. Machold, R., S. Andree, L. Van Kaer, H.-G. Ljunggren, and H. Ploegh, *Peptide influences the folding and intracellular transport of free major histocompatibility complex class I heavy chains.* J. Exp. Med. **181** (1995) 1111-1122.

158. Vitiello, A., T.A. Potter, and L.A. Sherman, *The role of beta 2-microglobulin in peptide binding by class I molecules.* Science **250** (1990) 1423-6.

159. Silver, M.L., K.C. Parker, and D.C. Wiley, *Reconstitution by MHC-restricted peptides of HLA-A2 heavy chain with beta 2-microglobulin, in vitro.* Nature **350** (1991) 619-22.

160. Parker, K.C., M.L. Silver, and D.C. Wiley, *An HLA-A2/beta-2-microglobulin/peptide complex assembled from subunits expressed separately in Escherichia coli.* Mol. Immunol. **29** (1991) 371-378.

161. Burshtyn, D.N. and B.H. Barber, *High occupancy binding of antigenic peptides to purified, immunoadsorbed H-2Db beta 2m molecules.* J. Immunol. **151** (1993) 3070-81.

162. Degen, E. and D. Williams, *Participation of a novel 88-Kd protein in the biogenesis of murine class I histocompatibilty molecules.* J. Cell. Biol. **112** (1991) 1099.

163. Rajagopalan, S. and M.B. Brenner, *Calnexin retains unassembled major histocompatibility complex class I free heavy chains in the endoplasmic reticulum.* J. Exp. Med. **180** (1994) 407-412.

164. Hochstenbach, F., V. David, S. Watkins, and M. Brenner, *Endoplasmic reticulum resident protein of 90 kilodaltons associates with the T- and B- cell antigen receptors and major histocompatibility complex antigens during their assembly.* Proc. Natl. Acad. Sci. USA **89**(1992) 4734-4738.

165. Degen, E., M. Cohen-Doyle, and D. Williams, *Efficient dissociation of the p88 chaperone from major histocompatibility complex class I molecules requires both ß-2 microglobulin and peptide.* J. Exp. Med. **175** (1992) 1653-1661.

166. Margolese, L., *et al.*, *Identification of the region on the class I histocompatibility molecule that interacts with the molecular chaperone, p88 (calnexin, IP90).* J. Biol. Chem. **268** (1993) 17959-17966.

167. Sugita, M. and M.B. Brenner, *An unstable beta-2-microglobulin : major histocompatibility complex class I heavy chain intermediate dissociates from calnexin and then is stabilized by binding peptide*. J. Exp. Med. **180** (1994) 2163-2171.

168. Ortmann, B., M.J. Androlewicz, and P. Cresswell, *MHC class I/beta 2-microglobulin complexes associate with TAP transporters before peptide binding*. Nature **368** (1994) 864-7.

169. Suh, W., *et al.*, *Interaction of MHC class I molecules with the transporter associated with antigen processing*. Science **264** (1994) 1322-1326.

170. Jackson, M.R., D.M.F. Cohen, P.A. Peterson, and D.B. Williams, *Regulation of MHC Class I Transport by the Molecular Chaperone, Calnexin (p88, IP90)*. Science (Washington D C) **263** (1994) 384-387.

171. Capps, G.G. and M.C. Zuniga, *Class I histocompatibility molecule association with phosphorylated calnexin: Implications for rates of intracellular transport*. J. Biol. Chem. **269** (1994) 11634-11639.

172. Sadasivan, B.K., A. Cariappa, G.L. Waneck, and P. Cresswell, *Assembly, peptide loading, and transport of MHC class I molecules in a calnexin-negaitve cell line*. Cold Spring Harbor Symp. Quant. Biol. **LX** (1995) 267-275.

173. Alexander, J., J.A. Payne, B. Shigekawa, J.A. Frelinger, and P. Cresswell, *The transport of class I major histocompatibility complex antigens is determined by sequences in the alpha 1 and alpha 2 protein domains*. Immunogenetics **31** (1990) 169-78.

174. Alexander, J., J.A. Payne, R. Murray, J. Frelinger, and P. Cresswell, *Differential transport requirements of HLA and H-2 class I glycoproteins*. Immunogenetics **29** (1989) 380-388.

175. Cerundolo, V., Elliott, T., Elvin, J., Bastin, J., Townsend, A., *Association of the human invariant chain to H-2 D^b molecules*. Eur. J. Immunol. **22** (1992) 2243-2248.

176. Li, Z. and P.K. Srivastava, *Tumor rejection antigen gp96/grp94 is an ATPase: implications for protein folding and antigen presentation.* EMBO J. **12** (1993) 3143-3151.

177. Williams, D., S. Swiedler, and G. Hart, *Intracellular transport of memebrane glycoproteins: two closely related histocompatibility antigens differ in their rates of transit to the cell surface.* J. Cell Biol. **101** (1985) 725-734.

178. Anderson, M., S. Paabo, T. Nilsson, and P. Peterson, *Impaired intracellular transport of class I MHC antigens as a possible means for adenoviruses to evade immune surveillance.* Cell **43** (1985) 215-222.

179. Cox, J.H., J.R. Bennink, and J.W. Yewdell, *Retention of adenovirus E19 glycoprotein in the endoplasmic reticulum is essential to its ability to block antigen presentation.* J. Exp. Med. **174** (1991) 1629-37.

180. Nuchtern, J.G., J.S. Bonifacino, W.E. Biddison, and R.D. Klausner, *Brefeldin A implicates egress from the endoplasmic reticulum in class I restricted antigen presentation.* Nature **339** (1989) 223-226.

181. Yewdell, J.W. and J.R. Bennink, *Brefeldin A specifically inhibits presentation of protein antigens to cytotoxic T lymphocytes.* Science **244** (1989) 1072-5.

182. Lapham, C., I. Bacik, J. Yewdell, K. Kane, and J. Bennink, *Class I molecules retained in the endoplasmic reticulum bind antigenic peptides.* J. Exp. Med.; **177** (1993) 1633-1641.

183. Tector, M., Q. Zhang, and R.D. Slater, *Phosphatase inhibitors block in vivo binding of peptides to class I major histocompatibility complex molecules.* J. Biol. Chem. **269** (1994) 25816-25822.

184. Henderson, R.A., *et al.*, *HLA-A2.1-associated peptides from a mutant cell line: A second pathway of antigen presentation.* Science **255** (1992) 1264-1266.

185. Wei, M.L. and P. Cresswell, *HLA-A2 molecules in an antigen processing mutant cell contain signal sequence-derived peptides.* Nature **356** (1992) 443-446.

186. Rammensee, H.-G., K. Falk, and O. Rötschke, *Peptides naturally presented by MHC class I molecules.* Annu. Rev. Immunol. **11** (1993) 213-244.

187. Ljunggren, H.G., *et al.*, *Empty MHC class I molecules come out in the cold.* Nature **346** (1990) 476-480.

188. Ortiz-Navarrete, V. and G.J. Hämmerling, *Surface appearance and instability of empty H-2 class I molecules under physiological conditions.* Proc. Natl. Acad. Sci. U S A **88** (1991) 3594-7.

189. Cox, A., *et al.*, *Identification of a peptide recognized by five melanoma-specific human cytotoxic T cell lines.* Science **264** (1994) 716-719.

190. Olsen, A.C., *et al.*, *A quantitative assay to measure the interaction between immunogenic peptides and purified class I major histocompatibility complex molecules.* Eur. J. Immunol. **24** (1994) 385-392.

191. Boyd, L.F., S. Kozlowski, and D.H. Margulies, *Solution binding of an antigenic peptide to a major histocompatibility complex class I molecule and the role of beta 2-microglobulin.* Proc. Natl. Acad. Sci. USA **89** (1992) 2242-6.

192. Matsumura, M., Y. Saito, M. Jackson, E. Song, and P. Peterson, *In vitro peptide binding to soluble empty class I major histocompatibility complex molecules isolated from transfected Drosophila melanogaster cells.* J. Biol. Chem. **267** (1992) 23589-23595.

193. Fahnestock, M.L., *et al.*, *Effects of peptide length and composition on binding to an empty class I MHC heterodimer.* Biochemistry **33** (1994) 8149-58.

194. Elvin, J., C. Potter, T. Elliott, V. Cerundolo, and A. Townsend, *A method to quantify binding of unlabeled peptides to class I molecules and detect their allele specificity.* J. Immunol. Methods **158** (1993) 161-171.

195. Christinck, E.R., M.A. Luscher, B.H. Barber, and D.B. Williams, *Peptide binding to class I MHC on living cells and quantitation of complexes required for CTL lysis.* Nature **352** (1991) 67-70.

196. Schumacher, T.N., *et al.*, *Direct binding of peptide to empty MHC class I molecules on intact cells and in vitro.* Cell **62** (1990) 563-7.

197. Stuber, G., *et al.*, *Identification of wild-type and mutand p53 peptides binding to HLA-A2 assessed by a peptide loading-deficient cell line assay and a novel major histocompatibility complex class I peptide binding assay*. Eur. J. Immunol. **24** (1994) 765-768.

198. Choppin, J., *et al.*, *Analysis of physical interactions between peptides and HLA molecules and application to the detection of human immunodeficiency virus 1 antigenic peptides*. J. Exp. Med. **172** (1990) 889-899.

199. Bodmer, H.C., J.M. Bastin, B.A. Askonas, and A.R. Townsend. *Influenza-specific cytotoxic T-cell recognition is inhibited by peptides unrelated in both sequence and MHC restriction*. Immunology **66** (1989) 163-9.

200. Maryanski, J.P., P. Pala, J.C. Cerottini, and G. Corradin. *Synthetic peptides as antigens and competitors in recognition by H-2 restricted cytolytic T cells specific for HLA*. J. Exp. Med. **167** (1988) 1391-1405.

201. Margulies, D.H., M. Corr, L.F. Boyd, and S.N. Khilko. *MHC class I/peptide interactions: binding specificity and kinetics [see comments]*. J. Mol. Recognit. **6** (1993) 59-69.

202. Ojcius, D.M., J.P. Abastado, F. Godeau, and P. Kourilsky. *Peptide binding to MHC class I proteins measured with a novel fluorescent technique*. C. R. Acad. Sci Iii **315** (1992) 337-41.

203. Frelinger, J.A., F.M. Gotch, H. Zweerink, E. Wain, and A.J. McMichael, *Evidence of widespread binding of HLA class I molecules to peptides*. J. Exp. Med. **172** (1990) 827-34.

204. Chen, B.P. and P. Parham, *Direct binding of influenza peptides to class I HLA molecules*. Nature **337** (1989) 743-5.

205. Benjamin, R.J., A. Madrigal, and P. Parham, *Peptide binding to empty HLA-B27 molecules of viable human cells*. Nature **351** (1991) 74-77.

206. Burshtyn, D.N. and B.H. Barber, *Dynamics of peptide binding to purified antibody-bound H-2Db and H-2Db beta 2m complexes*. J. Immunol. **151** (1993) 3082-93.

207. Elvin, J., V. Cerundolo, T. Elliott, and A. Townsend. *A quantitative assay of peptide-dependent class I assembly*. Eur. J. Immunol. **21** (1991) 2025-31.

208. Cerundolo, V., T. Elliott, and A. Townsend. *The kinetics of association of peptides with MHC class I molecules*. Progress in immunology **VIII** (1992) 175-180.

209. Khilko, S.N., *et al.*, *Direct detection of major histocompatibility complex class I binding to antigenic peptides using surface plasmon resonance. Peptide immobilization and characterization of binding specificity*. J. Biol. Chem. **268** (1993) 15425-34.

210. Chen, W., S. Khilko, J. Fecondo, D.H. Margulies, and J. McCluskey, *Determinant selection of major histocompatibility complex class I-restricted antigenic peptides is explained by class I-peptide affinity and is strongly influenced by nondominant anchor residues*. J. Exp. Med. **180** (1994) 1471-83.

211. Khilko, S.N., *et al.*, *Measuring interactions of MHC class I molecules using surface plasmon resonance*. J. Immunol. Methods **183** (1995) 77-94.

212. Boyd, L.F. and D.H. Margulies. *Tetrameric peptides bind to H-2D^d and H-2L^d molecules*. in *The 9th international congress of immunology*. 1995. San Francisco.

213. Schuck, P., *Kinetics of ligand binding to receptor immobilized in a polymer matrix, as detected with an evanescent wave biosensor. I. A computer simulation of the influence of mass transport*. Biophys. J. **70** (1996) 1230-1249.

214. Mottez, E., *et al.*, *A single-chain murine class I major transplantation antigen*. Eur J Immunol **21** (1991) 467-71.

215. Godeau, F., *et al.*, *Purification and ligand binding of a soluble class I major histocompatibility complex molecule consisting of the first three domains of H-2Kd fused to beta 2-microglobulin expressed in the baculovirus-insect cell system*. J. Biol. Chem. **267** (1992) 24223-9.

216. Ojcius, D.M., F. Godeau, J.P. Abastado, J.L. Casanova, and P. Kourilsky, *Real-time measurement of antigenic peptide binding to empty and preloaded single-chain major histocompatibility complex class I molecules*. Eur. J. Immunol. **23** (1993) 1118-24.

217. Ojcius, D.M., *et al.*, *Dissociation of the peptide-MHC class I complex limits the binding rate of exogenous peptide*. J. Immunol. **151** (1993) 6020-6.

218. Neefjes, J.J., J. Dierx, and H.L. Ploegh, *The effect of anchor residue modifications on the stability of major histocompatibility complex class I-peptide interactions*. Eur. J. Immunol. **23** (1993) 840-5.

219. Fahnestock, M.L., I. Tamir, L. Narhi, and P.J. Bjorkman, *Thermal stability comparisons of purified empty and peptide-filled forms of a class I MHC molecule*. Science **258** (1992) 1658-1662.

220. Jackson, M., E. Song, Y. Yang, and P. Peterson, *Empty and peptide containing conformers of class I major histocompatibility complex molecules expressed in Drosophila melanogaster cells*. Proc. Natl. Acad. Sci. USA **89** (1992) 12117-12121.

221. Gairin, J.E., H. Mazarguil, D. Hudrisier, and M.B. Oldstone, *Optimal lymphocytic choriomeningitis virus sequences restricted by H-2Db major histocompatibility complex class I molecules and presented to cytotoxic T lymphocytes*. J. Virol. **69** (1995) 2297-305.

222. Williams, D.B., B.H. Barber, R.A. Flavell, and H. Allen, *Role of beta-2 microglobulin in the intrcellular transport and surface expression of murine class I histocompatibility molecules*. J. Immunol. **142** (1989) 2796-2806.

223. Myers, N.B., W.R. Lie, M. Nett, R.J. Rubocki, and T.H. Hansen, *The conformation of L^d induced by beta-2 microglobulin is fixed during de novo synthesis and irreversible by exchange and dissociation*. J. Immunol. **142** (1989) 2751-2758.

224. Rohren, E.M., D.J. McCormick, and L.R. Pease, *Peptide-induced conformational changes in class I molecules - Direct detection by flow cytometry*. J. Immunol. **152** (1994) 5337-5343.

225. Bluestone, J.A., S. Jameson, S. Miller, and R.n. Dick, *Peptide-induced conformational changes in class I heavy chains alter major histocompatibility complex recognition*. J. Exp. Med. **176** (1992) 1757-1761.

226. Bluestone, J.A., A. Kaliyaperumal, S. Jameson, S. Miller, and R.n. Dick. *Peptide-induced changes in class I heavy chains alter allorecognition*. J. Immunol. **151** (1993) 3943-3953.

227. Chen, W., J. McCluskey, S. Rodda, and F.R. Carbone, *Chenges at peptide residues buried in the major histocompatibility complex (MHC) class I binding cleft influence T cell recognition: a possible role for indirect conformational alterations in the MHC class I or bound peptide in determining T cell recognition*. J. Exp. Med. **177** (1993) 869-873.

228. Solheim, J.C., *et al.*, *Binding of peptides lacking consensus anchor residue alters H-2L^d serologic recognition*. J. Immunol. **151** (1993) 5387-5397.

229. Hogquist, K.A., A.G. Grandea, and M.J. Bevan, *Peptide variants reveal how antibodies recognize major histocompatibility complex class I*. Eur. J. Immunol. **23** (1993) 3028-3036.

230. Chattopadhyay, S., M. Theobald, J. Biggs, and L.A. Sherman, *Conformational differences in major histocompatibility complex-peptide complexes can result in alloreactivity*. J. Exp. Med. **179** (1994) 213-219.

231. Ojcius, D.M., L. Gapin, and P. Kourilsky, *Dissociation of the peptide/MHC class I complex: pH dependence and effect of endogenous peptides on the activation energy*. Biochem. Biophys. Res. Commun. **197** (1993) 1216-22.

232. Wubbolts, R.W., J.J. Neefjes, and M. Fernandez-Borja, *MHC class II assembly and transport*, in *HLA and MHC: genes, molecules and function*, M.J. Browning and A.J. McMichael, Editor. 1996, BIOS Scientific Publishers: Oxford.

233. Brown, J.H., *et al.*, *Three-dimensional structure of the human class II histocompatibility antigen HLA-DR1*. Nature (1993) 33-39.

234. Sadegh-Nasseri, S. and H. McConnell, *A kinetic intermediate in the reaction of an antigenic peptide and I-E^k*. Nature **337** (1989) 274-276.

235. Dornmair, K., B. Rothenhausler, and H.M. McConnell, *Structural intermediates in the reactions of antigenic peptides with MHC molecules*. Cold Spring Harbor Symp. Quant. Biol. **44** (1989) 409-416.

236. Sadegh-Nasseri, S. and R. Germain, *A role for peptide in determining MHC class II structure.* Nature **353** (1991) 167-169.

237. Germain, R.N. and L.R. Hendrix, *MHC class II structure, occupancy, and surface expression determined by post-endoplasmic reticulum antigen binding.* Nature **353** (1991) 134-139.

238. Davidson, H.W., P.A. Reid, A. Lanzavecchia, and C. Watts, *Processed antigen binds to newly synthesized MHC class II molecules in antigen-specific B lymphocytes.* Cell **67** (1991) 105-116.

239. Qiu, Y., X. Xu, A. Wandinger-Ness, D.P. Dalke, and S.K. Pierce, *Separation of subcellular compartments containing distinct functional forms of MHC class II.* J. Cell Biol. **125** (1994) 595-605.

240. Hochman, J.H., Y. Shimizu, R. DeMars, and M. Edinin, *Specific associations of fluorescent beta 2-microglobulin with cell surfaces: the affinity of different H-2 and HLA antigens for beta 2-microglobulin.* J. Immunol. **140** (1988) 2322-2329.

241. Mage, M.G., *et al.*, *A recombinant, soluble, single-chain class I major histocompatibility complex molecule with biological activity.* Proc Natl Acad Sci U S A **89** (1992) 10658-62.

242. Abastado, J.P., *et al.*, *A soluble, single-chain Kd molecule produced by yeast selects a peptide repertoire indistinguishable from that of cell-surface-associated Kd.* Eur. J. Immunol. **23** (1993) 1776-83.

243. Hochuli, E., H. Dobeli, and A. Schacher, *New metal chelate adsorbent selective for proteins and peptides containing neighbouring histidine residues.* J. Chromatogr. **411** (1987) 177-84.

244. Crowe, J., *et al.*, *6xHis-Ni-NTA chromatography as a superior technique in recombinant protein expression/purification.* Methods Mol. Biol. **31** (1994) 371-87.

245. Kozak, M., *Point mutations define a sequence flanking the AUG initiator codon that modulates translation by eukaryotic ribosomes.* Cell **44** (1986) 283-292.

246. Zemmour, J. and P. Parham, *HLA class I nucleotide sequences, 1992*. Human Immunology **34** (1992) 225-241.

247. Bebbington, C.R. and C.C.G. Hentschel, *The use of vectors based on gene amplification for the expression of cloned genes in mammalian cells*, in *DNA cloning*, D. Glover, Editor. 1987, Academic Press. p. 163-186.

248. Bebbington, C.R., *Expression of antibody genes in nonlymphoid mammalian cells*. Methods **2** (1991) 136-145.

249. Krishna, S., P. Benaroch, and S. Pillai, *Tetrameric cell-surface MHC class I molecules*. Nature **357** (1992) 164-167.

250. Nozaki, Y. and C. Tanford, *Examination of titration behavior*. Meth. Enzymol. **11** (1967) 715-734.

251. Park, K.S., *et al.*, *Effect of enzymatic methylation of yeast iso-1-cytochrome c on its isoelectric point*. Arch. Biochem. Biophys. **267** (1988) 195-204.

252. Phillips, W.J. and R.A. Cerione, *Fluorescence investigations of receptor-mediated processes*, in *Biophysical and biochemical aspects of fluorescence spectroscopy*, T.G. Dewey, Editor. 1991, Plenum Press: New York and London. p. 135-168.

253. Lakowicz, J.R., *Principles of fluorescence spectroscopy*. 1983, New York: Academic Press.

254. Dewey, T.G.e., *Biophysical and biochemical aspects of fluorescence spectroscopy*. 1991, New York and London: Plenum Press.

255. Holzwarth, A.R., *Time-resolved fluorescence spectroscopy*. Methods in enzymology **246** (1995) 334-361.

256. Brand, L. and B. Witholt, *Fluorescence measurements*. Methods Enzymol. **11** (1967) 776-856.

257. Lehrer, S.S. and G.D. Fasman, *Fluorescence of lysozyme and lysozyme substrate complexes*. J. Biol. Chem. **242** (1967) 4644-4651.

258. Beecham, J.M. and L. Brand, *Time-resolved fluorescence of proteins*. Annu. Rev. Biochem. **54** (1985) 43-71.

259. Diaz, J.F. and J.M. Andreu, *Kinetics of dissociation of the tubulin-colchicine complex - complete reaction scheme and comparison to thermodynamic measurements*. J. Biol. Chem. **266** (1991) 2890-2896.

260. Miller, D.M., J.S. Olson, J.W. Pflugrath, and F.A. Quiocho, *Rates of ligand binding to periplasmic proteins involved in bacterial transport and chemotaxis*. J. Biol. Chem. **258** (1983) 13665-13672.

261. Voss, E.J., *Kinetic measurements of molecular interactions by spectrofluorimetry*. J. Mol. Recognit. **6** (1993) 51-58.

262. Fasman, G.D., ed. *Handbook of biochemistry and molecular biology*. 3rd ed. Vol. I. 1976, CRC Press: Cleveland.

263. Wetlaufer, D.B., *Ultraviolet spectra of proteins and amino acids*. Adv. Protein Chem. **17** (1962) 303-390.

264. Foote, J. and C. Milstein, *Kinetic maturation of an immune response*. Nature **352** (1991) 530-532.

265. Kropshofer, H., I. Bohlinger, H. Max, and H. Kalbacher, *Self and foreign peptides interact with intact and disassembled MHC class II antigen HLA-DR via tryptophan pockets*. Biochemistry **30** (1991) 9177-9187.

266. Strominger, J.L., *et al.*, *An evaluation of the significance of amino acid homologies in human histocompatibility antigens (HLA-A and HLA-B) with immunoglobulins and other proteins, using relatively short sequences*. Scand. J. Immunol. **11** (1980) 573-592.

267. Fersht, A., *Enzyme structure and mechanism*. 2nd ed. 1984, New York: W.H. Freeman and Company.

268. Roughton, F.J.W. and B. Chance, *Rapid reactions*, in *Techniques of organic chemistry*, S.L. Freiss, E.S. Lewis, andA. Weissberger, Editor. 1963, Wiley-Interscience: New York. p. 703-798.

269. Prinz, H., *Receptor-binding kinetics,* in *Receptor-ligand interactions - a practical approach,* E.C. Hulme, Editor. 1992, IRL Press: Oxford. p. 265-288.

270. Di Franco, A., *Reaction mechanism of L-glutamate dehydrogenase.* Eur. J. Biochem. **45** (1974) 407-424.

271. Christensen, U. and L. Mølgaard, *Stopped-flow fluorescence kinetic studies of Glu-plasminogen.* FEBS Lett. **278** (1991) 204-206.

272. Lambeir, A. and Y. Engelborghs, *A fluorescence stopped-flow study of colchicine binding to tubulin.* J. Biol. Chem. **256** (1981) 3279-3282.

273. von Hippel, P.H. and O.G. Berg, *Facilitated target location in biological systems.* J. Biol. Chem. **264** (1989) 675-678.

274. von Smoluchowski, M., *Versuch einer mathematischen Theorie der Koagulationskinetik kolloider Lösungen.* Z. Phys. Chem. **92** (1917) 129-168.

275. Shoup, D., G. Lipari, and A. Szabo, *Diffusion-controlled bimolecular reaction rates - the effect of rotational diffusion and orientation constraints.* Biophys. J. **36** (1981) 697-714.

276. Mason, D. and A. Williams, *The kinetics of antibody binding in solution and at the cell surface.* Biochem. J. **87** (1980) 1-20.

277. Berzofsky, J.A., S.L. Epstein, and I. Berkower, *Antigen-antibody interactions and monoclonal antibodies.* 1989, New York: Raven Press.

278. Pecht, I., *Antibody-hapten binding kinetics, conformational transitions and domains interactions,* in *Protein conformation as an immunological signal,* F. Celada, V.N. Schumaker, andE.E. Sercarz, Editor. 1983, Plenum Press: New York. p. 3-13.

279. Day, E.D., *Molecular basis of antigen-antibody interactions,* in *Methods of immunological analysis,* R.E. Masseyeff, W.H. Albert, andN.A. Staines, Editor. 1993, VCH: Weinheim. p. 80-90.

280. Wang, J.-X., H.I. Yamamura, W. Wang, and W.R. Roeske, *The use of the filtration technique in in vitro radioligand binding assays for membrane-bound and solubilized receptors*, in *Receptor-ligand interactions: a practical approach*, E.C. Hulme, Editor. 1992, IRL Press: Oxford. p. 213-234.

281. Buelow, R., S. Kuo, L. Paborsky, K.J. Wilson, and J.B. Rothbard, *Detergent-enhanced dissociation of endogenous peptides from PI-DRB1*0401*. Eur. J. Immunol. **24** (1994) 2181-5.

282. Frost, A.A. and R.G. Pearson, *Kinetics and mechanism*. Second ed. 1953, New York: John Wiley & Sons.

283. Weiland, G.A. and P.B. Molinoff, *Quantitative analysis of drug-receptor interactions: I. Determination of kinetic and equilibrium properties*. Life Sci **29** (1981) 313-30.

284. Dörr, F., *Basic Concepts of Thermodynamics*, in *Biophysics*, W. Hoppe, *et al.*, Editor. 1983, Springer-Verlag: Berlin. p. 316-322.

285. Molinoff, P.B., B.B. Wolfe, and G.A. Weiland, *Quantitative analysis of drug-receptor interactions: II. Determination of the properties of receptor subtypes*. Life Sci **29** (1981) 427-43.

286. Raffa, R.B. and F. Porreca, *Thermodynamic analysis of the drug-receptor interaction*. Life Sciences **44** (1989) 245-258.

287. Weiland, G.A., K.P. Minnemann, and P.B. Molinoff, *Fundamental difference between the molecular interactions of agonists and antagonists with the β-adrenergic receptor*. Nature **281** (1979) 114-117.

288. Testa, B., *et al.*, *Do thermodynamic studies provide information on both the binding and the activation of dopaminergic and other receptors?* Biochem. Pharmacol. **36** (1987) 4041-4046.

289. Naghibi, H., A. Tamura, and J.M. Sturtevant, *Significant discrepancies between van t'Hoff and calorimetric enthalpies*. Proc. Natl. Acad. Sci. USA **92** (1995) 5597-5599.

290. Dörr, F., *Theory of absolute reaction rates*, in *Biophysics*, W. Hoppe, *et al.*, Editor. 1983, Springer Verlag: Berlin etc. p. 328-330.

291. Arrhenius, S., *Über die Reaktionsgeschwindigkeit bei der Inversion von Rohrzucker durch Säuren*. Zeitschr. f. Phys. Chem. **4** (1889) 226-248.

292. Woody, R.W., *Circular dichroism*. Meth. Enzymol. **246** (1995) 34-71.

293. Creighton, T.E., *Proteins - structures and molecular properties*. 2nd ed. ed. 1993, New York: W.H. Freeman and Company.

294. Eftink, M.R., *Fluorescence quenching: theory and applications*, in *Topics in fluorescence spectroscopy*, J.R. Lakowicz, Editor. 1991, Plenum Press: New York and London. p. 53-126.

295. Eftink, M.R., *Fluorescence quenching reactions: probing macromolecular structures*, in *Biophysical and biochemical aspects of fluorescence spectroscopy*, T.G. Dewey, Editor. 1991, Plenum Press: New York and London. p. 1-42.

296. Bucci, E. and R.F. Steiner, *Anisotropy decay of fluorescence as an experimental approach to protein dynamics*. Biophys. Chem. **30** (1988) 199-224.

297. Steiner, R.F., *Fluorescence anisotropy: theory and applications*, in *Topics in fluorescence spectroscopy*, J.R. Lakowicz, Editor. 1991, Plenum Press: New York and London. p. 1-52.

298. Jameson, D.M. and W.H. Sawyer, *Fluorescence anisotropy applied to biomolecular interactions*. Meth. Enzymol. **246** (1995) 283-299.

299. Eisinger, J., B. Feuer, and A.A. Lamola, *Intramolecular energy transfer in adrenocorticotropin*. Biochemistry **8** (1969) 3902-3908.

300. Dittes, K., *et al.*, *Picosecond fluorescence spectroscopy of a single-chain class I major histocompatibility complex encoded protein in its peptide loaded and unloaded states*. Immunol. Lett. **40** (1994) 125-32.

301. Gakamsky, D.M., E. Haas, P. Robbins, J.L. Strominger, and I. Pecht, *Selective steady-state and time-resolved fluorescence spectroscopy of an HLA-A2-peptide complex*. Immunol. Lett. **44** (1995) 195-201.

302. Zimmermann, S.B., *Marcomolecular crowding: biochemical, biophysical, and physiological consequences*. Annu. Rev. Biophys. Biomol. Struct. **22** (1993) 27-65.

303. Burmeister, W.P., A.H. Huber, and P.J. Bjorkman, *Crystal structure of the complex of rat neonatal Fc receptor with Fc*. Nature **372** (1994) 379-383.

304. Burmeister, W.P., L.N. Gastinel, N.E. Simister, M.L. Blum, and P.J. Bjorkman, *Crystal structure at 2.2 Å resolution of the MHC-related neonatal Fc receptor*. Nature **372** (1994) 336-343.

305. Downing, A.K., *et al.*, *Solution structure of a pair of calcium-binding epidermal growth factor-like domains: implications for the Marfan syndrome and other genetic disorders*. Cell **85** (1996) 597-605.

306. Berg, O.G. and P.H. von Hippel, *Diffusion-controlled macromolecular interactions*. Ann. Rev. Biophys. Biophys. Chem. **14** (1985) 131-160.

307. Berg, H.C., *Random walks in biology*. 1983, Princeton: Princeton University Press.

308. Berg, H.C. and E.M. Purcell, *Physics of chemoreception*. Biophys. J. **20** (1977) 193-219.

309. Franklin, T.J., *Binding energy and the activation of hormone receptors*. Biochem. Pharmacol. **29** (1980) 853-856.

310. Strickland, S., G. Palmer, and V. Massey, *Determination of dissociation constants and specific rate constants of enzyme-substrate (or protein-ligand) interactions from rapid reaction kinetic data*. J. Biol. Chem. **250** (1975) 4048-4052.

311. Ortega, E., R. Schweitzer-Stenner, and I. Pecht, *Kinetics of ligand binding to the type I Fc_{ε} receptor on mast cells*. Biochemistry **30** (1991) 3473-3483.

312. Ortega, E., R. Schweitzer-Stenner, and I. Pecht, *Possible orientational constraints determine secretory signals induced by aggregation of IgE receptors on mast cells*. EMBO J. **7** (1988) 4101-4109.

313. Schimerlik, M.I. and R.P. Searles, *Ligand interactions with membrane-bound porcine atrial muscarinic receptor(s).* Biochemistry **19** (1980) 3407-3413.

314. Järv, J., B. Hedlund, and T. Bartfai, *Isomerisation of the muscarinic receptor • antagonist complex.* J. Biol. Chem. **254** (1979) 5595-5598.

315. Kranz, D.M., J.N. Herron, and E.W. Voss, *Mechanisms of ligand binding by monoclonal anti-fluorescyl antibodies.* J. Biol. Chem. **257** (1982) 6987-6995.

316. Foote, J. and C. Milstein, *Conformational isomerism and the diversity of antibodies.* Proc. Natl. Acad. Sci. USA **91** (1994) 10370-10374.

317. Lancet, D. and I. Pecht, *Kinetic evidence for hapten-induced conformational transition in immunoglobulin MOPC 460.* Proc. Natl. Acad. Sci. USA **73** (1976) 3549-3553.

318. Minton, A.P., *Macromolecular Crowding and Molecular Recognition.* J. Mol. Recogn. **6** (1993) 211-214.

319. Alberts, B., *et al.*, *Molecular biology of the cell.* Second ed. 1989, New York: Garland Publishing.

320. Nieland, T.J.F., *et al.*, *Isolation of an immunodominant viral peptide that is endogenously bound to the stress protein GP96/GRP94* Proc. Natl. Acad. Sci. USA **93** (1996) 6135-6139.

321. Beck, J.C., T.H. Hansen, S.E. Cullen, and D.R. Lee, *Slower processing, weaker beta 2-M association, and lower surface expression of H-2L^d are influenced by its amino terminus* J. Immunol. **137** (1986) 916-923.

322. Neefjes, J.J., and H.L. Ploegh, *Allele- and locus- specific differences in cell surface expression and the association of HLA class I heavy chain with beta 2-microglobulin: differential effects of inhibition of glycosylation on class I subunit association* Eur. J. Immunol. **18** (1988) 801-810.

323. Degen, E., and D.B. Williams, *Participation of a novel 88-kD protein in the biogenesis of murine class I histocompatibility molecules* J. Cell Biol. **112** (1991) 1099-1105.

324. Smith, J.D., N.B. Myers, J. Gorka, and T.H. Hansen. *Model for the in vivo assembly of nascent L^d molecules and for the expression of unfolded L^d molecules at the cell surface* J. Exp. Med. **178** (1993) 2035-2046.

325. Carreno, B.M., *et al., TAP associates with a unique class I conformation, whereas calnexin associates with multiple class I forms in mouse and man* J. Immunol. **155** (1995) 4726-4733.

326. Smith, J.D., J.C. Solheim, B.M. Carreno, and T.H. Hansen, *Characterisation of class I MHC folding intermediates and their disparate interactions with peptide and beta 2-microglobulin* Mol. Immunol. **32** (1995) 531-540.